University of Kentucky
UKnowledge

University of Kentucky Doctoral Dissertations Graduate School

2007

VISCOELASTIC RELAXATION CHARACTERISTICS OF RUBBERY POLYMER NETWORKS AND ENGINEERING POLYESTERS

Sumod Kalakkunnath
University of Kentucky, somudct@yahoo.com

Right click to open a feedback form in a new tab to let us know how this document benefits you.

Recommended Citation

Kalakkunnath, Sumod, "VISCOELASTIC RELAXATION CHARACTERISTICS OF RUBBERY POLYMER NETWORKS AND ENGINEERING POLYESTERS" (2007). *University of Kentucky Doctoral Dissertations*. 486.
https://uknowledge.uky.edu/gradschool_diss/486

This Dissertation is brought to you for free and open access by the Graduate School at UKnowledge. It has been accepted for inclusion in University of Kentucky Doctoral Dissertations by an authorized administrator of UKnowledge. For more information, please contact UKnowledge@lsv.uky.edu.

ABSTRACT OF DISSERTATION

Sumod Kalakkunnath

The Graduate School
University of Kentucky
2007

VISCOELASTIC RELAXATION CHARACTERISTICS OF RUBBERY POLYMER NETWORKS AND ENGINEERING POLYESTERS

ABSTRACT OF DISSERTATION

A dissertation submitted in partial fulfillment of the
requirements for the degree of Doctor of Philosophy in the
College of Engineering
at the University of Kentucky

By
Sumod Kalakkunnath
Lexington, Kentucky
Director: Dr. Douglass S. Kalika, Associate Professor of Chemical Engineering
Lexington, Kentucky
2007

Copyright © Sumod Kalakkunnath 2007

ABSTRACT OF DISSERTATION

VISCOELASTIC RELAXATION CHARACTERISTICS OF RUBBERY POLYMER NETWORKS AND ENGINEERING POLYESTERS

The relaxation characteristics of rubbery poly(ethylene oxide) [PEO] networks have been investigated as a function of network composition and architecture via dynamic mechanical analysis and broadband dielectric spectroscopy. A series of model networks were prepared via UV photopolymerization using poly(ethylene glycol) diacrylate [PEGDA] as crosslinker: variations in crosslink density were achieved either by the introduction of water in the prepolymerization reaction mixture, or by the inclusion of mono-functional acrylate such as poly(ethylene glycol) methyl ether acrylate [PEGMEA] or poly(ethylene glycol) acrylate [PEGA]. Copolymerization with mono-functional acrylate led to the insertion of flexible branches along the network backbone, and the corresponding glass-rubber relaxation properties of the copolymers (*i.e.,* T_g, relaxation breadth, fragility) were a sensitive function of network architecture and corresponding fractional free volume. Relatively subtle variations in network structure led to significant differences in relaxation characteristics, and a systematic series of studies was undertaken to examine the influence of branch length, branch end-group, and crosslinker flexibility on viscoelastic response. Dielectric spectroscopy was especially useful for the elucidation of localized, sub-glass relaxations in the polymer networks: the imposition of local constraint in the vicinity of the crosslink junctions led to the detection of a distinctive "fast" relaxation process in the networks that was similar to a comparable sub-glass relaxation observed in crystalline PEO and in the confined regions of PEO nanocomposites. Gas permeation studies on the model PEGDA networks confirmed their utility as highly-permeable, reverse-selective membrane materials, and strategic control of the network architecture could be used to optimize gas separation performance.

Dynamic mechanical and dielectric measurements have also been performed on a semicrystalline polyester, poly(trimethylene terephthalate) [PTT], in order to assess the influence of processing history on the resultant morphology and corresponding viscoelastic relaxation characteristics. Studies on both quenched and annealed PTT revealed the presence of a substantial fraction of rigid amorphous phase (RAP) material in the crystalline samples: dielectric measurements showed a strong increase in relaxation intensity above the glass transition indicating a progressive mobilization of the rigid amorphous phase with increasing temperature prior to crystalline melting.

KEYWORDS: dynamic mechanical analysis, broadband dielectric spectroscopy, UV photopolymerization, poly(ethylene oxide), poly(trimethylene terephthalate).

Sumod Kalakkunnath

03/12/2007

VISCOELASTIC RELAXATION CHARACTERISTICS OF RUBBERY POLYMER NETWORKS AND ENGINEERING POLYESTERS

By

Sumod Kalakkunnath

Dr. Douglass S. Kalika
Director of Dissertation

Dr. Barbara Knutson
Director of Graduate Studies

03/12/2007

RULES FOR THE USE OF DISSERTATIONS

Unpublished dissertations submitted for the Doctor's degree and deposited in the University of Kentucky Library are as a rule open for inspection, but are to be used only with due regard to the rights of the authors. Bibliographical references may be noted, but quotations or summaries of parts may be published only with the permission of the author, and with the usual scholarly acknowledgements.

Extensive copying or publication of the dissertation in whole or in part also requires the consent of the Dean of the Graduate School of the University of Kentucky.

A library that borrows this dissertation for use by its patrons is expected to secure the signature of each user.

Name	Date

DISSERTATION

Sumod Kalakkunnath

The Graduate School
University of Kentucky
2007

VISCOELASTIC RELAXATION CHARACTERISTICS OF RUBBERY POLYMER NETWORKS AND ENGINEERING POLYESTERS

DISSERTATION

A dissertation submitted in partial fulfillment of the
requirements for the degree of Doctor of Philosophy in the
College of Engineering
at the University of Kentucky

By
Sumod Kalakkunnath
Lexington, Kentucky
Director: Dr. Douglass S. Kalika, Associate Professor of Chemical Engineering
Lexington, Kentucky
2007

Copyright © Sumod Kalakkunnath 2007

ACKNOWLEDGEMENTS

First and foremost, warmest regards to my advisor, Dr. Douglass S. Kalika, without whom this work would have been impossible. A very genuine person at heart, Dr. Kalika has been a constant source of inspiration and assurance. He has helped me flourish not only as a researcher but also as a person, through his exemplary dedication towards both work and family. It has been an interesting and ongoing challenge to achieve his sense of perfection. I will always cherish the intellectually stimulating research meetings which were usually followed by lighter notes on music, sports and current affairs. In short, working with him over these years has been an enriching experience.

I would also like to thank, Dr. Benny Freeman (University of Texas at Austin) for providing the outstanding opportunity to collaborate with him. This joint effort has added a new dimension to my research and improved the quality of my work substantially. Special thanks to his team (Haiqing, Scott and Roy) for their assistance and input throughout the project.

The time spent here in Lexington has been memorable; thanks to all my friends. The road trips, get-togethers, coffee breaks and luncheon sessions will be forever etched in my mind. My dearest friends, Amita and Vivek, and my cousins, Sreeja and Manoj, deserve a special mention for being unwavering in their support.

Finally, I dedicate this work to my parents, Leela and Sethu, who will always remain a part of me. The values instilled by them will continue to help me strive to accomplish future goals.

TABLE OF CONTENTS

ACKNOWLEDGEMENTS……………………………………………………………iii

LIST OF TABLES………………………………………………………………vii

LIST OF FIGURES……………………………………………………………..viii

LIST OF FILES………………………………………………………….........xv

Chapter One: Introduction and Objectives………………………………….... 1

Chapter Two: Structure and Properties of Crosslinked Rubbery Networks and Semicrystalline Polymers...........4

2.1 TRANSPORT THROUGH RUBBERY NETWORKS…………………………… 4
2.2 REVERSE-SELECTIVE MEMBRANE NETWORKS…………………….......7
2.3 SEGMENTAL RELAXATION CHARACTERISTICS OF CROSSLINKED NETWORKS…………………………………………………9
2.4 TRANSPORT AND CHAIN DYNAMICS IN NANOCOMPOSITE MATERIALS…………………………………………………………...17
2.5 SEMICRYSTALLINE MORPHOLOGY OF LOW CRYSTALLINITY POLYMERS………………………………………………………….. 20

Chapter Three: Experimental Methods………………………………………. 34

3.1 MATERIALS……………………………………………………………...34
3.2 DYNAMIC MECHANICAL ANALYSIS (DMA)………………………………35
  3.2.1 Basic theory………………………………………………………35
  3.2.2 Time-temperature superposition…………………………………… 36
  3.2.3 Relaxation time and distribution parameter………………………... 37
  3.2.4 Experimental configuration and procedure………………………… 38
  3.2.5 Sample preparation and experimental technique……………………39
3.3 BROADBAND DIELECTRIC SPECTROSCOPY (BDS)………………………40
  3.3.1 Overview…………………………………………………………….40
  3.3.2 Derivation of phenomenological equations………………………… 40
    3.3.2.1 Static measurements……………………………………….. 40
    3.3.2.2 Dynamic measurements……………………………………..41
    3.3.2.3 Superposition principle……………………………………...42
    3.3.2.4 Description of non-Debye relaxation behavior……………...43

3.3.3 Dielectric relaxation phenomena at high temperatures and low frequencies……45
3.3.4 Correlation of dielectric relaxation intensity with inherent material properties……46
3.3.5 Experimental configuration and procedure……46
3.3.5.1 Sample preparation and experimental technique……48
3.3.5.2 Data analysis……48
3.4 DIFFERENTIAL SCANNING CALORIMETRY (DSC)……49
3.4.1 Basic theory……49
3.4.2 Sample preparation and experimental technique……50
3.4.3 Data Interpretation……51
3.4.3.1 Heat capacity measurement……51
3.4.3.2 Estimation of glass transition temperature……51
3.5 X-RAY DIFFRACTION (XRD)……52
3.5.1 Basic theory……52
3.5.2 Experimental technique……53

Chapter Four: Segmental Relaxation Characteristics of Crosslinked Poly(ethylene glycol) Networks: A Dynamic Mechanical Study……72

4.1 INTRODUCTION……72
4.2 EXPERIMENTAL……76
4.2.1 Materials……76
4.2.2 Polymer preparation……77
4.2.3 Dynamic Mechanical Analysis……78
4.2.4 Permeation and Sorption measurements……78
4.3 RESULTS AND DISCUSSION……79
4.3.1 Dynamic Mechanical Analysis……79
4.3.1.1 Networks based on variation in PEGDA molecular weight……79
4.3.1.2 PEGDA networks prepared with varying initial amounts of prepolymer……84
4.3.1.3 PEGDA networks prepared with varying amounts of acrylate monomer……87
4.3.1.4 PEGDA networks prepared with varying amounts of short-branch acrylate monomer……92
4.3.1.5 PEGDA networks prepared with variation in crosslinker……94
Networks prepared with PPGDA crosslinker……94
Networks prepared with BPAEDA crosslinker……97
4.3.2 Gas transport properties……98
4.3.3 PEGDA Nanocomposite networks……100
4.4 CONCLUSIONS……103

Chapter Five: Molecular Dynamics of Crosslinked Poly(ethylene glycol) Networks by Broadband Dielectric Spectroscopy………. 151

5.1 INTRODUCTION………. 151
5.2 EXPERIMENTAL………. 154
  5.2.1 Materials………. 154
  5.2.2 Polymer film preparation………. 154
  5.2.3 Dielectric Relaxation Spectroscopy………. 156
5.3 RESULTS AND DISCUSSION………. 156
  5.3.1 Properties of crosslinked PEGDA, PPGDA and PEO films………. 156
  5.3.2 Dielectric results for XLPEGDA, XLPPGDA, PEO films………. 157
  5.3.3 Properties of PEGDA and PPGDA copolymers………. 167
  5.3.4 Dielectric results for PEGDA/PEGMEA, PEGDA/PEGA copolymers………. 167
  5.3.5 Dielectric results for PEGDA/DGEEA copolymers………. 172
  5.3.6 Dielectric results for PPGDA/PPGMEA copolymers………. 175
  5.3.7 Properties of crosslinked BPAEDA and copolymers………. 177
  5.3.8 Dielectric results for crosslinked BPAEDA and copolymers………. 178
5.4 CONCLUSIONS………. 179

Chapter Six: Thermal Characterization of Poly(trimethylene terephthalate)………. 222

6.1 INTRODUCTION………. 222
6.2 EXPERIMENTAL………. 224
6.3 RESULTS AND DISCUSSION………. 225
  6.3.1 Calorimetric and X-ray analysis………. 225
  6.3.2 Dynamic Mechanical Analysis………. 229
  6.3.3 Broadband Dielectric Spectroscopy………. 232
6.4 CONCLUSIONS………. 236

Chapter Seven: Conclusions………. 254

References………. 258

Table of Nomenclature………. 266

VITA………. 270

LIST OF TABLES

Table 4.1: Relaxation characteristics of PEGDA networks. 107

Table 4.2: Relaxation characteristics of crosslinked PEGDA/water networks, based on PEGDA *n*=14 prepolymer. 108

Table 4.3: Characteristics of crosslinked PEGDA (*n*=14) and copolymer networks. 109

Table 4.4: Glass-rubber relaxation characteristics for PEGDA (*n*=14) and copolymer networks. 110

Table 4.5: Glass-rubber relaxation characteristics for PEGDA (*n*=14) and DGEEA (*n*=2) copolymer networks. 111

Table 4.6: Glass-rubber relaxation characteristics for PPGDA (*n*=12) and PPGMEA (*n*=2) copolymer networks. 112

Table 4.7: Glass-rubber relaxation characteristics for BPAEDA (*n*=4) and copolymer networks. 113

Table 4.8: Glass-rubber relaxation characteristics for PEGDA/MgO nanocomposites. 114

LIST OF FIGURES

Figure 2.1: Chemical structure of poly(ethylene glycol) diacrylate [PEGDA]. 25

Figure 2.2: Chemical structures of acrylate monomers. 26

Figure 2.3: Schematic of PEGDA-water crosslinked network. 27

Figure 2.4: Schematic showing the typical modulus behavior for crosslinked networks with decreasing crosslink density. 28

Figure 2.5: Arrhenius plot (log(τ) or log(a_T) versus $1/T$) showing the temperature dependence of the sub-glass and glass-rubber relaxation processes in polymer networks. 29

Figure 2.6: Schematic of the Fragility or Cooperativity plot (log(τ) or log(a_T) versus T_{REF}/T) showing the temperature sensitivity of the glass-rubber relaxation process as a function of crosslink density. 30

Figure 2.7: Kinked molecular conformation and repeat unit structure of PTT 31

Figure 2.8: Repeat unit structures of selected low crystallinity polymers. 32

Figure 2.9: Schematic showing the rigid amorphous phase in semicrystalline PTT. 33

Figure 3.1: Chemical structures of diacrylate monomers used as crosslinkers. 53

Figure 3.2: Chemical structures of acrylate co-monomers. 54

Figure 3.3: Determination of shift factor, a_T, to generate modulus-frequency master curve via time-temperature superposition method; frequency range of 0.1 to 10 Hz. 55

Figure 3.4: Modulus-frequency master curve obtained by time-temperature superposition. 56

Figure 3.5: Normalized curves for modulus and loss obtained by plotting the series solution for the KWW function with varying distribution parameter, $\beta = 0.1$, 0.3, 0.5 and 0.7. 57

Figure 3.6: Schematic representation of DMTA experimental set-up. 58

Figure 3.7: Single cantilever arrangement of a sample in the DMTA. 59

Figure 3.8: Representative dynamic mechanical (DMA) result for a polymeric material across the glass transition, plotted as a function of temperature for varying frequencies. 60

Figure 3.9: Parallel-plate capacitor arrangement for a dielectric material of thickness d, placed in an electric field E. 61

Figure 3.10: Cole – Cole model equations for dielectric constant (ε') and dielectric loss (ε'') plotted versus $\omega\tau_0$ on a semi-logarithmic plot. 62

Figure 3.11: Havriliak – Negami model equations for dielectric constant (ε') and dielectric loss (ε'') plotted versus $\omega\tau_0$ on a semi-logarithmic plot.. 63
Figure 3.12: Schematic representation of BDS experimental set-up. 64
Figure 3.13: Novocontrol Concept 40 BDS sample cell arrangement. 65
Figure 3.14: Schematic of the measurement circuit for the BDS Novocontrol Concept 40 spectrometer. 66
Figure 3.15: Perkin-Elmer DSC-7 Differential Scanning Calorimeter. 67
Figure 3.16: Typical DSC scan for a semicrystalline polymer. 68
Figure 3.17: Elastic scattering of X-rays from parallel crystal planes (1, 2 & 3) with a characteristic spacing *d*. 69
Figure 3.18: Typical WAXS pattern for a semicrystalline polymer plotted as intensity versus scattering angle (2θ). 70
Figure 4.1: FTIR spectra of liquid PEGDA and solid crosslinked PEGDA films ($n=3$). 113
Figure 4.2: Dynamic mechanical properties (E'; $tan\delta$) versus temperature for 100% PEGDA (n=14) network. 114
Figure 4.3: Dynamic mechanical properties (E'; $tan\delta$) for PEGDA networks based on diacrylates with varying ethylene oxide repeat length, n. 115
Figure 4.4: Ratio of temperature/rubbery modulus [T(K)/E_R] for PEGDA networks with varying ethylene oxide repeat length, n. 116
Figure 4.5: $tan\delta$ versus temperature (°C) for PEGDA networks in the sub-glass transition range. 117
Figure 4.6: Time-temperature master curve for PEGDA (n=14) network; $T_{REF} = -40°C$. 118
Figure 4.7: Time-temperature master curves for PEGDA networks with varying ethylene oxide repeat length, n. 119
Figure 4.8: Arrhenius plots of log(a_T) versus 1000/T(K) for PEGDA networks. 120
Figure 4.9: Storage modulus versus temperature for PEGDA (n=14) networks with varying amounts of water in the initial reaction mixture. 121
Figure 4.10: Time-temperature master curves for PEGDA/water networks. Curves are KWW best fits at $T_{REF} = -40°C$. 122
Figure 4.11: Cooperativity plots (log(a_T) versus T_α/T) for PEGDA/water networks.. 123
Figure 4.12: Dynamic mechanical properties (E'; $tan\delta$) versus temperature for PEGDA/PEGMEA copolymer networks. 124

Figure 4.13: Dynamic mechanical properties (E'; $tan\delta$) versus temperature for PEGDA/PEGA copolymer networks. 125

Figure 4.14: $tan\delta$ versus temperature for PEGDA/PEGMEA networks in the sub-glass transition range. 126

Figure 4.15: $tan\delta$ versus temperature for PEGDA/PEGA networks in the sub-glass transition range. 127

Figure 4.16: Time-temperature master curves for PEGDA copolymer networks; $T_{REF} = -40°C$. 128

Figure 4.17: Rubbery modulus (E_R, MPa) versus PEGDA content for PEGDA/PEGMEA, PEGDA/PEGA, and PEGDA/water networks. 129

Figure 4.18: KWW parameters for the glass-rubber relaxation in PEGDA networks; $T_{REF} = -40°C$. 130

Figure 4.19: Cooperativity plots ($\log(a_T)$ versus T_α/T) for PEGDA/PEGMEA copolymer networks. 131

Figure 4.20: Cooperativity plots ($\log(a_T)$ versus T_α/T) for PEGDA/PEGA copolymer networks. 132

Figure 4.21: Fragility index (m), as defined in Eq. 2.11, versus KWW distribution parameter (β_{KWW}) for PEGDA copolymer networks. 133

Figure 4.22: Dynamic mechanical properties (E'; $tan\delta$) versus temperature for PEGDA/DGEEA copolymer networks. 134

Figure 4.23: Time-temperature master curves for PEGDA/DGEEA copolymer networks; $T_{REF} = -40°C$. 135

Figure 4.24: Cooperativity plots ($\log(a_T)$ versus T_α/T) for PEGDA/DGEEA copolymer networks. 136

Figure 4.25: Dynamic mechanical properties (E'; $tan\delta$) versus temperature for 100% PEGDA and PPGDA/PPGMEA copolymer networks. 137

Figure 4.26: Time-temperature master curves for PPGDA/PPGMEA copolymer networks; $T_{REF} = -40°C$. 138

Figure 4.27: Cooperativity plots ($\log(a_T)$ versus T_α/T) for PPGDA/PPGMEA copolymer networks. 139

Figure 4.28: Dynamic mechanical properties (E'; $tan\delta$) versus temperature for BPAEDA/PEGMEA copolymer networks. 140

Figure 4.29: Dynamic mechanical properties (E'; $tan\delta$) versus temperature for BPAEDA/PEGA copolymer networks. 141

Figure 4.30: Time-temperature master curves for BPAEDA copolymer networks; $T_{REF} = 10°C$. 142

Figure 4.31: Cooperativity plots ($\log(a_T)$ versus T_α/T) for BPAEDA/PEGMEA copolymer networks. 143

Figure 4.32: Cooperativity plots (log(a_T) versus T_α/T) for BPAEDA/PEGA copolymer networks. 144

Figure 4.33: CO_2 transport properties determined at 35°C and infinite dilution for PEGDA/water networks. 145

Figure 4.34: CO_2 permeability (Barrer) determined at 35°C and infinite dilution for PEGDA networks. 146

Figure 4.35: Dynamic mechanical storage modulus (E') versus temperature for PEGDA networks with varying MgO (wt%) loading. 147

Figure 4.36: Dynamic mechanical loss factor ($tan\delta$) versus temperature for PEGDA networks with varying MgO (wt%) loading. 148

Figure 5.1: Dielectric constant (ε') and loss (ε'') vs. temperature for XLPEGDA; selected frequencies from 10 Hz to 0.5 MHz. 180

Figure 5.2: Contour plot of dielectric loss (ε'') vs. temperature (°C) vs. frequency (Hz) for XLPEGDA network. 181

Figure 5.3: Contour plot of dielectric loss (ε'') vs. temperature (°C) vs. frequency (Hz) for XLPPGDA network. 182

Figure 5.4: Contour plot of dielectric loss (ε'') vs. temperature (°C) vs. frequency (Hz) for PEO network. 183

Figure 5.5: Dielectric loss (ε'') vs. frequency (Hz) for XLPEGDA at -78°C. 184

Figure 5.6: Dielectric loss (ε'') vs. frequency (Hz) for XLPEGDA; temperatures from -98°C to -62°C at 4°C intervals. 185

Figure 5.7: Dielectric loss (ε'') vs. frequency (Hz) for XLPEGDA, XLPPGDA and PEO at -78°C. 186

Figure 5.8: HN curve fit parameters for XLPEGDA, XLPPGDA and PEO vs. temperature (°C). 187

Figure 5.9: Arrhenius plot of f_{MAX} (Hz) vs. 1000/T(K) for XLPEGDA, XLPPGDA and PEO. 188

Figure 5.10: Dielectric loss (ε'') vs. frequency (Hz) for XLPEGDA; temperatures from -38°C to -14°C at 4°C intervals. 189

Figure 5.11: Dielectric loss (ε'') vs. frequency (Hz) for XLPPGDA; temperatures from -34°C to -6°C at 4°C intervals. 190

Figure 5.12: Cole-Cole plots of dielectric loss (ε'') vs. dielectric constant (ε') for XLPEGDA and XLPPGDA at -34°C. 191

Figure 5.13: Contour plot of dielectric loss (ε'') vs. temperature (°C) vs. frequency (Hz) for 50/50 (wt%) PEGDA/PEGMEA network. 192

Figure 5.14: Dielectric properties of PEGDA/PEGMEA copolymer networks: (a) dielectric constant (ε'); (b) dielectric loss (ε'') vs. temperature. 193

Figure 5.15: Dielectric properties of PEGDA/PEGA copolymer networks: (a) dielectric constant (ε'); (b) dielectric loss (ε'') vs. temperature. 194

Figure 5.16: Dielectric loss (ε'') vs. temperature for PEGDA/PEGMEA copolymer networks across the sub-glass transition region. 195

Figure 5.17: Dielectric loss (ε'') vs. frequency for PEGDA/PEGMEA copolymer networks at -78°C. 196

Figure 5.18: Dielectric relaxation intensity ($\Delta\varepsilon$; determined from HN fits) vs. temperature for PEGDA/PEGMEA copolymer networks. 197

Figure 5.19: Havriliak-Negami [HN] broadening parameter vs. temperature for PEGDA/PEGMEA copolymer networks. 198

Figure 5.20: Dielectric loss (ε'') vs. frequency for PEGDA/PEGA copolymer networks at -78°C. 199

Figure 5.21: Arrhenius plot of f_{MAX} (Hz) vs. 1000/T(K): (a) PEGDA/PEGMEA copolymer networks; (b) PEGDA/PEGA copolymer networks. 200

Figure 5.22: Dielectric loss (ε'') vs. frequency for PEGDA/PEGMEA copolymer networks at -30°C. 201

Figure 5.23: Dielectric loss (ε'') vs. frequency for PEGDA/PEGA copolymer networks at -30°C. 202

Figure 5.24: Contour plot of dielectric loss (ε'') vs. temperature (°C) vs. frequency (Hz) for 60/40 (wt%) PEGDA/DGEEA copolymer network. 203

Figure 5.25: Dielectric loss (ε'') vs. frequency for PEGDA/DGEEA copolymer networks at -78°C. 204

Figure 5.26: Dielectric relaxation intensity ($\Delta\varepsilon$; determined from HN fits) vs. temperature for PEGDA/DGEEA copolymer networks. 205

Figure 5.27: Havriliak-Negami [HN] broadening parameter vs. temperature for PEGDA/DGEEA copolymer networks. 206

Figure 5.28: Arrhenius plot of f_{MAX} (Hz) vs. 1000/T(K) for PEGDA/DGEEA copolymer networks. 207

Figure 5.29: Dielectric loss (ε'') vs. frequency for PEGDA/DGEEA copolymer networks at -30°C. 208

Figure 5.30: Dielectric properties of PPGDA/PPGMEA copolymer networks: (a) dielectric constant (ε'); (b) dielectric loss (ε'') vs. temperature. 209

Figure 5.31: Dielectric loss (ε'') vs. frequency for PPGDA/PPGMEA copolymer networks at -78°C. 210

Figure 5.32: Dielectric loss (ε'') vs. frequency for PPGDA/PPGMEA copolymer networks at -30°C. 211

Figure 5.33: Cooperativity plots of τ/τ_α vs. T_α/T for PPGDA/PPGMEA copolymer networks. 212

Figure 5.34: Contour plot of dielectric loss (ε'') vs. temperature (°C) vs. frequency (Hz) for XLBPAEDA network. 213

Figure 5.35: Dielectric loss (ε'') vs. frequency (Hz) for XLBPAEDA; temperatures from -98°C to -54°C at 4°C intervals. 214

Figure 5.36: Dielectric properties of BPAEDA/PEGMEA copolymer networks: (a) dielectric constant (ε'); (b) dielectric loss (ε'') vs. temperature. 215

Figure 5.37: Dielectric properties of BPAEDA/PEGA copolymer networks: (a) dielectric constant (ε'); (b) dielectric loss (ε'') vs. temperature. 216

Figure 5.38: Dielectric loss (ε'') vs. frequency for BPAEDA/PEGMEA copolymer networks at -70°C. 217

Figure 5.39: Dielectric loss (ε'') vs. frequency for BPAEDA/PEGA copolymer networks at -70°C. 218

Figure 5.40: Dielectric relaxation intensity ($\Delta\varepsilon$; determined from HN fits) vs. BPAEDA content (wt%) for BPAEDA/PEGMEA and BPAEDA/PEGA copolymer networks. 219

Figure 6.1: DSC heating sweeps (10°C min^{-1}) for quenched and isothermally melt crystallized PTT. 236

Figure 6.2: DSC heating sweeps (10°C min^{-1}) for isothermally melt crystallized PTT: expanded view of glass transition region. 237

Figure 6.3: DSC heating sweeps (10°C min^{-1}) for isothermally melt crystallized PTT plotted versus time. 238

Figure 6.4: Incremental increase in heat capacity ($\Delta C_p(T_g)$; J/mol-K) versus net heat of fusion (ΔH_F; kJ/mol) for melt crystallized PTT. 239

Figure 6.5: Wide-angle X-ray diffraction patterns (intensity versus 2θ) for quenched and melt crystallized (T_c = 180°C) PTT. 240

Figure 6.6: Dynamic mechanical storage modulus (E'; Pa) and loss factor ($tan\delta$) versus temperature for quenched PTT. 241

Figure 6.7: Dynamic mechanical storage modulus (filled symbols) and loss factor ($tan\delta$) (empty symbols) versus temperature for melt crystallized (T_c = 160°C) PTT. 242

Figure 6.8: Time-temperature master curve for melt crystallized (T_c = 160°C) PTT; T_{REF} = 80°C 243

Figure 6.9: Dynamic mechanical $tan\delta$ versus temperature for melt crystallized PTT. 244

Figure 6.10: Dielectric constant (ε') and loss (ε'') versus temperature for quenched PTT. 245

Figure 6.11: Dielectric constant (ε') and loss (ε'') versus temperature for melt crystallized (T_c = 170°C) PTT. 246

Figure 6.12: Dielectric loss (ε'') versus frequency for quenched PTT across the glass-rubber (α) and sub-glass (β) relaxation regions. 247

Figure 6.13: Dielectric loss (ε'') versus frequency for melt crystallized (T_c = 170°C) PTT across the glass-rubber (α) and sub-glass (β) relaxation regions. 248

Figure 6.14: Arrhenius plot of f_{MAX} (Hz) versus 1000/T(K) for quenched and melt crystallized PTT. 249

Figure 6.15: Comparison of $\tan\delta$ versus temperature curves for quenched PTT........ 250

Figure 6.16: Dielectric relaxation intensity ($\Delta\varepsilon = \varepsilon_R - \varepsilon_U$) versus temperature for quenched and melt crystallized PTT; sub-glass (β) and glass-rubber (α) relaxations. 251

LIST OF FILES

Sumod Kalakkunnath_PhD Dissertation……………………………………………17.7 MB

Chapter One

Introduction and Objectives

Polymeric materials have become ubiquitous in modern society owing to their wide spectrum of applicability. These materials find use in applications ranging from electrical, automotive and structural parts to textile fibers, barrier packaging and membranes. The potential application of a polymeric material with desired characteristics requires insight into its inherent structure-property-performance relationships. It is of immense value to establish the correlations between molecular and morphological character and performance in-situ, the goal being to enhance performance characteristics by intelligent variation in chemical composition, backbone structure and processing history. The optimization of a polymer for a specific engineering application calls for a fundamental understanding of molecular architecture, chain dynamics, and phase behavior as a function of composition, synthesis, and processing, with simultaneous evaluation of macroscopic performance properties. The projects described herein undertake this approach for the investigation of two classes of polymeric materials: crosslinked poly(ethylene glycol) (PEG)-based rubbery networks for use as gas separation membranes, and a commercial semicrystalline polyester, poly(trimethylene terephthalate) (PTT), currently processed for high performance fiber applications.

Rubbery crosslinked membrane networks have shown promise for the separation of gas mixtures, particularly for the preferential separation of quadrupolar gases such as CO_2 over light gases like H_2. This low-energy separation technique is of tremendous industrial importance, as it provides a method for the potential sequestration of CO_2 as well as for the purification of H_2 for use as fuel or chemical feedstock. A series of model crosslinked membranes based on PEG have been formulated with the intention to achieve high solubility selectivity and minimal size-sieving for the transport of polar gases over smaller, non-polar molecules. A thorough experimental study has been undertaken to fully characterize the relaxation characteristics of these networks with systematic variation in structure and crosslink density. In addition, the gas transport properties of the membranes have been measured in collaboration with the research group of Prof. Benny Freeman at the University of Texas at Austin. The correlation of chain dynamics, morphology and mechanical integrity with gas separation performance for these rubbery networks facilitates the establishment of molecular-based design rules for the preparation of membranes with optimized properties.

The specific objectives of this project are as follows:

> Investigation of the glass-rubber (α) relaxation for model PEG networks via dynamic thermal analysis techniques; *i.e.*, Dynamic Mechanical Analysis (DMA) and Broadband Dielectric Spectroscopy (BDS).
>
> Detailed characterization of the sub-glass (β) relaxations in these networks using the more sensitive BDS technique; elucidation of the sub-glass transition behavior and its correlation with molecular confinement.
>
> Investigation of copolymer series with systematic variations in network architecture and crosslink density. This includes variation in the crosslinker structure, variation in the network composition, and variation in the branch length and/or end group of the co-monomer.
>
> Correlation of gas permeation measurements and free volume properties with dynamic relaxation characteristics for the determination of those network structural elements most appropriate for optimal gas separation performance.

Poly(trimethylene terepthalate) (PTT), a relatively new member of the terephthalate polyester family, is gaining significant commercial importance in the areas of textile fibers and structural materials. PTT proves to be a suitable alternative to its predecessors (*e.g.*, PET, PBT) both in terms of its processability and excellent dimensional stability. Also, PTT possess a unique kinked molecular conformation which appears to be responsible for its exceptional elastic properties. The semicrystalline morphology of PTT contains a fraction of chains that remain immobile through the glass transition, known as the rigid amorphous phase (RAP) fraction. The character of the rigid amorphous phase, which is a function of processing history, can be critical in determining macroscopic properties such as fracture toughness and barrier performance. Dynamic mechanical and dielectric measurements have been performed in order to explore the sensitivity of the relaxation characteristics in PTT to the resultant crystalline architecture, with corresponding evaluation of its structure using calorimetric and X-ray methods. The key consideration here is to understand the semicrystalline morphology that emerges in PTT and its correlation with performance properties.

The specific objectives associated with the characterization of PTT are:

> Elucidation of glass-rubber (α) and sub-glass (β) relaxation characteristics in quenched and annealed PTT as a function of prior thermal history using dynamic mechanical and dielectric techniques.
>
> Correlation of dynamic properties with crystalline morphology, as characterized by calorimetric and X-ray methods.
>
> Estimation of RAP fraction as a function of processing history.

Chapter 2 of the dissertation provides an overview of structure and properties for both the rubbery crosslinked networks and PTT. The experimental methods and phenomenological equations employed to analyze these material systems are discussed in detail in Chapter 3. Chapters 4 and 5 summarize the relaxation characteristics of the crosslinked membrane networks: Chapter 4 focuses on results obtained from dynamic mechanical analysis, while Chapter 5 is dedicated to broadband dielectric studies. Chapter 6 details the static and dynamic properties of PTT as influenced by thermal processing history. Finally, Chapter 7 presents a review of the most significant results from this work.

Copyright © Sumod Kalakkunnath 2007

Chapter Two

Structure and Properties of Crosslinked Rubbery Networks and Semicrystalline Polymers

Understanding structure-property relationships is key to developing materials with enhanced or optimum performance. It is therefore pertinent to have fundamental insight into the chain dynamics and morphology of the materials under consideration, and how variations in structure correlate with potential applicability. This chapter examines the fundamentals of transport phenomena in rubbery networks, compositional factors that affect separation performance, the influence of crosslinking on chain dynamics and relaxation phenomena, and how the morphology and transport behavior of polymer membranes vary with the inclusion of inorganic fillers. It also explores the morphology that exists in low crystallinity thermoplastics as a function of polymer backbone structure and sample preparation history.

2.1 TRANSPORT THROUGH RUBBERY NETWORKS

The employment of rubbery networks as membrane materials is gaining interest for use in industrial gas separations. In particular, these membranes are attractive for the selective removal and sequestration of CO_2 from mixtures of light gases (*e.g.*, H_2, N_2, air, CH_4). This application is of immense industrial importance for a number of processes, such as the separation of CO_2 from H_2 upon steam reforming of hydrocarbons, or the removal of CO_2 from CH_4 for natural gas purification.[1] Performance requirements for such a membrane include high CO_2 permeability coupled with high CO_2/light gas selectivity, so that CO_2 (typically the minority component) permeates to the low pressure side of the membrane while the light gas component (*i.e.*, H_2, CH_4) is retained at elevated pressure on the feed side for subsequent transport and use. These criteria can be realized via the application of rubbery networks that rely on preferential solubility rather than size discrimination for selective separation. This section pertains to understanding the transport of gases through such networks and the need to design and characterize rubbery networks for use as "reverse selective" membranes.

Consider the steady state flux (N_A, cm^3(STP)/cm^{2}s) of a gas A through a rubbery membrane of thickness l (cm). If p_2 and p_1 are the partial pressures of gas A at the feed (high pressure) and permeate (low pressure) sides, respectively, then its permeability (P_A) through the membrane is given as:[2]

$$P_A = \frac{N_A \cdot l}{p_2 - p_1} \qquad [2.1]$$

If the downstream pressure, p_1, is much lower than the upstream pressure, p_2, and the Fick's law of diffusion is obeyed, then the permeability can be expressed as:[2]

$$P_A = D_A \times S_A \qquad [2.2]$$

where D_A is the effective concentration-averaged diffusivity. S_A is the apparent solubility coefficient given by the relation:

$$S_A = \frac{C_2}{p_2} \qquad [2.3]$$

where C_2 is the concentration of gas A sorbed on the upstream side of the membrane. Diffusivity of a gas is often correlated to the free volume of the polymer by the relation:[3,4]

$$D_A = A_D \exp\left(-\frac{B}{FFV}\right) \qquad [2.4]$$

where A_D is a pre-exponential factor, B is a constant that depends on the penetrant size and FFV is the fractional free volume present in the polymer. FFV is generally defined by the equation:[5]

$$FFV = \frac{V - V_o}{V} \qquad [2.5]$$

where V is the specific volume of the polymer in its amorphous form at a given temperature and V_0 is the specific occupied volume at 0 K. V_0 is typically estimated as 1.3 times the van der Waals volume, as calculated using group contribution methods.[6]

Ideal selectivity of a membrane gives a measure of the degree of preferential separation for one component in a mixture. For a binary mixture of gases A and B, the ideal selectivity ($\alpha_{A/B}$) is defined as the ratio of their corresponding pure gas permeabilities:[7]

$$\alpha_{A/B} = \frac{P_A}{P_B} = \left[\frac{D_A}{D_B}\right] \times \left[\frac{S_A}{S_B}\right] \qquad [2.6]$$

where D_A/D_B, the ratio of the diffusivities of the two gases, is termed the diffusivity selectivity and S_A/S_B, the ratio of their respective solubility coefficients, is known as the solubility selectivity. Diffusivity selectivity depends primarily on the difference in gas molecule size and thus reflects the size-sieving ability of the membrane. Solubility selectivity, on the other hand, is controlled by two factors: (i) the relative affinity of the penetrant gas molecules for the polymer, and (ii) the difference in the degree of condensability of the penetrants in the polymer.[2,8] Condensability of a gas is often assumed to be directly related to its critical temperature. Solubility, unlike diffusivity, depends only weakly on the free volume of the polymer and its corresponding size sieving character.

Following the above discussion, it is possible to differentiate the transport behavior in glassy and rubbery membranes. On account of their primarily rigid backbone structure, glassy polymers tend to have less free volume and lower chain mobility, thus rendering them more size selective in nature. These polymers therefore have high diffusivity selectivity, which distinguishes them from flexible rubbery polymers. Commercial applications to date have emphasized the use of glassy polymers and their optimization to obtain high diffusivity selectivities.[2,9] By contrast, the application of rubbery membranes for industrial gas separations has remained relatively unexplored.[10,11] Rubbery membranes, which have flexible chain backbones and inherently high free volume, tend to be weakly size sieving, with the separation driven primarily by solubility selectivity.

This characteristic can be used as an advantage for preferentially separating larger, more soluble gas molecules (*e.g.*, acid or polar gases like CO_2 or H_2S) from smaller, non-polar gases that exhibit low solubility.

Rubbery membranes that preferentially permeate larger, more soluble gas molecules based on solubility selectivity are termed “reverse-selective” membranes owing to the opposite or “reverse” character of separation as compared to the size discrimination mechanism typically encountered with glassy polymers. The desired separation is achieved by simultaneously decreasing the diffusivity selectivity (size-based separation) and increasing the solubility selectivity (affinity-based separation) of the membrane. Flexible rubbery polymers that exhibit favorable interactions with one of the components in the feed mixture are ideal candidates for such a class of membranes. The polymer chain flexibility renders the membrane less size selective and decreases the diffusivity selectivity, while a positive matrix-molecule interaction increases the solubility selectivity.

2.2 REVERSE-SELECTIVE MEMBRANE NETWORKS

The discussion in this section will pertain to the development of networks intentionally designed for the reverse-selective removal of CO_2 from light gas mixtures, specifically the preferential transport of (larger) CO_2 over (smaller) H_2. To achieve this, the membrane material should be minimally size sieving. Also, selective permeation of the minority component (*i.e.*, CO_2) reduces the required membrane area and eliminates the need to re-pressurize the H_2 recovered on the high-pressure feed side; both are factors that render the membrane separation more economical. These goals requires the use of polymers that contain polar groups (*e.g.*, ether oxygens, nitriles, *etc.*) which foster high CO_2 solubility along with favorable CO_2/H_2 solubility selectivity on account of their interaction with the quadrupolar moment of CO_2.[12,13] Previous studies have reported polar ether oxygens present in ethylene oxide to be the best species that can maintain high CO_2/H_2 solubility selectivity.[14-17] Hence, the logical approach is to prepare high free volume (*i.e.*, rubbery) membranes based on polymers rich in polar ether oxygen units, for example, poly(ethylene oxide) [PEO].**[18]** Unfortunately, the high degree of crystallinity in PEO precludes the possibility of achieving high permeation rates as practically no gas permeation occurs through the ordered crystalline regions.**[17]** The introduction of chemical crosslinks, however, is an effective method to suppress crystallization in PEO and thereby dramatically enhance permeability. In fact, if the distance between crosslinks is sufficiently short, completely non-crystalline PEO polymers can be achieved. Graham has reported that fully amorphous crosslinked networks of PEO are obtained when the molecular weight of the ethylene oxide segments between crosslink junctions is 1500 grams per mole or less (*i.e.*, approximately 35 ethylene oxide [EO] units).**[19]** Priola *et al.* indicate a somewhat lower value (~ 875 g/mole between crosslinks) to maintain the amorphous character of the PEO network.**[20]**

In order to incorporate the high ethylene oxide content of PEO and maintain an amorphous rubbery matrix, highly crosslinked networks of ultraviolet (UV) photopolymerized polyethylene glycol diacrylate (PEGDA) have been prepared. The basic structure of PEGDA and the crosslinked network formed on photopolymerization are shown in **Figure 2.1**. The length of the repeat unit (n=14) is selected such that the overall ethylene oxide content remains high and the rubbery character of the network is maintained. Lower values of n can lead to a glassy network, while higher values of n can reduce the crosslink density to the point of crystallization.

Optimization of membrane performance requires systematic variation of the membrane architecture, with an ultimate goal of establishing design rules that can be applied for specific gas separation objectives. This entails, for example, the use of different strategies to control crosslink density, while simultaneously tailoring membrane free volume. One approach to prepare these networks is by the inclusion of monofunctional acrylate groups in the prepolymer reaction mixture. The structures of selected acrylate monomers, poly(ethylene glycol) methyl ether acrylate [PEGMEA] and poly(ethylene glycol) acrylate [PEGA], along with the crosslinked network structure formed on copolymerizing these monomers with PEGDA, are shown in **Figure 2.2**. PEGDA acts as a crosslinker or bridge between the backbone chains, while the acrylate monomers are inserted as branch or pendant groups in the network. The length of the repeat segment for the PEGA and PEGMEA monomers is selected such that the copolymer networks retain their amorphous nature, as well as an approximately constant overall ethylene oxide content. This approach facilitates the characterization of networks with varying free volume, but similar chemical composition.

A second approach for controlling crosslink density of the networks is by introduction of appropriate amounts of water as diluent, thus systematically varying the concentration of prepolymer in the reaction mixture.[21-23] Lower prepolymer concentration can lead to the formation of "wasted" crosslinks (see **Figure 2.3**) due to an increase in intramolecular cyclization. These loops fail to contribute to the mechanical integrity of the network, but are effective in suppressing crystallization. This method again renders it possible to prepare amorphous networks with varying crosslink density and similar chemical composition.

The above mentioned approaches afford the possibility of preparing a wide range of wholly amorphous model membranes having high ethylene oxide content. The corresponding structures can then be tailored to optimize CO_2 permeability and CO_2/light gas selectivity. Possible modifications to the structure of the networks include varying the repeat segment length of the crosslinker or acrylate pendant group, or introducing somewhat more rigid or bulkier crosslinkers.

2.3 SEGMENTAL RELAXATION CHARACTERISTICS OF CROSSLINKED NETWORKS

This section examines the relationships between network structure and segmental relaxation characteristics in crosslinked polymer networks. Dynamic mechanical analysis and broadband dielectric spectroscopy provide fundamental insight into the motional dynamics of polymer chain segments over a wide range of temperature and experimental timescale. These experimental techniques afford an enhanced understanding of segmental relaxation behavior as a function of the local molecular environment, as influenced by polymer composition and network architecture. Detailed information can be obtained on the time-temperature character of each relaxation, relaxation breadth, and the overall distribution of relaxation times. The sensitivity of these methods to relatively subtle changes in network structure renders them highly useful in elucidating those refinements that are most effective in tailoring membrane properties for specific separations.

The segmental relaxation properties of polymer networks are strongly influenced by the presence of crosslinking. A number of studies have been undertaken to investigate the segmental constraint and dynamic heterogeneity that arise due to crosslinks in polymer networks, and the influence of varying crosslink density on the measured glass transition temperature (T_g).**[24-33]** The introduction of crosslinks leads to a decrease in the conformational freedom of the chains and results in areas of restricted mobility in the vicinity of the crosslink junctions. The constraint imposed by the crosslinks typically manifests itself by an increase in T_g with increasing crosslink density. The positive shift in T_g is most prominent at high crosslink densities where the average distance between crosslinks approaches the characteristic length scale of local segmental rearrangement. A recent study by Schroeder and Roland on crosslinked poly(dimethylsiloxane) networks demonstrates this behavior, where an increase in T_g of over 50°C was observed when the distance between the crosslinks was reduced to ~ 14 Å.**[30]** The increase in T_g was accompanied by broadening of the glass-rubber relaxation which can be attributed to the increased heterogeneous environment experienced by the relaxing chains at higher crosslink densities.

The crosslink density of a network, or the effective number of network junctions per unit volume (υ_e, mol/cm^3), is inversely related to the molecular weight between crosslinks (M_c, g/mol) as follows:**[34]**

$$\upsilon_e = \frac{\rho_p}{M_c} \qquad [2.7]$$

where ρ_p is the bulk polymer density (g/cm^3). Equilibrium water swelling measurements and/or the value of the modulus in the rubbery plateau region (obtained via dynamic mechanical testing) can be used to estimate M_c. The rubbery modulus is correlated to the effective crosslink density according to classical rubber elasticity theory:[35-37]

$$\upsilon_e = \frac{E_R}{3RT} \qquad [2.8]$$

where E_R is the rubbery modulus value, T is the absolute temperature and R is the universal gas constant. Thus, elasticity theory predicts a relation between M_c and the ratio T/E_R such that lower crosslink density corresponds to a lower rubbery modulus. **Figure 2.4** shows a schematic of typical mechanical behavior for a polymer network with varying crosslink density. A decrease in the crosslink density is manifested by a drop in the value of the rubbery modulus and may be accompanied by a negative offset in T_g.

The concept of time-temperature interdependence can be used to gain an understanding of the molecular relaxation behavior associated with these networks over a wide range of experimental timescales. By shifting the modulus data obtained from dynamic mechanical analysis relative to a single reference temperature, modulus-frequency master curves are generated (see time-temperature superposition method, Section 3.2).[38] These master curves can be analyzed using a suitable model to assess the influence of effective crosslink density on the characteristics of the relaxation environment. One such model that accounts for both intramolecular and intermolecular cooperation, as typically encountered across the glass-rubber relaxation, is the Kohlrausch-Williams-Watts (KWW) function:[29]

$$\phi(t) = \exp[-(t/\tau_0)^{\beta}] \qquad [2.9]$$

The KWW “stretched-exponential” function satisfactorily describes the glass-rubber relaxation in terms of τ_0, the observed relaxation time and β, the distribution parameter. τ_0 is an average value for the distribution of relaxation times experienced by the network, while β quantifies the breadth of the relaxation. Lower values of β are indicative of increased intermolecular coupling and inhomogeneous broadening.[29] Williams *et al.* have provided series approximations of the modulus and loss for the KWW model in the frequency domain; these can be used as a basis for curve fits to determine the characteristic parameters.[39] Alternatively, Ngai *et al.* have proposed an equation similar to the KWW function that expresses the effective relaxation time in relation to the intermolecular coupling factor (*n*), with *n* reflecting the intermolecular constraints present between non-bonded relaxing species.[40,41]

Dielectric relaxation spectroscopy is an effective tool to investigate molecular relaxations in crosslinked networks, and is a logical complement to dynamic mechanical analysis. The dielectric response of a material, expressed in terms of the complex dielectric constant (ε^*), reflects the reorientation of dipoles along the polymer chain segments in response to an applied electric field of varying frequency. The dielectric dispersion associated with the glass transition undergoes broadening and shifts to lower frequencies (longer relaxation times) as the hindrance to chain motion increases with increasing crosslink density. A number of empirical models have been proposed to relate the shape of the dielectric relaxation data to segmental motions of the polymer chains (see Section 3.3). Among them, the Havriliak-Negami (HN) equation[42] appears to be the most versatile for describing the entire dielectric relaxation spectrum, as it can readily account for the asymmetric relaxation broadening typically encountered in crosslinked networks:

$$\varepsilon^* = \varepsilon_U + \frac{\varepsilon_R - \varepsilon_U}{[1 + (i\omega\tau_{HN})^a]^b} \qquad [2.10]$$

The parameters appearing in the HN equation are defined as follows: ε_R is the relaxed dielectric constant value, obtained at very low frequencies ($\omega \to 0$), and ε_U is the unrelaxed dielectric constant, corresponding to high frequencies ($\omega \to \infty$). τ_{HN} represents the average relaxation time of the network, while *a* (broadening parameter) and *b* (skewing parameter) characterize the shape of the relaxation curves. The dielectric relaxation intensity ($\Delta\varepsilon$) is given by the difference, $\varepsilon_R - \varepsilon_U$.

In addition, the application of a suitable model (such as the HN model) can be used to establish the intensity of a particular relaxation, thus providing insight into the number and character of the network dipoles participating in a specific relaxation process. The specificity of the dielectric "probe" (*i.e.*, network dipoles) and the wide frequency range of the dielectric technique make it especially useful for studying the influence of network modifications on polymer chain mobility.

The temperature dependence of segmental relaxations is of vital importance in understanding the dynamics of polymer networks. Local transitions, for example sub-glass relaxations, are typically non-cooperative, activated processes. The short-range motions inherent to these relaxations usually follow the Arrhenius model, such that a semi-logarithmic plot of relaxation time [log(τ)] versus $1/T$ results in a straight line. Alternatively, the glass-rubber transition is a large-scale, cooperative process that displays non-Arrhenius behavior. Such processes depend on free volume availability and can be described using the Williams-Landel-Ferry (WLF) equation (see **Figure 2.5**).[38] The wide distribution of relaxation times observed in crosslinked polymer networks can mask the influence of intermolecular coupling on the relaxation behavior. In order to address this issue, Angell has proposed the generation of normalized semi-logarithmic Arrhenius plots in the vicinity of the glass-rubber transition, known as cooperativity plots.[29,43] In **Figure 2.6**, the relaxation time (τ) or the shift factor (a_T) is plotted versus reciprocal temperature, normalized with respect to an appropriate reference temperature (usually chosen as the glass-rubber transition temperature, T_g). The data can then be fit to the WLF model to capture the non-Arrhenius behavior of the glass-rubber relaxation, and temperature normalization enables direct comparison of networks with different T_g's on a single plot.

The fragility of a material can be used as an index to quantify the temperature sensitivity of segmental relaxation for different systems. Generally, materials with a rigid backbone and/or high crosslink density display greater temperature dependence reflective of their higher intermolecular association, and correspondingly higher fragility. On the other hand, polymers with a flexible backbone and a more open structure have lower fragility.[44] The temperature sensitivity of each material is reflected in the fragility (or steepness) index (m), which is determined based on the slope of the respective cooperativity curve at a particular reference temperature ($T_{REF} = T_g$) as follows:

$$m = \left.\frac{d\log(\tau)}{d(T_{REF}/T)}\right|_{T=T_{REF}} = \left.\frac{d\log(a_T)}{d(T_{REF}/T)}\right|_{T=T_{REF}} \qquad [2.11]$$

where $a_T = \tau/\tau_{REF}$. The fragility index, m, can also be correlated to the corresponding apparent activation energy (E_A) at that temperature:

$$m = \frac{E_A(T_{REF})}{2.303RT_{REF}} \qquad [2.12]$$

Thus, a network with lower crosslink density and reduced segmental constraints will exhibit lower values of slope and fragility index m, and hence a lower activation energy. This behavior is suggestive of a more open, less restricted network and indicates a decrease in the temperature sensitivity of segmental relaxation due to a reduction in the intermolecular cooperativity.

Numerous investigators have employed several complementary experimental techniques in conjunction with empirical models to characterize relaxation behavior in crosslinked polymeric networks. Litvinov and Dias,[24] for example, have investigated copolymer networks of UV cured poly(ethylene glycol) diacrylate [PEGDA] crosslinker with 2-ethylhexyl acrylate [HEA] using dynamic mechanical analysis and NMR techniques. The network structure and crosslink density were altered by varying the amount of HEA monomer, thus changing the fraction of pendant or dangling chains in the corresponding network. Mechanical and NMR testing showed an increase in the molar mass between crosslinks (M_c) accompanied by a drop in T_g, indicating the formation of a more open, less-constrained network with increasing HEA content. Similar dynamic mechanical studies have been performed by Alves *et al.*[25] on networks prepared by copolymerizing poly(methyl methacrylate) [PMMA] with different amounts of the crosslinker, ethylene glycol dimethacrylate [EGDMA]. Increases in crosslink density were manifested by a positive offset in T_g of ~ 20°C over the range of samples studied, with a corresponding shift in the glass-rubber (α) relaxation to longer times. The modulus data were analyzed using the KWW equation, and indicated an increase in the breadth of the glass-rubber relaxation as reflected in decreasing values of the β_{KWW} parameter. The fragility concept was applied to assess the temperature dependence of the characteristic relaxation times for the different samples. The fragility index (*m*) increased with increasing crosslinker content suggesting a stronger non-Arrhenius behavior at higher crosslink densities. The sub-glass (β) relaxation characteristics, however, were found to be independent of crosslink density. This reflects a minimal influence of crosslinker content at the small length scales of non-cooperative motion.

Kannurpatti *et al.*[26-28] have investigated the preparation of ideal crosslinked networks via the use of living radical polymerizations that eliminate the trapping of radicals in the emerging network. As such, the networks remain chemically inert on further increase of temperature. This offers the possibility of preparing networks with widely varying crosslink density that remain fully stable during the course of thermal analysis. Dynamic mechanical studies on copolymers of poly(ethylene glycol) dimethacrylate [PEGDMA] and diethylene glycol dimethacrylate [DEGDMA] reveal an increase in the heterogeneity of the polymer matrix upon inclusion of increasing amounts of the shorter, less flexible DEGDMA monomer into the network. The T_g was found to increase linearly with crosslink density along with a decrease in the β_{KWW} value. Networks were also prepared by copolymerizing the above dimethacrylates with monomers such as n-octyl methacrylate [OcMA] and n-heptyl acrylate [HepA]. From a stoichiometric standpoint, DEGDMA copolymer networks should be more highly crosslinked as compared to the flexible PEGDMA networks. However, counter-intuitively, the molecular weight between crosslinks (M_c) for DEGDMA was found to be higher than in the PEGDMA networks. This suggested the extensive formation of loops in crosslinked DEGDMA through cyclization, leading to higher apparent values of M_c as reflected in the rubbery modulus. Thus, the length of the crosslinker agent was found to be strongly influential in the resulting relaxation behavior of the network. Dielectric analysis carried out on these networks revealed a secondary, local (β) transition at higher frequencies and shorter relaxation times. The intensity of the β peak was found to correlate with the number of unreacted double bonds in the network; at higher cure times, lower β relaxation intensity was measured. At the same time, higher extents of conversion led to broadening of the glass-rubber (α) relaxation, which shifted to longer relaxation times.

Roland and co-workers[29,30] have performed relaxation studies on various crosslinked polymer networks including poly(vinylethylene) [PVE] and poly(dimethylsiloxane) [PDMS]. Dielectric analysis revealed segmental relaxation characteristics similar to the networks described above, with positive offsets in T_g, increased fragility and relaxation broadening observed with increasing crosslink density. In the case of the PVE networks, it was possible to distinguish the effect of crosslinking on intermolecular cooperativity as opposed to variations in local friction. It was shown that the uncorrelated segmental relaxation time (as determined by the Hall-Helfand equation[45]), which signifies intramolecular correlations, showed only a modest increase with increase in crosslink density as compared to the relaxation time given by the KWW expression. This reflected the dominant influence of intermolecular coupling on the relaxation characteristics of the networks in comparison to the effect of local friction. In studies on the PDMS system, a significant increase was observed in T_g and fragility when M_c approached a value comparable to the segmental relaxation length scale.

A number of other investigators have examined the dielectric relaxation characteristics of model crosslinked polymer networks with well-controlled architectures. Glatz-Reichenbach *et al.*[31] studied styrene-butyl-acrylate [SB] divinylbenzene [DVB] copolymers, for example, while Yu Kramarenko *et al.*[32] prepared model heterocyclic polymer networks via simultaneous trimerization of 1,6-hexamethylene diisocyanate [HMDI] and hexyl isocyanate [HI]. Fitz and Mijovic[33] used poly(methylphenylsiloxane) [PMPS] chains with reactive end groups in order to control the distance between crosslinks, and measured the effective cooperativity length for these networks. Analysis of the dielectric relaxation spectra in the above studies was accomplished by fitting the relaxation data to the Havriliak-Negami (HN) function. The shape of the dielectric loss curves can be characterized by scaling the HN parameters (a and b) using a model proposed by Schöhnals and Schlosser.[46] The scaling parameters of the model are given by $m=a$ and $n=a\bullet b$. m is sensitive to the low frequency side of the spectrum and reflects large scale cooperative motions. n, on the other hand, encompasses the high frequency limit and the corresponding small scale, local motions. Both m and n can be studied with variation in temperature and crosslink density to gauge the relaxation behavior. In the copolymers studied by Glatz-Reichenbach and Yu Kramarenko, *m* decreased with crosslink density while *n* remained invariant. This suggests that the local environments in the network are not influenced by changes in the crosslinker content. Fragility studies can be coupled with shape parameter analysis to establish the length scale of cooperative relaxation. In the PMPS networks examined by Fitz and Mijovic, invariance in the fragility index and relaxation shape across the range of samples studied indicated that the cooperative length of the relaxing segments was less than the distance between crosslinks for their particular series of networks.

The strategic formulation of crosslinked networks, and the characterization of static and dynamic properties is crucial for the intelligent design of membrane materials with desired performance attributes. The molecular relaxation of poly(ethylene glycol) based networks, and their relation to gas separation performance, are detailed in Chapter 4 (dynamic mechanical studies) and Chapter 5 (dielectric measurements).

2.4 TRANSPORT AND CHAIN DYNAMICS IN NANOCOMPOSITE MATERIALS

Over the last decade, polymer nanocomposites have proven to be promising membrane materials for selective gas separations.[47] However, the large polymer-particle surface area generated by the nanosized filler particles often results in significant modifications to the thermomechanical properties of the polymer matrix, modifications that can have a strong influence on the separation properties of the composite.[48-50] The establishment of a fundamental understanding of the morphology and dynamics of nanocomposites and their relationship to gas separation is an important step in optimizing performance. This section examines the transport behavior of nanoparticle-filled polymer systems and considers the extent to which the presence of nanoscale filler affects the dynamics associated with polymer chain motion, and the resulting gas separation properties of the polymer matrix.

Impermeable filler particles dispersed in a polymer film act as impediments to the molecules diffusing through the matrix. The penetrant molecules have to follow a more tortuous diffusion path and hence cover a longer distance to pass through the film. Also, the overall permeability suffers since the total area available for permeation decreases. If τ is the tortuosity factor and ϕ is the volume fraction, then the effective diffusivity and permeability are given by:[51]

$$D_{eff} = \frac{D_p}{\tau} \qquad [2.13]$$

$$P_{eff} = \frac{\phi_p P_p}{\tau} \qquad [2.14]$$

where subscripts *eff* and *p* denote the filled and pure polymer phases, respectively. The tortuosity factor τ accounts for the additional distance traversed by the molecules in a tortuous path and has been defined by several theoretical expressions incorporating particle shape, orientation and interaction with the matrix. Maxwell provides a simple expression for the definition of τ:[52]

$$\tau = 1 + \frac{\phi_f}{2} \qquad [2.15]$$

where ϕ_f is the volume fraction of the filler particles. Thus, from equations 2.14 and 2.15, the effective permeability for a two-phase system comprised of a continuous polymer phase and a dispersed filler particle phase is given by:

$$\frac{P_{eff}}{P_p} = \frac{1 - \phi_f}{1 + \frac{\phi_f}{2}} \qquad [2.16]$$

For non-porous filler with negligible sorption of the penetrant molecules, the permeability decreases with increasing filler content and the corresponding increase in τ. For this binary system, the solubility is given by:

$$S = \phi_p S_p \qquad [2.17]$$

where S_p is the solubility of the pure polymer phase. In the event of sorption by the filler particles, the solubility equation is expanded as follows:[53]

$$S = \phi_p S_p + (1-\phi_p) S_f \qquad [2.18]$$

where S_p and S_f are the penetrant solubilities in the polymer phase and the filler phase, respectively.

The transport behavior described above is true for larger filler particles, typically of size greater than 100 nm. However, a contradictory effect is observed upon dispersion of particles of a smaller sizescale. In fact, nanoscale particles can interact chemically or physically with the surrounding polymer matrix, thereby modifying the chain dynamics and the corresponding transport characteristics. Studies by Merkel *et al.* have demonstrated this behavior where significant permeability enhancement was observed when nanoparticles were dispersed into rigid, glassy polymer membranes.[47,54,55] Methane permeability was found to increase by more than 300% upon addition of 25 vol% of 13 nm fumed silica particles in poly(4-methyl-2-pentyne) [PMP], a rigid polyacetylene. The permeability increase can be attributed to disruption in the rigid chain packing, thus enhancing the free volume available for penetrant transport. Recently, Matteucci and coworkers[56] have observed improved permeation rates in rubbery polymer systems. Inclusion of ~ 30 vol% of spherical MgO nanoparticles (nominal diameter: 2.5nm, specific surface area: 640 m^2/g) in 1,2 polybutadiene was found to enhance CO_2 permeability by more than an order of magnitude, with significant improvement in CO_2/light gas selectivity as compared to the unfilled polymer.

In a nanocomposite matrix, the particle-polymer interactions, as well as physical confinement effects, can have tremendous influence on the polymer chain mobility. Consequently, the restriction of chain motion can alter the thermomechanical properties of the polymer.[48-50] Previous studies have shown that inclusion of inorganic particles like carbon black or silica can significantly increase the glass transition temperature of the matrix.[57] In certain systems, reports have indicated the emergence of a second, higher T_g reflecting a more constrained population of polymer chain segments in the vicinity of the particle surface.[58-62] Early studies by Yim *et al.* reported a dual T_g behavior on inclusion of silica particles (specific surface area: 200 m^2/g) in polymers such as poly(dimethyl siloxane) [PDMS], polystyrene [PS] and poly(ethylene glycol) [PEG].[58] Similar results have also been reported on inclusion of silica particles into acrylic polymers like poly(acrylic acid) and poly(methyl acrylate).[59] Interestingly, experiments conducted by Tsagaropoulos[60,61] with varying silica particle size (nominal diameters of 7 nm and 44 μm, respectively) revealed the existence of a higher offset T_g only for the nanosized particles, the extent of influence of the inorganic particles on the polymer matrix correlating with their effective surface area. Conversely, studies have shown a negative offset in T_g for systems in which the polymer does not completely wet the particles. Arrighi *et al.*[62] indicated a drop in T_g for styrene-butadiene rubber [SBR] filled with modified hydrophobic silica particles (specific surface area: ~ 160 m^2/g) while Ash *et al.*[50] reported a reduction of ~ 25°C in T_g upon dispersion of alumina particles (nominal diameter: 38 nm, specific surface area: 44 m^2/g) in poly (methyl methacrylate) [PMMA].

A recent review article by Torkelson[63] discusses work undertaken to understand the variation in T_g in ultra-thin polymer films. T_g was found to strongly decrease with decreasing film thickness for a free surface film or films coated on neutral or repulsive substrates (film thicknesses below ~ 100 nm). On the contrary, for thin films applied on a substrate with favorable polymer-substrate interaction, T_g was observed to increase with decreasing film thickness. For the rubbery nanocomposites studied here, the average interparticle distance may be on the order of 10 nm, resulting in a significant influence of nanocofinement on polymer chain mobility. The sensitive nature of polymer-substrate interactions at the nanoscale and their corresponding influence on gas transport properties makes the study of nanocomposite morphology and dynamics important in glassy systems, and in filled rubbery polymer networks; see Section 4.3.3.

2.5 SEMICRYSTALLINE MORPHOLOGY OF LOW CRYSTALLINITY POLYMERS

"Low crystallinity" polymers is a broad term used for polymers with a semiflexible backbone structure and a bulk crystallinity level of usually less than 50%.[64] Poly(trimethylene terephthalate) [PTT], a low crystallinity thermoplastic, exhibits unique stress-recovery characteristics that has led to its growing use in the fibers and apparel industry. It is speculated that the "kinked" structure possessed by PTT is largely responsible for its distinctive mechanical performance (see **Figure 2.7**). A broad understanding of the thermomechanical properties of PTT can be achieved by investigating the dynamic mechanical and dielectric relaxation behavior of specimens prepared with varying thermal histories. Of particular interest is the relationship between the crystalline morphology and thermomechanical behavior; *e.g.*, the characteristics of the glass-rubber relaxation, as compared to similar semiflexible low crystallinity polymers.

Low crystallinity polymers typically exhibit slow crystallization kinetics that make it possible to capture them in a wholly amorphous state. This provides an opportunity to generate a wide range of crystalline morphologies with controlled processing history, and to contrast the thermomechanical properties of these materials with the quenched, amorphous glass. The semicrystalline morphology of such polymers will be examined in this section by reviewing the relaxation characteristics of two widely-studied low crystallinity polymers that possess a relatively rigid, linear backbone structure: poly(ethylene terephthalate) [PET] and poly(ether ether ketone) [PEEK]. The properties of these polymers will be further assessed by considering the influence of "kinks" incorporated within the backbone structure via copolymerization. Copolymers to be discussed include (low crystallinity) poly(ether ketone ketone) [PEKK] and meta-phenylene modified poly(phenylene sulfide) [PPS]. The molecular structures of the polymers of interest are shown in **Figure 2.8**.

In many ways, the crystallization and morphology of PET and PEEK are similar, owing to their relatively rigid, straight-chain or para-connected aromatic backbone structure. The relaxation behavior of PET has been established through a large number of dynamic mechanical and dielectric studies.[46,64-75] Typical to low crystallinity polymers, PET displays two motional transitions: a short range, non-cooperative sub-glass (β) relaxation and a long range, cooperative glass-rubber (α) relaxation. While the β relaxation remains largely unaffected by the presence of crystallinity, the α relaxation is altered by the spatial constraints imposed by the crystal regions on the relaxing amorphous segments.

The presence of crystallinity leads to a broadening of the glass-rubber relaxation and a positive offset of ~ 10-25°C in T_g as compared to a wholly amorphous sample, mainly due to the development of a constrained relaxation environment. The observed positive offset in the relaxation temperature varies with the thermal history; *e.g.*, cold crystallization temperature. Small angle X-ray scattering (SAXS) studies by Dobbertin *et al.* have shown an inverse relation between the relaxation temperature and the amorphous interlayer thickness of the PET crystals.[74] With increasing cold crystallization temperature the crystal lamellae were found to be thicker, leading to less segmental constraint and a somewhat lower value of T_g.

The relaxation characteristics of PEEK have been examined extensively using dielectric, dynamic mechanical and calorimetric methods, [76-85] and display a behavior very similar to that of PET. Again, the glass-rubber relaxation properties were found to be strongly influenced by the constraints imposed by the crystal layer, with T_g offset to higher temperatures in the crystallized samples as compared to the quenched glass. For PEEK, samples prepared using solvent crystallization and thermal crystallization were compared on the basis of their dynamic mechanical glass transition temperature, T_α. The offset in T_α for solvent crystallized samples was ~ 10-15°C higher than that observed for the thermally crystallized samples, emphasizing the sensitivity of T_g to variations in the semicrystalline morphology. SAXS studies[80,84] have revealed the existence of a thinner amorphous interlayer and correspondingly tighter morphology in the solvent crystallized samples, leading to the observed increase in T_α.

A distinctive behavior seen in PET and PEEK is that of a disproportionate decrease in the glass-rubber relaxation intensity upon crystallization. When a polymer crystallizes, some portion of chain segments are incorporated into the three-dimensional crystal structure and remain immobile at temperatures below the melting temperature (T_m). The fraction of such segments, which fail to contribute to the relaxation intensity, can be determined by a number of methods, such as calorimetry or X-ray diffraction. However, in the case of low crystallinity polymers like PET and PEEK, the observed decrease in intensity is substantially lower than the fraction of polymer chain segments immobilized within the crystalline phase. This behavior has been attributed to the existence of a third phase, known as the "rigid amorphous phase (RAP)" (see **Figure 2.9**), which consists of non-crystalline material that remains immobile at the glass transition and which has been shown to relax gradually between T_g and T_m.[69,71,85] Calorimetric studies on PET[74] and PEEK[76,85] have indicated the presence of a RAP fraction in the range of 0.2-0.4 for various sample processing histories; the highest amount of RAP is observed for the lowest cold crystallization temperatures, which correspond to the most restrictive crystallization conditions. Higher cold crystallization temperatures or less restrictive crystallization conditions (*e.g.*, slow cooling from the melt) allow for greater chain mobility during crystallization, thereby decreasing the RAP fraction. However, for PET and PEEK, a finite amount of RAP fraction was found to remain even at the least restrictive crystallization conditions.

Variation in the backbone structure of these relatively rigid, semiflexible polymers can lead to the development of a strikingly different relaxation behavior. Features observed in PET and PEEK (*i.e.*, large offset in T_g for crystallized samples and the presence of a significant RAP fraction) are dramatically reduced by the random copolymerization of up to ~ 10 mol% of 1,3 meta-phenylene linkages into the polymer backbone. This trend is observed in the case of poly(ether ketone ketone) [PEKK] copolymers and modified poly(phenylene sulfide) [PPS] (see Figure 2.8). Studies on PEKK[86,87] and PPS[88-90] reveal a lower offset in T_g for the crystallized copolymer samples as compared to their wholly amorphous counterparts, with the degree of offset varying inversely with the fraction of random kinks (meta content) in the copolymer backbone. In fact, PEKK and PPS samples prepared under the least restrictive crystallization conditions, (*i.e.*, high cold crystallization temperatures or slow cooling from melt) exhibit T_g values equivalent to that of a completely amorphous sample, despite the presence of ~ 30 wt% crystallinity.

A second distinctive aspect of the "kinked" copolymer morphology is the progressive and complete mobilization of the rigid amorphous phase with varying copolymer composition and thermal history. Less restrictive crystallization conditions and/or higher meta phenylene content led to a sharp reduction in the RAP fraction. Dielectric studies on

PEKK[87] and PPS[89] copolymers have shown the mobile amorphous fraction reaching a value of 0.65-0.70, indicating nearly full mobilization of the non-crystalline material. It appears that the segregation of meta linkages at the crystal-amorphous interface results in a disruption of the constraining influence that the crystalline segments impose on the interlamellar amorphous chains, thereby accounting for greater chain mobility across the glass transition and a corresponding minimization of the RAP phenomenon.

PTT possesses a similar kinked backbone. However, PTT has a regular kinked structure, as opposed to the random structures evident in the PEKK and PPS copolymers. It is of interest to study the crystalline morphology in PTT in terms of its influence on T_g, the overall RAP fraction, and RAP mobilization as a function of sample preparation history. A complete experimental study of the relaxation characteristics of PTT, as related to crystalline morphology, is presented in Chapter 6.

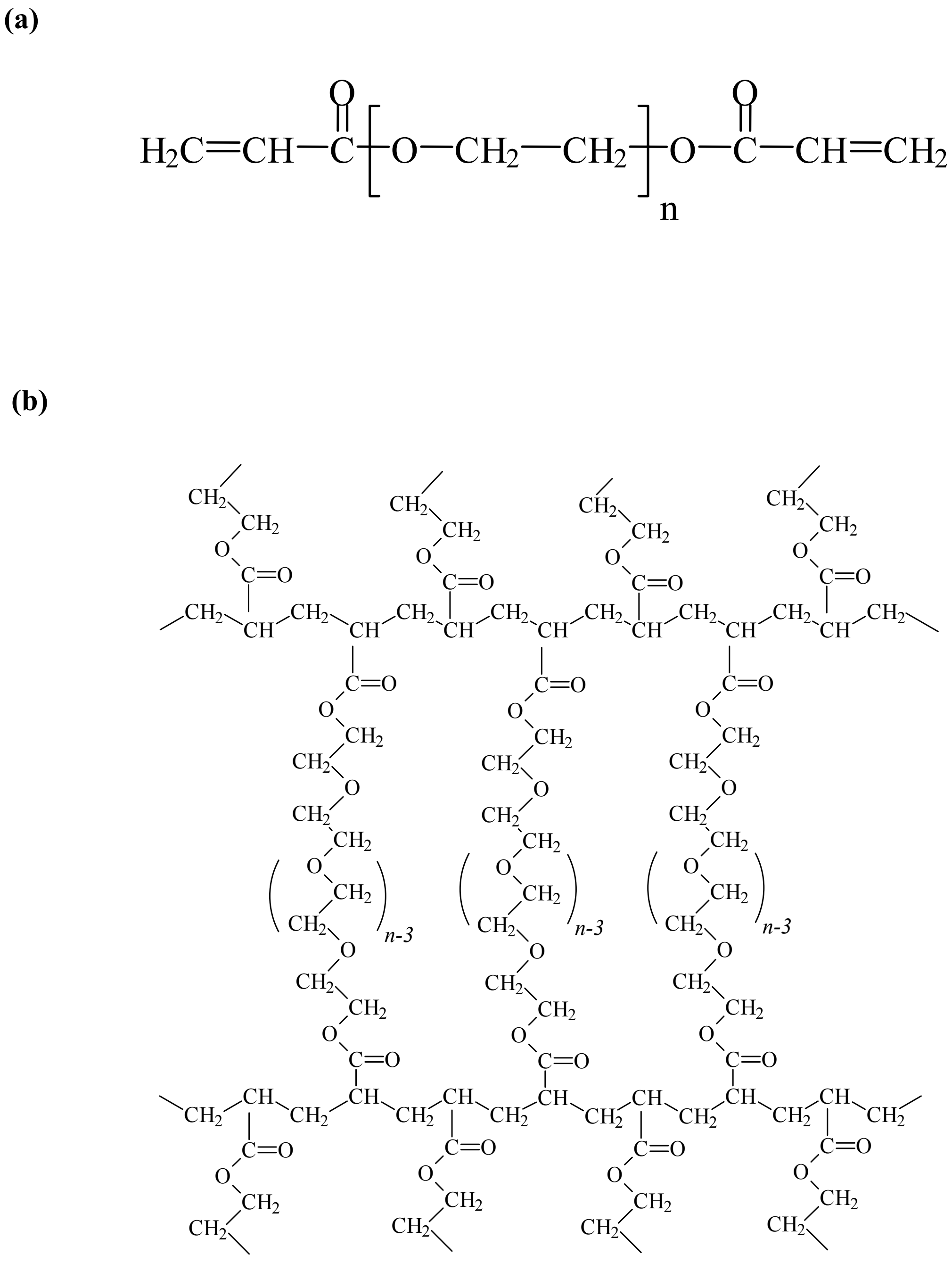

$$H_2C{=}CH-\overset{O}{\overset{\|}{C}}-\left[O-CH_2-CH_2\right]_n-O-\overset{O}{\overset{\|}{C}}-CH{=}CH_2$$

Figure 2.1: (a) Chemical structure of poly(ethylene glycol) diacrylate [PEGDA]; (b) Schematic of idealized crosslinked network for 100% PEGDA.

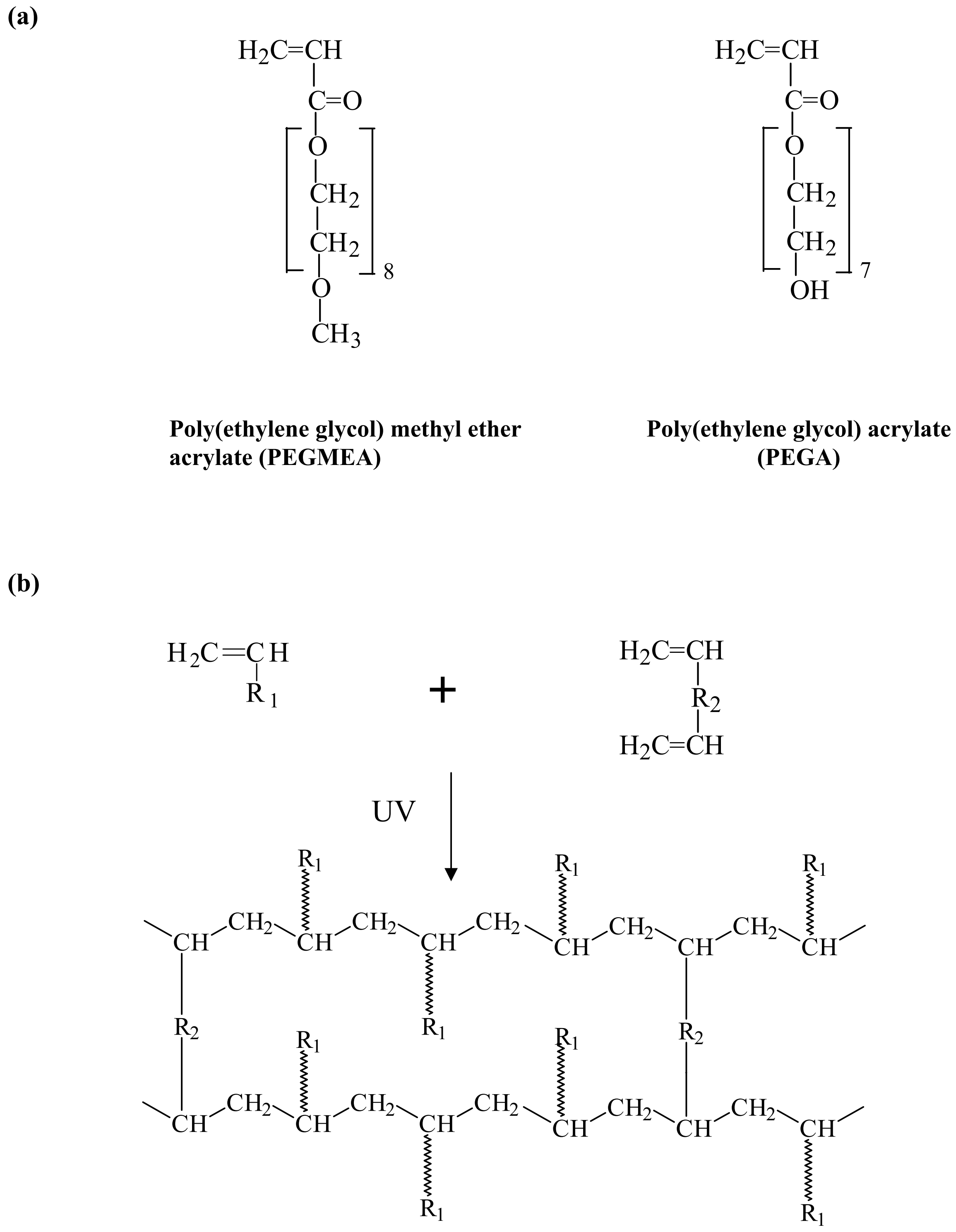
(a)
H2C=CH
C=O
O
CH2
CH2
8
O
CH3
H2C=CH
C=O
O
CH2
CH2
7
OH
Poly(ethylene glycol) methyl ether acrylate (PEGMEA)
Poly(ethylene glycol) acrylate (PEGA)
(b)
H2C=CH
R1
+
H2C=CH
R2
H2C=CH
UV
R1
CH
CH2
R2

Figure 2.2: (a) Chemical structures of acrylate monomers; (b) Formation of crosslinked copolymer network.

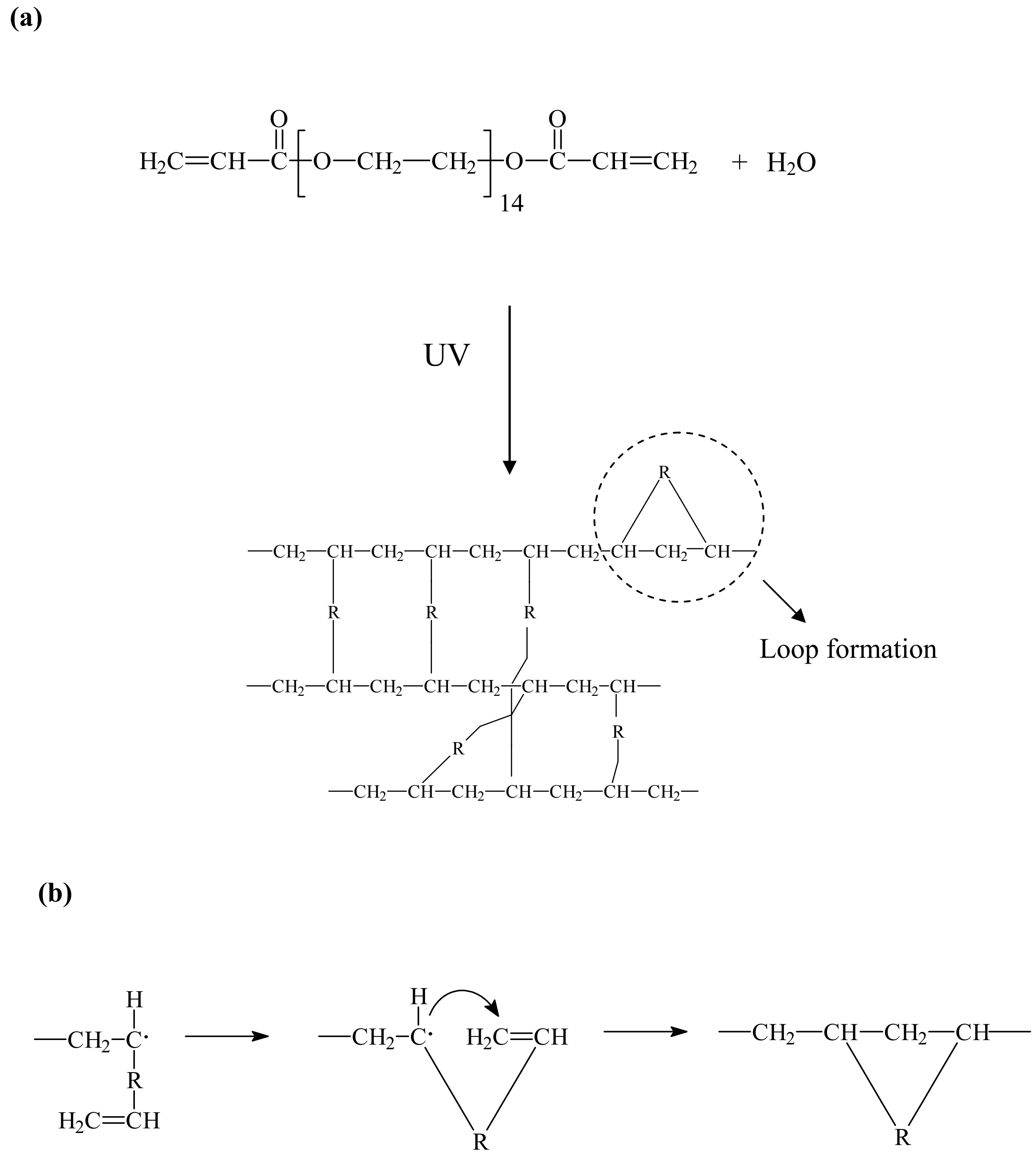
(a)
O
O
14
+ H₂O
UV
Loop formation
R
(b)
H
R
H₂C=CH

Figure 2.3: (a) Schematic of PEGDA-water crosslinked network; (b) Formation of loops or “wasted” crosslinks in PEGDA-water networks.

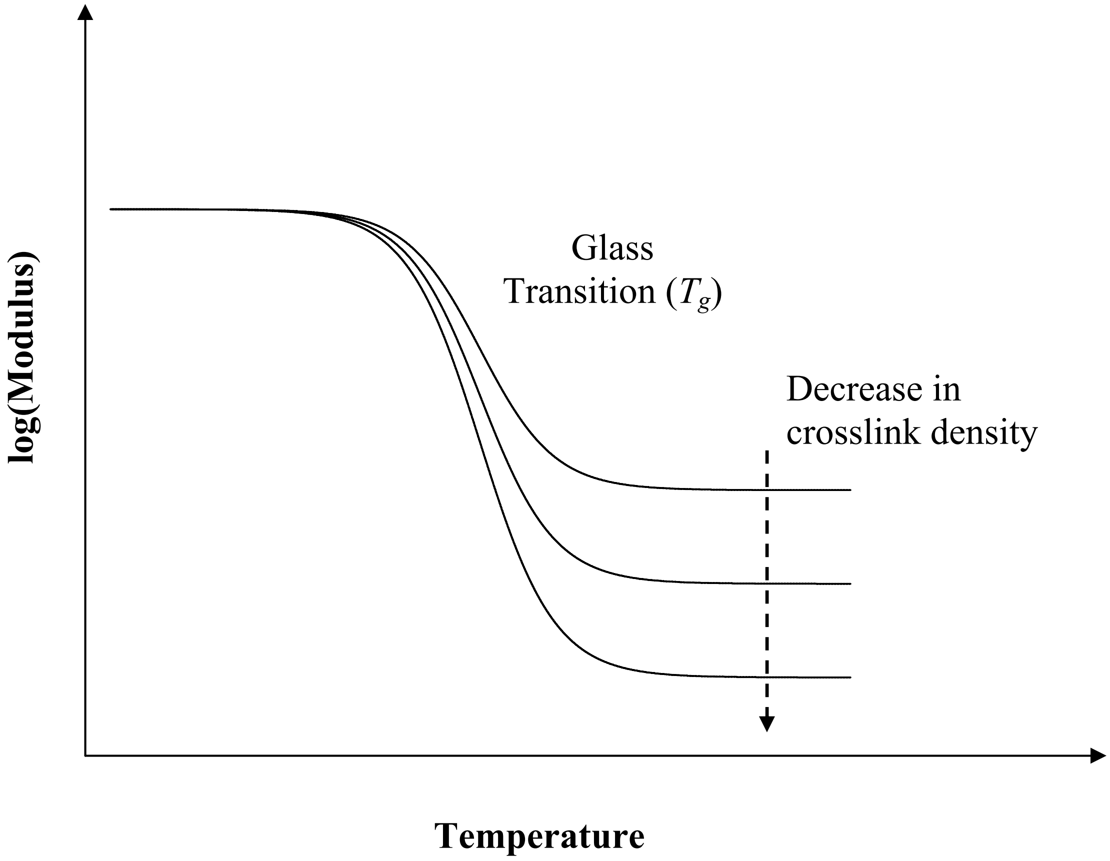

Figure 2.4: Schematic showing the typical modulus behavior for crosslinked networks with decreasing crosslink density.

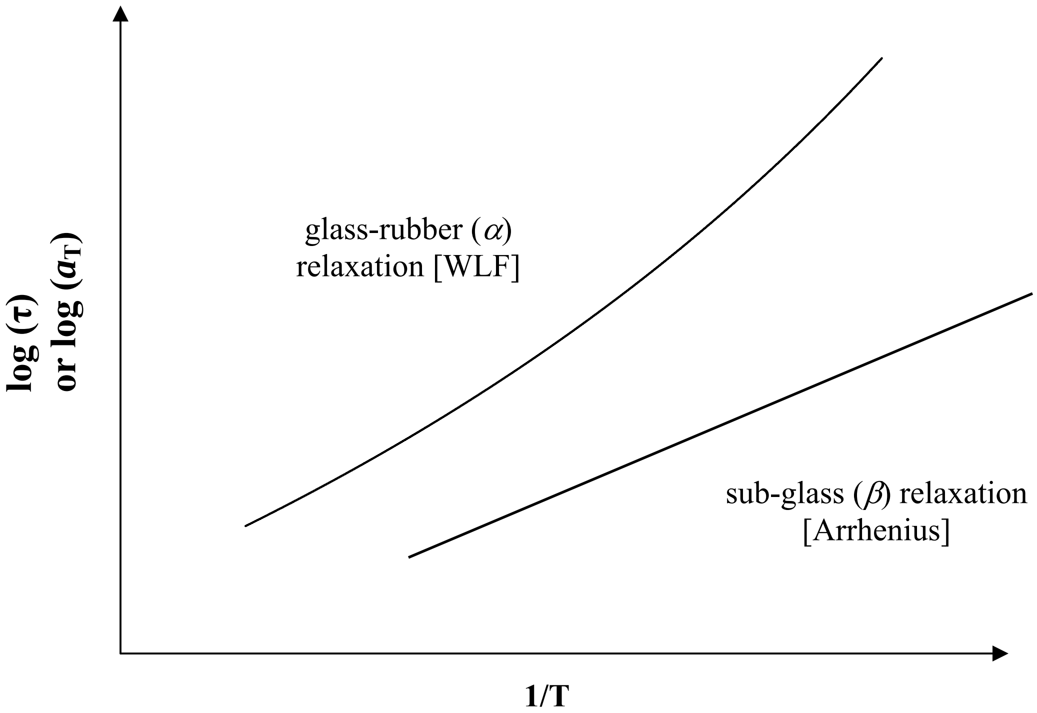

Figure 2.5: Arrhenius plot (log(τ) or log(a_T) versus 1/T) showing the temperature dependence of the sub-glass and glass-rubber relaxation processes in polymer networks.

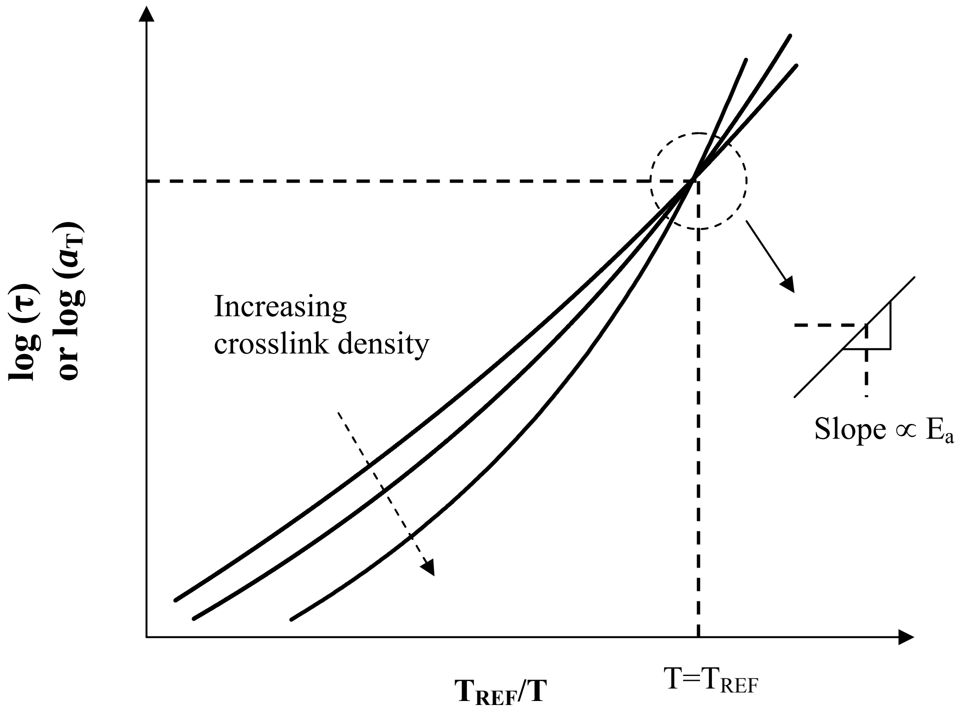
log (τ) or log (a_T)
Increasing crosslink density
Slope ∝ E_a
T_{REF}/T
$T=T_{REF}$

Figure 2.6: Schematic of the Fragility or Cooperativity plot (log(τ) or log(a_T) versus T_{REF}/T) showing the temperature sensitivity of the glass-rubber relaxation process as a function of crosslink density.

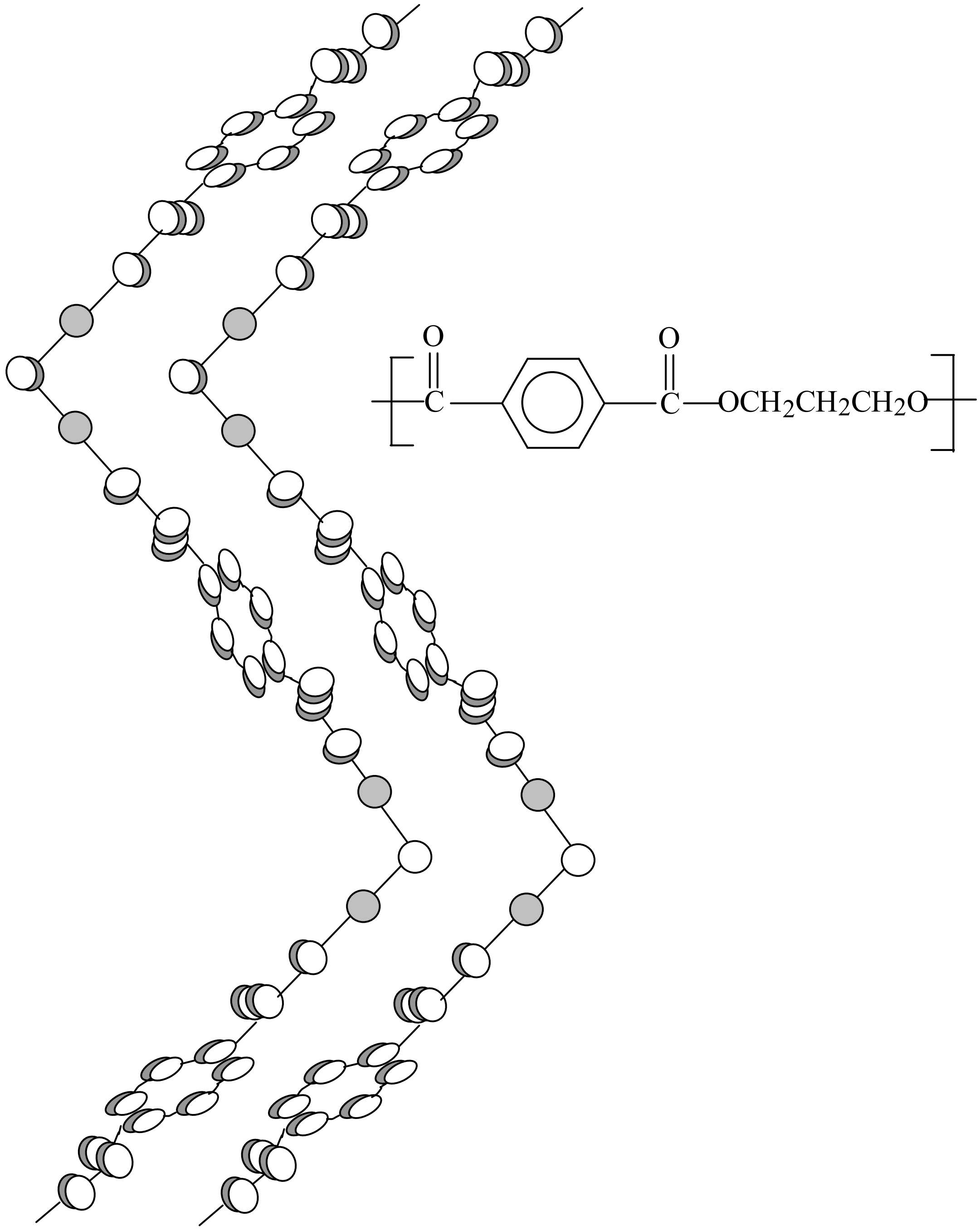

Figure 2.7: Kinked molecular conformation$^+$ and repeat unit structure of PTT. ($^+$ - Adapted from: http://www.swicofil.com/ptt.html)

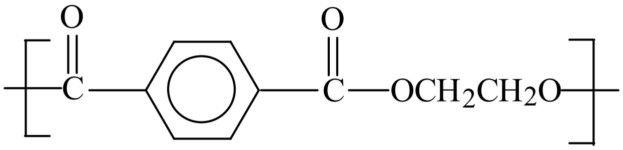

Poly(ethylene terephthalate) [PET]

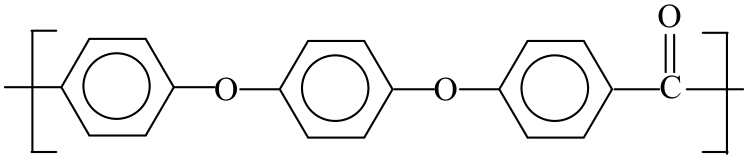

Poly(ether ether ketone) [PEEK]

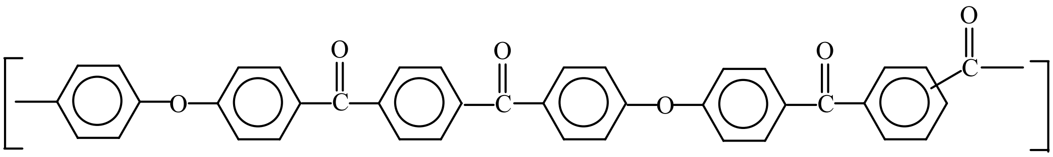

Poly(ether ketone ketone) [PEKK]

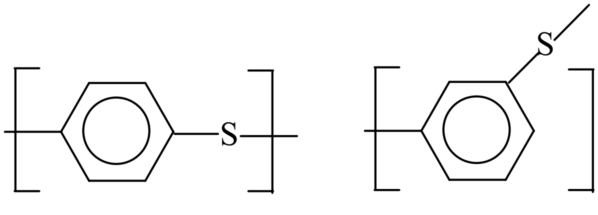

Poly(phenylene sulfide) copolymer [PPS]

Figure 2.8: Repeat unit structures of selected low crystallinity polymers.

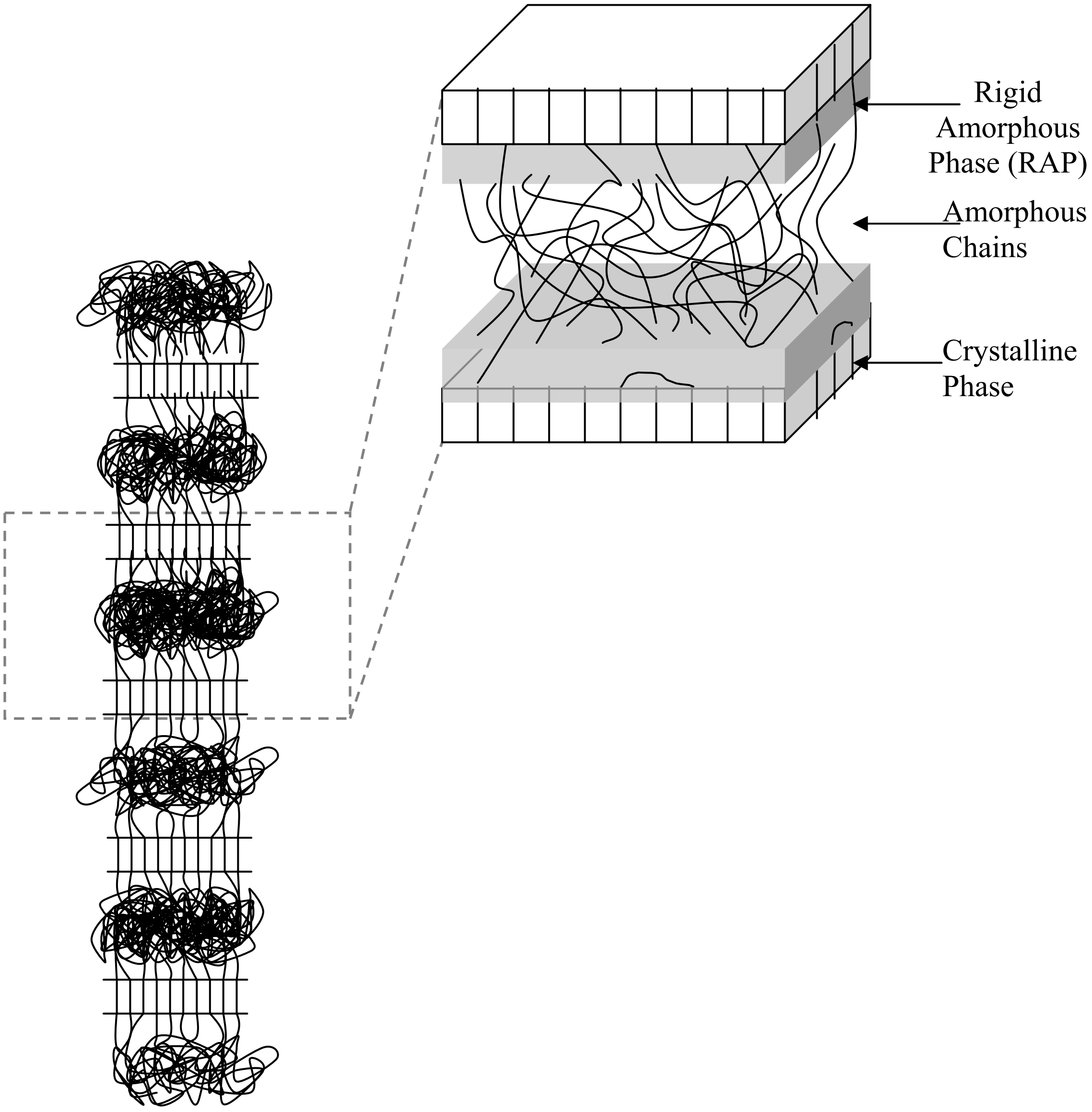
Rigid Amorphous Phase (RAP)
Amorphous Chains
Crystalline Phase

Figure 2.9: Schematic showing the rigid amorphous phase in semicrystalline PTT.

Copyright © Sumod Kalakkunnath 2007

Chapter Three

Experimental Methods

The primary objective of this work is the fundamental characterization of molecular architecture, chain dynamics and phase behavior in semicrystalline polymers and membranes as a function of composition, synthesis and processing history. Thermal analysis techniques will be employed to elucidate the structure-property relationships for two types of materials: (i) polyethylene glycol (PEG) – based rubbery networks for use in gas separation membranes, and (ii) poly(trimethylene terephthalate) (PTT), a semicrystalline thermoplastic which is a recent addition to the family of commercial aromatic polyesters.

3.1 MATERIALS

The focus of studies undertaken in this work is the characterization of rubbery copolymer membranes strategically formulated from liquid monomers to achieve high solubility selectivity for larger, polar or quadrupolar gas molecules over small, non polar gases. These are typically highly crosslinked networks prepared via UV photopolymerization of polyethylene oxide (PEO) based diacrylates, which act as the crosslinker, and PEO-based acrylates, which introduce side-chains into the networks. The inclusion of branch groups via reaction with monofunctional acrylates alters the crosslink density and the fractional free volume of the network, and thereby influences the gas permeation properties. **Figures 3.1** and **3.2** show the chemical structures of the monomers used for this work; all monomers were obtained from Sigma-Aldrich (Milwaukee, WI). Proton nuclear magnetic resonance (^{1}H NMR) and fast atom bombardment mass spectrometry (FAB-MS) were performed at the University of Texas at Austin to confirm the molecular weight and polydispersity index of the monomers.

The second material under investigation is a semicrystalline thermoplastic, poly(trimethylene terephthalate) (PTT). PTT, a member of the terephthalate polyester family, shows properties intermediate to its commercial predecessors; polyethylene terephthalate (PET) and polybutylene terephthalate (PBT). The chemical structure of PTT is shown in Figure 2.7. Due to its distinctive, kinked molecular structure PTT finds varied commercial applications ranging from textile and carpet fibers to structural materials.[91] Quenched PTT has a glass transition temperature (T_g) of around 42°C with an equilibrium melting temperature of ~ 237°C.[92] For experimental purposes, PTT resin was obtained in pellet form through the courtesy of Shell Chemical Company, Houston, TX (CORTERRA^{TM} PTT 200, intrinsic viscosity: 0.921 dl/g).

3.2 DYNAMIC MECHANICAL ANALYSIS (DMA)

3.2.1 Basic theory

Polymers typically show a viscoelastic response to an externally applied load; *i.e.*, their response behavior is intermediate between that of an elastic solid and a viscous liquid. At low temperatures and high rates of strain, polymers typically behave as an elastic solid and follow Hooke's law, where stress is proportional to strain and independent of the rate of loading:

$$\sigma = Ee \qquad [3.1]$$

On the other hand, at high temperatures and low rates of strain, polymers tend to follow Newton's law for a purely viscous liquid, where stress is proportional to the rate of strain and independent of strain:

$$\sigma = \eta \frac{de}{dt} \qquad [3.2]$$

At low strains, deformation in polymers is reversible but time and temperature dependent. Thus, DMA can be used as a tool to investigate the dynamic mechanical properties of the polymer as it involves the measurement of stress response to a periodic strain as a function of the experimental time scale (*i.e.*, the frequency of perturbation), with simultaneous variation in temperature.

In a typical dynamic mechanical experiment, an oscillating sinusoidal stress is applied and the resulting strain is measured. For a viscoelastic material, the strain response lags the applied sinusoidal stress by a phase angle δ, or similarly the stress leads the strain by a phase angle δ. This can be expressed in complex notation as:

$$\sigma(t) = \sigma_0 \exp i(\omega t + \delta) \qquad [3.3]$$

$$e(t) = e_0 \exp(i\omega t) \qquad [3.4]$$

Since modulus is defined as stress/strain, the complex modulus (E^*) can be written as:

$$E^* = \frac{\sigma(t)}{e(t)} = \frac{\sigma_0}{e_0}\exp(i\delta) = \frac{\sigma_0}{e_0}(\cos\delta + i\sin\delta) \qquad [3.5(a)]$$

$$E^* = \left(\frac{\sigma_0}{e_0}\cos\delta\right) + i\left(\frac{\sigma_0}{e_0}\sin\delta\right) = E_1 + iE_2 \qquad [3.5(b)]$$

and

$$\tan\delta = \frac{E_2}{E_1} \qquad [3.5(c)]$$

where E_1 represents the in-phase elastic component of the complex modulus or the fully recoverable energy stored per cycle and is termed the storage modulus; E_2 is the loss modulus, *i.e.*, the out-of-phase viscous component quantifying the viscous dissipation or the loss of energy; *tan δ* is the loss factor and is defined as the ratio of the loss modulus to the storage modulus.

3.2.2 Time-temperature superposition

An experimental limitation of dynamic mechanical analysis is the relatively narrow range of experimentally-accessible frequencies (~ 10^{-2} to 10^{2} Hz). This is overcome by elucidation of the complete modulus-frequency behavior using the principle of time-temperature interdependence, *i.e.*, by capturing the full relaxation behavior of a material at a single reference temperature.[38] This method is based on the expectation that the viscoelastic behavior of a polymer at a particular temperature can be correlated to its response at a different temperature by a simple shift in the experimental timescale (see **Figure 3.3**).[93] The experimental modulus or loss data are superimposed relative to a single reference temperature via the introduction of a horizontal offset, also known as the shift factor (a_T), to generate a master curve in the frequency domain as shown in **Figure 3.4**. This broadens the range of effective frequencies over which the sample can be analyzed. Typically, the reference temperature (T_{REF}) is chosen close to the glass transition temperature. The master curve plot then has a horizontal axis given by:

$$\log(\omega_{MC}) = \log(\omega_{\exp}) + \log(a_T) = \log(\omega_{\exp} a_T) \qquad [3.6]$$

3.2.3 Relaxation time and distribution parameter

The relaxation of a polymeric material across the glass transition can often be described by a "stretched" form of the exponential decay model, also known as the Kohlrausch-Williams-Watts (KWW) model, in order to encompass the wide range of relaxation time-distribution:

$$\phi(t) = \exp[-(t/\tau_0)^{\beta}] \qquad [2.9]$$

This asymmetric model is based on the assumption that the relaxation function $\phi(t)$ is influenced solely by intermolecular coupling amongst relaxing polymer chain segments. It contains two parameters, a single central relaxation time constant (τ_0) and a distribution parameter (β). β varies with the strength of interaction, thus mapping the influence of the intermolecular coupling to the segmental relaxation. Values of β range from 0 to 1, with lower values of β indicating a more heterogeneous or constrained environment for segmental motion.[29]

Upon completion of the time-temperature superposition, the experimental data obtained are compared with a library of normalized curves generated using series solutions reported by Williams.[39] **Figure 3.5** shows a series of such curves obtained via the KWW reported by Williams.[39] **Figure 3.5** shows a series of such curves obtained via the KWW function for varying values of β. With increasing β, a more narrow and correspondingly homogenous relaxation is obtained.

3.2.4 Experimental configuration and procedure

Dynamic mechanical analysis is a versatile technique for probing a broad spectrum of molecular motions in polymeric materials. Measurements in dynamic mechanical experiments can be based on two methodologies, either by decay of free vibration or by employing a forced vibration. Typically, polymeric materials are analyzed using a forced vibration technique which allows for dynamic excitation over a range of frequencies without a change in sample dimensions.[94] Forced vibration testing encompasses two deformation geometries: the tensile and bending modes.

In tensile mode, the sample is mounted such that the linear force is applied along the length of the sample. This method is particularly useful for materials that may relax with temperature, *e.g.*, films and fibers. The alternative is the bending mode in which the sample, usually a rectangular bar, is clamped rigidly at the two ends (dual cantilever mode) with a sinusoidal force applied at its central point, or fixed at one end with the other end free to vibrate (single cantilever mode). The bending mode is typically the most versatile and can be used for a wide variety of materials. In particular, the single cantilever geometry is preferred for high temperature measurements and samples that tend to undergo large changes in dimensions during the experiment.

Figure 3.6 shows a schematic of the configuration for the Polymer Laboratories Dynamic Mechanical Thermal Analyzer (DMTA). The sample is mounted inside the test head; the environment inside the test chamber is controlled by heating coils that run spirally around the chamber, a liquid N_2 cooling jacket, and entry/exit points for supplying inert gas (N_2). The sample is mounted in single cantilever mode as shown in **Figure 3.7**. The head is connected to a temperature controller and an analyzer which in turn are interfaced with a computer. The analyzer is programmed to generate and control the applied sinusoidal stress and simultaneously measure sample displacement. The measured responses are processed along with calibration values of the equipment and sample dimensions. Incorporation of these values into an equation expressing the forced vibration of the system generates the numeric values for storage modulus (E') and loss factor ($\tan\delta = E''/E'$).[95]

Figure 3.8 shows a schematic plot of storage modulus and *tanδ* for a model material scanned over a range of frequencies across the glass-rubber relaxation. The drop in the storage modulus with the simultaneous peak in *tanδ* represents the onset of large scale conformational motions corresponding to the glass transition. The loss factor exhibits a maximum in the temperature scan when the frequency of the motional processes inside the sample resonates with the experimental frequency. The peak position shifts to higher temperatures with increasing experimental frequency, reflecting the higher level of thermal energy required for the polymer segments to respond to the applied perturbation.

3.2.5 Sample preparation and experimental technique

The dynamic mechanical measurements were carried out using a Polymer Laboratories MK-II DMTA configured in bending mode with single cantilever geometry. Liquid N_2 was used as coolant to perform sub-ambient runs, and N_2 purge gas was maintained to provide an inert testing atmosphere. Sample films (0.5 to 1.0 mm thickness) were cut into rectangular bars of 10 mm x 30 mm and were vacuum dried prior to measurement. Experiments were conducted over a temperature range of -120°C to 200°C with a heating rate of 1°C/min. Storage modulus and *tanδ* were recorded at frequencies ranging from 0.1 Hz to 10 Hz. Dynamic mechanical transition temperatures were established according to the peak in *tanδ* at 1 Hz; based on the heating and data collection rates inherent to the dynamic mechanical measurements, the precision associated with the peak temperatures was ± 1°C.

3.3 BROADBAND DIELECTRIC SPECTROSCOPY (BDS)

3.3.1 Overview

Broadband Dielectric Spectroscopy is a non-intrusive technique suitable for probing molecular motions and morphology in a variety of material systems. In this study, it involves measurement of the dielectric response of a polymeric material subjected to an alternating electric field as a function of the frequency (time) and temperature. Application of an electric field leads to polarization of the material. Polarization can be the outcome of (i) an instantaneous distortion of the electron cloud associated with the constituent molecules termed electronic polarization or induced-dipole polarization, (ii) the re-alignment of the molecular dipoles present along the polymer chain, referred to as orientation polarization, or (iii) interfacial polarization, which involves the migration and trapping of charged species at impenetrable interfaces or boundaries.

The primary focus of the dielectric studies described here is the elucidation of orientation polarization as it involves the alignment of dipoles along the polymer chain, thus providing insight into polymer chain motions and their relation to molecular structure and morphology. These motions can encompass large scale cooperative relaxation of the chains, typically associated with the glass transition, or local (non-cooperative) sub-glass relaxations such as the rotation of side groups or the vibration of small segments. The measured intensity of the relaxations reflects the strength of the dipoles and the scale of the corresponding motions.[96]

3.3.2 Derivation of phenomenological equations

3.3.2.1 Static measurements

Consider a parallel-plate capacitor as shown in **Figure 3.9**, with an electric field *E* applied across the plates; the plates have an area *A* and are separated by a distance *d*, with

d much smaller than the dimension of the plates. When a dielectric medium is positioned between the plates, the resulting capacitance is given by:

$$C = \frac{\sigma A}{Ed} = \frac{Q}{V} \quad [3.7]$$

where σ is the charge density, Q is the magnitude of charge on each plate, and V is the potential difference across the plates due to the charge. If the dielectric medium is replaced by vacuum, the voltage required to maintain the same magnitude of charge increases, thereby reducing the capacitance across the plates to C_0. The static dielectric constant (ε_S) is then defined as:

$$\varepsilon_S = \frac{C}{C_0} \quad [3.8]$$

with $\varepsilon_S = 1$ for vacuum, and $\varepsilon_S > 1$ for all dielectric media.

Polarization (P) of a material can be expressed in terms of the dielectric displacement (D) of the material and the electric field strength (E) as follows:

$$D = E + 4\pi P \quad [3.9]$$

where D can also be defined in terms of the static dielectric constant,

$$D = \varepsilon_s E \quad [3.10]$$

3.3.2.2 Dynamic measurements

The above equations are applicable for a time-independent or static electric field. However, when a viscoelastic material is subjected to an alternating electric field, there is a simultaneous fluctuation in the dielectric displacement or polarization response of the material such that it lags the applied electric field by a phase angle, δ.

In complex notation, the time-dependent electric field [$E(t)$] and corresponding dielectric displacement [$D(t)$] can be expressed as:

$$E(t) = E_0 \exp(i\omega t) \qquad [3.11(a)]$$

$$D(t) = D_0 \exp i(\omega t - \delta) \qquad [3.11(b)]$$

Therefore, the complex dielectric constant (ε^*) can be defined as:

$$\varepsilon^* = \frac{D(t)}{E(t)} = \frac{D_0}{E_0}\exp(-i\delta) = \varepsilon_0(\cos\delta - i\sin\delta) \qquad [3.12(a)]$$

$$\varepsilon^* = (\varepsilon_0 \cos\delta) - i(\varepsilon_0 \sin\delta) = \varepsilon' - i\varepsilon'' \qquad [3.12(b)]$$

and

$$\tan\delta = \frac{\varepsilon''}{\varepsilon'} \qquad [3.12(c)]$$

where ε' is the real part of the complex dielectric constant, known as the dielectric constant or permittivity, ε'' is the dielectric loss and corresponds to the imaginary part of the complex dielectric constant, and *tanδ* is the dielectric loss factor or dissipation factor.

3.3.2.3 Superposition principle

In order to understand the frequency response of ε^* and to relate it to the inherent dynamics of the material, it is imperative to develop appropriate phenomenological equations. The superposition principle expresses the instantaneous dielectric displacement $D(t)$ as a sum of the displacements resulting from the incremental electric fields applied at all times for $x \le t$.[67]

$$D(t) = \underbrace{\varepsilon_U E(t)}_{\textit{Instantaneous term}} + \underbrace{(\varepsilon_R - \varepsilon_U)\int_{-\infty}^{t} E(x)\alpha(t-x)\,dx}_{\textit{Summation term}} \qquad [3.13]$$

ε_R is the relaxed dielectric constant attained at very low frequencies where the polymer dipoles have sufficient time to align with the applied electric field; ε_U is the unrelaxed dielectric constant realized at the other end of the frequency spectrum, *i.e.*, for frequencies approaching infinity where the dipolar molecules are unable to orient with the alternating field. The intensity of the measured dielectric response as a result of orientation polarization is given by the difference, $\Delta\varepsilon = \varepsilon_R - \varepsilon_U$, termed the dielectric relaxation intensity.[97]

As a first (empirical) approach, the dielectric relaxation can be described by an exponential decay function, $\alpha(t)$, encompassing a single relaxation time (τ_0),

$$\alpha(t) = \frac{1}{\tau_0}\exp(-t/\tau_0) \qquad [3.14]$$

Substituting equation [3.14] into the summation term of [3.13] and differentiating with respect to t gives:

$$\tau_0 \frac{dD(t)}{dt} + D(t) = \tau_0 \varepsilon_U \frac{dE(t)}{dt} + \varepsilon_R E(t) \qquad [3.15]$$

Introducing equations [3.11(a)] and [3.11(b)] into [3.15] results in the Debye relation[67] for the complex dielectric constant as a function of frequency:

$$\varepsilon^* = \varepsilon_U + \frac{\varepsilon_R - \varepsilon_U}{1 + i\omega\tau_0} \qquad [3.16(a)]$$

which when resolved into its real and imaginary components gives:

$$\varepsilon' = \varepsilon_U + \frac{\varepsilon_R - \varepsilon_U}{1 + \omega^2\tau_0^2} \qquad [3.16(b)]$$

$$\varepsilon'' = (\varepsilon_R - \varepsilon_U)\frac{\omega\tau_0}{1 + \omega^2\tau_0^2} \qquad [3.16(c)]$$

3.3.2.4 Description of non-Debye relaxation behavior

Polymeric materials typically show a broad distribution of relaxation times considering their macromolecular nature and the physical constraints associated with chain motions. Hence, the relaxations are much broader as compared to a single relaxation time Debye response. The behavior is best captured using empirical equations with adjustable exponents based on modifications to the Debye equation.

Cole-Cole modification

The Cole-Cole model[98] employs a "broadening" parameter (*a*) to encompass symmetric relaxations that are broader than those predicted by the Debye model.

$$\varepsilon^* = \varepsilon_U + \frac{\varepsilon_R - \varepsilon_U}{1 + (i\omega\tau_0)^a} \qquad [3.17]$$

Equation 3.17 can be resolved into its real and imaginary parts[99] and plotted as dielectric constant or loss versus frequency for varying values of *a* ($0 < a \leq 1$) (see **Figure 3.10**). The lower the value of *a*, the broader the relaxation. A value of *a* equal to unity corresponds to the Debye equation.

Davidson-Cole Modification

The Davidson-Cole[100] model modifies the Debye equation through the introduction of a "skewing" parameter (*b*) to account for high frequency non-symmetric broadening of the dielectric loss data:

$$\varepsilon^* = \varepsilon_U + \frac{\varepsilon_R - \varepsilon_U}{(1 + i\omega\tau_0)^b} \qquad [3.18]$$

The value of *b* varies from 0 to 1, with lower values of *b* indicating a higher degree of asymmetry; $b = 1$ corresponds to the Debye model.

Havriliak-Negami model

A widely used empirical equation is obtained by the combination of the above two models as proposed by Havriliak and Negami.[42] The model incorporates both the "broadening" and "skewing" parameters and offers enough flexibility to describe the behavior of a majority of polymer systems, thereby providing insight into the nature of the relaxation time distribution:

$$\varepsilon^* = \varepsilon_U + \frac{\varepsilon_R - \varepsilon_U}{[1 + (i\omega\tau_{HN})^a]^b} \qquad [2.10]$$

Figure 3.11 shows Havriliak - Negami plots with $a = 0.5$ and b ranging from 0 to 1. Here, τ_0 corresponds to τ_{HN}, the single relaxation time predicted by the Havriliak-Negami model. The position of the loss maximum is given by the following relation:

$$\tau_{MAX} = \tau_{HN} \left[\frac{\sin(\frac{\pi a b}{2+2b})}{\sin(\frac{\pi a}{2+2b})} \right]^{1/a} \qquad [3.19]$$

For a perfectly symmetric relaxation, $b = 1$ and $\tau_{MAX} = \tau_{HN}$.

3.3.3 Dielectric relaxation phenomena at high temperatures and low frequencies

The dielectric response of a material at high temperatures and low frequencies is often dominated by conduction effects. The processes that contribute to the dielectric response under these conditions include the migration of mobile charge carriers across the medium and the trapping of charges at interfaces and boundaries. While the motion of charge carriers can increase the dielectric loss by several orders of magnitude, charge trapping influences both the dielectric constant and dielectric loss. This additional polarization is a result of (i) accumulation of charges at the electrode-sample interface termed “electrode polarization” and/or (ii) the separation of charges at internal phase boundaries referred to as Maxwell-Wagner-Sillars (MWS) polarization. MWS polarization is generally evident in non-homogenous materials like multiphase polymers, blends and colloids, and occurs across smaller size scales as compared to electrode polarization. In certain cases, this large scale polarization can mask the dielectric orientation response of the material.[99]

3.3.4 Correlation of dielectric relaxation intensity with inherent material properties

The dielectric relaxation intensity ($\Delta\varepsilon = \varepsilon_R - \varepsilon_U$) associated with a particular motional process can be used to elucidate the underlying characteristics of the material. Several equations have been proposed to correlate the dielectric response of a material with its composition and corresponding polarizability.**[101-103]** A relatively general equation was proposed by Fröhlich,**[104]** known as the Fröhlich-Onsager expression:

$$\Delta\varepsilon = \frac{3\varepsilon_R}{(2\varepsilon_R + \varepsilon_U)} \frac{4\pi N}{3kT} \left(\frac{\varepsilon_U + 2}{3} \right)^2 g\mu_0^2 \qquad [3.20(a)]$$

where:

$$\Delta\varepsilon = \varepsilon_R - \varepsilon_U \qquad [3.20(b)]$$

The Fröhlich theory gains its applicability for different material systems by inclusion of the Kirkwood correlation factor (g), which accounts for short-range orientation correlations between molecules. A value of $g = 1$ provides the dielectric relaxation intensity ($\Delta\varepsilon$) of an isotropic material with totally uncorrelated dipoles. However, in the case of a polymeric material, for example, the dipolar response is influenced by both intramolecular and intermolecular correlations that result in a value of g different than unity. $g > 1$ suggests an enhancement in the dipolar response relative to the isotropic case due to the alignment or correlation of the individual dipole moments, while $g < 1$ indicates a system where the individual dipoles are correlated such that some degree of dipolar cancellation occurs, leading to a lower net response.

3.3.5 Experimental configuration and procedure

The Novocontrol Concept 40 Broadband Dielectric Spectrometer is state-of-art equipment with significant enhancements in cell design and analyzer controls. This has led to the possibility of probing the sample over a broad range of frequencies (10^{-3} to 10^{7} Hz) and temperatures (-150°C to 400°C) with outstanding accuracy and data processing capabilities. Measurements can be made either at discrete temperatures, or with a temperature ramp and concomitant sweeping through the entire range of frequencies.

A schematic for the Concept 40 BDS instrument is shown in **Figure 3.12**. Liquid nitrogen, held in a dewar, is vaporized and used for controlling the sample temperature. The liquid N_2 passes through a gas heating module which in turn is connected to the temperature controller that provides a precision of 0.1°C. The sample holder or cryostat is a double-walled metallic cylinder, with a high vacuum maintained in between the walls to isolate the sample and avoid external ice formation. The sample cell is placed inside the cryostat and consists of the electrode-coated sample sandwiched between two gold-plated electrodes to form a parallel-plate capacitor arrangement (see **Figure 3.13**). The temperature controller is connected through three channels to the dewar and sample cell, which completes the analyzer circuitry. The data are collected, stored and analyzed via a computer connected to the instrument.[105]

The circuit used for the dielectric measurements is shown in **Figure 3.13**. An alternating voltage at a particular frequency is applied across the sample and the current generated is measured. The current typically lags the voltage by a phase angle δ and varies with the sample material and geometry. The complex notations of voltage and current amplitude can be shown as:

$$U^* = U_0 \exp i(\omega t) \qquad [3.21]$$

$$I^* = I_0 \exp i(\omega t - \delta) \qquad [3.22]$$

The applied voltage and measured current can be related to the complex capacitance of the sample (C_p^*) through the following equation:

$$C_p^* = -i \frac{I^*}{\omega U^*} - C_{edge} - C_S \qquad [3.23]$$

where C_{edge} is the additional capacitance resulting from the electrical stray fields emanating from the borders of the sample capacitor, and C_s reflects the additional capacitance due to external factors such as the capacitance of electrode connection wires or that due to teflon spacers. Sample capacitance can be further related to the complex dielectric constant to evaluate the material properties at varying temperature and frequency as shown below:

$$\varepsilon^* = \varepsilon' - i\varepsilon'' = \frac{C_p^*}{C_0} \qquad [3.24]$$

where C_0 is defined as the empty cell capacitance.

3.3.5.1 Sample preparation and experimental technique

Experiments were carried out on previously vacuum dried sample films with thickness in the range of 0.25 to 0.4 mm. A VEECO 7700 series thermal evaporator was used to evaporate concentric silver electrodes onto the polymer films to ensure good electrical contact. The samples were mounted on a mask and placed inside the thermal evaporator under vacuum; silver pellets were then evaporated from a heated tungsten filament to form 33 mm electrodes on either side of the polymer film. Quenched PTT films were coated using a silver paint, obtained from SPI Inc., West Chester (PA), to avoid exposure to elevated temperatures (and possible crystallization) during the thermal evaporation process. Typically, dielectric constant (ε') and loss (ε'') were measured from -150°C to 150°C at discrete temperature intervals of 4°C over a frequency range of 0.1Hz – 1MHz.

3.3.5.2 Data analysis

The WINFIT® software package bundled with the spectrometer provided the tools for rigorous analysis of the experimental data. The glass and sub-glass relaxations were curve fit to the Havriliak-Negami model (equation 2.10) and the corresponding parameters were determined. The software resolves possible conduction contributions to the dielectric response by incorporating a conductivity term in the Havriliak-Negami equation, as shown:

$$\varepsilon^* = \varepsilon' - i\varepsilon'' = \underbrace{\varepsilon_{U_1}}_{\text{Instantaneous polarization term}} + \sum_{k=1}^{3} \underbrace{\left[\frac{\Delta\varepsilon_k}{\left(1 + (i\omega\tau_{HN_k})^{a_k}\right)^{b_k}} \right]}_{\text{Orientation polarization component}} - \underbrace{i\left(\frac{\sigma_0}{\varepsilon_0 \omega} \right)^N}_{\text{Conductivity term}} \qquad [3.25]$$

where σ_0 is the conductivity and ε_0 is the vacuum permittivity. For ideal conduction (isotropic medium with no internal boundaries), $N \longrightarrow 1$.

3.4 DIFFERENTIAL SCANNING CALORIMETRY (DSC)

3.4.1 Basic theory

One of the most widely used methods to measure the energetic effects associated with phase transitions in polymers is Differential Scanning Calorimetry (DSC). Physical and chemical transformations in polymers such as crystallization, melting, glass transition and curing, which are typically associated with heat effects, are effectively captured in both a qualitative and quantitative manner by the DSC. The basic configuration of a modern DSC instrument[106] is shown in **Figure 3.15** and consists of two thermally insulated cells, one for the sample of interest and the other for the reference. The reference sample is chosen such that it remains stable within the experimental temperature range. The underlying principle of DSC involves the measurement of the difference in heat flow required to maintain both the sample and reference pans at the same temperature for the entire experiment. The temperature program of a conventional DSC is designed such that sample pan temperature increases linearly with time. This technique allows the identification of key physical transformations like melting, an endothermic event, which necessitates more heat flow to the sample cell in order to maintain the same temperature as the reference during heating. This phenomenon is shown in a typical DSC scan for a semicrystalline polymer with peak melting temperature at T_m in **Figure 3.16**. Similarly, we can distinguish the glass transition behavior as a step-wise change in the curve at T_g, and the exothermic crystallization event indicated by the downward peak at T_c.

DSC is generally operated in a power-compensation mode which relies on two overlapping control loops. The first loop is designed to provide the same heat flow rate to both the sample and reference cells, while the second loop provides a differential power input to the sample cell such that temperature differences arising due to the various phase transitions are eliminated. The electrical nature of measurement allows conversion of heat flow into heat capacity or enthalpy completely independent of temperature.[107]

3.4.2 Sample preparation and experimental technique

A Perkin-Elmer DSC-7 Differential Scanning Calorimeter was employed to analyze PTT samples prepared with varying thermal histories. The sample, prepared by melt-pressing, was placed in the sample cell sealed inside an aluminum pan (~ 50 mm^3 volume) and crimped with an aluminum lid, while an empty crimped pan was placed in the reference cell. The previously vacuum dried samples were used in the form of thin strips with a low sample mass of ~ 10 mg to ensure good thermal contact. An inert atmosphere of N_2 was maintained in the overhead space above the cells.

High-purity calibration standards, indium and zinc, were used to calibrate the measured heat flow and temperature of the calorimeter, while the heat capacity calibration was performed using a sapphire standard. A typical scanning rate of 10°C/min was employed for all the experiments. Empty pan (baseline) runs were performed and subtracted from the sample run to eliminate any slope or curvature effects introduced by the instrument or sample pans.

3.4.3 Data Interpretation

3.4.3.1 Heat capacity measurement

The heat capacity was determined by calibration with a sapphire standard using the method described by Wunderlich.[108] The method requires three separate runs; an empty pan baseline run, a sapphire calibration run, and a sample run to be performed under the same experimental conditions. The sample heat capacity can then be determined from the measured amplitudes of the respective runs using the following equation:

$$m_s C_p(sample) = \frac{[a_s(T) - a_r(T)]}{kq} \qquad [3.26(a)]$$

$$kq = \frac{[a_{cal}(T) - a_r(T)]}{m_c C_p^{cal}(T)} \qquad [3.26(b)]$$

where a_r, a_{cal} and a_s are the heat flow amplitudes of the empty pan, calibration and sample runs, respectively, while m_s and m_c are the respective masses of the sample and sapphire (calibrant) standard. C_p^{cal} is the sapphire heat capacity obtained from literature.[109] k is a proportionality constant and q is the experimental temperature scan rate.

3.4.3.2 Estimation of glass transition temperature

The glass to rubber transition is detected as a step change in the heat flow or the heat capacity (see Inset of Figure 3.16). In the case of a wholly amorphous polymer, the material transforms from a glassy solid to a rubbery liquid across the glass transition temperature (T_g). A similar glass-rubber relaxation is observed across T_g in the non-crystalline regions of a semicrystalline polymer. Once the C_p *(sample)* is determined by the method described above, the glassy (solid) and the rubbery baselines are extrapolated (see Figure 3.16). T_g is then defined as the temperature at half the extrapolated incremental increase in C_p, and is obtained from the equation:

$$0.5 = \frac{C_p^{Sample}(T_g) - C_p^{Solid}(T_g)}{C_p^{Rubber}(T_g) - C_p^{Solid}(T_g)} \qquad [3.27]$$

3.5 X-RAY DIFFRACTION (XRD)

3.5.1 Basic theory

X-ray diffraction is a widely used tool to elucidate the crystal structure in semicrystalline polymers. The pattern obtained from the elastic scattering of X-rays reveals the inherent atomic arrangement and morphology of the polymer. The crystalline regions of semicrystalline polymers have well-defined geometries that reflect a periodic three-dimensional structure based upon a primary unit cell.

Consider **Figure 3.17**, wherein atomic planes in the crystal are separated by a fixed distance, *d*, known as the plane spacing. The X-ray waves interact with the atoms to produce an interference pattern. For example, the rays scattered off of layer 2 travel further than those scattered from layer 1. Depending on the distance traveled by the X-ray before it is scattered, the resulting radiation can interfere either destructively (nullify each other) or constructively (increase in amplitude by addition of respective intensities). According to Bragg's law, constructive interference is observed when *d* is such that the distance traveled by the X-ray is an integral multiple of the incident wavelength (λ).

$$n\lambda = 2d\sin\theta \qquad [3.28]$$

This principle can be used to probe the sample at varied size scales ranging from 1Å (to measure atomic periodicity) to 2000Å (to investigate morphological variations). The technique used at small size scales (1Å-10Å) to determine the crystal unit structure, the degree of crystallinity, and the size and perfection of crystallites is termed Wide Angle X-ray Scattering (WAXS). The constructive diffraction peaks are shown in a typical WAXS plot for a semicrystalline polymer in **Figure 3.18**. The peak positions correspond to different characteristic spacings of the crystal planes given by Equation 3.28. The lattice or crystal planes can be identified and lattice geometry understood by employing the reciprocal nomenclature of Miller's Indices.[110] A halo pattern devoid of any peaks is obtained for polymers that can be quenched into a wholly amorphous state. The degree of crystallinity can then be evaluated based on the difference in area under the crystalline diffraction peaks relative to that of the amorphous halo (see Figure 3.17*)*, with the assumption that the amorphous halo is consistent with the scattering pattern obtained from the amorphous regions in the semicrystalline polymer.

3.5.2 Experimental technique

Selected quenched and melt-crystallized PTT films were examined using a Siemens 5000 diffractometer with Cu K_α radiation (λ = 1.5406Å). Data were recorded at room temperature across a range of scattering angles (2θ) from 5 to 50°; the scan rate was 2° min^{-1}, with a data interval of 0.02°.

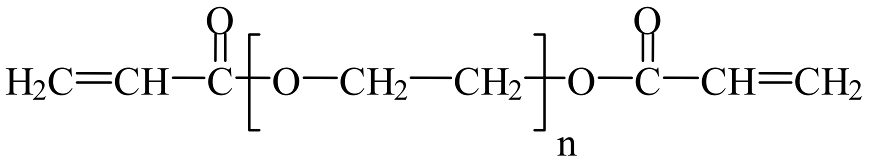

$$H_2C{=}CH-\overset{O}{\overset{\|}{C}}-\left[O-CH_2-CH_2\right]_n-O-\overset{O}{\overset{\|}{C}}-CH{=}CH_2$$

Poly(ethylene glycol) diacrylate (PEGDA; n=3, 10, 14)

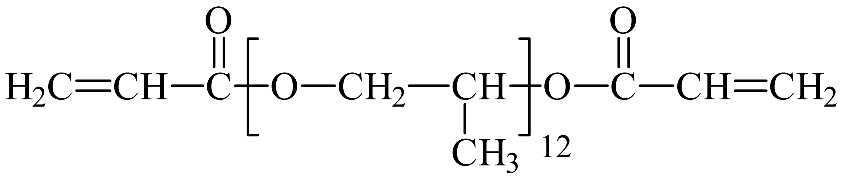

$$H_2C{=}CH-\overset{O}{\overset{\|}{C}}-\left[O-CH_2-\underset{CH_3}{\underset{|}{CH}}\right]_{12}-O-\overset{O}{\overset{\|}{C}}-CH{=}CH_2$$

Poly(propylene glycol) diacrylate (PPGDA)

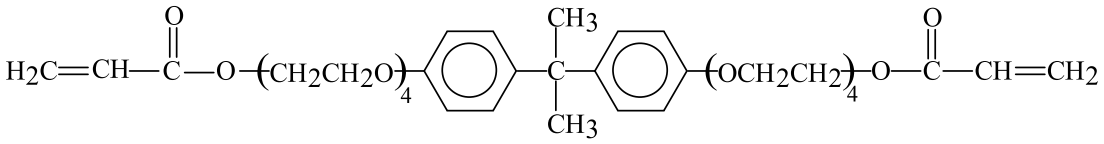

Bisphenol A ethoxylate diacrylate (BPAEDA)

Figure 3.1: Chemical structures of diacrylate monomers used as crosslinkers.

.

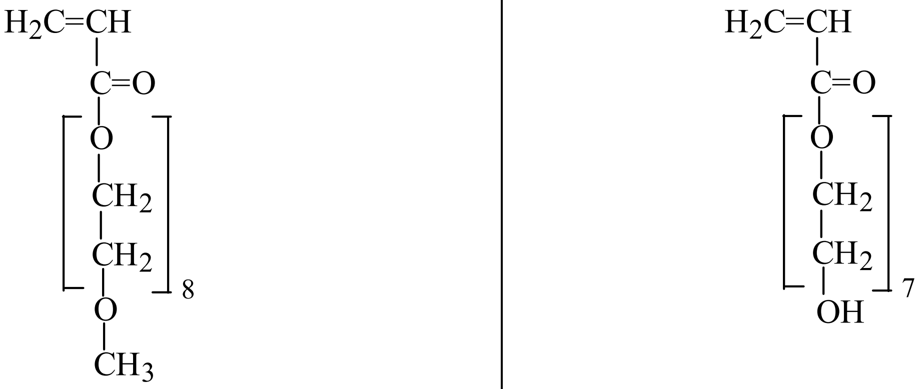

Poly(ethylene glycol) methyl ether acrylate (PEGMEA)

Poly(ethylene glycol) ether acrylate (PEGA)

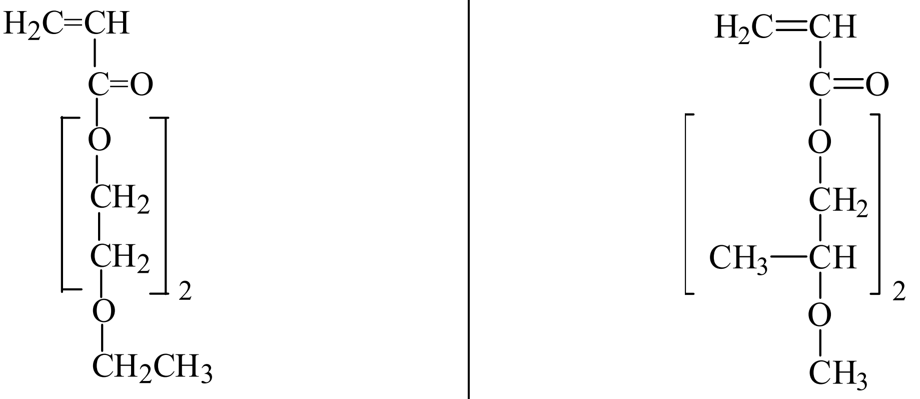

Diethylene glycol ethyl ether acrylate (DGEEA)

Poly(propylene glycol) methyl ether acrylate (PPGMEA)

Figure 3.2: Chemical structures of acrylate co-monomers.

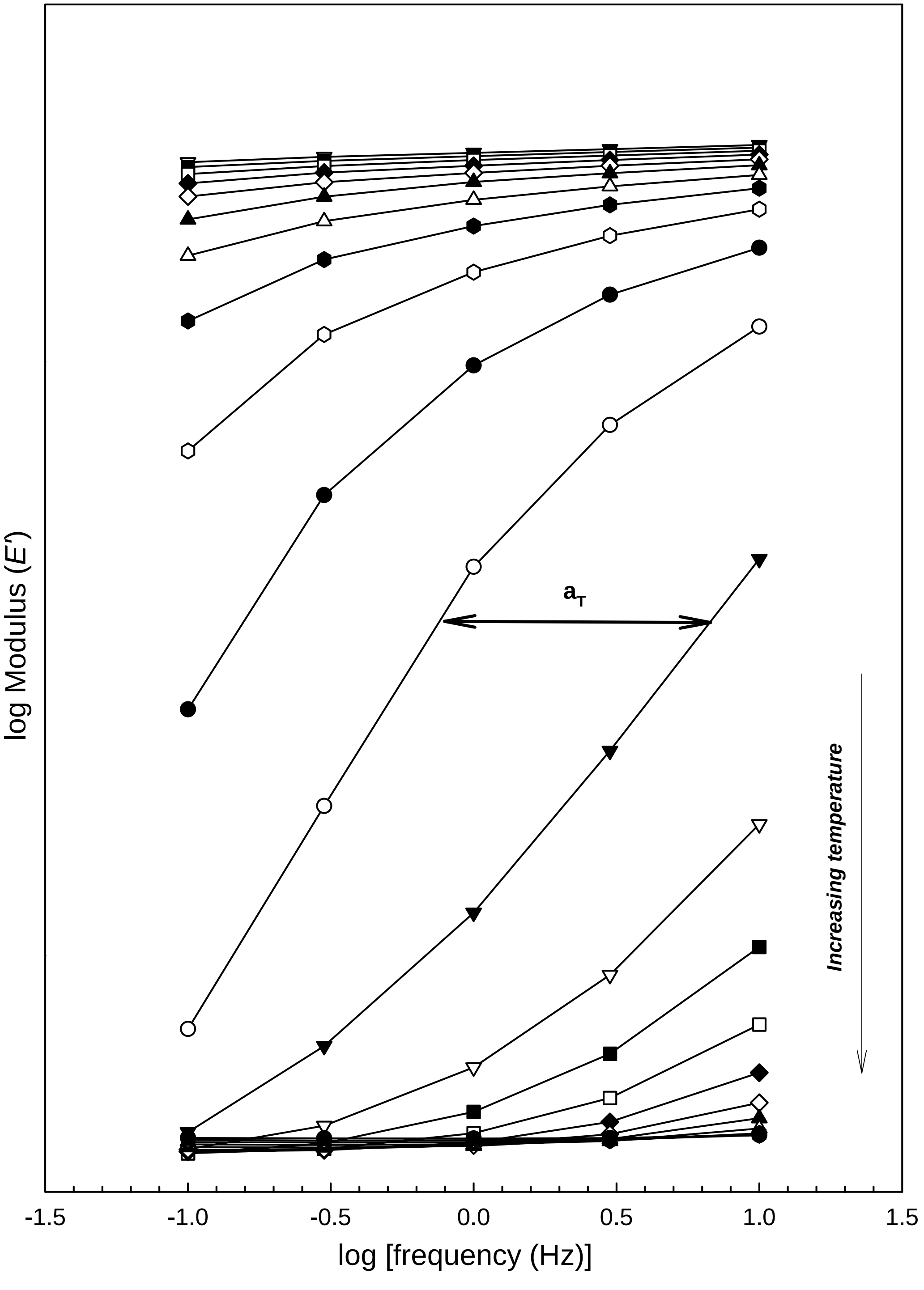

Figure 3.3: Determination of shift factor, a_T, to generate modulus-frequency master curve via time-temperature superposition method; frequency range of 0.1 to 10 Hz.

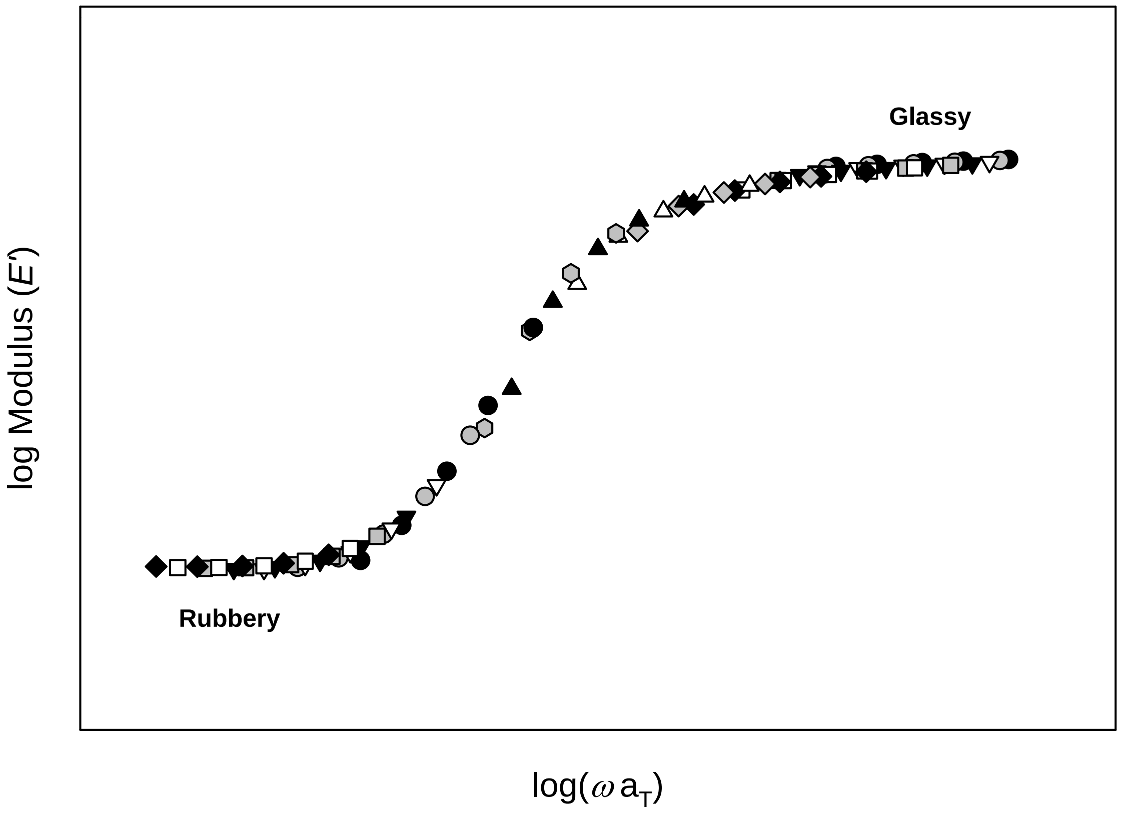

Figure 3.4: Modulus-frequency master curve obtained by time-temperature superposition; groups of data points (*i.e.*, same symbols) correspond to discrete temperatures.

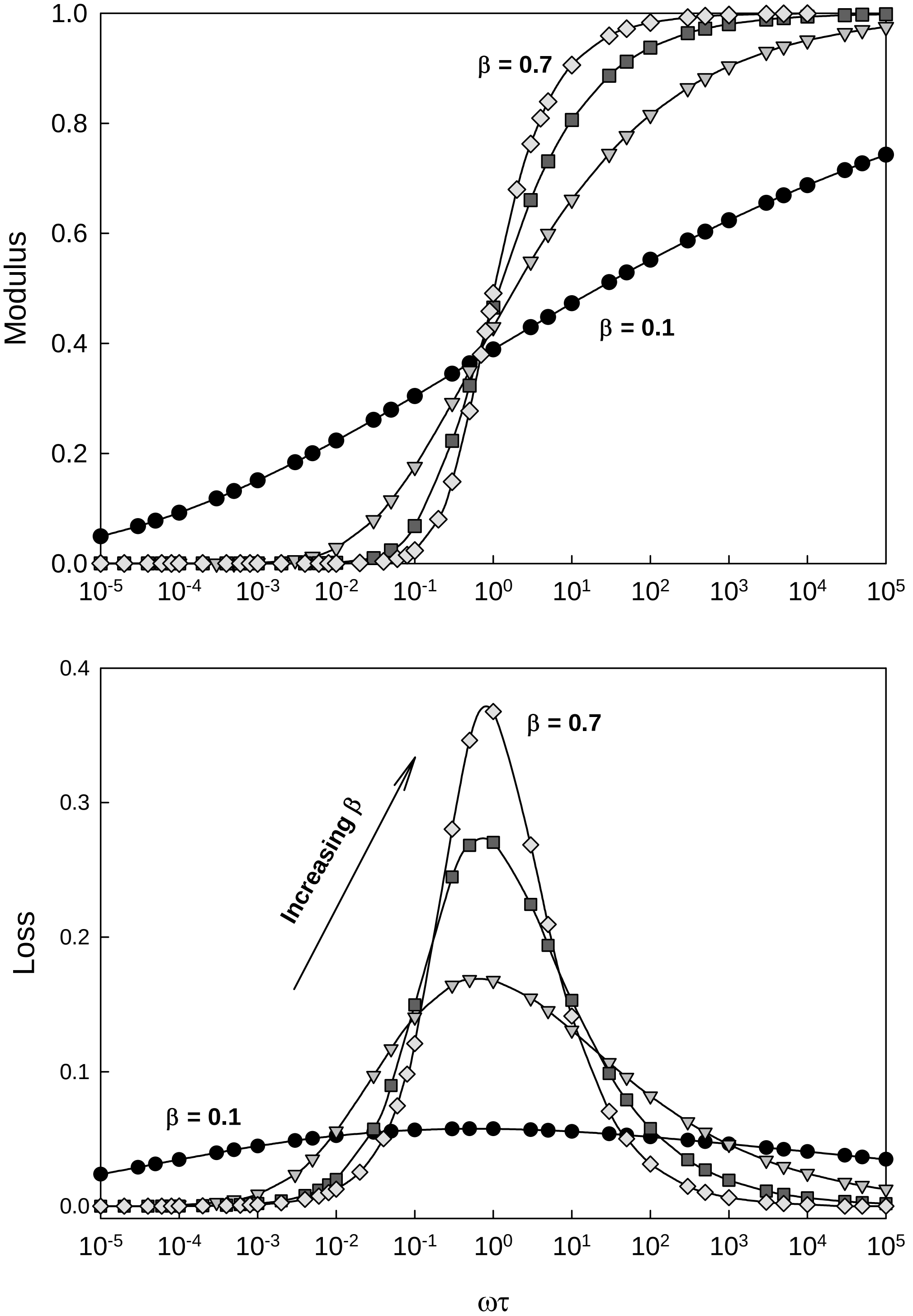

Figure 3.5: Normalized curves for modulus and loss obtained by plotting the series solution for the KWW function[39] with varying distribution parameter, $\beta = 0.1$, 0.3, 0.5 and 0.7.

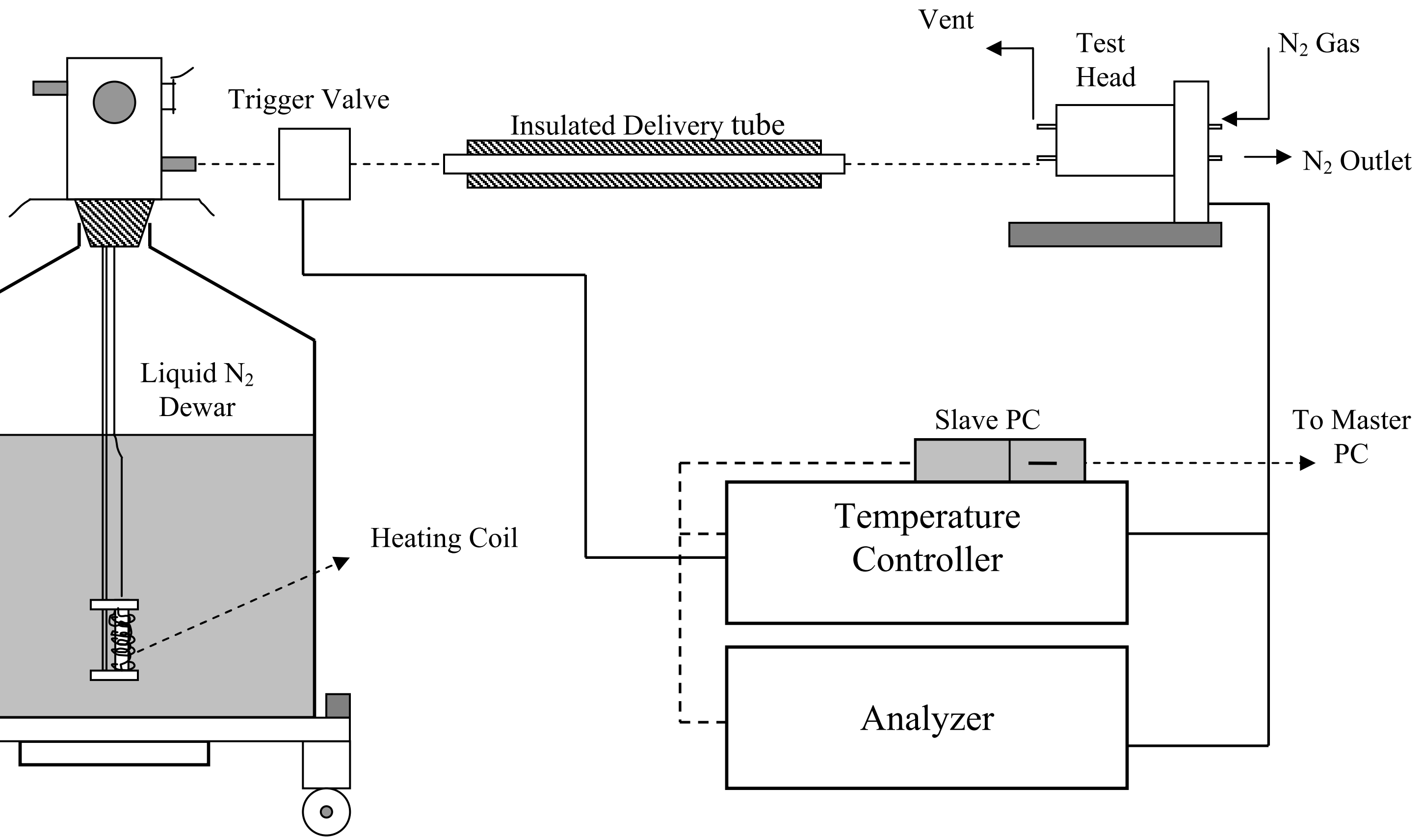
Vent
Test Head
N$_2$ Gas
Trigger Valve
Insulated Delivery tube
N$_2$ Outlet
Liquid N$_2$ Dewar
Slave PC
To Master PC
Heating Coil
Temperature Controller
Analyzer

Figure 3.6: Schematic representation of DMTA experimental set-up.

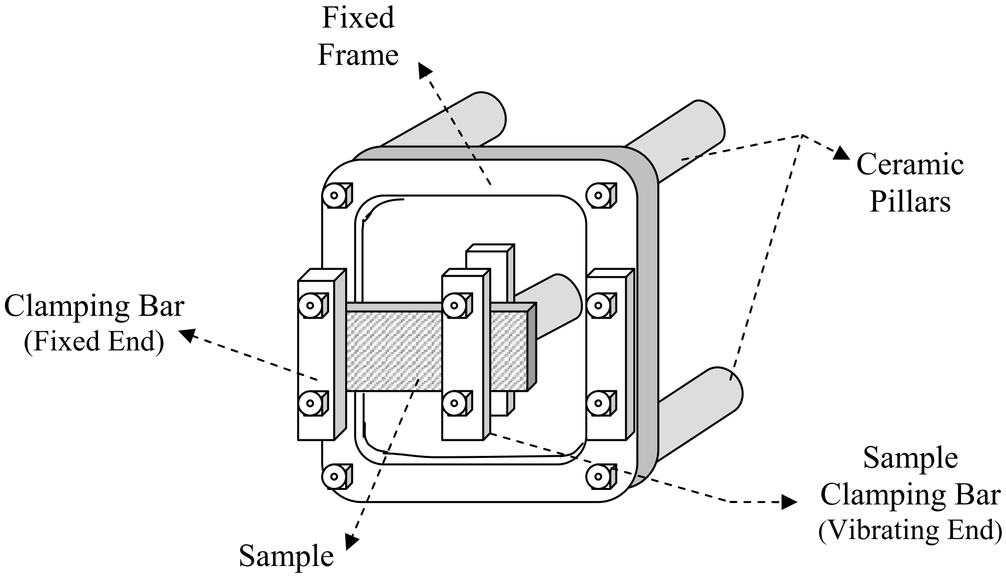
Fixed
Frame
Ceramic
Pillars
Clamping Bar
(Fixed End)
Sample
Clamping Bar
(Vibrating End)
Sample

Figure 3.7: Single cantilever arrangement of a sample in the DMTA.

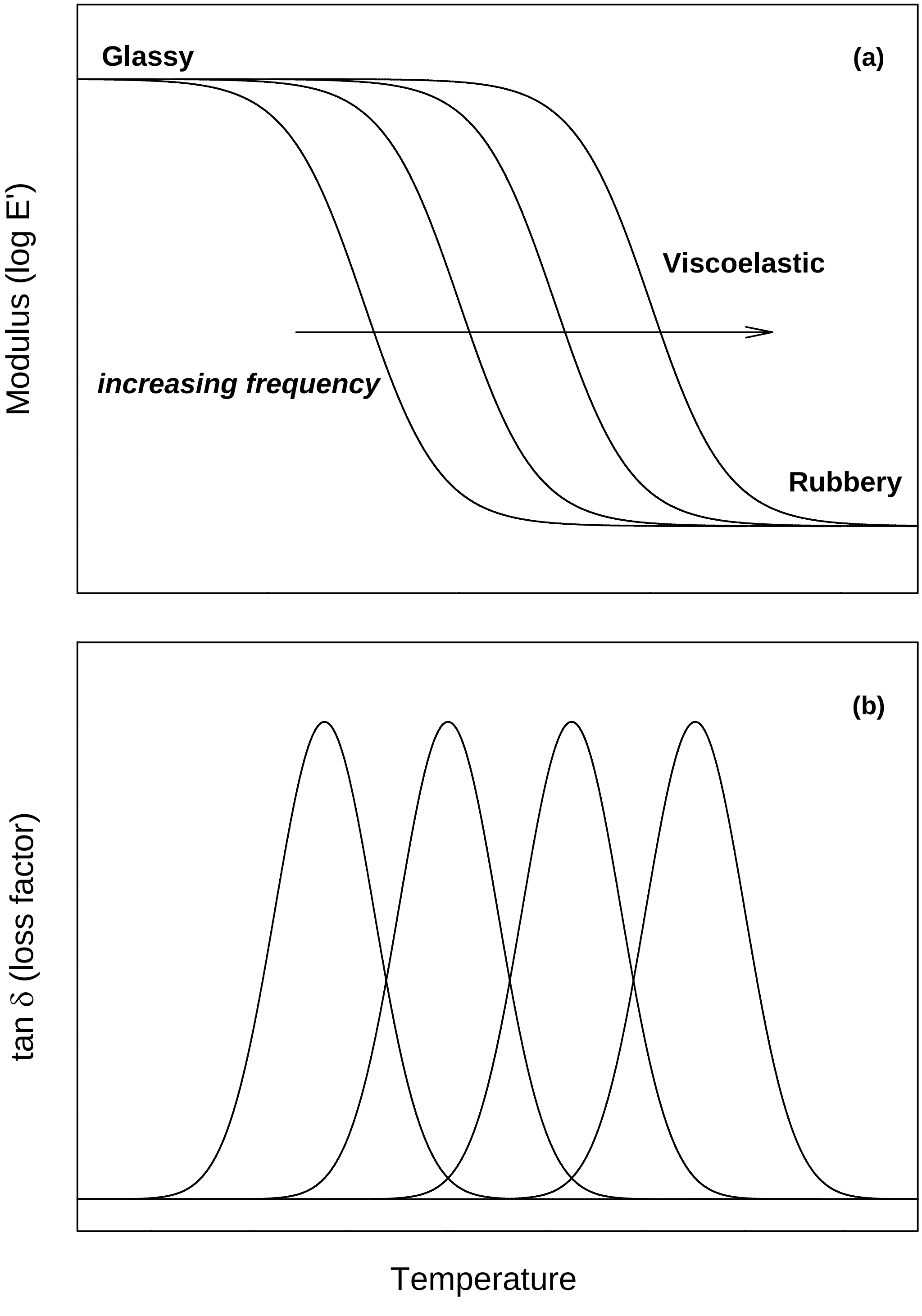

Figure 3.8: Representative dynamic mechanical (DMA) result for a polymeric material across the glass transition, plotted as a function of temperature for varying frequencies; (a): Storage modulus (E'), (b): tan δ (loss factor).

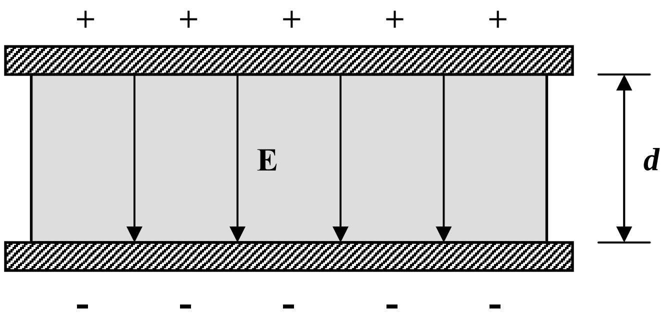

Figure 3.9: Parallel-plate capacitor arrangement for a dielectric material of thickness *d*, placed in an electric field *E*.

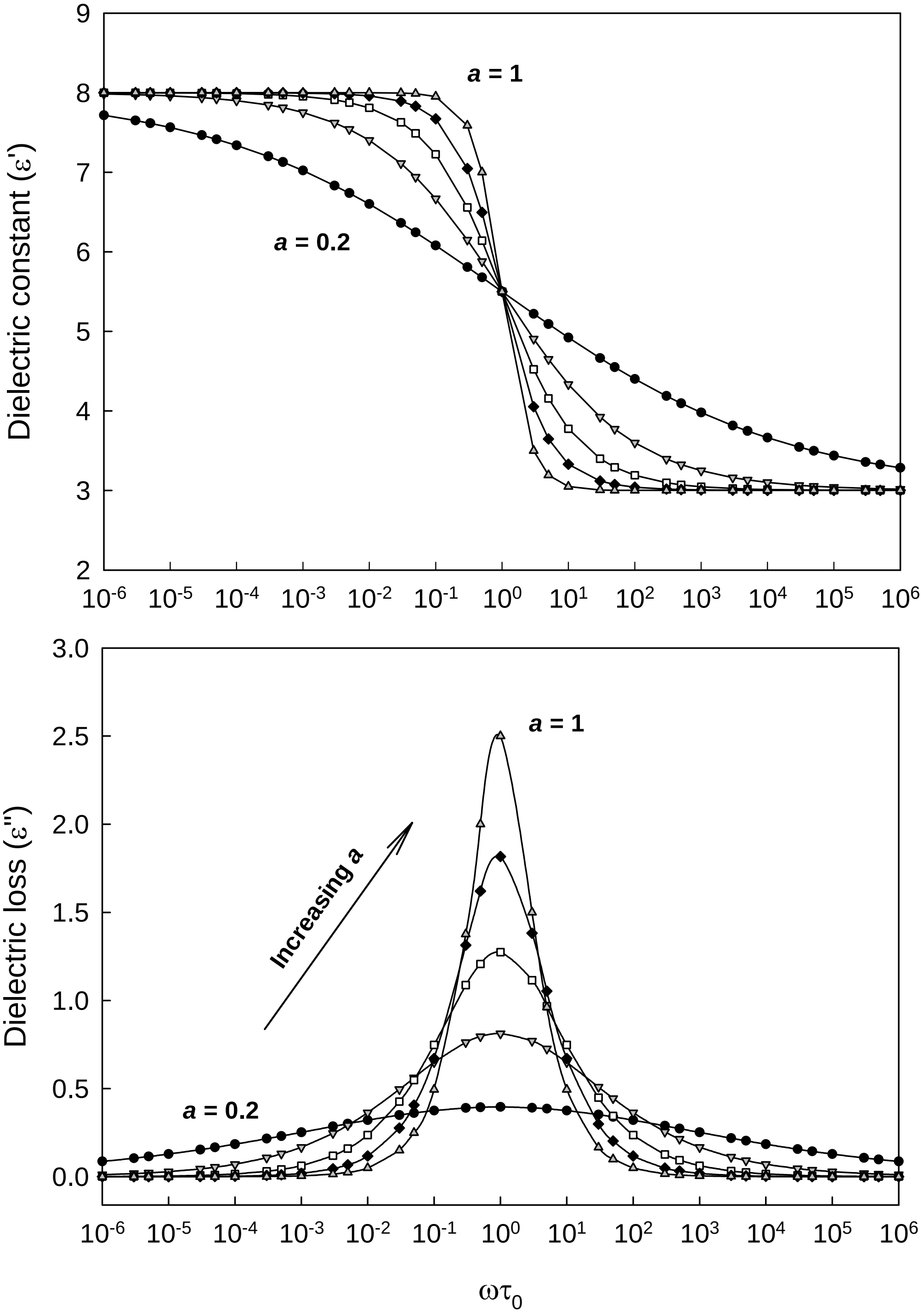

Figure 3.10: Cole – Cole model equations for dielectric constant (ε') and dielectric loss (ε'') plotted versus $\omega\tau_0$ on a semi-logarithmic plot (see Equation 3.17). Broadening parameter (a) = 1 gives the Debye model. For this example, $\varepsilon_U = 3$, $\varepsilon_R = 8$ and $a = 0.2$, 0.4, 0.6, 0.8 and 1.

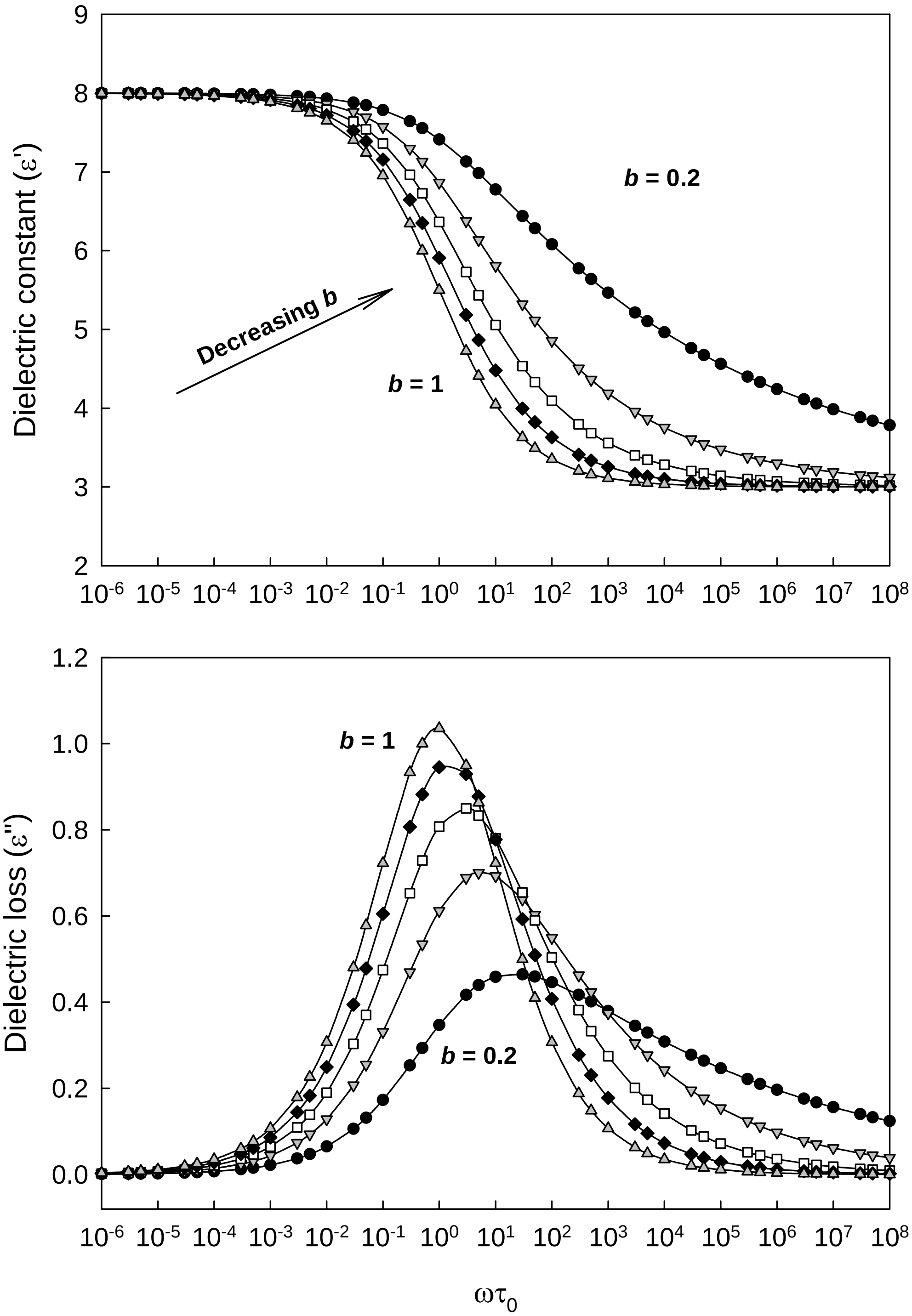

Figure 3.11: Havriliak – Negami model equations for dielectric constant (ε') and dielectric loss (ε'') plotted versus $\omega\tau_0$ on a semi-logarithmic plot (see Equation 2.10). Broadening parameter (a) = 0.5. Skewing parameter (b) = 1 gives the Cole-Cole model. For this example, $\varepsilon_U = 3$, $\varepsilon_R = 8$ and $b = 0.2$, 0.4, 0.6, 0.8 and 1.

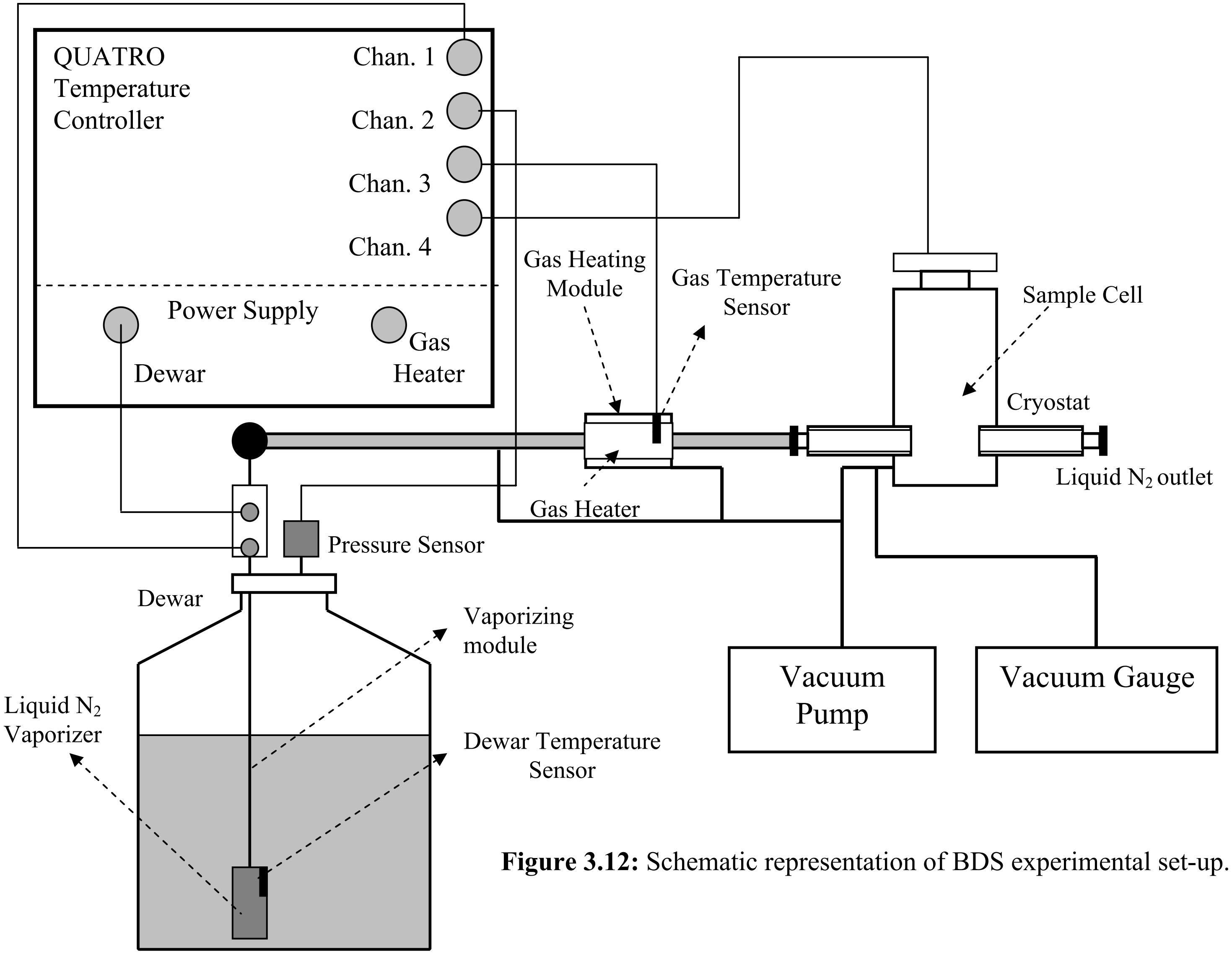
QUATRO
Temperature
Controller
Chan. 1
Chan. 2
Chan. 3
Chan. 4
Power Supply
Dewar
Gas
Heater
Gas Heating
Module
Gas Temperature
Sensor
Sample Cell
Cryostat
Liquid N_2 outlet
Gas Heater
Pressure Sensor
Dewar
Vaporizing
module
Liquid N_2
Vaporizer
Dewar Temperature
Sensor
Vacuum
Pump
Vacuum Gauge

Figure 3.12: Schematic representation of BDS experimental set-up.

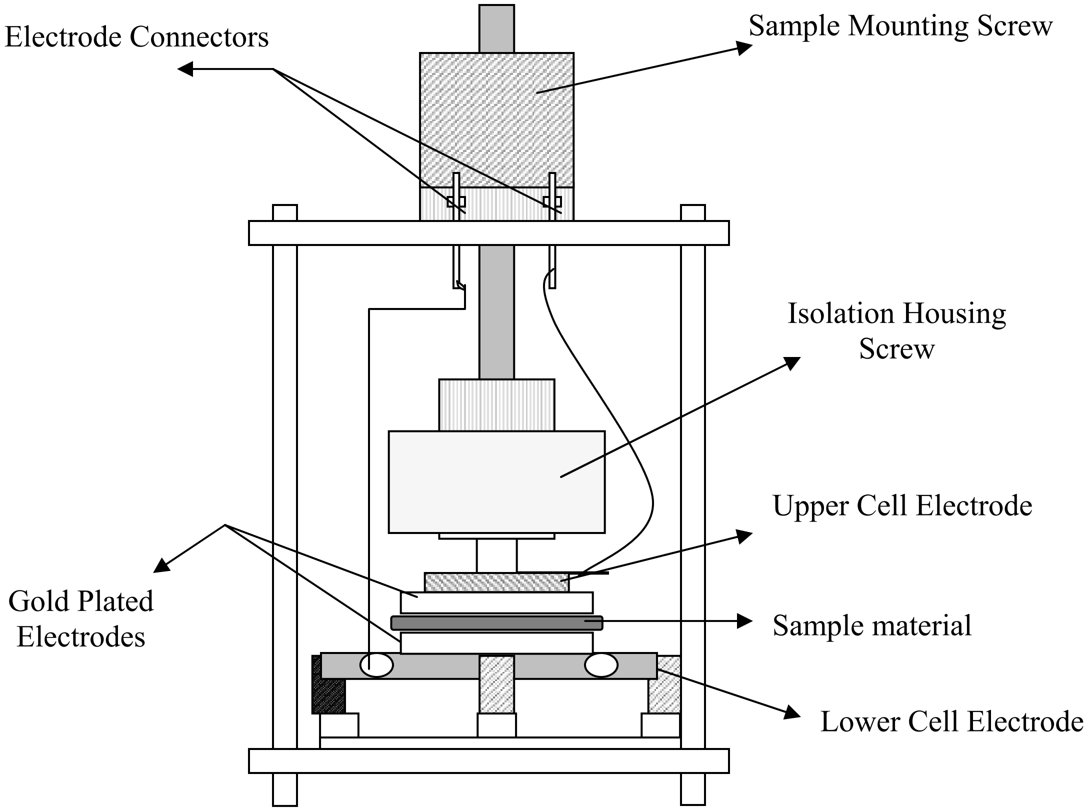
Electrode Connectors
Sample Mounting Screw
Isolation Housing Screw
Upper Cell Electrode
Gold Plated Electrodes
Sample material
Lower Cell Electrode

Figure 3.13: Novocontrol Concept 40 BDS sample cell arrangement.

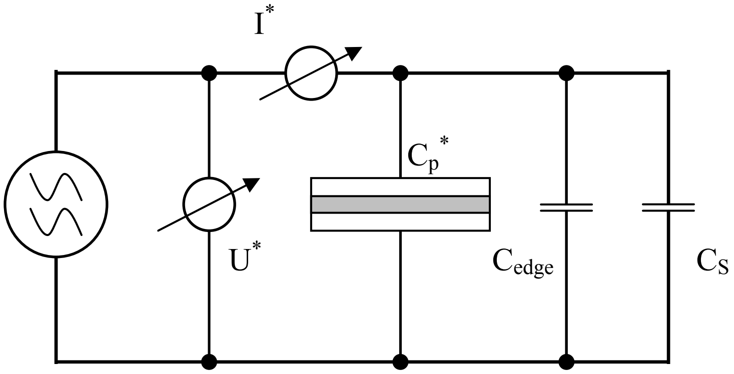
I*
Cp*
U*
Cedge
CS

Figure 3.14: Schematic of the measurement circuit for the BDS Novocontrol Concept 40 spectrometer.

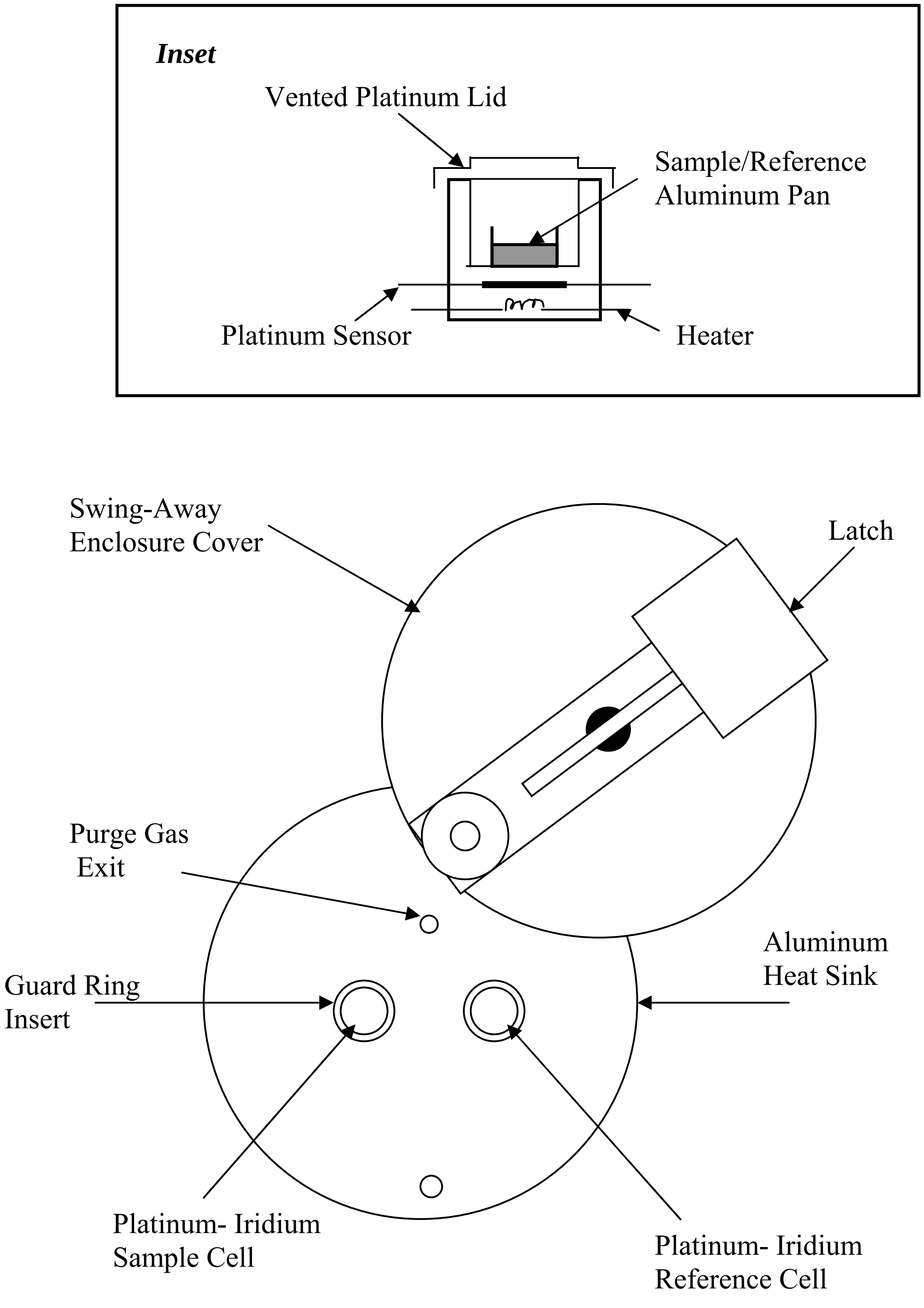
Inset
Vented Platinum Lid
Sample/Reference Aluminum Pan
Platinum Sensor
Heater
Swing-Away Enclosure Cover
Latch
Purge Gas Exit
Aluminum Heat Sink
Guard Ring Insert
Platinum- Iridium Sample Cell
Platinum- Iridium Reference Cell

Figure 3.15: Perkin-Elmer DSC-7 Differential Scanning Calorimeter. *Inset:* Detailed view of a sample/reference cell.[106]

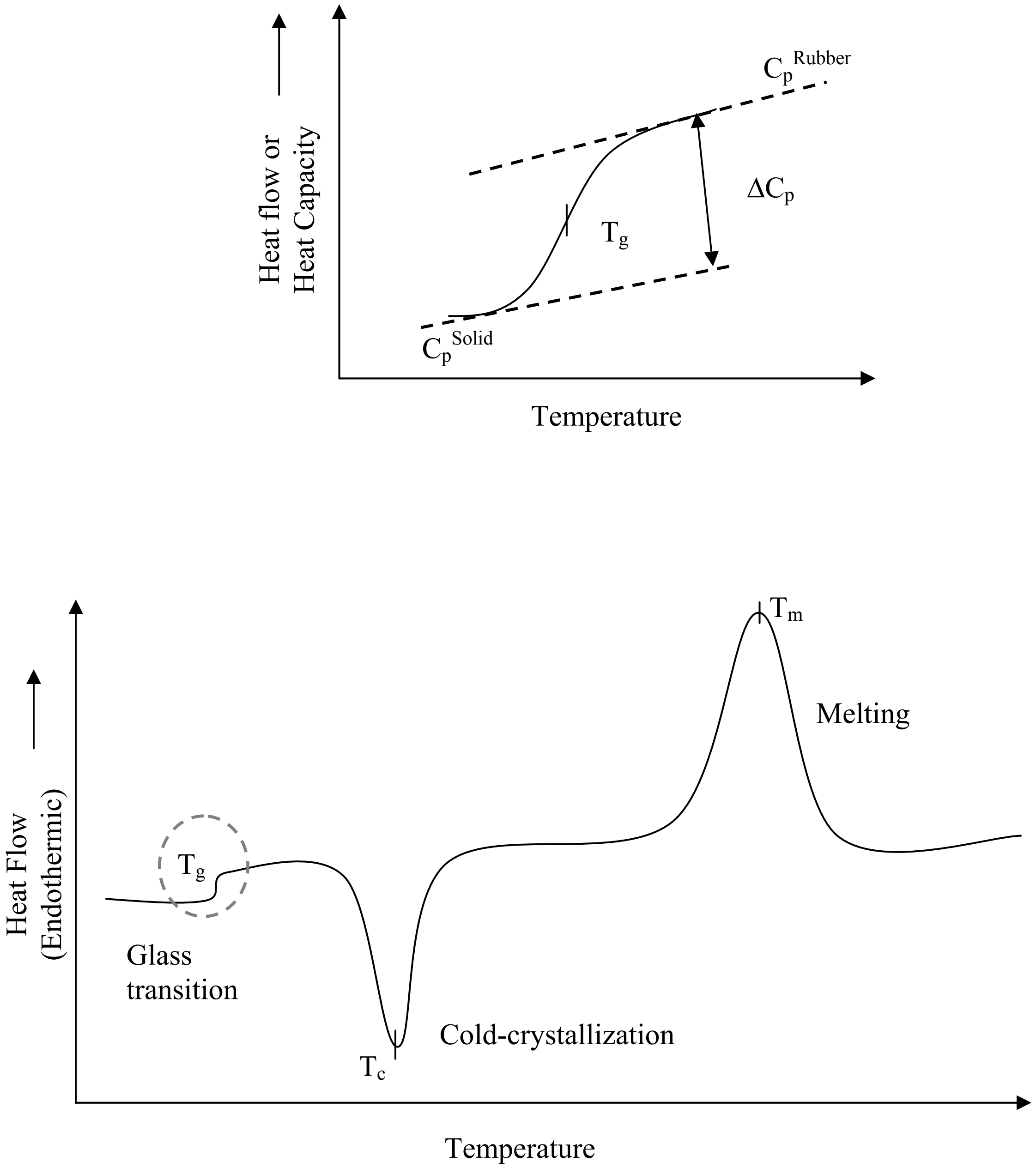
Heat flow or
Heat Capacity
C_p^{Rubber}
ΔC_p
T_g
C_p^{Solid}
Temperature
Heat Flow
(Endothermic)
T_m
Melting
T_g
Glass
transition
Cold-crystallization
T_c
Temperature

Figure 3.16: Typical DSC scan for a semicrystalline polymer. *Inset:* Expanded view of glass-rubber transition and estimation of T_g.

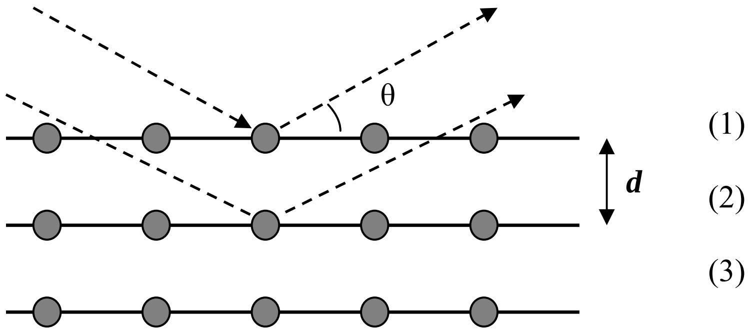

Figure 3.17: Elastic scattering of X-rays from parallel crystal planes (1, 2 & 3) with a characteristic spacing *d*.

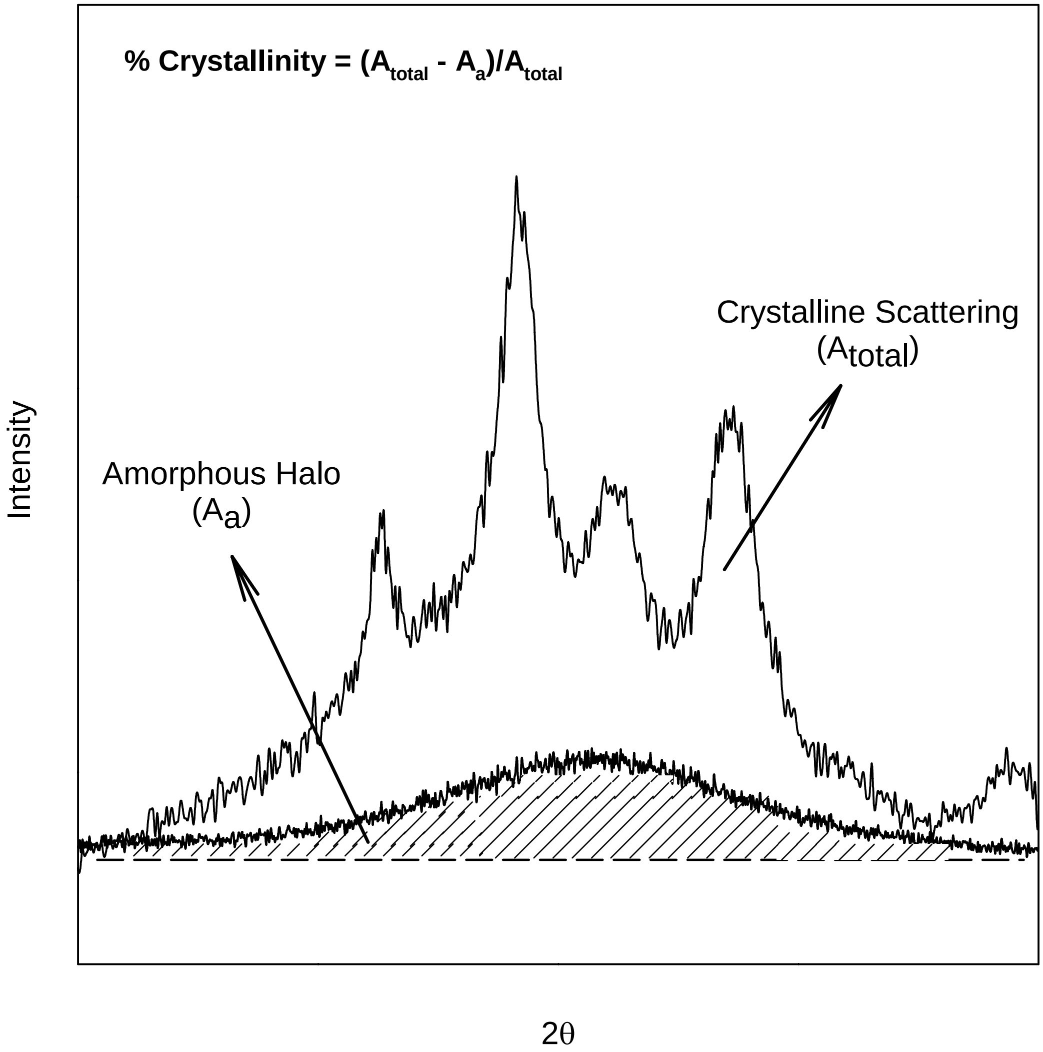

Figure 3.18: Typical WAXS pattern for a semicrystalline polymer plotted as intensity versus scattering angle (*2θ*).

Copyright © Sumod Kalakkunnath 2007

Chapter Four

Segmental Relaxation Characteristics of Crosslinked Poly(ethylene glycol) Networks: A Dynamic Mechanical Study

This chapter is based on work published as:

(i) S. Kalakkunnath, D.S. Kalika, H. Lin, B.D. Freeman, *"Segmental Relaxation Characteristics of Crosslinked Poly(ethylene oxide) Copolymer Networks"*, Macromolecules, **38(23)**, 9679-9687 (2005). Copyright 2005 American Chemical Society.

(ii) S. Kalakkunnath, D.S. Kalika, H. Lin, B.D. Freeman, *"Viscoelastic Characteristics of UV Polymerized Poly(ethylene glycol) Diacrylate Networks with Varying Extents of Crosslinking"*, Journal of Polymer Science Part B: Polymer Physics, **44(15)**, 2058-2070 (2006). Copyright 2006 Wiley Periodicals, Inc.

(iii) R.D. Raharjo, H. Lin, D.F. Sanders, B.D. Freeman, S. Kalakkunnath, D.S. Kalika, *"Relation Between Network Structure and Gas Transport in Poly(propylene glycol diacrylate)"*, Journal of Membrane Science, **283(1-2)**, 253-265 (2006). Copyright 2006 Elsevier Ltd.

4.1 INTRODUCTION

The selective removal of carbon dioxide from mixtures containing light gases is a process of immense industrial importance, and there is growing interest in the implementation of membrane technologies to achieve such separations for a number of applications; *e.g.*, the separation of CO_2 from hydrogen upon steam reforming of hydrocarbons, or the removal of CO_2 from CH_4 for natural gas purification.[111] For many of these applications, membrane materials with high CO_2 permeability and high CO_2/light gas selectivity are desired, so that the CO_2 will permeate to the low pressure side of the membrane, while the light gas component is retained at or near the feed pressure for subsequent transport and use. One method to achieve membranes with high CO_2 permeability and favorable overall CO_2 selectivity is to select and/or tailor materials with high CO_2 solubility and high CO_2/light gas solubility selectivity. The quadrupolar character of CO_2 can be exploited in this regard, since CO_2 will tend to interact favorably with polar groups present in the membrane.[12] A recent review of potential CO_2 interactions has shown ether oxygens to be amongst the most promising polar groups for the achievement of favorable CO_2 solubility and solubility selectivity.[18] The formulation of rubbery polymeric materials incorporating high levels of the flexible ether oxygen moieties should lead to membranes with strong CO_2 solubility, as well as high diffusivity. The net result would be membranes with the potential to deliver the desired separation properties both in terms of overall CO_2 permeability, as well as the purity of the resulting product streams.

Poly(ethylene oxide) [PEO; $\mathbf{-(-OCH_2CH_2-)_n-}$] has been identified as an effective membrane material for the selective separation of quadrupolar-nonpolar gas pairs.[17] However, PEO has a strong tendency to crystallize, and the presence of a significant crystalline fraction reduces permeability in these materials to non-viable levels for industrial separations. One approach to inhibit crystallization in PEO is the introduction of chemical crosslinks. By limiting the number of ethylene oxide segments (n) between crosslink junctions to about 20 or less, fully amorphous crosslinked networks can be obtained.[19,20] The possibility of preparing wholly amorphous networks with high ethylene oxide content suggests a number of potential membrane architectures that could be designed to achieve optimum CO_2 permeability and selectivity characteristics.

The strategic formulation of gas separation membranes based on PEO networks with high CO_2 permeability as well as high CO_2/light gas selectivity requires a fundamental understanding of the relationships between gas transport and the static and dynamic characteristics of the membrane material. In this work, various series of crosslinked polyethylene oxide networks prepared by ultraviolet (UV) photopolymerization of poly(ethylene glycol) diacrylate [PEGDA] (structure shown in Figure 2.1(a)) have been characterized by dynamic mechanical analysis with a focus on assessing how systematic changes in crosslink density affect the physical and gas transport characteristics of the membranes. For the first series of networks, the distance between crosslinks was varied by the photopolymerization of commercial PEG diacrylates with different values of the repeat unit length (*n*); the range of *n* values was limited so that only amorphous networks were obtained. For the second series of networks, the crosslink density was systematically varied by changing the concentration of prepolymer in the reaction mixture (see Figure 2.3).[21-23] The introduction of water into the reaction mixture leads to a decrease in effective crosslink density, as lower prepolymer concentration increases the probability of intramolecular cyclization or loop formation.[23] The resulting loops, which do not contribute to the elastic character of the network, are typically associated with wasted crosslinks. Nonetheless, these crosslinks are effective in suppressing crystallization for the PEG networks. By changing the concentration of prepolymer in the reaction mixture, it is possible to prepare a series of amorphous networks with identical chemical composition, but varying effective crosslink density.

In addition to the materials described above, model networks with varying crosslink density were prepared by copolymerizing PEGDA with either poly(ethylene glycol) methyl ether acrylate [PEGMEA], or poly(ethylene glycol) acrylate [PEGA] (see chemical structures in Figure 2.2(a)). The inclusion of mono-functional acrylate in the reaction mixture leads to the introduction of fixed-length pendant groups in the resulting crosslinked network, as well as an increase in the distance between crosslinks, as illustrated in Figure 2.2(b). For this study, the molecular weights of the acrylates (PEGMEA and PEGA) were selected so as to maintain an approximately constant ethylene oxide (EO) content in the networks (~ 82 wt% EO). As a result, any measured changes in gas transport properties can be attributed to structural variations: *i.e.*, changes in the crosslink density, as well as the nature of the pendant chain end. The key difference between the two copolymer series is the end group associated with the acrylate species: $-OCH_3$ (PEGMEA) versus $-OH$ (PEGA).

Different strategies have been employed for the further optimization of these networks; for example, variation in the chain length of acrylate monomer and/or variation in the crosslinker backbone structure. A series of networks have been prepared by copolymerizing PEGDA with diethylene glycol ethyl ether acrylate [DGEEA] (see structure in Figure 3.1(b)), with a repeat unit length $n = 2$, in order to assess the influence of short pendant groups on the overall physical properties. Further, the basic nature of the network was varied by copolymerizing the crosslinker, poly(propylene glycol) diacrylate [PPGDA], with poly(propylene glycol) methyl ether acrylate [PPGMEA], where both monomers have a propylene oxide (PO) repeat unit (see Figures 3.1 (a) and (b)). This led to networks with more inherent free volume and varying chemical composition. Alternatively, networks have been prepared by copolymerization of a rigid crosslinker, bisphenol A ethoxylate diacrylate [BPAEDA], with PEGMEA and PEGA (see Figure 3.1 (a)). BPAEDA was used as a crosslinker in an effort to increase the mechanical integrity of the resulting networks. Finally, a new generation of PEGDA-based membranes, filled with nanoscale MgO particles, has been examined in anticipation of possible enhancements in bulk gas transport properties.

Dynamic thermal analysis techniques, such as dynamic mechanical analysis, can be used to investigate the segmental relaxation characteristics of crosslinked networks across a wide range of temperature and timescale.[24-27] In polymeric networks, the presence of the crosslinks results in a restriction of segmental mobility in the vicinity of the crosslink junctions. This restriction, which reduces the conformational freedom of the chains, is manifested by an increase in the measured glass transition temperature with increasing crosslink density. The positive offset in T_g is most pronounced at high crosslink densities, where the average distance between crosslinks approaches the length scale characteristic of the local segmental dynamics.[30] In addition to the offset in T_g, inhomogeneous broadening of the glass-rubber relaxation is observed with increasing crosslink density. This broadening reflects the range of local environments experienced by the relaxing segments and their corresponding proximity to the crosslink junctions. For the copolymer networks, the dynamic relaxation characteristics will be influenced not only by changes in crosslink density, but also by the presence of non-reactive oligomeric pendant groups in the network.[24] Further, an increase in intermolecular cooperativity is typically encountered at higher degrees of crosslinking, with greater time-temperature sensitivity and correspondingly larger apparent activation energies associated with the relaxation process.[112,113] Such behavior has been shown to increase the "fragility" of the network with increased crosslinking.[43,44,114]

In this chapter, dynamic mechanical analysis was employed as a means to measure the relaxation characteristics and the bulk mechanical properties (*i.e.*, modulus) for the different series of crosslinked networks described above. By application of time-temperature superposition methods,[38] it was possible to establish modulus-frequency master curves over the entire range of the glass-rubber relaxation (12-16 decades in frequency), and the resulting curves could be satisfactorily described by the Kohlrausch-Williams-Watts [KWW] stretched exponential function.[39] The construction of fragility plots was used to assess changes in intermolecular cooperativity with varying network structure.[43,44] The characteristics of the networks were subsequently related to their gas transport properties.

4.2 EXPERIMENTAL

4.2.1 Materials

Poly(ethylene glycol) diacrylate [PEGDA: Mol.Wt. = 258, 575, and 700 g/mol], poly(propylene glycol) diacrylate [PPGDA: Mol.Wt. = 900 g/mol], bisphenol A ethoxylate diacrylate [BPAEDA: Mol.Wt. = 688 g/mol], poly(ethylene glycol) methyl ether acrylate [PEGMEA: Mol.Wt. = 460 g/mol], poly(ethylene glycol) acrylate [PEGA: Mol.Wt. = 380 g/mol], di(ethylene glycol) ethyl ether acrylate [DGEEA: Mol.Wt. = 188 g/mol] and poly(propylene glycol) methyl ether acrylate [PPGMEA: Mol.Wt. = 202 g/mol] were purchased from Aldrich Chemical Company (Milwaukee, WI); the nominal molecular weights provided by the supplier are as indicated. 1-hydroxylcyclohexyl phenyl ketone [HCPK] initiator was also purchased from Aldrich. All reagents were used as received. The inorganic MgO nanoparticles (nominal diameter: 2.5nm, specific surface area: 640 m^2/g) were obtained from NanoScale Materials, Inc. (Manhattan, KS).

Proton nuclear magnetic resonance (^1H NMR) and fast atom bombardment mass spectrometry (FAB-MS) were used to verify the molecular weight of the prepolymers; all ^1H NMR and FAB-MS measurements were completed at the University of Texas at Austin. For PEGDA with the highest molecular weight, ^1H NMR indicated a value of 743 g/mole, which corresponds to a monomeric repeat value of $n \sim 14$. For the other monomers, the measured values were: PPGDA (n=12), BPAEDA (n=4), PEGMEA (n=8), PEGA (n=7), DGEEA (n=2) and PPGMEA (n=2), respectively. In addition, FAB-MS measurements indicated a narrow distribution of molecular weight in all cases (polydispersity index < 1.10). The molecular weights were in good agreement with the values reported by the supplier; additional experimental details have been reported previously.[115]

4.2.2 Polymer preparation

Prepolymer solutions were prepared by adding 0.1 wt.% initiator (HCPK) to the appropriate diacrylate-acrylate liquid blend of required concentration. For the PEGDA-water system, a known amount of ultrapure water was added to the prepolymer mixture to achieve the target composition. After stirring, each solution was sonicated for 10 minutes to eliminate bubbles (Ultrasonic cleaner, Model FS60, Fisher Scientific, Pittsburg, PA). The solution was sandwiched between two quartz plates, which were separated by spacers to control film thickness. The dimensions of the spacers were varied in order to obtain consistent thickness in the final (dried) polymer films. The solution was polymerized by exposure to 312 nm UV light in a UV Crosslinker (Model FB-UVXL-1000, Fisher Scientific) for 90 seconds at 3 mW/cm^2. The solid films obtained by this process were three dimensional networks and contained a negligible amount of low molecular weight polymer (*i.e.*, sol) that was not bound to the network. After polymerization, the PEGDA- and PPGDA-based samples were extracted using toluene in a Soxhlet extraction system. Virtually no measurable weight change was observed in the films before and after extraction, confirming that essentially no unbound sol was present in the as-polymerized networks. For the remaining network systems, immersion in a large amount of ultrapure water was found to be sufficient to remove the low molecular weight sol, if present. The PEGDA nanocomposite membranes were prepared by inclusion of appropriate amounts of MgO particles in the prepolymer reaction mixture, followed by UV photopolymerization as described above.

Attenuated total reflection Fourier transform infrared spectroscopy (FTIR-ATR) was used to determine the conversion of acrylate groups in the films (see ref. 115 for experimental details). The disappearance of acrylate double bonds due to polymerization leads to the decrease of sharp peaks at 810 cm^{-1} (ascribed to the twisting vibration of the acrylic CH_2=CH bond),[116] at 1410 cm^{-1} (deformation of the CH_2=CH bond)[117,118] and at 1190 cm^{-1} (acrylic C=O bond).[117]

4.2.3 Dynamic Mechanical Analysis

Dynamic mechanical thermal analysis was performed using a Polymer Laboratories DMTA operating in single cantilever bending geometry. The dried polymer films had a thickness of 0.8-1.0 mm and were held under vacuum at room temperature prior to measurement. Storage modulus (E') and loss tangent ($tan\delta$) were recorded at a heating rate of 1°C/min with test frequencies in the range of 0.1 to 10 Hz; all measurements were carried out under inert (N_2) atmosphere. Dynamic mechanical transition temperatures were established according to the peak in $tan\delta$ at 1 Hz; based on the heating and data collection rates inherent to the dynamic mechanical measurements, the precision associated with the peak temperatures was ± 1°C.

4.2.4 Permeation and Sorption measurements

CO_2 pure gas permeability in the solid polymer networks was measured using a constant-volume, variable pressure apparatus.[115] Gas solubility was determined using a dual-volume, dual-transducer unit based on the barometric, pressure-decay method. CO_2

diffusion coefficients at infinite dilution were calculated based on the measured values of permeability and solubility, as discussed in ref. 115. All transport measurements reported herein were conducted at the University of Texas at Austin.

4.3 RESULTS AND DISCUSSION

4.3.1 Dynamic Mechanical Analysis

4.3.1.1 Networks based on variation in PEGDA molecular weight

Three amorphous networks were prepared via the UV polymerization of 100% PEGDA with varying molecular weight. Based on the molecular weight values reported by the supplier, and the ^{1}H NMR and FAB-MS studies described above, these networks corresponded to crosslinked PEGDA with nominal n values of 3, 10, and 14, respectively.

Polymerization of acrylate monomers using ultraviolet radiation is a well-established technology. Acrylate double bonds exhibit high reactivity, with rapid conversion of the acrylate groups under typical polymerization conditions.**[119]** A full discussion of the UV polymerization of PEGDA and the corresponding reaction parameters selected for this work (*i.e.*, choice and amount of initiator, reaction time) is presented in ref. 115.

FTIR-ATR was used to probe the amount of unreacted acrylate groups in the resulting polymer networks. For those networks that remained rubbery throughout the polymerization reaction, essentially 100% conversion of acrylate groups was achieved, as verified by the complete disappearance of the characteristic acrylate peaks in the corresponding IR spectra.**[115]** This was the case for the networks prepared using the n=10 and n=14 PEGDA monomers. For the network based on the n=3 PEGDA monomer, however, crosslinking leads to a glassy material at room temperature, with FTIR-ATR indicating a small amount of unreacted acrylate groups in the resulting films. **Figure 4.1** compares spectra from the liquid PEGDA (n=3) with spectra taken from both sides of the crosslinked polymer film; the carbonyl (C=O) band at 1725 cm^{-1} was used as a reference to facilitate comparison of the spectra. Examination of the characteristic peaks at 810, 1190, and 1410 cm^{-1} verifies that residual acrylate groups are present in the network, most likely as dangling chain ends. In addition, there appears to be a modest dependence on film depth, with the film surface originally positioned closer to the UV source (labeled "top" in Figure 4.1) showing a higher extent of acrylate conversion. Conversion estimates based on the relative area of the 810 cm^{-1} peak indicate an overall conversion of ~95% at the top surface, and ~88% at the bottom surface (film thickness of 1.0 mm).

The presence of unreacted acrylate groups (and possibly trapped radicals) in the networks suggests the possibility of additional reactions occurring upon heating of the crosslinked polymer films during thermal analysis studies.**[26]** To assess the effect of higher temperature exposure, the crosslinked PEGDA film (n=3) was annealed under vacuum at 100°C for one hour; the resulting IR spectra are shown in Figure 4.1. The annealing, which was intentionally conducted at a temperature above the glass transition, led to additional acrylate conversion, especially at the bottom surface of the film. The overall acrylate conversion for the annealed film was estimated to be 95 to 97%.

Dynamic mechanical results over the entire temperature range studied (−120°C to 20°C) are presented for the 100% PEGDA (n=14) network in **Figure 4.2**. Storage modulus and $tan\delta$ are plotted isochronally for five measurement frequencies ranging from 0.1 to 10 Hz. The data show a clear, step-wise decrease in modulus centered at −35°C that corresponds to the glass-rubber relaxation in these fully crosslinked networks. The drop in modulus is accompanied by a narrow peak in $tan\delta$ which shifts to higher temperatures with increasing frequency (*i.e.*, decreasing experimental timescale). The nominal glass transition temperature, T_α, is defined here as corresponding to the peak in $tan\delta$ at a frequency of 1 Hz. For 100% PEGDA, T_α = −35°C. **Figure 4.3** compares the 1 Hz dynamic mechanical data for the three (n = 3, 10, 14) PEGDA networks. For the n=10 and n=14 networks, a sharp step-change in storage modulus (E') is evident in the vicinity of the glass-rubber relaxation; the transition is considerably broadened for the n=3 material with a shift observed in T_α to higher temperatures with decreasing PEGDA molecular weight (*i.e.*, decreasing segmental length between crosslinks).

The dynamic mechanical transition temperatures for the networks are reported in **Table 4.1**. The strong positive offset in T_α, as well as the observed broadening of the glass transition, indicates that the distance between crosslinks for these samples is sufficiently short so as to approach the length scale associated with segmental relaxation. The presence of the crosslinks leads to local constraint of those segments positioned closest to the network junctions, and the degree to which the segmental motion is hindered will vary with varying distance from the crosslink site. The net result is an inhomogeneous broadening of the relaxation in the temperature or frequency domain, and a shift of the relaxation to higher temperatures.

Classical rubber elasticity theory is often used to relate the measured mechanical modulus in the rubbery plateau region to the effective crosslink density.[35-37] Theory predicts that the molecular weight between crosslinks should correlate with the ratio T/E_R, where T is absolute temperature and E_R is the corresponding rubbery modulus.[27] **Figure 4.4** shows a plot of T/E_R versus n for the three PEGDA networks. The values of E_R were determined by the construction of time-temperature master curves for each network in the vicinity of its corresponding glass transition (see discussion of time-temperature superposition, below). Figure 4.4 reveals a direct correlation between the measured rubbery modulus (expressed as T/E_R) and the nominal distance between crosslinks, as established by the molecular weight of the PEGDA prepolymer.

Dynamic mechanical results in the sub-glass region are provided as plots of tanδ versus temperature in **Figure 4.5** (10 Hz). For the highly crosslinked n=3 network, two distinct sub-glass relaxations are evident, labeled β_1 and β_2, respectively, with increasing temperature. Sub-glass relaxations in polymers typically reflect highly-localized processes such as side-group rotations, or limited in-chain motions.[67] Given the relatively smooth, flexible character of the PEG segments, it is not difficult to envision local relaxations occurring along these segments even at very high crosslink densities.

Mechanical and dielectric studies of crystalline PEO indicate two relaxations that originate in the amorphous regions of the polymer:[67] a cooperative process corresponding to the glass transition, and a non-cooperative process corresponding to local twisting along the PEO segments (γ relaxation).[120] Recently, Runt and co-workers have reported dielectric results wherein two sub-glass (γ) relaxations were observed for PEO, and these relaxations were attributed to local mode motions occurring (i) along amorphous PEO segments well-removed from the crystal surface, and (ii) within more constrained PEO segments, located closer to the crystal-amorphous interface (*i.e.*, order-disorder transition region).[121] Based on this finding, two distinct topological origins can similarly be inferred for the two sub-glass relaxations observed in the n=3 network, with the β_1 relaxation corresponding to localized motions occurring farther from the crosslink junctions, and the β_2 relaxation reflecting more constrained motions occurring closer to the crosslink points.

Dynamic mechanical scans for the n=10 and n=14 networks do not display a clear, dual-relaxation behavior in the sub-glass region. For the n=10 network, there is an indication of a very shallow lower temperature relaxation centered at about −110°C, while for the n=14 network, only a single sub-glass relaxation is observed. However, broadband dielectric studies on these networks show two distinct sub-glass relaxations (details in Chapter 5). The failure to observe two sub-glass mechanical relaxations in these samples may be due to the localized, non-cooperative character of the ethylene oxide motions, which have only a very weak influence on the bulk mechanical response of the material when originating away from the crosslink junctions. Also, the position of the β_1 relaxation for the n=14 network may simply lie outside the accessible temperature range of our dynamic mechanical instrument (*i.e.*, below −120°C). The $tan\delta$ peak temperatures for the sub-glass relaxations are reported in Table 4.1; the β_2 transition is offset to progressively higher temperatures with increasing crosslink density.

Time-temperature superposition was used to construct modulus-frequency master curves in the vicinity of the glass transition.[38] A representative result for the n=14 network is provided in **Figure 4.6**; the inset shows the shift factor (a_T) as a function of temperature.

The glass-rubber relaxation can be described using the Kohlrausch-Williams-Watts (KWW) "stretched exponential" relaxation time distribution function:

$$\phi(t) = \exp[-(t/\tau_o)^{\beta}] \qquad [2.9]$$

where τ_o is the observed relaxation time and β is the distribution parameter. β ranges in value from 0 to 1, with values close to unity corresponding to a narrow, single relaxation time (*i.e.*, Debye) response. Lower values of β reflect increased intermolecular coupling, as well as inhomogeneous relaxation broadening owing to the presence of crosslinks.[29] Series approximations reported by Williams *et al.* express modulus and loss for the KWW model in the frequency domain, and these equations were used as the basis for the curve fits reported here.[39] The KWW modulus curve for PEGDA (n=14) is included in Figure 4.6, with a corresponding value of the distribution parameter, $\beta = 0.30$.

Modulus master curves for all three PEGDA networks are shown in **Figure 4.7**. The data are presented as modulus versus ωa_T, where ω is the applied test frequency ($\omega = 2\pi f$, with f expressed in Hz) and a_T is the shift factor. Since each master curve was constructed using a different reference temperature, the data were shifted along the horizontal axis based on their respective relaxation time, τ_o. Specifically, modulus is plotted versus $\omega a_T/\omega_o$, where $\omega_o = 1/\tau_o$. Figure 4.7 clearly shows the increase in relaxation breadth encountered with increasing crosslink density for the PEGDA samples, with the KWW distribution parameter varying from 0.30 (n=14) to 0.11 (n=3).

The time-temperature shift factor for each network is plotted versus reciprocal temperature (*i.e.*, Arrhenius plot) in **Figure 4.8**. For all three networks, those data corresponding to temperatures $T > T_g$ could be satisfactorily fit to the Williams-Landel-Ferry (WLF) equation.[38] The observed deviation of the data from the WLF relation at lower temperatures (higher values of $1/T$) is consistent with behavior reported for other networks (*e.g.*, crosslinked poly(methyl methacrylate)), and correlates with the transition of the material into the glassy state.[25] The deviation of the shift factor near T_g results in a relative maximum in the apparent activation energy, which is reflected in the local slope of the data.

4.3.1.2 PEGDA networks prepared with varying initial amounts of prepolymer

PEGDA (*n*=14) networks were prepared with varying proportions of prepolymer and ultrapure water in the reaction mixture in order to produce chemically-identical crosslinked materials with systematic variation in the effective crosslink density.[22,23] The materials remained fully rubbery throughout the reaction process and subsequent drying, such that there was no network collapse during the drying process. Modulus versus temperature curves for the networks are shown in **Figure 4.9**. As discussed earlier, it was anticipated that a reduction in the concentration of prepolymer would lead to increased loop formation (*i.e.*, wasted crosslinks) and a lower effective crosslink density. This is evident in the progressive decrease in E_R (rubbery plateau modulus) with increasing water content in the reaction mixture, suggesting that from an elastic response standpoint, a much looser network is obtained at lower prepolymer concentrations. The results are consistent with equilibrium water swelling measurements for these same networks, which indicate a progressive decrease in the calculated crosslink density with decreasing PEGDA content in the reaction mixture.[115]

Although a systematic variation in effective crosslink density is indicated for the PEGDA/water networks, virtually no change in the glass-rubber relaxation temperature (T_α) is observed with varying reaction mixture composition ($T_\alpha = -34$°C; see **Table 4.2**). The invariance of T_α suggests that the segmental motions associated with the glass transition occur over a length scale such that the observed relaxation time is minimally affected by the underlying structural changes in the network brought about by lowering the prepolymer concentration. However, the observed decrease in effective crosslink density does lead to a narrowing of the glass-rubber relaxation process. **Figure 4.10** shows the time-temperature master curves for the PEGDA/water samples, along with the corresponding KWW curve fits. For the 80/20 and 50/50 PEGDA/water networks, satisfactory KWW fits are obtained across the entire frequency range of the relaxation, with corresponding values of the distribution parameter (β) equal to 0.37 and 0.39, respectively. For the 20/80 PEGDA/water network, the KWW function can only be fit at relatively high frequencies, with a corresponding value of β = 0.47. The progressive increase in β (re: Table 4.2) is consistent with an overall narrowing of the glass transition for these networks, the loosening of the elastic constraints leading to a more homogenous segmental relaxation environment.

One method by which to assess changes in the character of the segmental relaxation in these networks is via the construction of fragility or cooperativity plots, normalized, semi-logarithmic Arrhenius plots of shift factor [log(a_T)] versus T_α/T in the vicinity of the glass transition.[29,43] **Figure 4.11** shows the cooperativity curves for the PEGDA/water networks, with the solid lines corresponding to WLF fits to the data. The curves show a decrease in slope (*i.e.*, decreasing temperature sensitivity) at lower effective crosslink density. This behavior suggests a corresponding reduction in the intermolecular cooperativity inherent to the glass transition as the networks become more open, with less overall segmental constraint. The results obtained for the PEGDA/water (diluent) series are largely consistent with previous studies on polymeric networks (*e.g.*, poly(vinylethylene),[29,113] poly(dimethylsiloxane),[30] poly(methyl methacrylate)[25]) wherein crosslink density was controlled stoichiometrically.

The sensitivity of the glass-rubber relaxation time (or corresponding shift factor) to temperature can be interpreted in terms of the dynamic fragility of the material. Materials that display strong degradation of structure with temperature (*i.e.,* high temperature sensitivity) are designated as “fragile” liquids, and their relaxation typically reflects a high degree of intermolecular coupling. Polymers with compact, flexible backbones that lack pendant groups tend to experience less intermolecular constraint, and as a result display lower fragility.[44] This would presumably be the case with the ethylene oxide segments that comprise the PEGDA network. The fragility (or steepness) index, *m*, can be determined based on the slope of each cooperativity curve evaluated at $T = T_{REF}$ according to the following expression:

$$m = \left.\frac{d\log(\tau)}{d(T_{REF}/T)}\right|_{T=T_{REF}} = \left.\frac{d\log(a_T)}{d(T_{REF}/T)}\right|_{T=T_{REF}} \qquad [2.11]$$

where $a_T = \tau/\tau_{REF}$.

The value of *m* depends upon the definition of T_{REF}: for the glass transition, the convention has been to assign T_{REF} such that the corresponding relaxation time, $\tau(T_{REF}) = 100$ seconds. Values of the fragility index determined on this basis range from $m = 16$ (strong limit) to $m \geq 200$ (fragile limit);[122] tabulations of dynamic and thermodynamic fragility have been reported in the literature for a variety of polymers and small molecule glass formers.[114,122,123] The value of *m* can be related to the apparent activation energy (E_A) evaluated at T_{REF}:

$$m = \frac{E_A(T_{REF})}{2.303RT_{REF}} \qquad [2.12]$$

where *R* is the gas constant. For the data reported here, the convention $T_{REF} = T_\alpha$ (peak temperature at 1 Hz) has been adopted, which is appropriate given the range of experimental frequencies used in the measurements. In this context, the value of *m* should be considered a relative quantity: direct comparisons of the fragility index with other values reported in the literature are valid only if T_{REF} is assigned to the same relaxation time.

For the 100% PEGDA network (n=14), the data presented in Figure 4.11 indicate a value of $m = 78$. As the effective crosslink density is reduced, the fragility index is observed to decrease. Values of *m* for the PEGDA/water series of networks were calculated to be 72 (80/20 PEGDA/water), 66 (50/50) and 49 (20/80), respectively. The corresponding values of E_A, evaluated at T_α, are reported in Table 4.2. For a wide range of materials, an inverse relationship has been reported between the KWW distribution parameter (β) and the fragility index (m).[122] That is, an increase in the overall breadth of the relaxation (decreasing value of β) tends to correlate with an increase in fragility. This behavior is observed for the PEGDA/water network series studied here, demonstrating an apparent linkage between the degree of non-exponentiality as encompassed in equation 2.9, and the extent of intermolecular cooperativity.

The overall viscoelastic characteristics of the PEGDA/water networks, wherein effective crosslink density was changed by the introduction of varying amounts of water in the reaction mixture, are comparable to those reported for other network series prepared with controlled crosslink density. In general, higher levels of crosslinking lead to broader relaxations, evidence of greater intermolecular cooperativity, and, at the highest crosslink densities, a positive offset in glass transition temperature. For the networks prepared using PEGDA with n=14, no variation in T_α was observed, despite the clear changes in effective crosslink density as evident in the rubbery modulus, as well as in water swelling measurements. This outcome would seem to indicate that for networks based on the n=14 prepolymer, the distance between crosslink junctions is such that any reduction in local constraint brought about by the presence of the diluent during crosslinking would not be manifested by a change in the glass transition temperature. Typically, variations in the measured glass transition temperature can be correlated with changes in the fractional free volume (FFV), and for the PEGDA/water series, the invariance of T_α would imply a constant FFV.[18] Independent determinations of FFV in the networks via density measurements are consistent with this expectation, and show relatively little variation across the series (see Table 4.2).[115] As a result, the PEGDA/water networks present an exceptional opportunity to investigate the influence of network structure on gas transport properties independent of changes in network composition or fractional free volume (see discussion of gas transport properties in Section 4.3.2).

4.3.1.3 PEGDA networks prepared with varying amounts of acrylate monomer

Dynamic mechanical results for the PEGDA/PEGMEA series of copolymers (1 Hz) are presented in **Figure 4.12**. For the various copolymer samples studied, the ratio of PEGDA to PEGMEA in the initial reaction mixture is indicated on a weight basis (*e.g.*, 80/20 PEGDA/PEGMEA corresponds to a network based on 80 wt% PEGDA, 20 wt% PEGMEA). The data show a progressive decrease in the glass-rubber relaxation temperature with PEGMEA content, as both the step change in E' and peak in $tan\delta$ are shifted to the left with increasing PEGMEA. The T_α values for the series are reported in **Table 4.3**, as well as glass transition temperatures (T_g) determined by DSC.[124] The T_α and T_g values show good overall correspondence. The small, consistent difference between T_α and T_g (~ 5°C) reflects the inherent difference in experimental timescale for the dynamic mechanical (1 Hz) and DSC measurements.

The introduction of an increasing amount of PEGMEA in the reaction mixture leads to a corresponding decrease in the crosslink density of the network. This decrease in crosslink density is manifested by a decrease in the storage modulus in the rubbery plateau region (E_R). For the 30/70 PEGDA/PEGMEA sample, the crosslink density is insufficient to fully suppress PEO crystallization in the network. This is evident in the modulus-temperature curve for the 30/70 specimen, which shows an increase in E' just above the glass transition that appears to correspond to the onset of cold crystallization. For the dynamic mechanical measurements, the samples were mounted in the dynamic mechanical thermal analyzer at room temperature, and then cooled rapidly to the start temperature of −120°C (effective cooling rate of −15°C/min). Given the relatively rapid cooling rate, it is likely that the sample initially contained little or no crystallinity. The subsequent dynamic mechanical heating scan was conducted at a much slower rate (+ 1°C/min), allowing the sample ample time to crystallize in-situ upon passing the glass transition, followed eventually by the onset of melting at −20°C. The room temperature modulus then corresponds to a fully amorphous, rubbery material. The observed behavior is consistent with DSC sweeps (20°C/min) conducted on these copolymers, which showed cold crystallization exotherms for copolymers containing high levels of PEGMEA.[124]

The decrease in glass transition temperature observed for the PEGDA/PEGMEA series is attributable primarily to the introduction of pendant groups along the network backbone. For the PEGDA/water networks described earlier, no variation in T_α nor fractional free volume (FFV) was observed with varying effective crosslink density. By contrast, for the PEGDA/PEGMEA films, a significant decrease in T_α is encountered with the reduction in crosslink density that accompanies copolymerization of the PEGMEA. A systematic increase in FFV for the PEGDA/PEGMEA films is also observed over the range of compositions examined (see Table 4.3).**[124]** Although the topographical details for the PEGDA/water and PEGDA/PEGMEA systems are likely to be quite different, the contrast in their glass transition characteristics suggests that the key structural element for the observed behavior in the PEGDA/PEGMEA series is the flexible pendant branches, which lead to both a greater fractional free volume and a correspondingly shorter relaxation time.

Dynamic mechanical data for the PEGDA/PEGA series are provided in **Figure 4.13**. The results are similar to those obtained for the PEGDA/PEGMEA specimens, with both a negative shift in T_α and a progressive decrease in rubbery modulus observed with increasing PEGA content. For the PEGDA/PEGA series, however, the relative downward shift in relaxation temperature over the composition range is much less ($\Delta T_\alpha = T_\alpha^{30/70} - T_\alpha^{100/0} = -7°\mathrm{C}$) as compared to the PEGDA/PEGMEA system ($\Delta T_\alpha = -17°\mathrm{C}$). Also, neither crystallization nor melting is observed during the dynamic mechanical scans. As noted above, the main structural difference between the PEGMEA and PEGA components is the pendant end group, *i.e.*, $-\mathrm{OCH_3}$ versus $-\mathrm{OH}$.

Dynamic mechanical results in the sub-glass transition region are presented as plots of $\tan\delta$ versus temperature (10 Hz) in **Figure 4.14** (PEGDA/PEGMEA) and **Figure 4.15** (PEGDA/PEGA). In all cases, only a single broad sub-glass relaxation is observed, designated as the β relaxation. The corresponding peak temperatures, T_β, are reported in Table 4.3. Notably, however, dielectric studies on crosslinked PEGDA and the copolymer networks show two sub-glass transitions across the same temperature range (see Sections 5.3.2 and 5.3.4, respectively), which is consistent with the DMA data for PEGDA (n=3) and previously reported dielectric results for crystalline PEO.**[121]** For the crosslinked copolymer networks studied here, isolated motions well removed from the crosslink junctions would have only a very weak influence on the bulk mechanical properties of the network, and they would be difficult to detect via dynamic mechanical measurements. As such, the single (β) relaxation that is observed most likely reflects local motions that occur in relatively close proximity to the crosslink junctions, leading to a stronger overall mechanical response. This scenario is consistent with the observed negative shift in T_β with increasing acrylate content (re: PEGDA/PEGMEA series), as the resulting decrease in crosslink density and increased branch content would presumably lead to a less constrained local relaxation environment.

Time-temperature superposition was used to construct modulus-frequency master curves for the crosslinked copolymer networks at a common reference temperature of −40°C.[38] Examination of the time-temperature master curves in **Figure 4.16** clearly shows a systematic variation in relaxation time and rubbery modulus with increasing acrylate co-monomer in the network. The rubbery plateau modulus (E_R), as determined by the KWW fits at −40°C, is plotted versus network composition in **Figure 4.17**. In addition to the data for the PEGDA/PEGMEA and PEGDA/PEGA series, results for the networks based on PEGDA/water (re: Figure 4.10) are also included. According to classical rubber elasticity theory, the mechanical modulus measured in the rubbery plateau region should be proportional to the crosslink density.[35-37] In Figure 4.17, a single relationship is evident between rubbery modulus and PEGDA content for all three network systems. This implies that the effective crosslink density in the various networks depends solely on the amount of PEGDA crosslinker present in the reaction mixture, even though the structural details of the resulting networks may differ substantially.

In **Figure 4.18**, the KWW parameters (τ_o, β) are plotted versus PEGDA content for the various networks. For both the PEGDA/PEGMEA and PEGDA/PEGA series, τ_o decreases with decreasing PEGDA fraction at a fixed reference temperature. This behavior reflects the shift in glass transition to lower temperatures (or higher frequencies) with increasing co-monomer content. A decrease in PEGDA crosslinker also leads to a progressive increase in the KWW distribution parameter (β), reflecting a narrowing of the glass-rubber relaxation with decreasing crosslink density; the trend is consistent across all three network systems examined. The observed narrowing of the glass-rubber relaxation with decreasing crosslink density suggests an overall reduction of the elastic constraints imposed by the crosslink junctions, leading to a more homogeneous segmental relaxation environment; this result is in agreement with KWW parameters reported for other networks of varying crosslink density.[25-28,30] For the networks examined here, comparable relaxation narrowing is observed regardless of the method used to reduce crosslink density; *i.e.*, either through the addition of diluent to the reaction mixture, or via copolymerization and the introduction of flexible pendant branches in the network.

Figures 4.19 and **4.20** show cooperativity plots for the PEGDA/PEGMEA and PEGDA/PEGA networks, respectively, based on the T_α values reported in Table 4.3. The solid curves correspond to WLF fits to the data. For both series of networks, the curves show a decrease in slope (*i.e.*, decrease in time-temperature sensitivity) with decreasing crosslink density. This behavior suggests a net decrease in the intermolecular cooperativity inherent to the glass transition with a reduction in crosslink density and concomitant introduction of flexible PEG branches within the network. The trend is consistent with results reported for other homopolymer networks with varying crosslink density.[25,29,30] The activation energies, $E_A(T_\alpha)$, and fragility values for PEGDA and the copolymer networks are reported in **Table 4.4**. For both copolymer systems, a progressive decrease in the fragility value is evident with increasing acrylate content, indicating a lower degree of intermolecular cooperativity across the glass transition with decreasing crosslink density; this result is very similar to the trend obtained for the PEGDA/water networks. As noted above, an inverse relation has been reported between the KWW distribution parameter (β) and the fragility index (m).[122] Increases in the distribution parameter, which are indicative of a narrowing of relaxation breadth, tend to correlate with a decrease in the fragility value. Such a correlation is observed for the PEGDA copolymer networks, as demonstrated in **Figure 4.21**.

The segmental relaxation characteristics of the PEGDA copolymer networks, and their relation to variations in crosslink density, are largely consistent with the behavior reported for other polymer networks with controlled crosslink density. The systematic decrease in crosslink density (with no net change in chemical composition) achieved by the copolymerization of flexible pendant groups into the network leads to a narrowing of the glass transition that reflects a more homogeneous relaxation environment, as the constraining influence of the acrylate junctions is reduced. This is accompanied by a decrease in fragility index, suggesting less intermolecular cooperativity inherent to the glass-rubber relaxation. These trends, which are common to many homopolymer network systems with varying crosslink density, would seem to indicate that the relaxation mechanism in the PEGDA networks is not substantially changed upon introduction of the pendant branches. That is, the segmental motions that occur along the ethylene oxide linkages of the branches (n = 7 or 8 in length) are likely to be quite similar in character to those occurring across the crosslinked PEGDA bridges (n=14). As such, the underlying motional origin of the glass transition appears to remain more or less the same. However, the introduction of the pendant branches does lead to a decrease in the measured glass transition temperature for the copolymer networks, as the non-reactive chain ends introduce defects into the network structure. This effect is more pronounced for the PEGMEA co-monomer ($-OCH_3$ chain end) as compared to PEGA ($-OH$ end group) and is accompanied by a systematic increase in fractional free volume for the PEGDA/PEGMEA series (refer to Table 4.3). Notably, for the PEGDA/PEGA series, a modest decrease in FFV is observed with increasing PEGA content.

4.3.1.4 PEGDA networks prepared with varying amounts of short-branch acrylate monomer

Dynamic mechanical data for PEGDA networks copolymerized with the short branch DGEEA monomer are shown in **Figure 4.22**: these copolymers exhibit a substantial reduction in crosslink density with increasing DGEEA content as manifested by the strong decrease observed in the rubbery plateau modulus (E_R) (see Figure 4.22). The nominal glass transition temperature (T_α; 1 Hz peak value) varies by 3°C over the range of sample compositions examined indicating only a modest decrease in T_α with co-monomer content, a result that is consistent with the DSC measurements (see **Table 4.5**). This is in contrast to the PEGDA/PEGMEA copolymers, which show a much larger drop in T_α over the same composition range. The key difference for the PEGDA/DGEEA series is the shorter repeat unit length of the acrylate monomer. The DGEEA monomer, with a repeat unit length of $n = 2$, is inserted into the PEGDA network as short branch defects. While the short branches produce a net increase in FFV that is comparable to the result for PEGDA/PEGMEA, they are closer to bulky pendants rather than flexible branches, and this limits the decrease in glass transition temperature that might otherwise be expected based on the reduction in crosslink density and corresponding increase in FFV.[125] This trend in T_α is consistent with dynamic mechanical results reported for PEGDA networks prepared with even shorter (n=1) branched, $-OCH_3$ terminated acrylate monomer.[126]

Time-temperature superposition was used to construct master curves of storage modulus (E') versus frequency at a reference temperature of –40°C;[38] results for the complete PEGDA/DGEEA series with corresponding KWW curve fits are shown in **Figure 4.23**. The β parameter values indicate an overall narrowing of the relaxation at higher DGEEA content, possibly due to the net decrease in crosslink density. However, this behavior is not as strong when compared to the PEGMEA series of networks. It is speculated that the DGEEA branches impart a certain degree of heterogeneity to the network owing to their substantially short length as compared to the flexible bridging groups. This could possibly result in a trade off between the crosslink density and pendant content leading to a lesser degree of narrowing.

Figure 4.24 shows cooperativity plots for the PEGDA/DGEEA networks, with T_α corresponding to the dynamic mechanical peak temperature for each network at a frequency of 1Hz. Each data set has been successfully described by the non-linear Williams-Landel-Ferry (WLF)[38] equation (see solid curves in Figure 4.24). The activation energy (E_A) (slope of each curve at T_α) and the fragility index (m) (calculated as per equation 2.11) are reported in Table 4.5. Addition of small amounts of DGEEA monomer into the PEGDA network results in the reduction of the time-temperature sensitivity (and hence the intermolecular cooperativity) associated with the glass-rubber relaxation of the network. This is reflected in the decrease in activation energy and fragility index with decrease in crosslink density as compared to a 100% PEGDA network, as seen for the 80/20 PEGDA/DGEEA copolymer. However, further increases in the amount of co-monomer fail to decrease the intermolecular cooperativity to a significant degree.

4.3.1.5 PEGDA networks prepared with variation in crosslinker

Networks prepared with PPGDA crosslinker

Dynamic mechanical results for networks formed from 100% PPGDA crosslinker (n = 12), as well as for films prepared from the copolymerization of PPGDA with PPGMEA (n = 2) are shown in **Figure 4.25**. The dynamic mechanical studies encompass copolymer compositions up to 40 wt% PPGMEA co-monomer. The position of the $tan\delta$ peak (T_α = –37°C; 1 Hz) is independent of co-monomer content, indicating that the nominal glass transition temperature of the networks is not affected by composition for the range of specimens examined. Similar to PEGDA/DGEEA series, the incorporation of PPGMEA co-monomer into the PPGDA network results in the insertion of short branches (n = 2) along the network backbone. However, the PPGDA networks encompass an inherently larger free volume as compared to the PEGDA networks (0.160 for 100% PPGDA vs. 0.118 for 100% PEGDA). Consequently, the insertion of the short PPGMEA branches and corresponding increase in free volume does not measurably alter the glass transition temperature in these networks (see **Table 4.6**). This is in contrast to the modest influence of co-monomer content on T_α in the PEGDA/DGEEA copolymer networks (see Table 4.5), and in sharp distinction to the PEGDA/PEGMEA copolymers, for which a progressive decrease in T_α of nearly 20°C was observed with increasing PEGMEA (n = 8) branch content. The insertion of longer PEGMEA branches into the initially tighter PEGDA network has a much stronger influence on the central segmental relaxation time and corresponding glass transition temperature as compared to the inclusion of shorter PPGMEA chains into the relatively open PPGDA network.

The storage modulus curve for the 100% PPGDA network (n = 12) is compared with the result obtained for the 100% PEGDA sample (n = 14) in Figure 4.25. Network theory^{37}

predicts that the storage modulus measured in the rubbery plateau region (E_R) should be proportional to the effective crosslink density (υ_e), where υ_e (mol/cm^3) is defined as:[34]

$$\upsilon_e = \frac{\rho_p}{M_c} \qquad [2.7]$$

where ρ_p (g/cm^3) is the bulk polymer density and M_c (g/mol) is the molecular weight between crosslink junctions. For both networks, M_c is nominally established by the number of repeat units in the crosslinker; *i.e.*, for PPGDA (n = 12), M_c = 768 g/mol, while for PEGDA (n = 14), M_c = 688 g/mol. The density of the 100% PPGDA network (1.065 gm/cm^3) is considerably lower than that measured for the 100% PEGDA network (1.183 gm/cm^3, see ref. 115), and reflects the higher fractional free volume present in the PPGDA matrix. The introduction of these physical parameters into the definition for υ_e predicts a reduction in effective crosslink density of ~ 20% for PPGDA versus PEGDA, and this is manifested in the measured decrease in E_R as shown in Figure 4.25. The modulus results obtained here are largely consistent with previous room-temperature mechanical measurements reported by Patel *et al.* on crosslinked PPGDA and PEGDA.[127] For the PPGDA/PPGMEA copolymers, E_R decreases systematically with increasing PPGMEA concentration, reflecting the stoichiometry-driven decrease in effective crosslink density with PPGMEA content in the polymerization reaction mixture.

Time-temperature superposition was used to construct master curves of storage modulus (E') versus frequency at a reference temperature of –40°C;[38] results for the entire PPGDA/PPGMEA series fit to the KWW model are shown in **Figure 4.26**. For the 100% PPGDA network, a value of β = 0.26 was obtained, indicating a somewhat broader, less homogeneous relaxation for the PPGDA sample as compared to the 100% PEGDA network (β = 0.30), most likely due to the presence of the $-CH_3$ pendant along the propylene oxide ($-OCH_2CHCH_3-$) repeat unit. Figure 4.26 shows a reasonable KWW fit for each copolymer composition, with β = 0.26 ± 0.01. For the range of copolymer compositions studied here, no systematic trend in relaxation breadth was observed with varying copolymer content.

Figure 4.27 shows cooperativity plots for the PPGDA/PPGMEA networks, as well as for a 100% PEGDA specimen, with T_α corresponding to the dynamic mechanical peak temperature for each network at a frequency of 1 Hz. In every case, the $\log(a_T)$ – reciprocal temperature relationship is non-linear, and can be described by the Williams-Landel-Ferry (WLF) equation[38] (see solid curves in Figure 4.27). The apparent activation energy of the glass-rubber relaxation (E_A) and the fragility index (m) can be evaluated using the slope of each cooperativity curve. For the 100% PPGDA network, a value of E_A = 300 kJ/mol is obtained. The introduction of PPGMEA into the network (and the corresponding drop in effective crosslink density) results in a reduction in the apparent activation energy, suggesting a decrease in the cooperativity inherent to the glass transition. Values of $E_A(T_\alpha)$ for the PPGDA/PPGMEA copolymer series are reported in Table 4.6; the trend observed is similar to that obtained for the PEGDA/PEGMEA networks (see Table 4.4). The reduction in crosslink density achieved through copolymerization leads to a decrease in the constraint imposed by the crosslink junctions, such that less segmental cooperation is required across the glass transition.

Comparison of the cooperativity curves for 100% PPGDA (n = 12) versus 100% PEGDA (n = 14) in Figure 4.27 reveals a stronger time-temperature sensitivity for the PEO network, indicating a higher degree of intermolecular cooperativity (*i.e.*, higher fragility) for the segmental motions in crosslinked PEGDA. From a structural standpoint, this result is somewhat counter-intuitive, as the bulkier character of the PPO repeat unit would be expected to encompass a higher degree of cooperative motion in the PPGDA networks as compared to the relatively smooth, compact character of the PEO moiety.[44] However, the comparison must also take into account the observed difference in effective crosslink density for these two materials ($\upsilon_{e\,[\mathrm{PEGDA}]} > \upsilon_{e\,[\mathrm{PPGDA}]}$), as well as the difference in fractional free volume present in the networks. The relatively high degree of fractional free volume that is obtained in crosslinked PPGDA appears to be a decisive factor, leading to a more open relaxation environment that can accommodate motion of the PPO segments with less overall inter-segmental cooperation.

Networks prepared with BPAEDA crosslinker

Dynamic mechanical data for the BPAEDA/PEGMEA series of copolymers (1 Hz) are presented in **Figure 4.28**. The data show a significant decrease in the glass-rubber relaxation temperature with PEGMEA content, as both the step change in E' and peak in $tan\delta$ are shifted strongly to the left with increasing PEGMEA. The T_α values for the series exhibit the same trend as the glass transition temperatures (T_g) determined by DSC (see **Table 4.7**). The key observation here is the positive offset in T_α for a 100% BPAEDA network (T_α = 11°C) as compared to the 100% PEGDA (T_α = -35°C) polymer. This can be attributed primarily to the bulky, relatively rigid character of the BPAEDA backbone (8 ethylene oxide repeat units, in addition to the bisphenol A group) as compared to the flexible PEGDA chains (14 ethylene oxide repeat units). Also, the 100% BPAEDA network has a lower value of molecular weight between crosslinks (M_c = 634 g/mol) as compared to a 100% PEGDA network (M_c = 688 g/mol), resulting in a more constrained morphology. Inclusion of increasing amounts of PEGMEA monomer drives a progressive decrease in the effective crosslink density as manifested by the observed drop in the rubbery modulus (E_R); similar trends in the dynamic mechanical results are obtained for the BPAEDA/PEGA series (see **Figure 4.29**)

Modulus-frequency master curves for both copolymer networks were constructed by applying the time-temperature superposition method, at a common reference temperature of 10°C.[38] Examination of the time-temperature master curves in **Figure 4.30** indicates a systematic variation in relaxation time and rubbery modulus with increasing acrylate co-monomer in the network. The data were curve fit to the KWW model (see solid curves in Figure 4.30) to obtain the distribution parameter (β). For the 100% BPAEDA network, a value of β = 0.21 was obtained (see Table 4.7), indicating a much broader, heterogeneous relaxation as compared to the 100% PEGDA network (β = 0.30). Also, the fractional free volume measured for the 100% BPAEDA network (0.109) is comparatively less than that for PEGDA (0.118). These characteristics are most likely due to the presence of the bulkier bisphenol A group along the crosslinker. Introduction of acrylate monomer into the network results in a slight broadening of the relaxation as reflected in the decreasing

β values for both copolymer series. This is counter-intuitive to the typical narrowing of the glass-rubber relaxation observed with decreasing crosslink density. It is speculated that the significant structural difference between the crosslinker and the flexible acrylate monomers results in the overall relaxation encompassing two distinct relaxing entities, which leads to the observed broadening.

Figures 4.31 and **4.32** show cooperativity plots for the BPAEDA/PEGMEA and BPAEDA/PEGA networks, respectively, based on the T_α values reported in Table 4.7. The solid curves correspond to WLF fits to the data.[38] For both series of networks, inclusion of the flexible acrylate monomer results in a decrease in slope, *i.e.*, a decrease in the time-temperature sensitivity or intermolecular cooperativity associated with the glass-rubber relaxation, in comparison to the relatively rigid 100% BPAEDA network. However, further decrease in crosslink density via inclusion of additional co-monomer does not seem to influence the cooperativity of the resulting network. As a result, a single WLF curve and corresponding value of the activation energy and fragility index can successfully describe the time-temperature behavior for each series of copolymers (see Table 4.7).

4.3.2 Gas transport properties

Rubbery, amorphous polymer networks based on PEGDA have been identified as promising membrane materials for the selective removal of CO_2 in mixtures with light gases such as CH_4, N_2, and H_2.[18] One goal of the current work is to understand the relationships between structure and composition, crosslink density, and gas transport properties in these network polymers. Recent companion studies on crosslinked PEGDA and PEGDA copolymers, undertaken at the University of Texas at Austin, detail the gas permeability and selectivity of these networks as a function of PEGDA content, crosslink density, and resulting fractional free volume.

The motivation behind these studies lies in the opportunity to explore the influence of network crosslink density on gas transport behavior. For the PEGDA/water networks, it appears that the sizeable variation in effective crosslink density, achieved independent of changes in composition or fractional free volume, has relatively little effect on the gas transport properties. **Figure 4.33**, for example, shows normalized CO_2 solubility and diffusivity data for the PEGDA/water networks as a function of initial reaction composition. Despite the significant changes in crosslink density observed for these materials, very little change in solubility or diffusivity is measured, with the corresponding CO_2 permeability increasing only by about 30% across the range of compositions studied.[115] Thus, for the PEGDA/water networks, the relatively invariant transport properties suggest that the key factor influencing gas permeation in network polymers is not simply crosslink density, and that any attempt to correlate gas transport to network structure must necessarily consider the broader relationships between crosslink density, segmental mobility, and fractional free volume.

Pure gas permeability measurements performed on the PEGDA/PEGMEA and PEGDA/PEGA series are shown in **Figure 4.34**.[115,124] The result obtained for the PEGDA/PEGA series is similar to that for the PEGDA/water networks, with a slight decrease in CO_2 permeability observed with increasing PEGA content. The decrease in permeability that is observed for the PEGDA/PEGA series is consistent with a small decrease in estimated fractional free volume for these materials as reported in Table 4.3. The behavior for the PEGDA/PEGA networks is in sharp contrast to the results for the PEGDA/PEGMEA series, where a dramatic increase in CO_2 permeability is observed with increasing PEGMEA branch content in the rubbery network (see Figure 4.34); this increase is driven primarily by an increase in the diffusivity of CO_2 in the polymer, as ethylene oxide content (and corresponding CO_2 solubility) remains virtually unchanged over the range of copolymer compositions.[124] The increase in CO_2 pure gas permeability correlates directly with the measured increase in fractional free volume for this polymer series. In addition, the PEGDA networks display favorable pure gas selectivity for reverse-selective separations (*e.g.*, preferential permeation of CO_2 over H_2). For 100% crosslinked PEGDA, pure gas CO_2/H_2 selectivity ($\alpha = P_{CO_2}/P_{H_2}$) has a value of approximately 8 for measurements conducted at 35°C; this value remains nearly constant across both the PEGDA/water and PEGDA/PEGA series of networks. For the

PEGDA/PEGMEA copolymer series, a progressive increase in selectivity is observed with increasing PEGMEA content: a CO_2/H_2 selectivity value of 13 is measured for minimally-crosslinked networks containing 99 wt% PEGMEA.

The contrasting gas transport performance observed for the PEGDA/PEGMEA and PEGDA/PEGA copolymer series demonstrates the sensitivity of these materials to minor changes in network structure or composition. In the case of the copolymer networks, the only obvious difference is the nature of the end group on the pendant branches: $-OCH_3$ versus $-OH$. This distinction leads to much greater variations in glass transition temperature and permeability across the PEGDA/PEGMEA series as compared to the PEGDA/PEGA specimens, variations that correlate primarily with the fractional free volume contained in the network. One possible explanation for the observed difference in these copolymer series is the potential for the $-OH$ chain ends in the PEGDA/PEGA polymers to form hydrogen bonds within the network structure, leading to local interactions that could potentially offset the changes in T_g and free volume typically encountered with the insertion of branch-like defects. The sensitivity of these membranes to relatively small variations in structure highlights the importance of developing fundamental understanding regarding how such changes influence membrane performance properties, and how intelligent design and control of membrane structure can be exploited to optimize separation performance for specific applications.

4.3.3 PEGDA Nanocomposite networks

The inclusion of nanoscale particles in a polymer matrix can produce significant enhancements in the physical properties of the composite material. Introduction of nanoparticles results in a dramatic increase in the particle-polymer surface area. This can potentially perturb the static and dynamic characteristics of the polymer matrix owing to physical confinement effects and particle-polymer interactions; such effects often improve the macroscopic performance of the material. Prior work by Yim *et al.*[58] has shown the emergence of a second, higher temperature T_g upon inclusion of untreated silica (specific surface area: 200 m^2/gm; 31 vol% loading) in poly(ethylene) glycol.

Similar effects have been observed for poly(dimethyl siloxane) [PDMS] and polystyrene [PS] at sufficient particle loadings. The higher temperature relaxation was speculated to originate in the layer of polymer chains physically immobilized on the silica particles, the thickness of which was estimated at 2 to 3 nm. An extensive dynamic mechanical study undertaken by Tsagaropoulos and Eisenberg[61] on different polymers (*e.g.*, poly(methyl methacrylate) [PMMA], PS) reveals the existence of a second $tan\delta$ peak at higher particle loadings (10 wt% and above), with ΔT_g as high as 122°C for the PMMA-silica nanocomposites. However, for larger silica particles, with lower specific area (~ 1 m^2/gm versus 380 m^2/gm), no such T_g effect was observed.[60] A detailed literature survey of work undertaken to elucidate polymer nanocomposite relaxation characteristics can be found in Section 2.4. The goal in this work is to develop fundamental structure-property relationships to facilitate the preparation of rubbery polymer nanocomposite membranes for the preferential transport of polar or quadrupolar gas molecules (such as CO_2) over light gases (such as H_2). Dynamic mechanical analysis has been used to gain an initial perspective into the nanocomposite morphology, and to develop insight as to how increased loading of nanoparticles alters the dynamic characteristics of the polymer.

Dynamic mechanical studies have been performed on a series of PEGDA-based networks prepared with increasing amounts of spherical MgO nanoparticle (0 to 44 wt% MgO, which corresponds to a volume fraction of 0 to 20 vol% MgO). The results are shown as storage modulus (E') and loss factor ($tan\delta$) versus temperature in **Figures 4.35** and **4.36**, respectively. At low particle loadings (≤ 26 wt%), there is slight enhancement in the glassy modulus accompanied by a progressive increase in the rubbery modulus. This result is typical of the bulk mechanical behavior observed for polymers with relatively inert, micron scale fillers, as observed by Schwarzl *et al.*[128] for polyurethane rubber filled with NaCl. With increased particle loading (30 wt% and above), the modulus curve exhibits a "two-step" character, indicative of two separate relaxation events. The emergence of a second, higher temperature relaxation is speculated to correspond to the fraction of polymer chains in the vicinity of the particle surface experiencing restricted mobility as a result of constraints imposed either through physical confinement and/or adsorption. Also, at higher filler content, the rubbery modulus value appears to be independent of the polymer composition (see Figure 4.35). Matteucci and co-workers have shown that the inclusion of MgO particles in a PEGDA matrix results in a significant increase in the void fraction, with a nominal MgO content of 40 vol% leading to a void volume fraction as high as 0.6.[129] This dramatic increase in the included free space within the polymer matrix appears to offset the influence of higher particle loading, thereby resulting in an invariant rubbery modulus for progressively stiffer networks.

The plot of loss factor ($tan\delta$) versus temperature (see Figure 4.36) confirms the presence of a dual-T_g behavior, with the lower temperature relaxation ($T_{\alpha 1}$) corresponding to the bulk polymer (PEGDA) matrix, and the higher temperature transition ($T_{\alpha 2}$) corresponding to polymer chains confined in the vicinity of the MgO particle surface. The peak intensity of the α_1 relaxation decreases as the transition becomes progressively broader, reflecting a more heterogeneous motional environment with increased filler content. **Table 4.8** provides the relaxation temperatures for the entire series of nanocomposites. A single glass transition is observed up to particle loadings of 26 wt%, with the peak temperature ($T_{\alpha 1}$) slightly higher than that of 100% PEGDA and independent of filler content. However, for particle loadings of 30 wt% and greater, two relaxations are evident. The upper transition peak temperature ($T_{\alpha 2}$) and the corresponding $tan\delta$ peak intensity increase with increasing particle content, a manifestation of the increased fraction of surface-constrained polymer chains. Surprisingly, the lower transition temperature ($T_{\alpha 1}$) decreases at higher particle loadings, to values lower than the T_g for neat PEGDA. This is possibly due to the ability of the MgO particles to "dewet" the surrounding PEGDA matrix, a trend consistent with the results reported by Arrighi *et al.*[62] for styrene-butadiene rubber (SBR) filled with organophillic-modified silica particles.

The dynamic mechanical results obtained for these polymer nanocomposites raise a number of interesting issues relative to the influence of nanofillers on the dynamics of rubbery crosslinked networks, and their ultimate effect on gas transport properties. With regard to this, future work would involve key variables pertaining to (i) the particle size and the corresponding specific surface area; (ii) the extent of particle loading and its influence on the thickness of the resulting surface-immobilized polymer layer; (iii) the surface chemistry of the filler particles, and their interaction strength with the bulk matrix; and (iv) the details of the network architecture, including variations in crosslink density, changes in backbone structure or introduction of pendant groups.

4.4 CONCLUSIONS

The viscoelastic characteristics of crosslinked polymer networks synthesized via UV photopolymerization have been investigated by dynamic mechanical analysis. For networks prepared using poly(ethylene glycol) diacrylates of varying molecular weight, the resulting rubbery modulus correlated directly with distance between crosslinks in a manner consistent with rubber elasticity theory. Decreasing the effective distance between crosslink junctions from n=14 (*i.e.*, fourteen $-OCH_2CH_2-$ units) to n=3 led to a strong positive offset in the glass transition temperature, as well as broadening of the glass-rubber relaxation. Time-temperature master curves for these networks could be satisfactorily fit to the KWW stretched exponential relaxation function, and the observed decrease in the KWW distribution parameter with increasing crosslink density reflected inhomogeneous broadening of the glass-rubber relaxation owing to local network constraints.

Networks prepared from PEGDA (n=14) with varying amounts of water in the reaction mixture showed a systematic decrease in effective crosslink density with increasing water content as determined from rubbery modulus measurements and prior swelling experiments. For these networks, a narrowing of the glass-rubber relaxation was observed with decreasing crosslink density, but with little variation in the measured glass transition temperature or fractional free volume. Cooperativity plots showed a progressive decrease in fragility with decreasing crosslink density, in agreement with other network studies reported in the literature.

The introduction of mono-functional acrylate in the prepolymer reaction mixture was used to control crosslink density in the resulting polymers and led to the insertion of flexible oligomeric branches within the networks. For the model PEGDA copolymer networks, the molecular weights of the PEGMEA and PEGA co-components were selected so as to maintain a constant ethylene oxide content within the final networks. For both series, the introduction of the acrylate co-monomer led to a decrease in the measured glass transition temperature as well as a systematic reduction in crosslink density as reflected in the rubbery modulus of the network. KWW curve fits to time-temperature modulus master curves indicated a narrowing of the glass-rubber relaxation with reduced crosslink density that correlated with a decrease in fragility, suggesting a more homogeneous, less cooperative relaxation environment in the copolymer networks. The influence of the copolymer branches was more pronounced in the PEGDA/PEGMEA series, which displayed a much larger variation in glass transition temperature with changing PEGDA content.

Insertion of the short branch DGEEA monomer into the PEGDA network had only a modest effect on the glass transition temperature with varying crosslink density. The KWW distribution parameter indicated only a slight narrowing of the relaxation breadth for the entire series of networks prepared, irrespective of the systematic decrease in the effective crosslink density. This could be attributed to the insertion of short, relatively rigid DGEEA branches which appears to introduce heterogeneity in the relaxation environment. The temperature sensitivity for the copolymer networks remained fairly consistent for the entire range of compositions which reflected in the modest decrease in fragility with increasing co-monomer content.

A series of rubbery crosslinked copolymers based on poly(propylene glycol) diacrylate have been examined. The presence of the bulky propylene oxide segment along the PPGDA crosslinker and PPGMEA branches led to relatively large amounts of free volume in these networks. The insertion of short branches along the network backbone via copolymerization with PPGMEA resulted in a systematic decrease in effective crosslink density and a progressive increase in FFV. Dynamic mechanical studies indicated virtually no variation in the glass transition temperature with increasing PPGMEA content. The presence of the flexible PPGMEA branches (and the corresponding reduction in crosslink density) did, however, result in a progressive decrease in network fragility at the glass-rubber transition.

The 100% BPAEDA network, which has an inherently stiffer crosslink structure, undergoes glass transition at a significantly higher temperature as compared to the PEGDA material. Inclusion of flexible acrylate PEGMEA and PEGA chains into the BPAEDA network led to a strong decrease in the glass transition temperature with decreasing effective crosslink density. However, a contrasting behavior was observed with increasing co-monomer content resulting in a gradual broadening of the glass-rubber relaxation. This has been attributed to the substantial structural difference between the crosslinker and the acrylate monomers, which leads to greater overall relaxation heterogeneity despite decreasing crosslink density in the networks.

Inclusion of MgO nanoparticles into the PEGDA network (*i.e.,* PEGDA/MgO nanocomposites) resulted in the emergence of a dual-T_g behavior in dynamic mechanical studies: the lower temperature relaxation ($T_{\alpha 1}$) originated in the bulk matrix phase while the second, higher temperature relaxation ($T_{\alpha 2}$) corresponded to polymer chains constrained in the vicinity of the particle surface due to physical confinement and segmental adsorption effects. Increased particle loading led to a progressively more heterogeneous relaxation response as manifested by a substantial broadening of the $T_{\alpha 1}$ relaxation. The position of the lower transition temperature ($T_{\alpha 1}$) was found to decrease slightly at higher particle loadings, possibly due to dewetting of the PEGDA matrix in the vicinity of MgO agglomerates. This was accompanied by a small increase in the second transition temperature ($T_{\alpha 2}$) due to the increased fraction of surface-constrained polymer chains.

Gas permeation measurements on the PEGDA/water networks indicated only a very small variation in gas transport properties, despite the sizeable variation in apparent crosslink density achieved in these materials. This result suggests that the controlling structural factor for gas transport in the networks is not crosslink density alone, and that attempts to correlate gas transport to network structure must necessarily consider the broader relationships between crosslink density, segmental mobility, and fractional free volume. A clear difference was evident in the transport behavior of the PEGDA/PEGMEA and PEGDA/PEGA copolymer networks, with the PEGDA/PEGMEA membranes displaying a strong variation in permeability and selectivity over the range of copolymer compositions examined. Both the observed glass transition and transport behavior correlated with measured variations in fractional free volume for these networks.

Table 4.1: Relaxation characteristics of PEGDA networks: T_α, dynamic mechanical peak temperature for glass transition (1 Hz); T_β, dynamic mechanical peak temperature for sub-glass transition (10 Hz); β_{KWW}, KWW distribution parameter for glass-rubber relaxation.

	T_α (1 Hz) (°C)	**$T_{\beta 1}$ (10 Hz) (°C)**	**$T_{\beta 2}$ (10 Hz) (°C)**	**β_{KWW}**
PEGDA (*n*=3)	79	-71	-37	0.11
PEGDA (*n*=10)	-26	-110	-66	0.19
PEGDA (*n*=14)	-35	--	-70	0.30

Table 4.2: Relaxation characteristics of crosslinked PEGDA/water networks, based on PEGDA *n*=14 prepolymer: T_{α}, dynamic mechanical peak temperature for glass transition (1 Hz); β_{KWW}, KWW distribution parameter for glass-rubber relaxation; FFV, fractional free volume based on density measurements; $E_A(T_{\alpha})$, apparent activation energy (kJ/mole) evaluated at T_{α}; *m*, fragility index based on equation 2.11. FFV determined at the University of Texas at Austin.

PEGDA/water	**T_{α} (1 Hz) (°C)**	**β_{KWW}**	**FFV**	**$E_A(T_{\alpha})$**	***m***
100:0	-35	0.30	0.118	354	78
80:20	-34	0.37	0.117	328	72
50:50	-34	0.39	0.119	302	66
20:80	-34	0.47	0.124	226	49

Table 4.3: Characteristics of crosslinked PEGDA (*n*=14) and copolymer networks: T_α, dynamic mechanical peak temperature for glass transition (1 Hz); T_g, calorimetric glass transition temperature;[124] T_β, dynamic mechanical peak temperature for sub-glass transition (10 Hz); β_{KWW}, KWW distribution parameter for glass-rubber relaxation; FFV, fractional free volume based on density measurements. T_g (DSC) and FFV determined at the University of Texas at Austin.

	T_α (1 Hz) (°C)	T_g (DSC) (°C)	T_β (10 Hz) (°C)	β_{KWW}	FFV
PEGDA	-35	-40	-70	0.30	0.118
PEGDA/PEGMEA					
80/20	-41	-44	-77	0.33	0.122
50/50	-47	-52	-79	0.34	0.127
30/70	-52	-57	-82	-----	0.128
PEGDA/PEGA					
80/20	-38	-40	-73	0.34	0.112
50/50	-41	-42	-73	0.35	0.112
30/70	-42	-44	-----	0.38	0.110

Table 4.4: Glass-rubber relaxation characteristics for PEGDA (*n*=14) and copolymer networks: T_{α}, dynamic mechanical peak temperature for glass transition (1 Hz); $E_A(T_{\alpha})$, apparent activation energy (kJ/mole) evaluated at T_{α}; *m*, fragility index based on equation 2.11.

	T_{α} (1 Hz) (°C)	**$E_A(T_{\alpha})$**	***m***
PEGDA	-35	354	78
PEGDA/PEGMEA			
80/20	-41	310	70
50/50	-47	262	60
PEGDA/PEGA			
80/20	-38	283	63
50/50	-41	231	52
30/70	-42	215	49

Table 4.5: Glass-rubber relaxation characteristics for PEGDA (*n*=14) and DGEEA (*n*=2) copolymer networks: T_α, dynamic mechanical peak temperature for glass transition (1 Hz); T_g, calorimetric glass transition temperature; β_{KWW}, KWW distribution parameter for glass-rubber relaxation; FFV, fractional free volume based on density measurements; $E_A(T_\alpha)$, apparent activation energy (kJ/mole) evaluated at T_α; *m*, fragility index based on equation 2.11. T_g (DSC) determined at the University of Texas at Austin.

	T_α (1 Hz) (°C)	**T_g (DSC) (°C)**	**β_{KWW}**	**FFV**	**$E_A(T_\alpha)$**	***m***
PEGDA	-35	-40	0.30	0.118	354	78
PEGDA/DGEEA						
80/20	-36	-41	0.29	0.114	276	61
60/40	-38	-44	0.33	0.125	250	56
50/50	-38	-45	0.32	0.128	250	56

Table 4.6: Glass-rubber relaxation characteristics for PPGDA (*n*=12) and PPGMEA (*n*=2) copolymer networks: T_α, dynamic mechanical peak temperature for glass transition (1 Hz); $E_A(T_\alpha)$, apparent activation energy (kJ/mole) evaluated at T_α; *m*, fragility index based on equation 2.11.

	T_α (1 Hz) (°C)	**$E_A(T_\alpha)$**	***m***
PPGDA	-36	300	67
PPGDA/PPGMEA			
90/10	-36	280	62
80/20	-37	235	52
60/40	-35	210	46

Table 4.7: Glass-rubber relaxation characteristics for BPAEDA (*n*=4) and copolymer networks: T_α, dynamic mechanical peak temperature for glass transition (1 Hz); T_g, calorimetric glass transition temperature; β_{KWW}, KWW distribution parameter for glass-rubber relaxation; $E_A(T_\alpha)$, apparent activation energy (kJ/mole) evaluated at T_α; *m*, fragility index based on equation 2.11. T_g (DSC) determined at the University of Texas at Austin.

	T_α (1 Hz) (°C)	**T_g (DSC) (°C)**	**β_{KWW}**	**$E_A(T_\alpha)$**	***m***
BPAEDA	11	1	0.21	283	52
BPAEDA/PEGMEA					
80/20	-8	-16	0.22	232	49
60/40	-24	-35	0.23		
50/50	-30	-43	0.19		
BPAEDA/PEGA					
80/20	-2	-11	0.21	221	45
60/40	-15	-27	0.20		
50/50	-21	-34	0.18		

Table 4.8: Glass-rubber relaxation characteristics for PEGDA/MgO nanocomposites: $T_{\alpha 1}$, dynamic mechanical peak temperature for glass transition (1 Hz) of the bulk matrix; $T_{\alpha 2}$, dynamic mechanical peak temperature for glass transition (1 Hz) of the polymer chains confined in the vicinity of the MgO particle surface.

	$T_{\alpha 1}$ (1 Hz) (°C)	**$T_{\alpha 2}$ (1 Hz) (°C)**
PEGDA (*n*=14)	-35	--
MgO content (wt%)		
14	-33	--
20	-33	--
26	-33	--
30	-33	10
35	-37	12
39	-38	16
44	-40	17

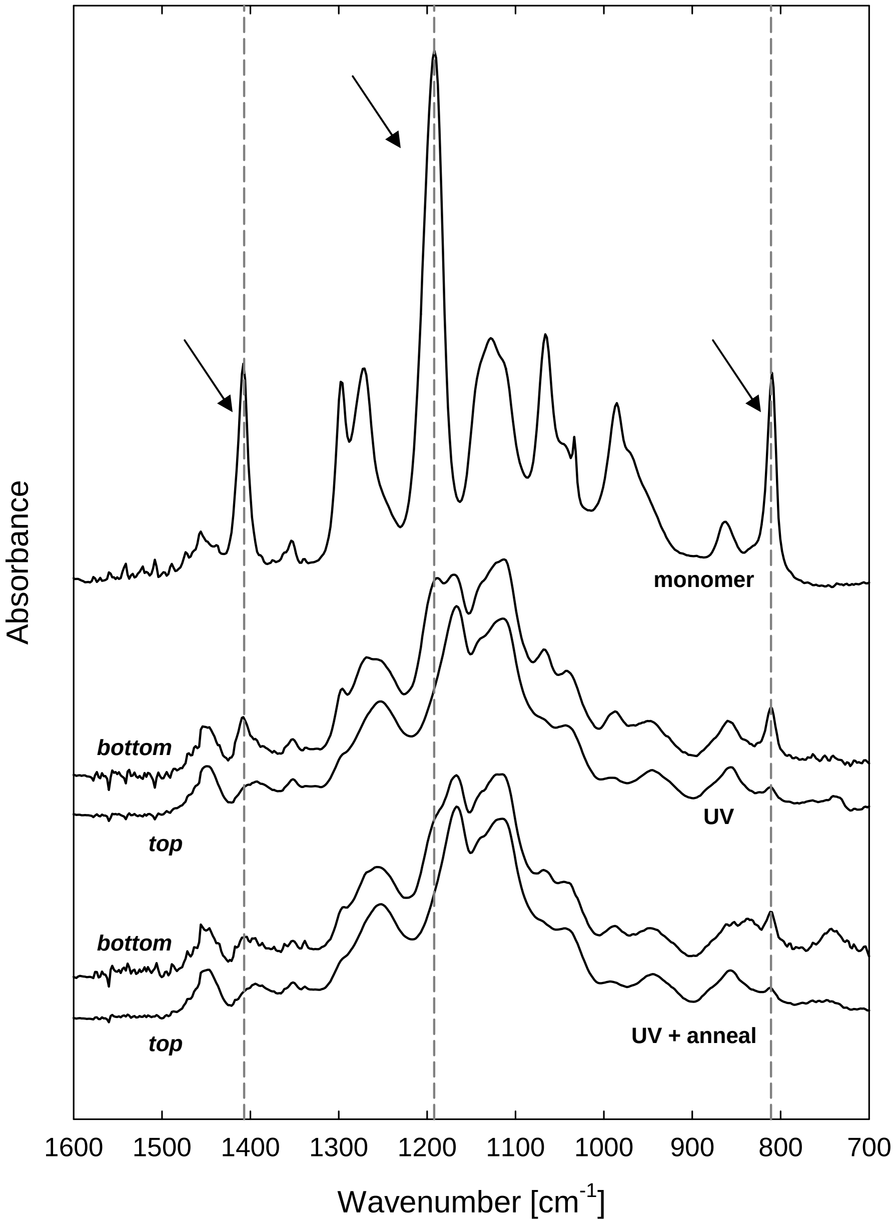

Figure 4.1: FTIR spectra of liquid PEGDA and solid crosslinked PEGDA films (*n=3*). For the solid polymer films, one side was exposed directly to UV light ("top"), and the other side was positioned opposite to the UV source ("bottom"). Annealed films were held at 100°C for one hour after UV exposure.

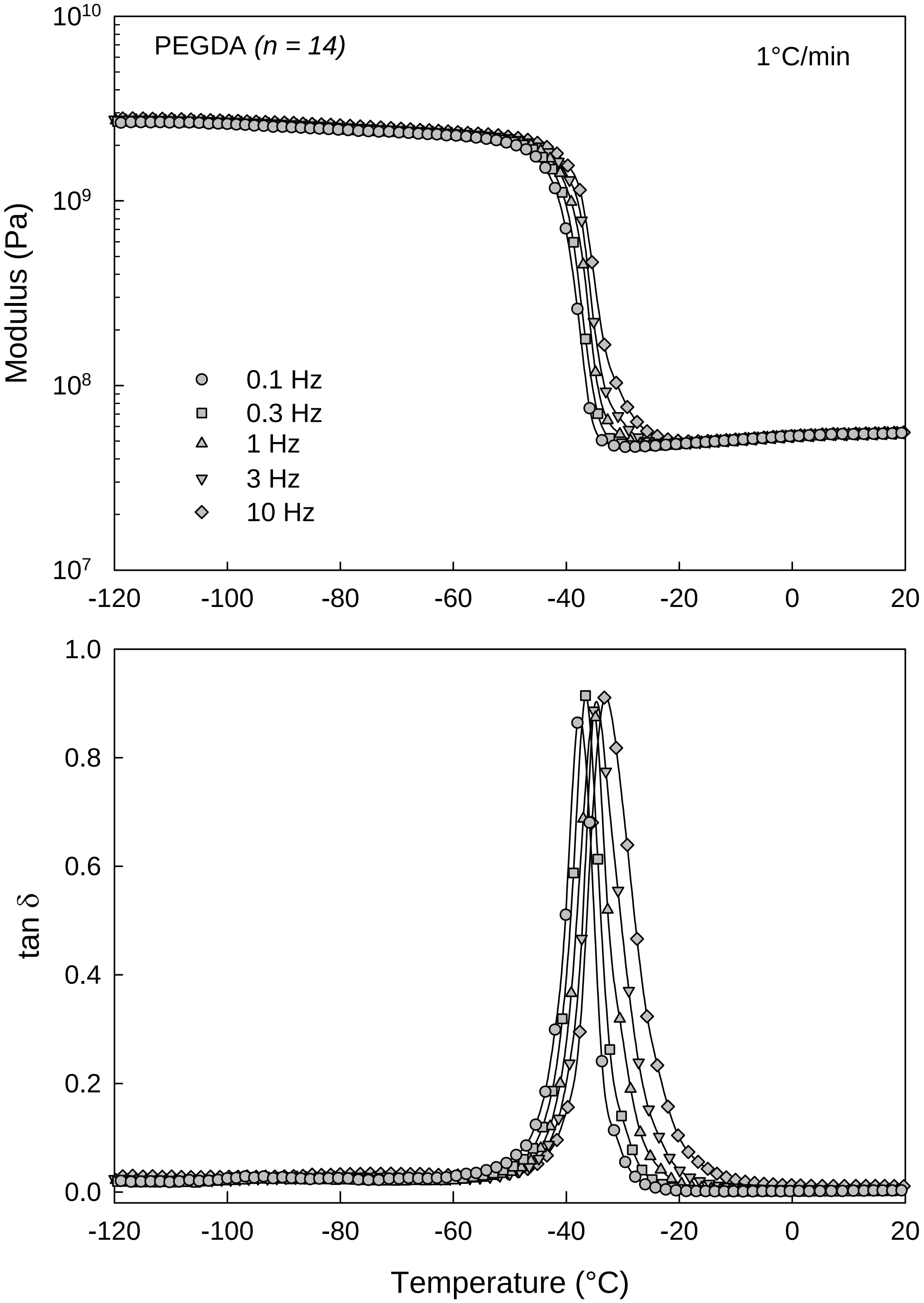

Figure 4.2: Dynamic mechanical properties (*E′*; *tanδ*) versus temperature for 100% PEGDA (*n*=14) network; heating rate of 1°C/min.

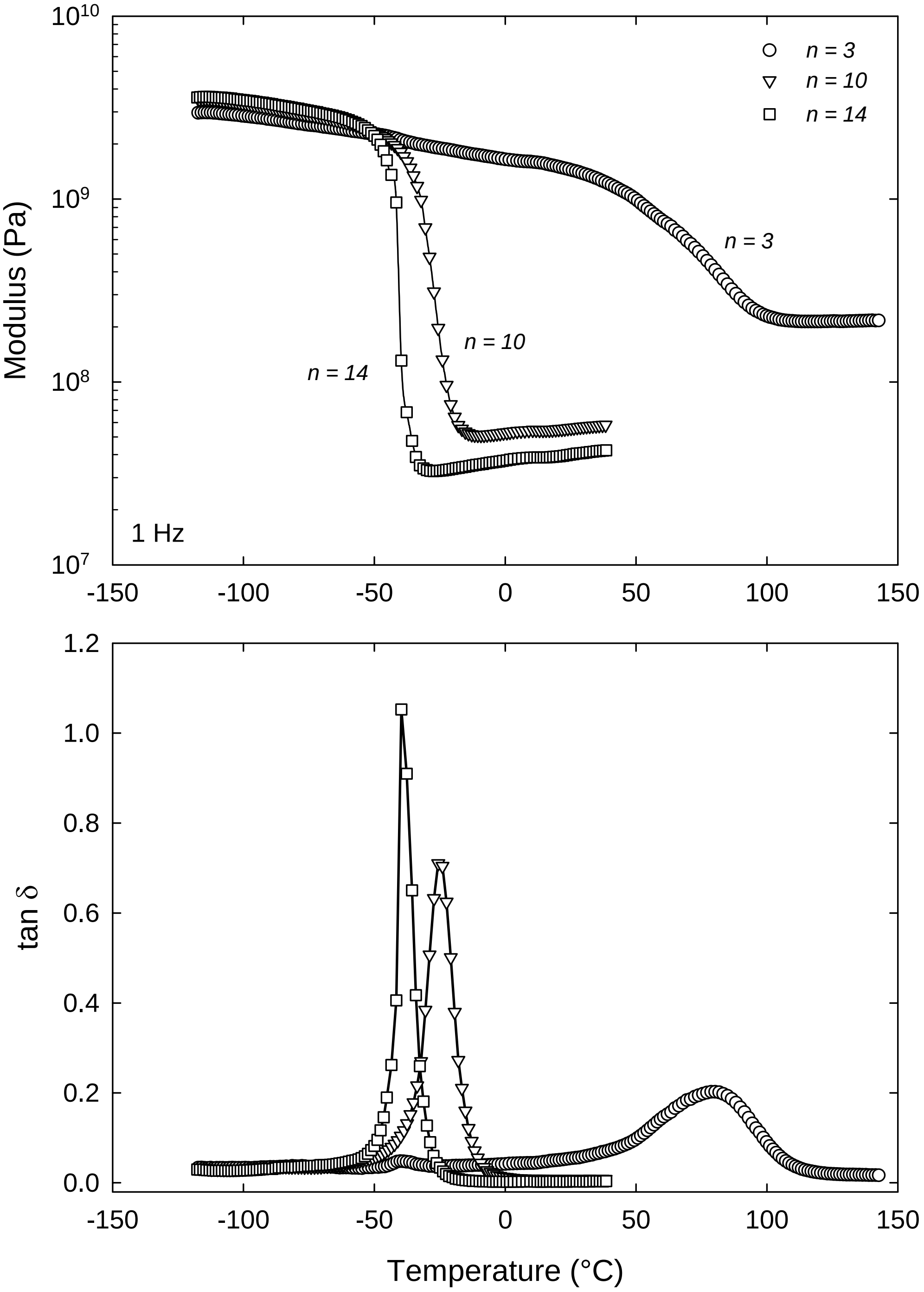

Figure 4.3: Dynamic mechanical properties (E'; $tan\delta$) for PEGDA networks based on diacrylates with varying ethylene oxide repeat length, *n*. Frequency of 1 Hz; heating rate of 1°C/min.

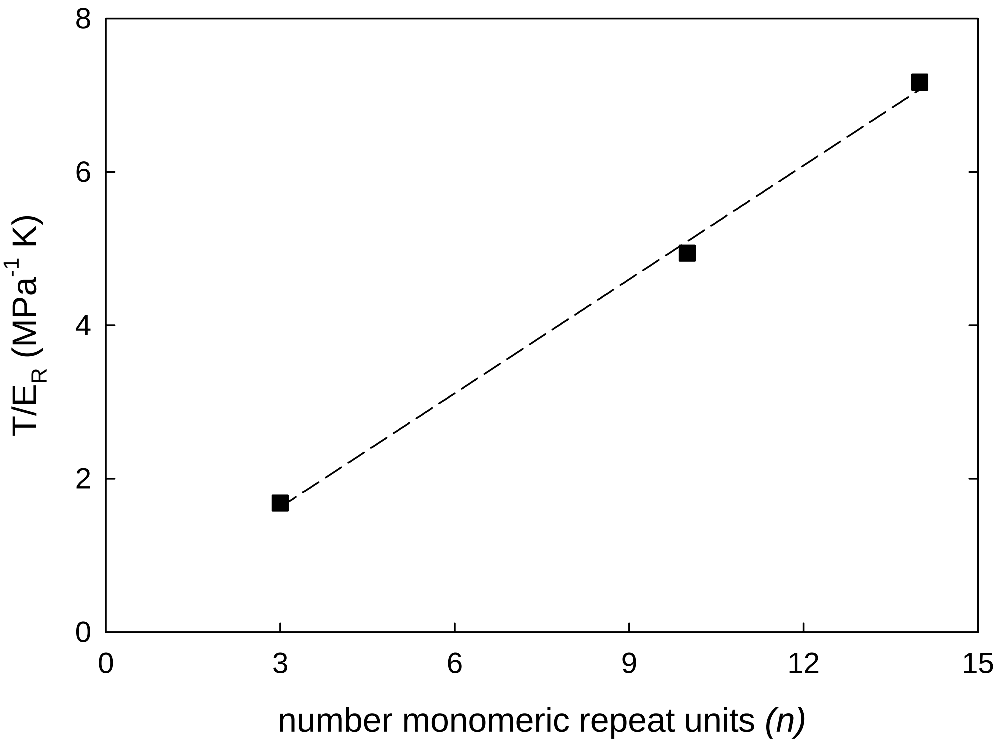

Figure 4.4: Ratio of temperature/rubbery modulus [T(K)/E_R] for PEGDA networks with varying ethylene oxide repeat length, *n*. Values of the rubbery modulus, E_R, established from time-temperature master curves.

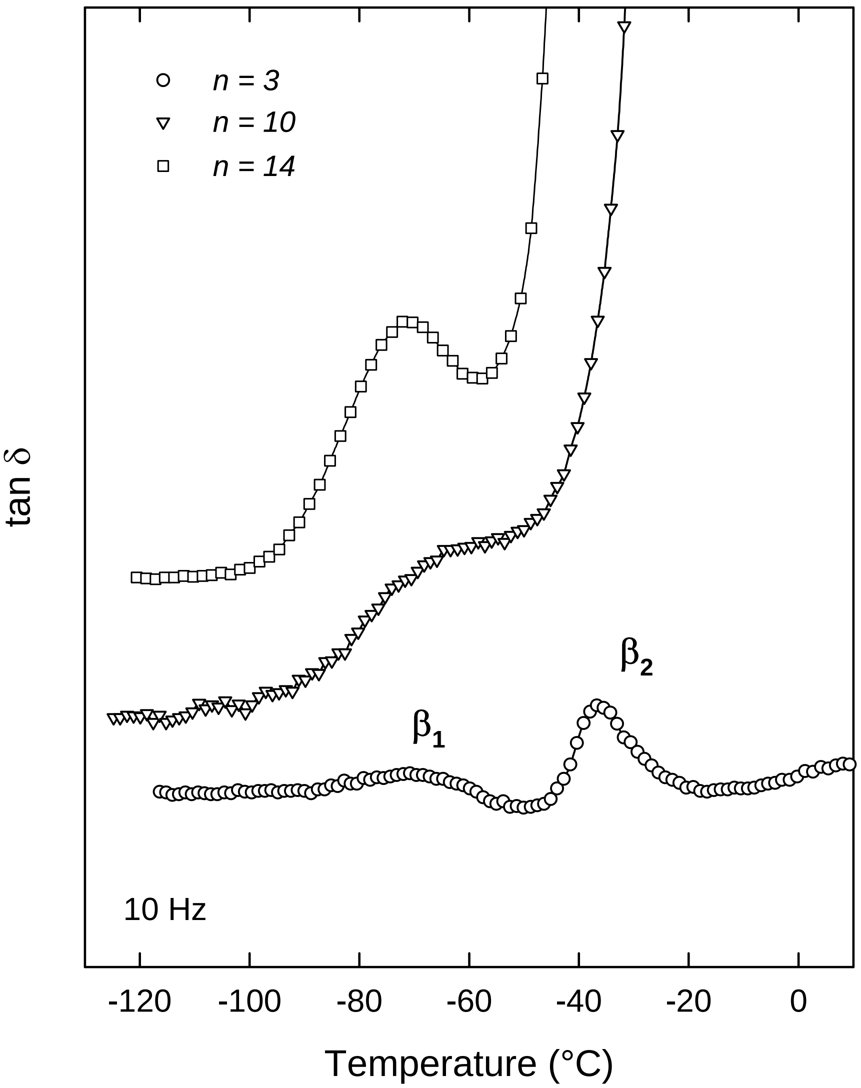

Figure 4.5: *tanδ* versus temperature (°C) for PEGDA networks in the sub-glass transition range. Curves are offset vertically for clarity. Frequency of 10 Hz; heating rate of 1°C/min.

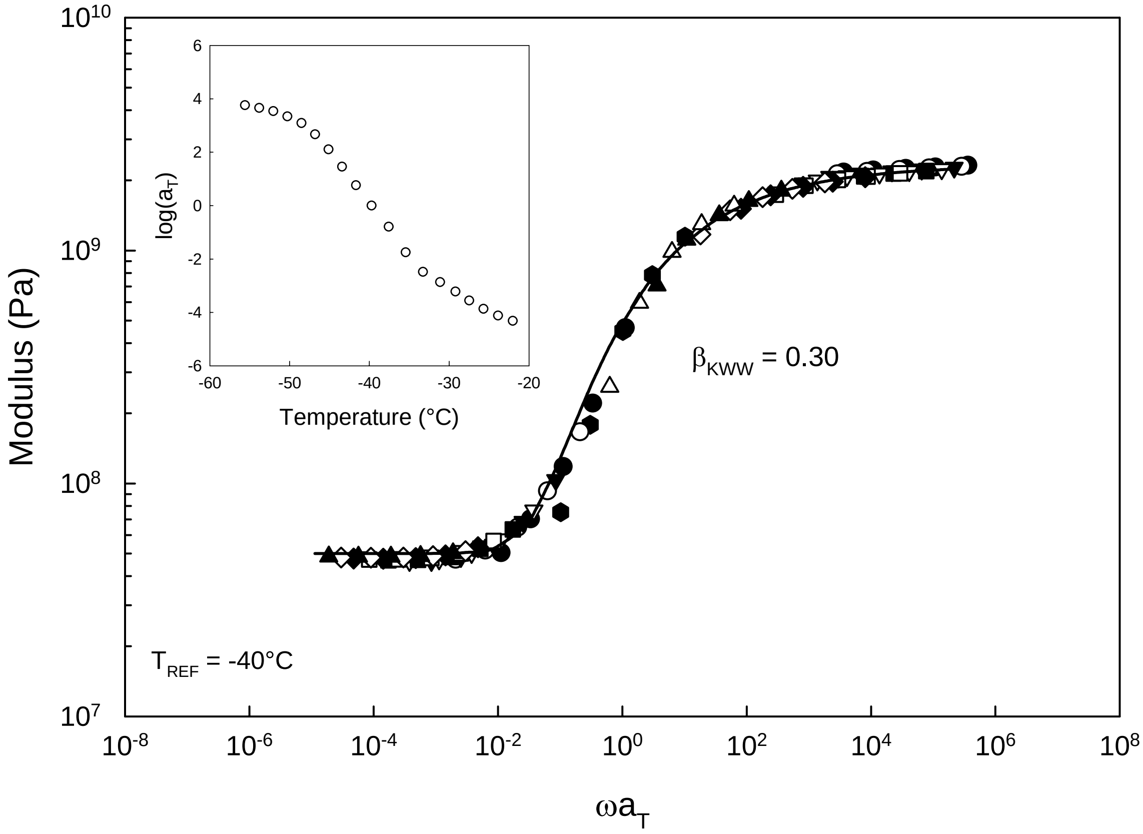

Figure 4.6: Time-temperature master curve for PEGDA (*n*=14) network; T_{REF} = –40°C. Solid curve is KWW best-fit. *Inset:* log(shift factor, a_T) versus temperature (°C).

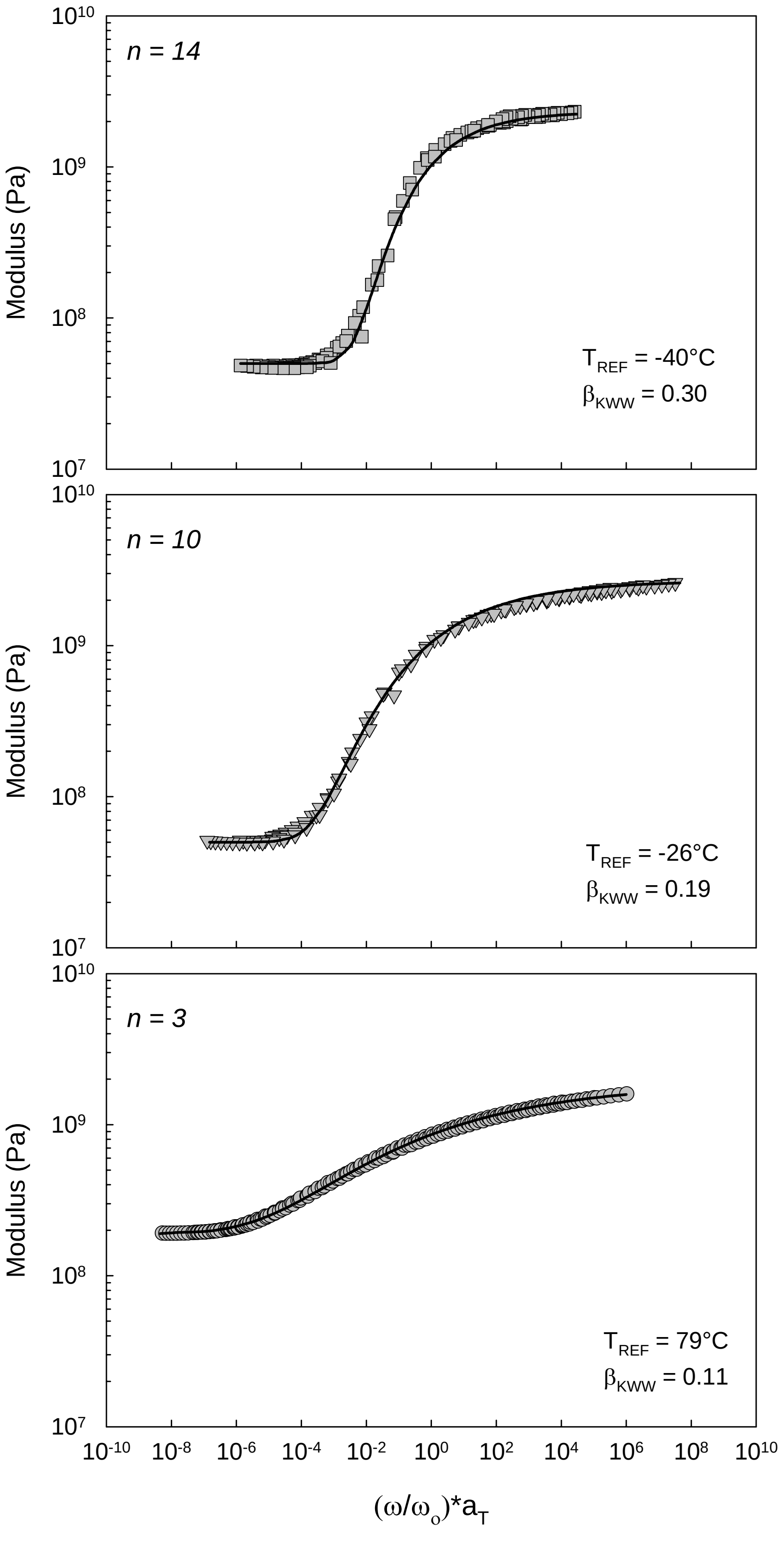

Figure 4.7: Time-temperature master curves for PEGDA networks with varying ethylene oxide repeat length, *n.* Solid curves are KWW best fits.

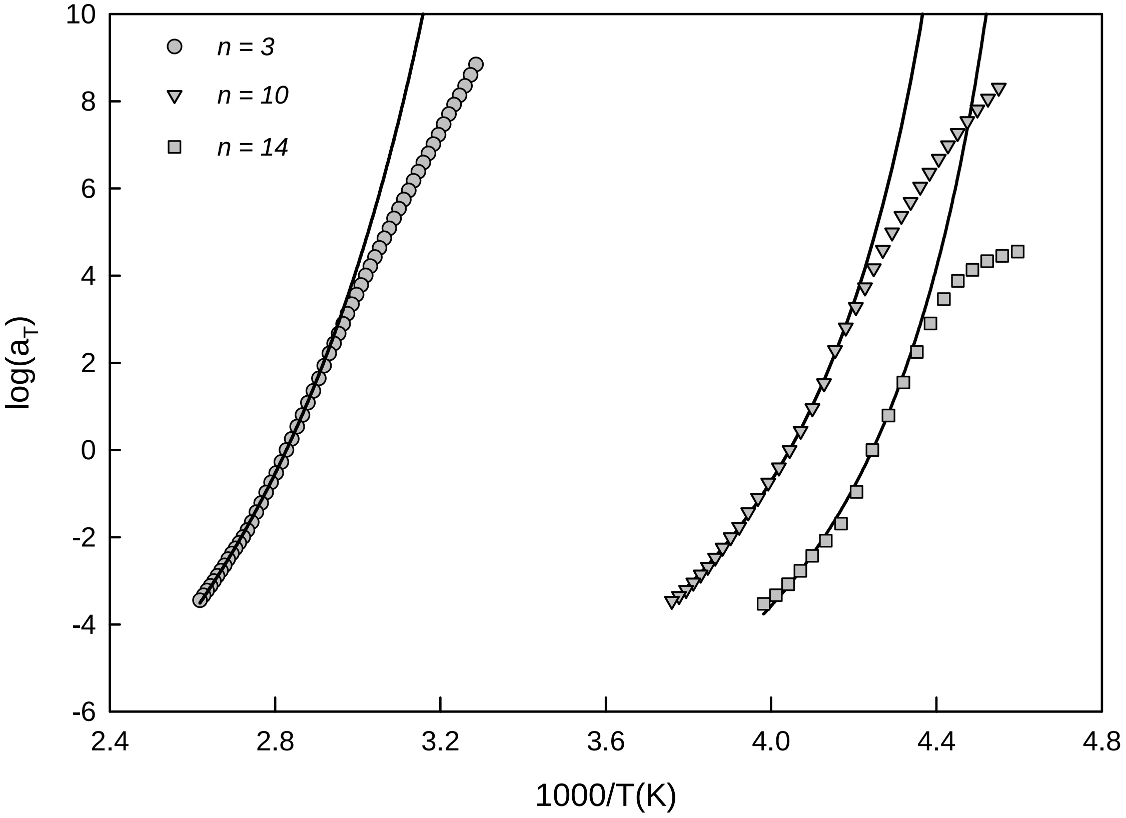

Figure 4.8: Arrhenius plots of log(a_T) versus 1000/T(K) for PEGDA networks. Solid curves are WLF fits.

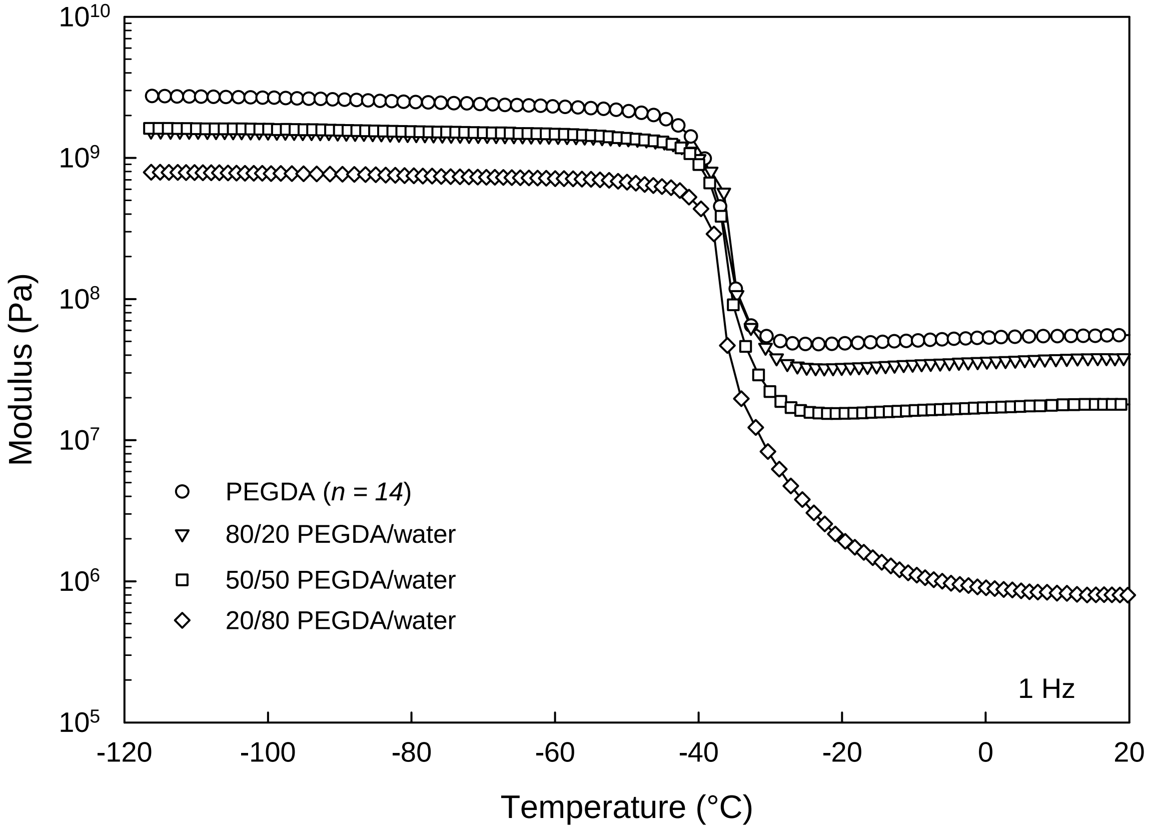

Figure 4.9: Storage modulus versus temperature for PEGDA (*n*=14) networks with varying amounts of water in the initial reaction mixture. Frequency of 1 Hz; heating rate of 1°C/min.

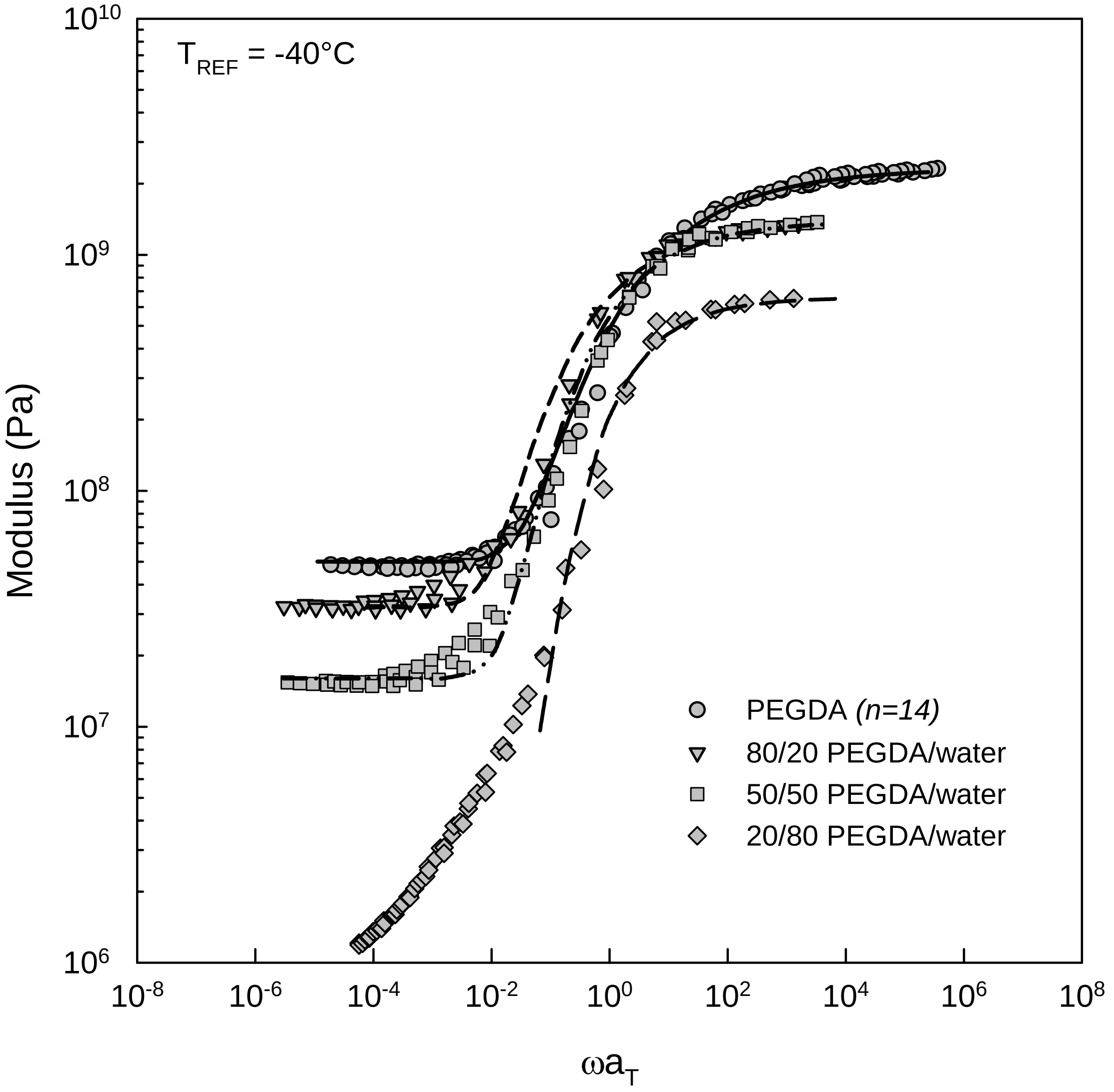

Figure 4.10: Time-temperature master curves for PEGDA/water networks. Curves are KWW best fits at $T_{REF} = -40$°C.

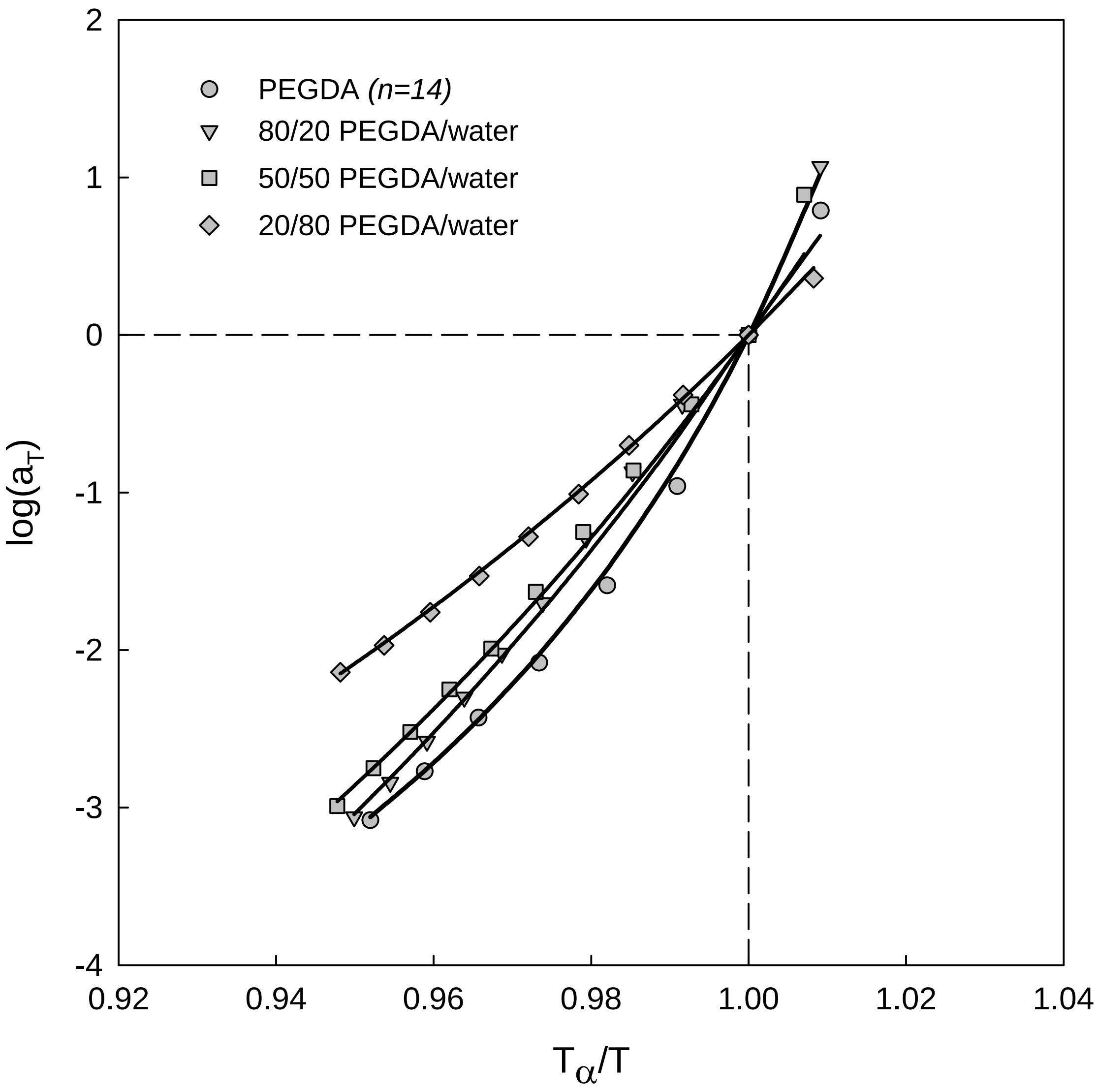

Figure 4.11: Cooperativity plots (log(a_T) versus T_α/T) for PEGDA/water networks. Solid curves are WLF fits.

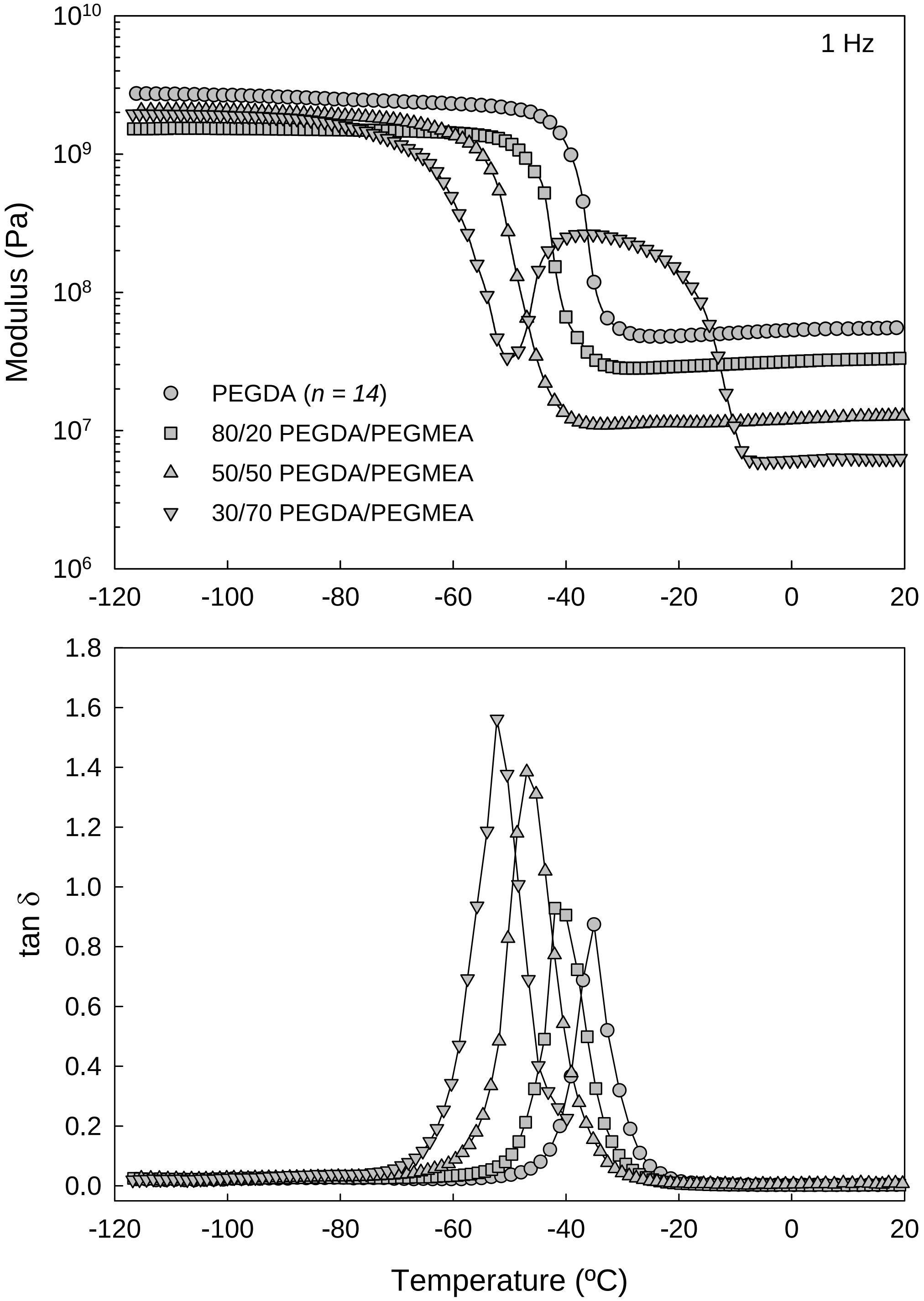

Figure 4.12: Dynamic mechanical properties (*E'*; *tanδ*) versus temperature for PEGDA/PEGMEA copolymer networks. Frequency of 1 Hz; heating rate of 1°C/min.

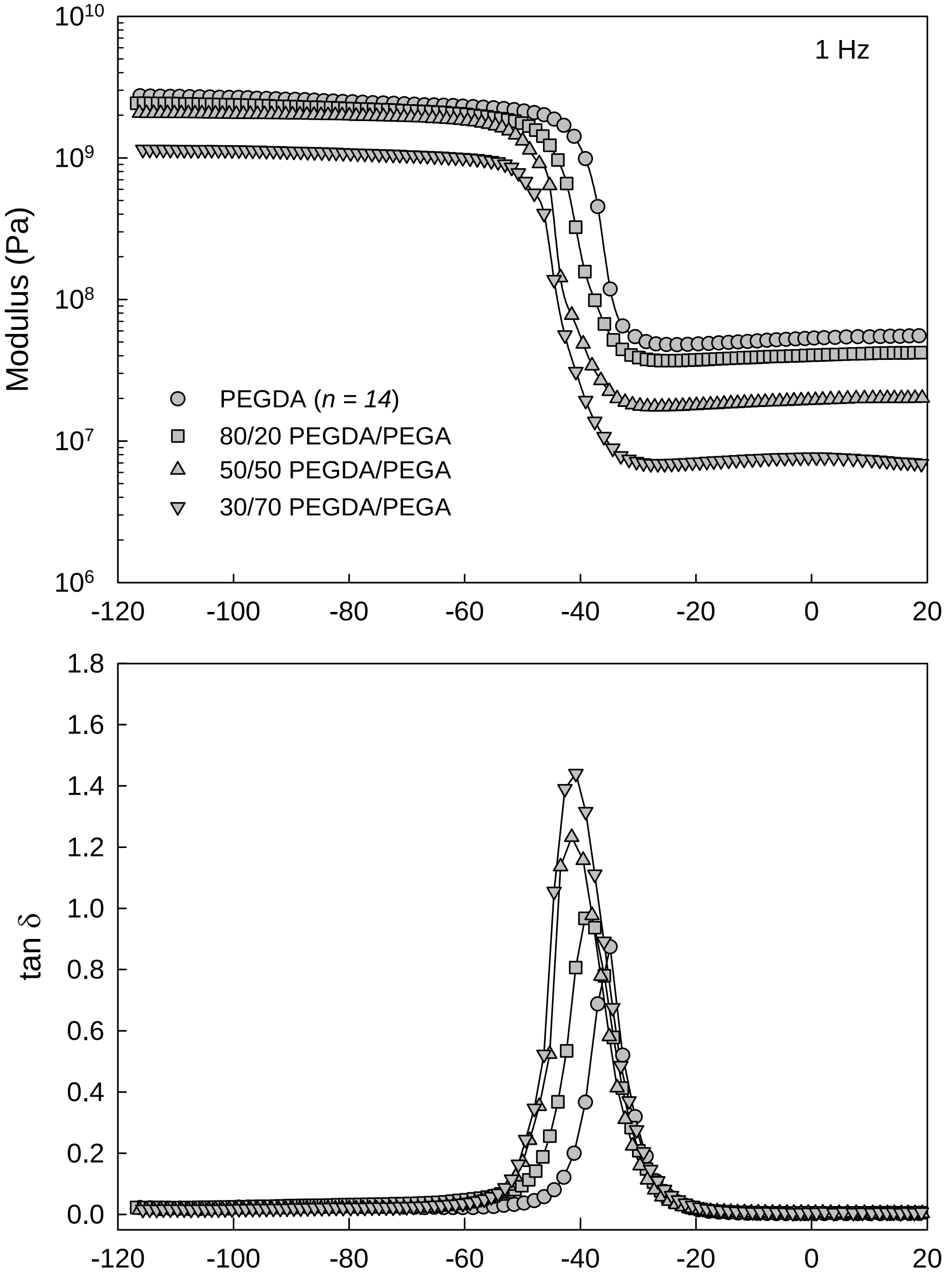

Figure 4.13: Dynamic mechanical properties (*E′*; *tanδ*) versus temperature for PEGDA/PEGA copolymer networks. Frequency of 1 Hz; heating rate of 1°C/min.

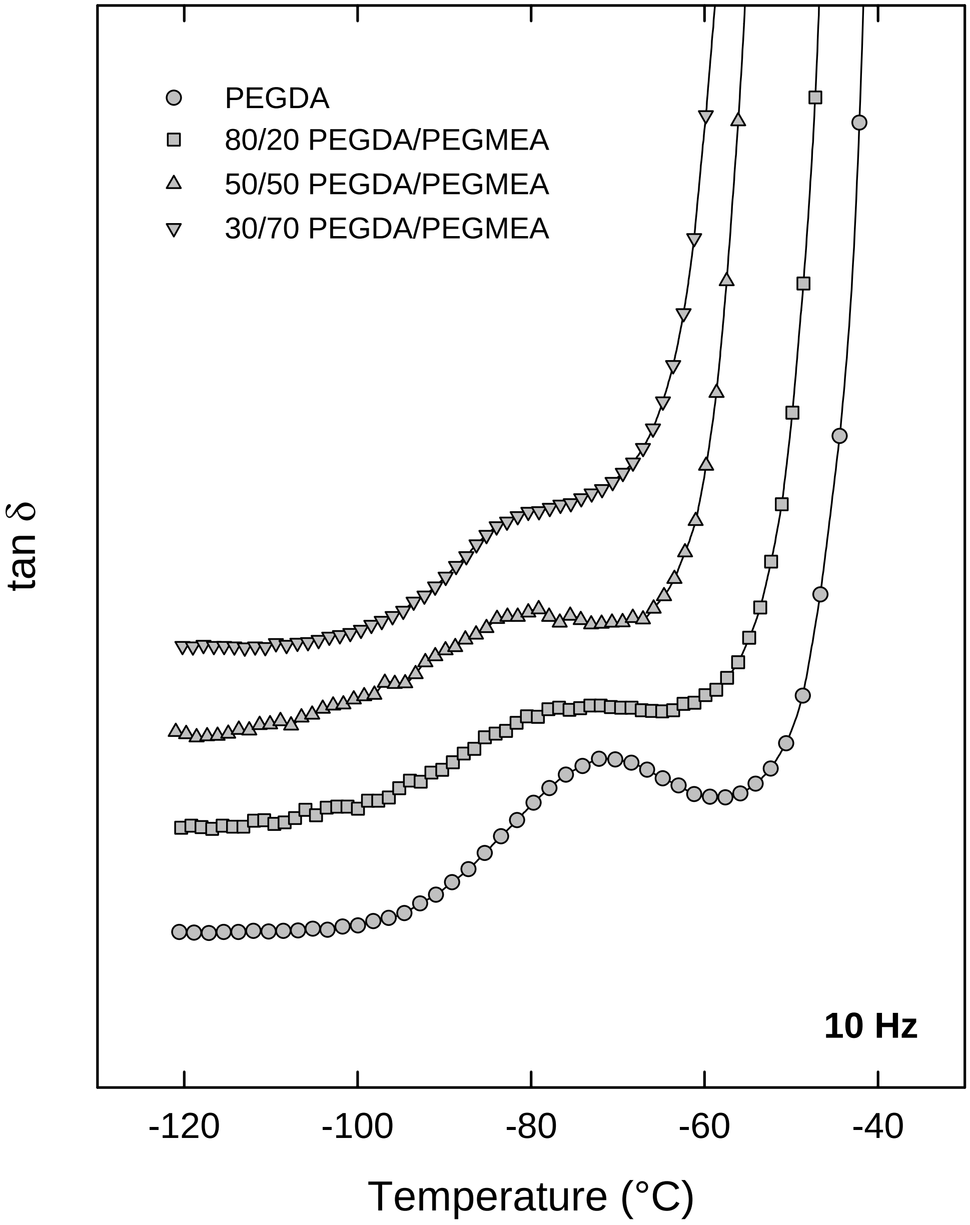

Figure 4.14: *tanδ* versus temperature for PEGDA/PEGMEA networks in the sub-glass transition range. Curves are offset vertically for clarity. Frequency of 10 Hz; heating rate of 1°C/min.

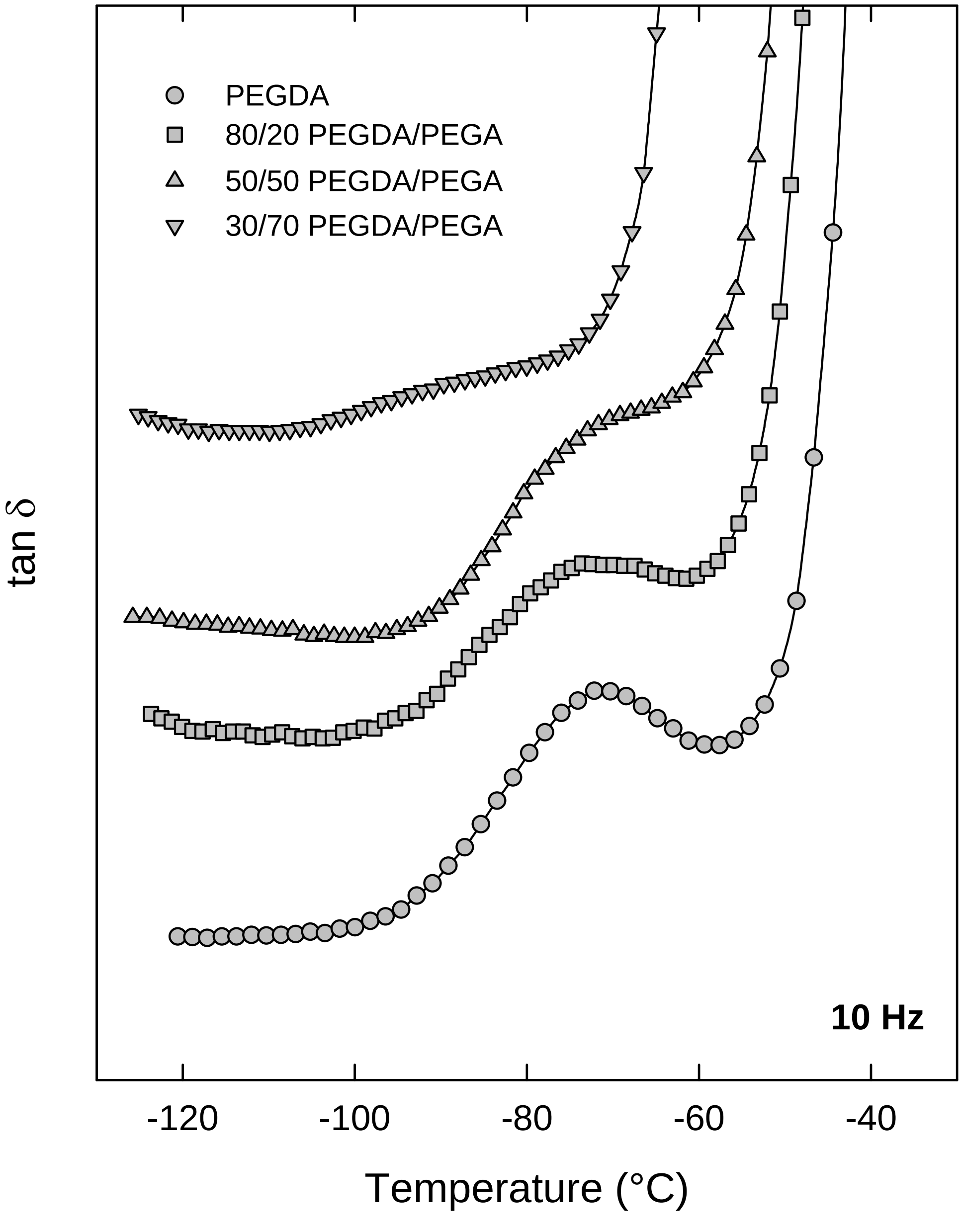

Figure 4.15: *tanδ* versus temperature for PEGDA/PEGA networks in the sub-glass transition range. Curves are offset vertically for clarity. Frequency of 10 Hz; heating rate of 1°C/min.

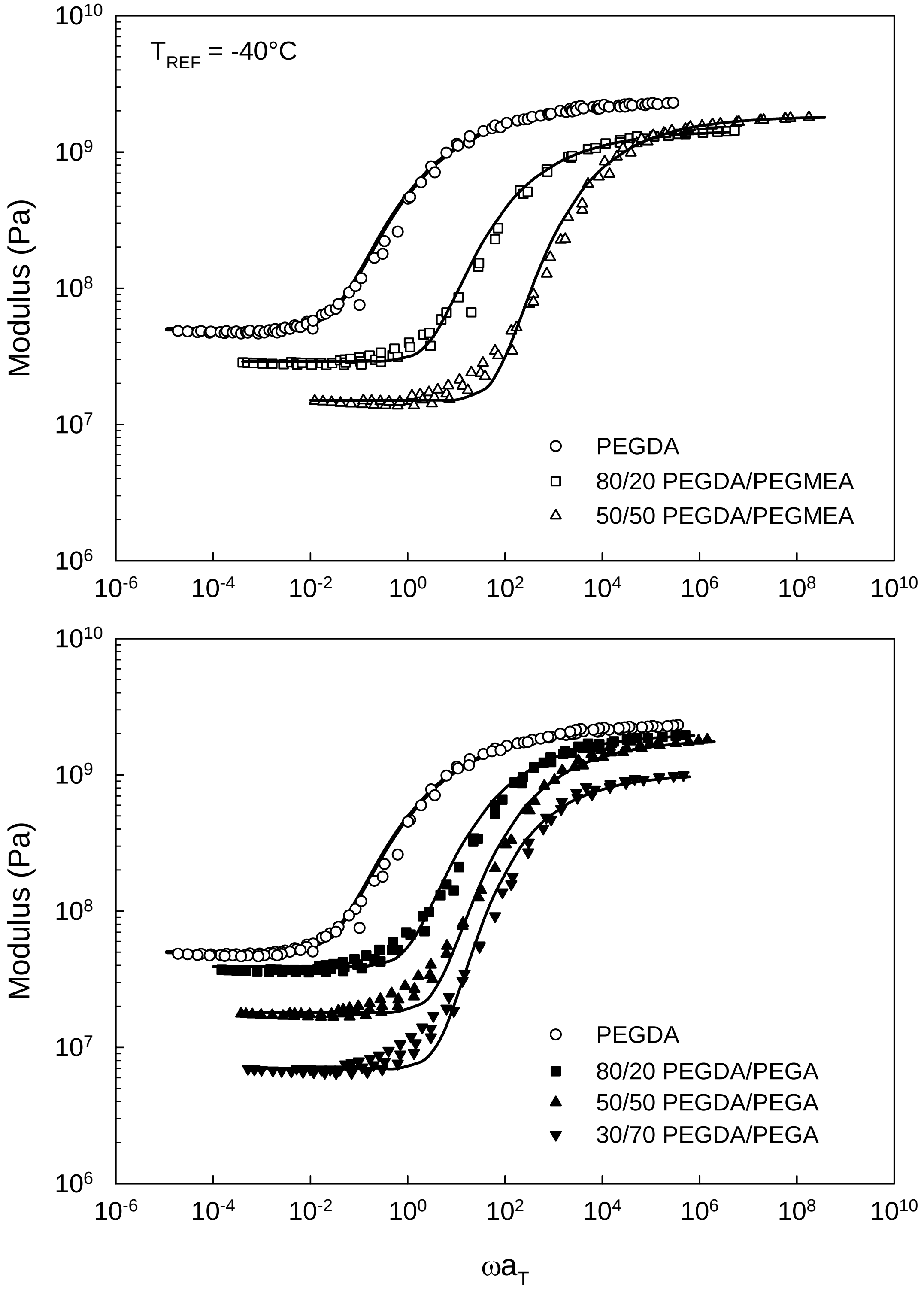

Figure 4.16: Time-temperature master curves for PEGDA copolymer networks; T_{REF} = –40°C. Solid curves are KWW best fits.

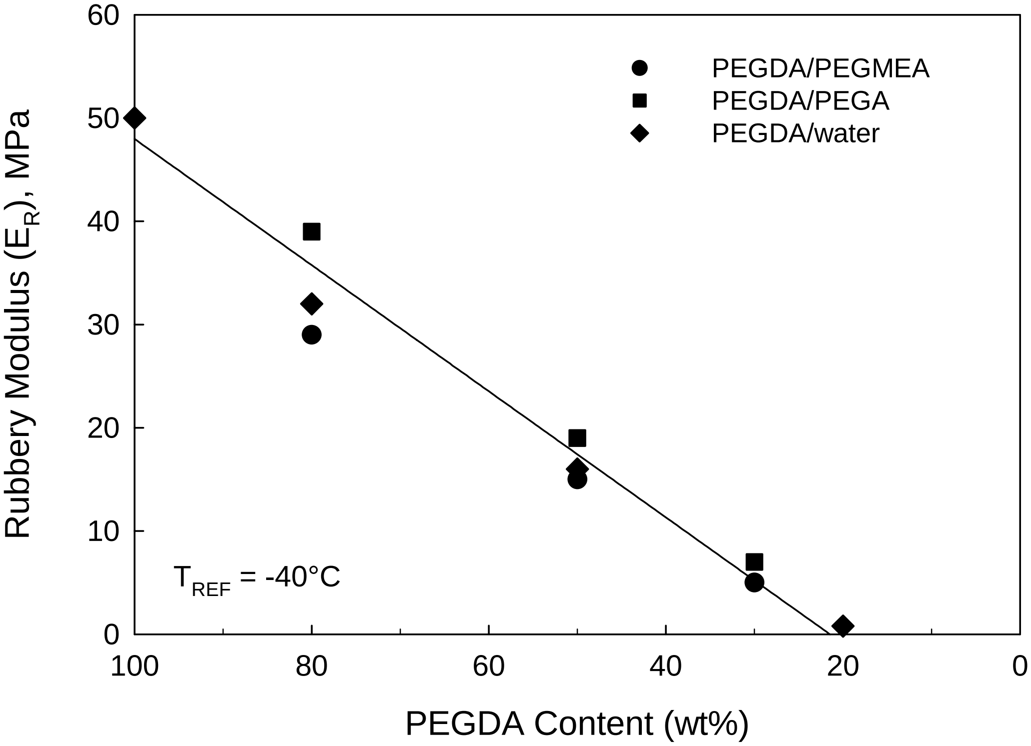

Figure 4.17: Rubbery modulus (E_R, MPa) versus PEGDA content for PEGDA/PEGMEA, PEGDA/PEGA, and PEGDA/water networks. E_R evaluated from time-temperature master curves at –40°C.

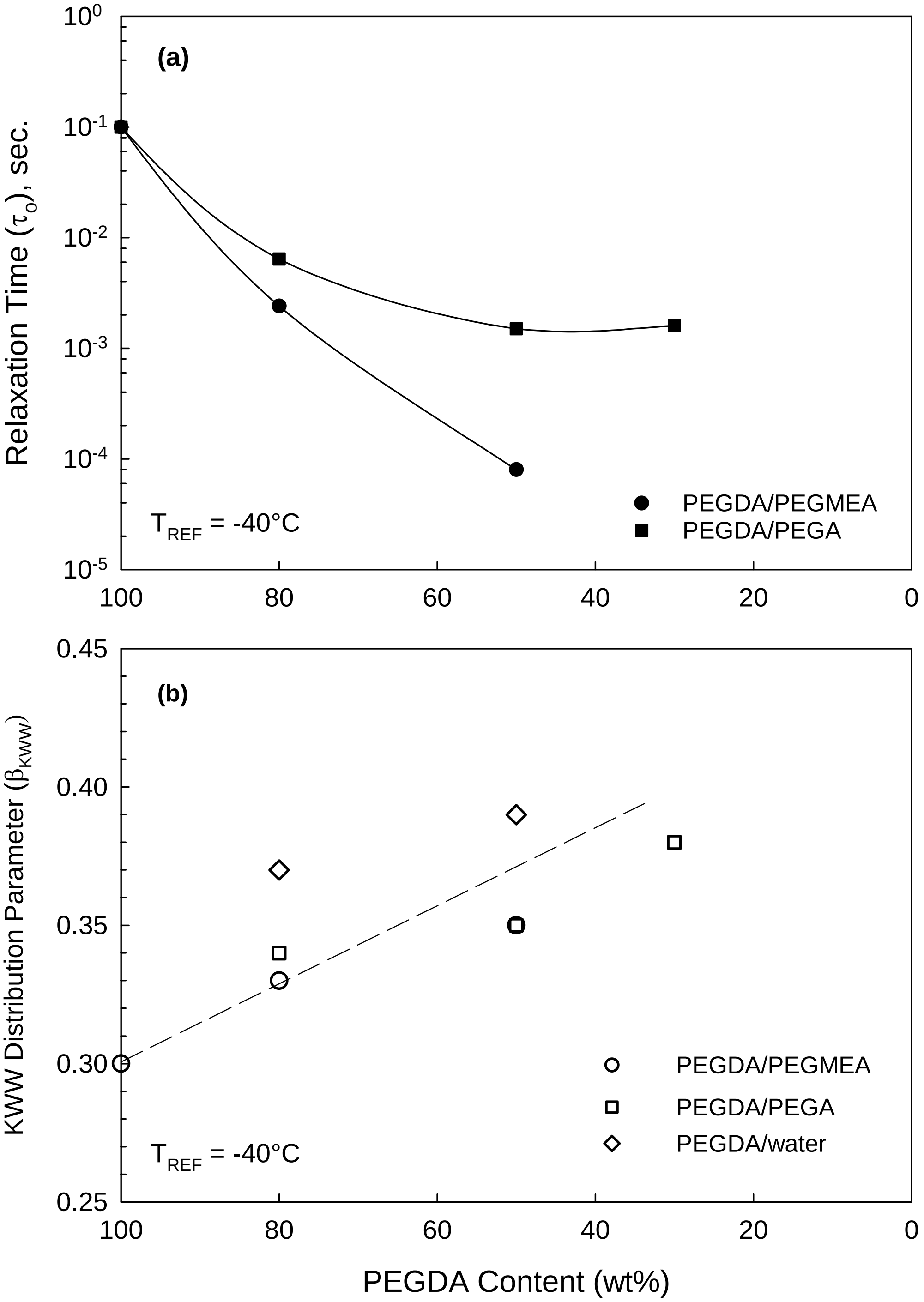

Figure 4.18: KWW parameters for the glass-rubber relaxation in PEGDA networks; T_{REF} = –40°C. (a) Relaxation time (τ_o, sec) versus PEGDA content; (b) Distribution parameter (β_{KWW}) versus PEGDA content.

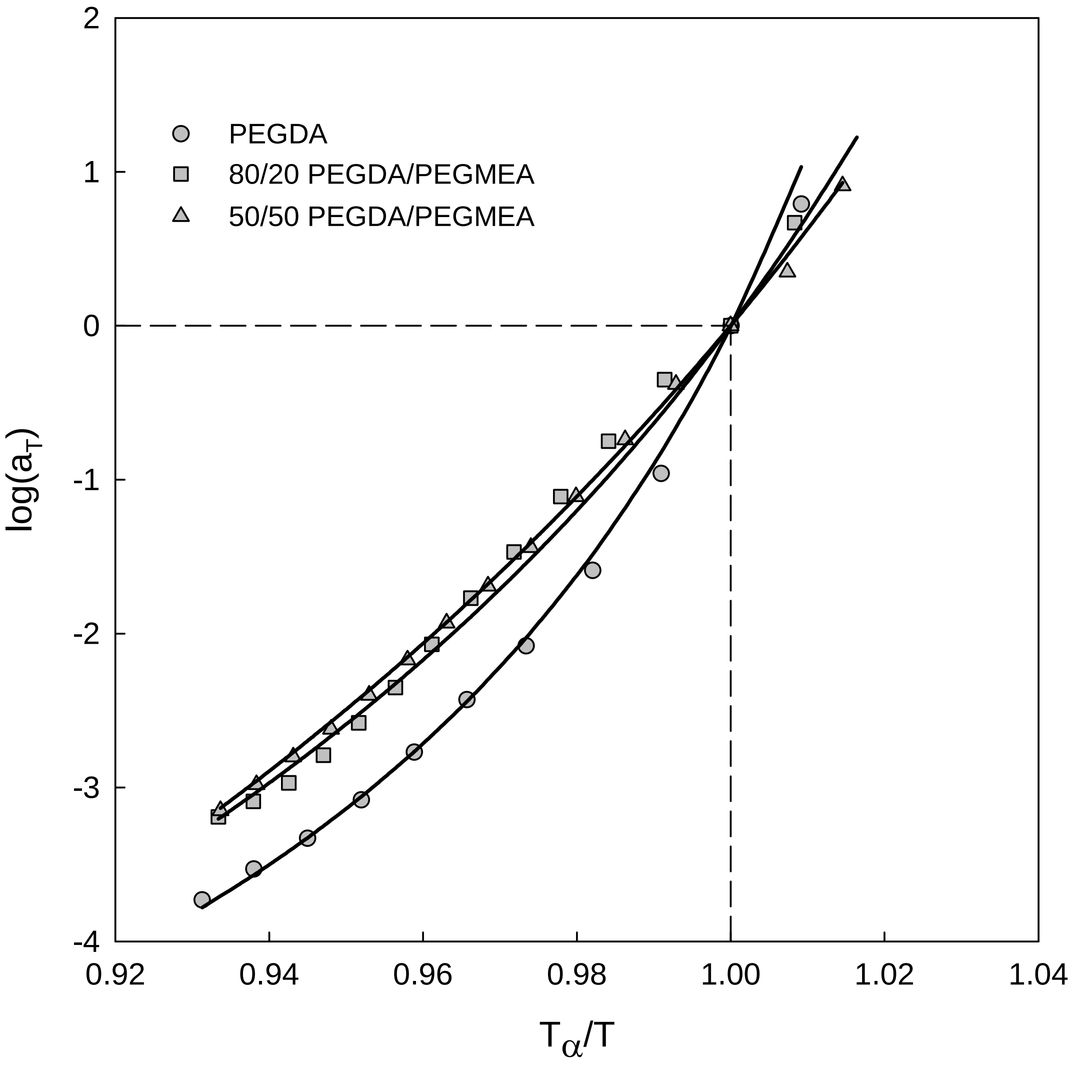

Figure 4.19: Cooperativity plots (log(a_T) versus T_α/T) for PEGDA/PEGMEA copolymer networks. Solid curves are WLF fits.

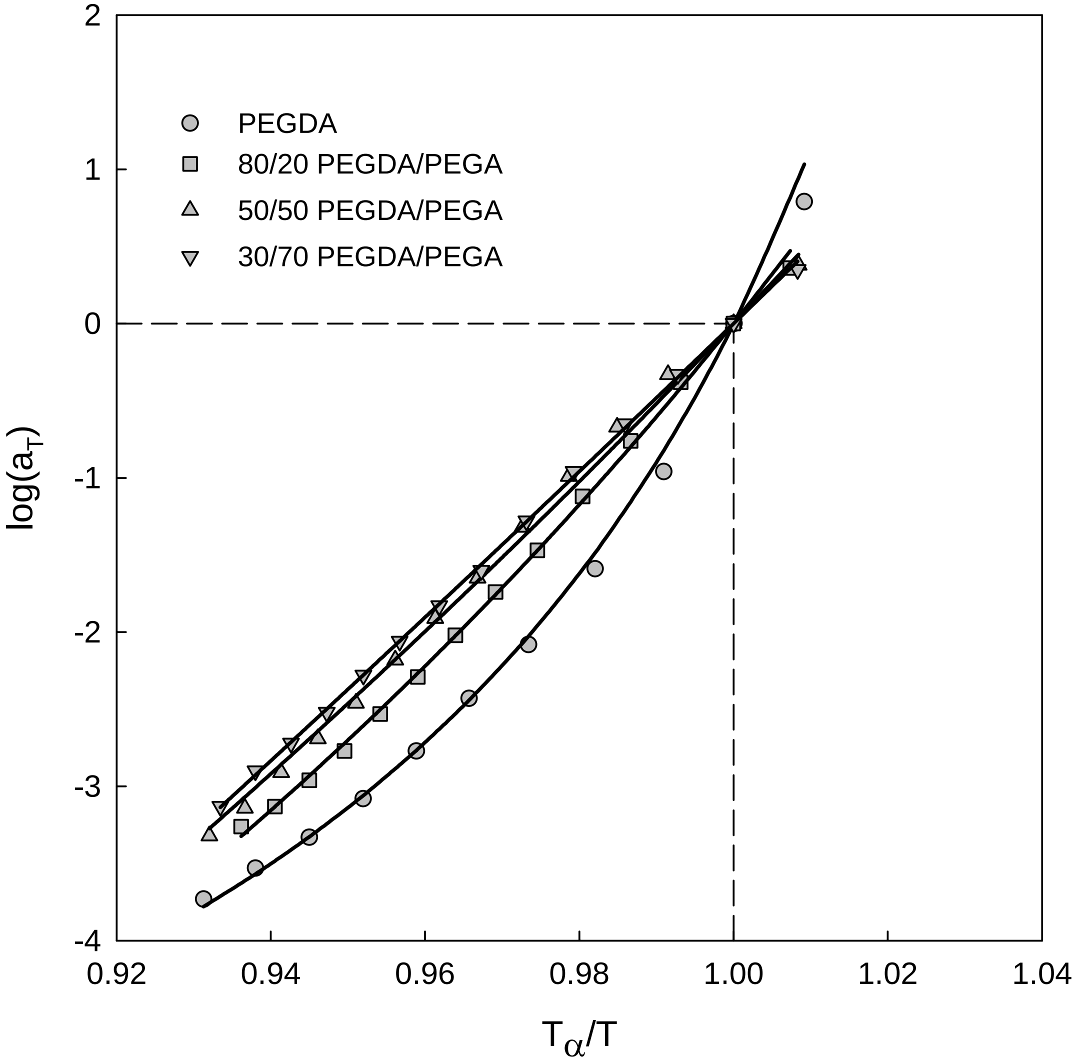

Figure 4.20: Cooperativity plots (log(a_T) versus T_α/T) for PEGDA/PEGA copolymer networks. Solid curves are WLF fits.

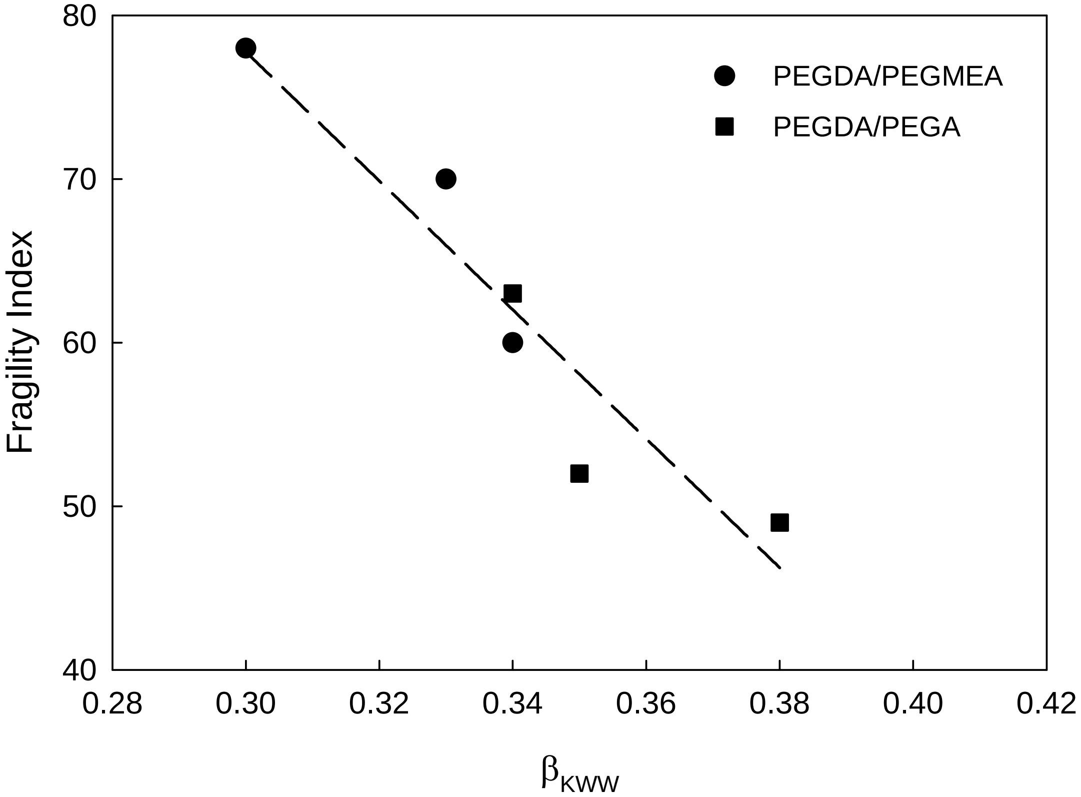

Figure 4.21: Fragility index (m), as defined in Eq. 2.11, versus KWW distribution parameter (β_{KWW}) for PEGDA copolymer networks.

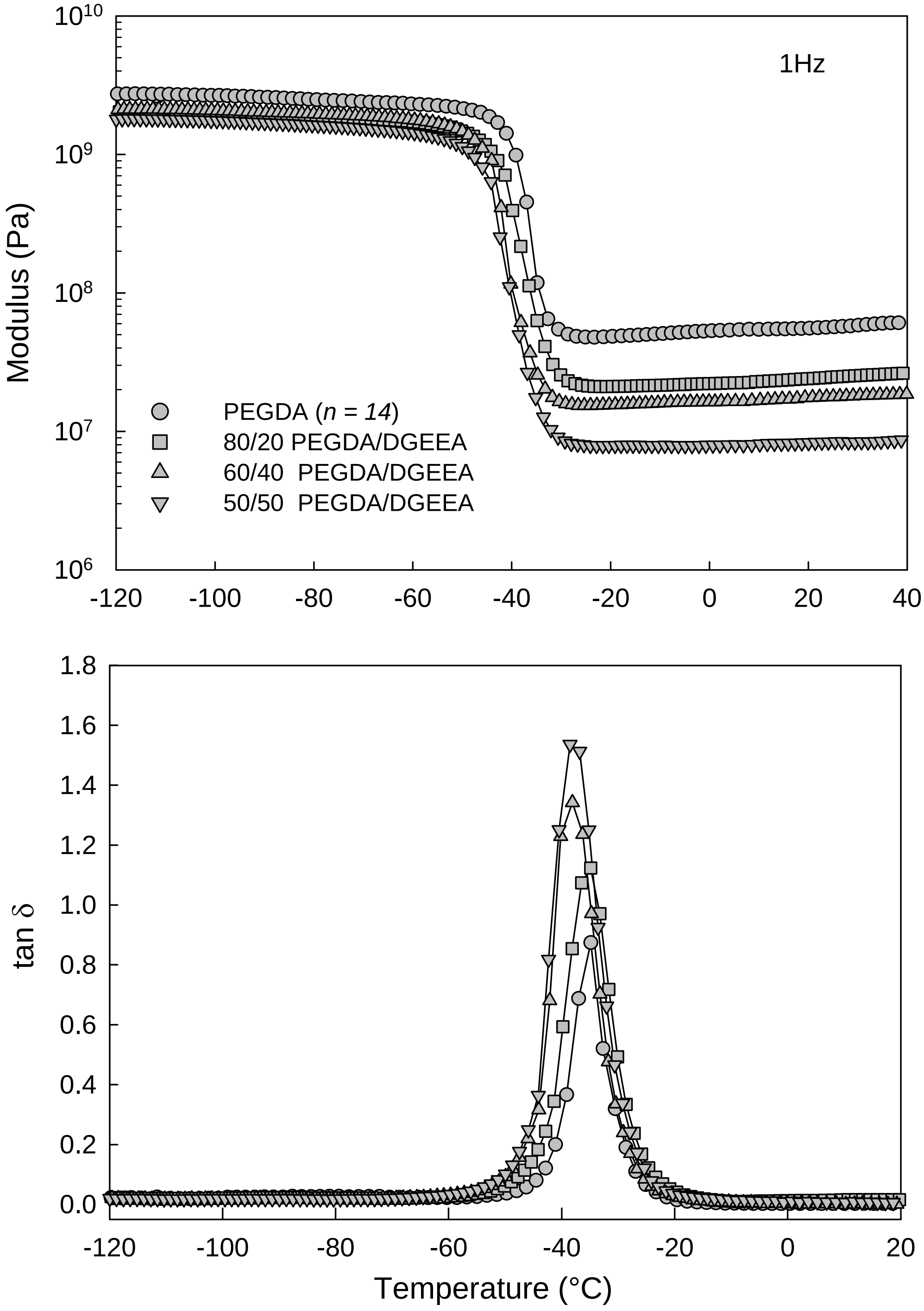

Figure 4.22: Dynamic mechanical properties (*E'*; *tanδ*) versus temperature for PEGDA/DGEEA copolymer networks. Frequency of 1 Hz; heating rate of 1°C/min.

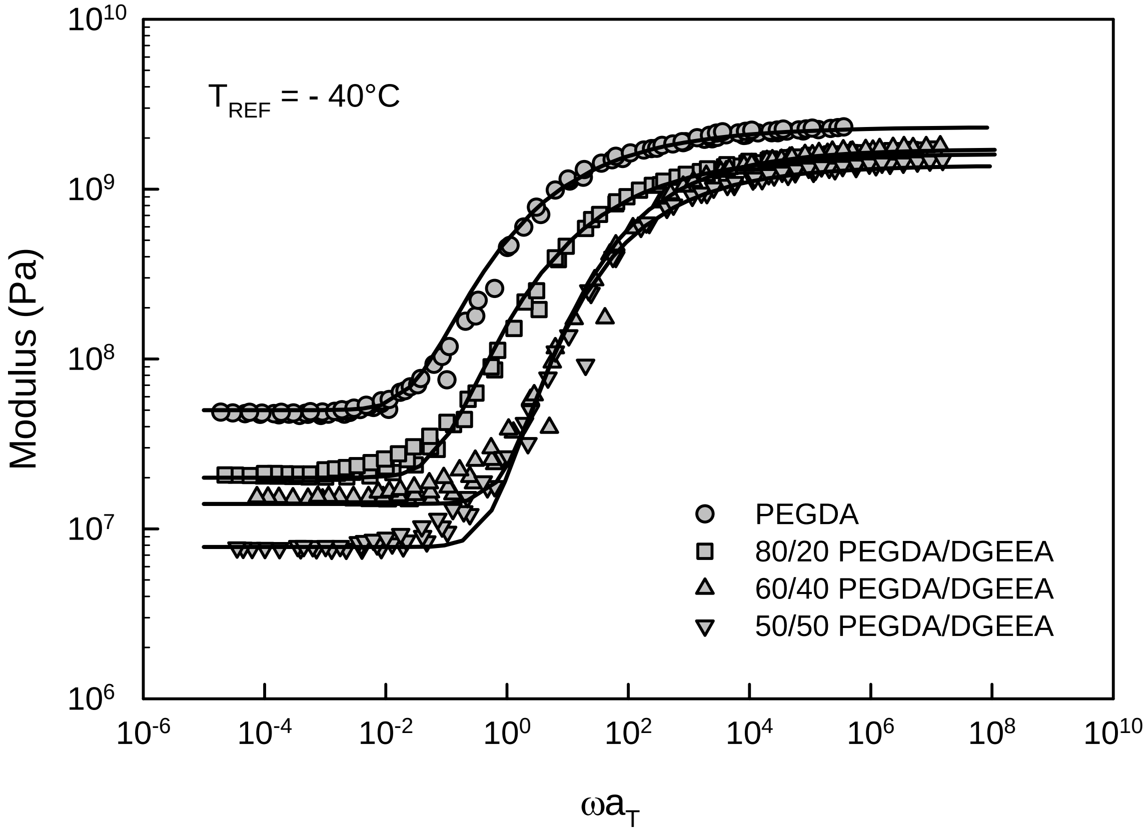

Figure 4.23: Time-temperature master curves for PEGDA/DGEEA copolymer networks; $T_{REF} = -40$°C. Solid curves are KWW best fits.

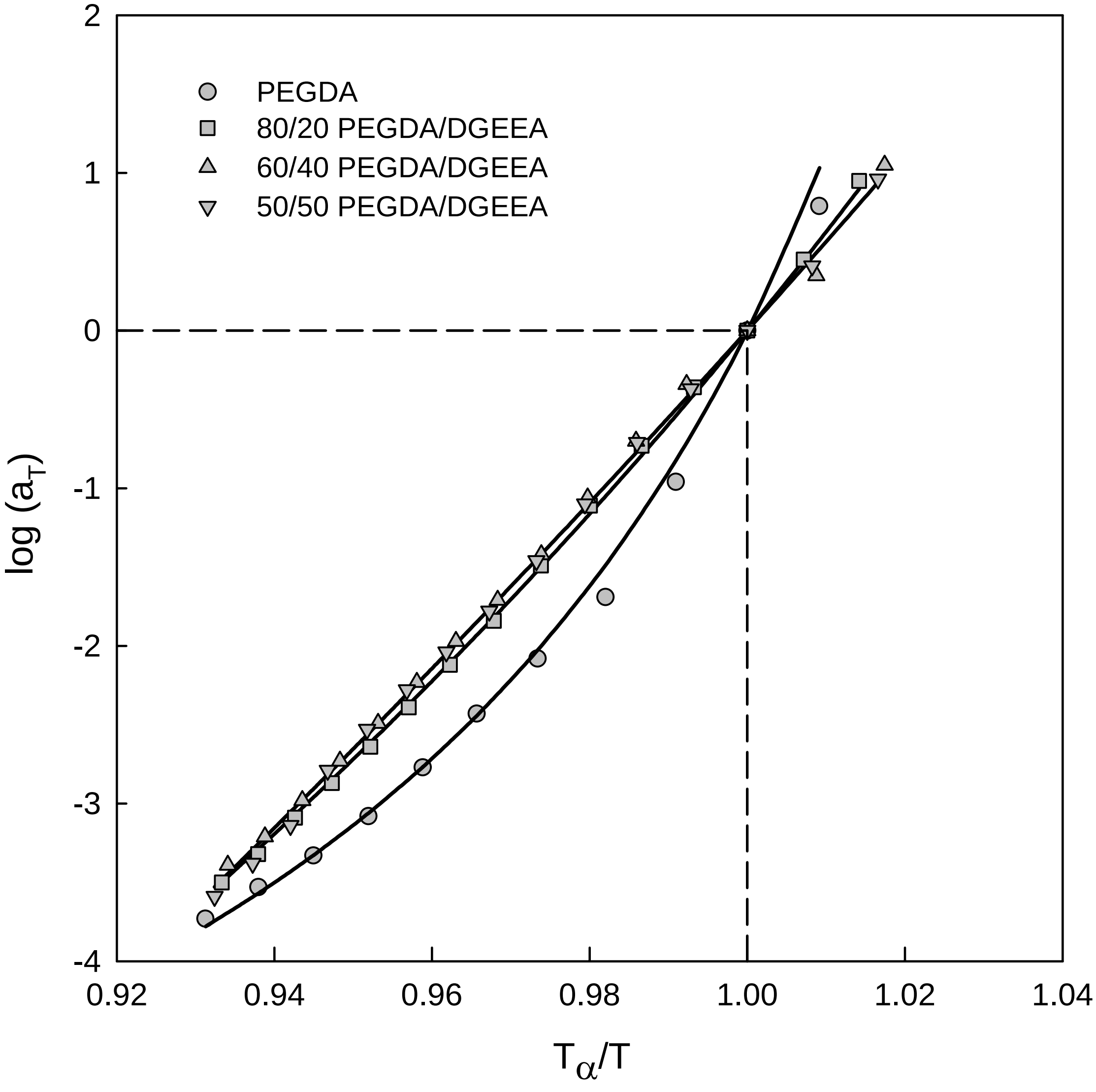

Figure 4.24: Cooperativity plots (log(a_T) versus T_α/T) for PEGDA/DGEEA copolymer networks. Solid curves are WLF fits.

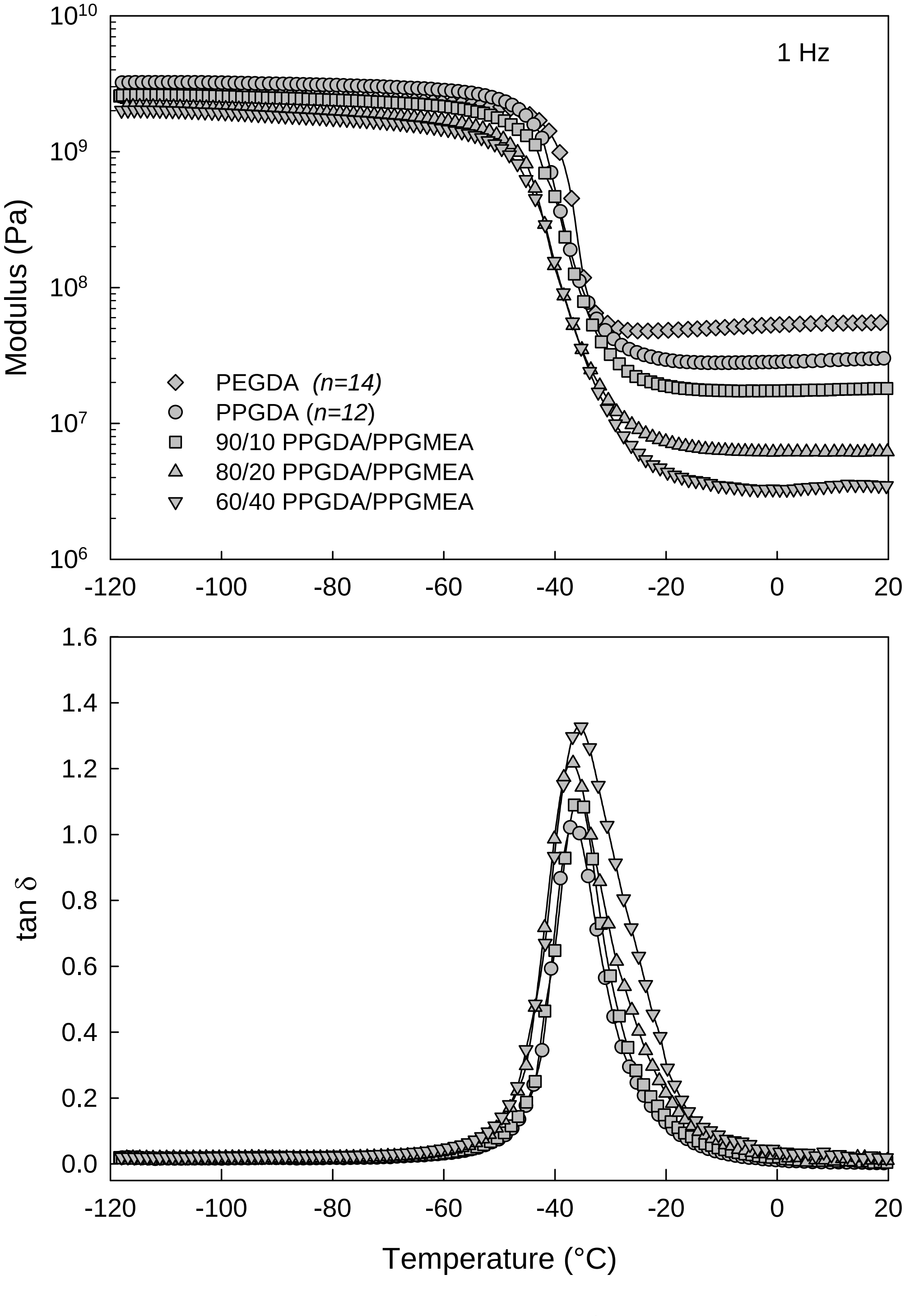

Figure 4.25: Dynamic mechanical properties (*E′*; *tanδ*) versus temperature for 100% PEGDA and PPGDA/PPGMEA copolymer networks. Frequency of 1 Hz; heating rate of 1°C/min.

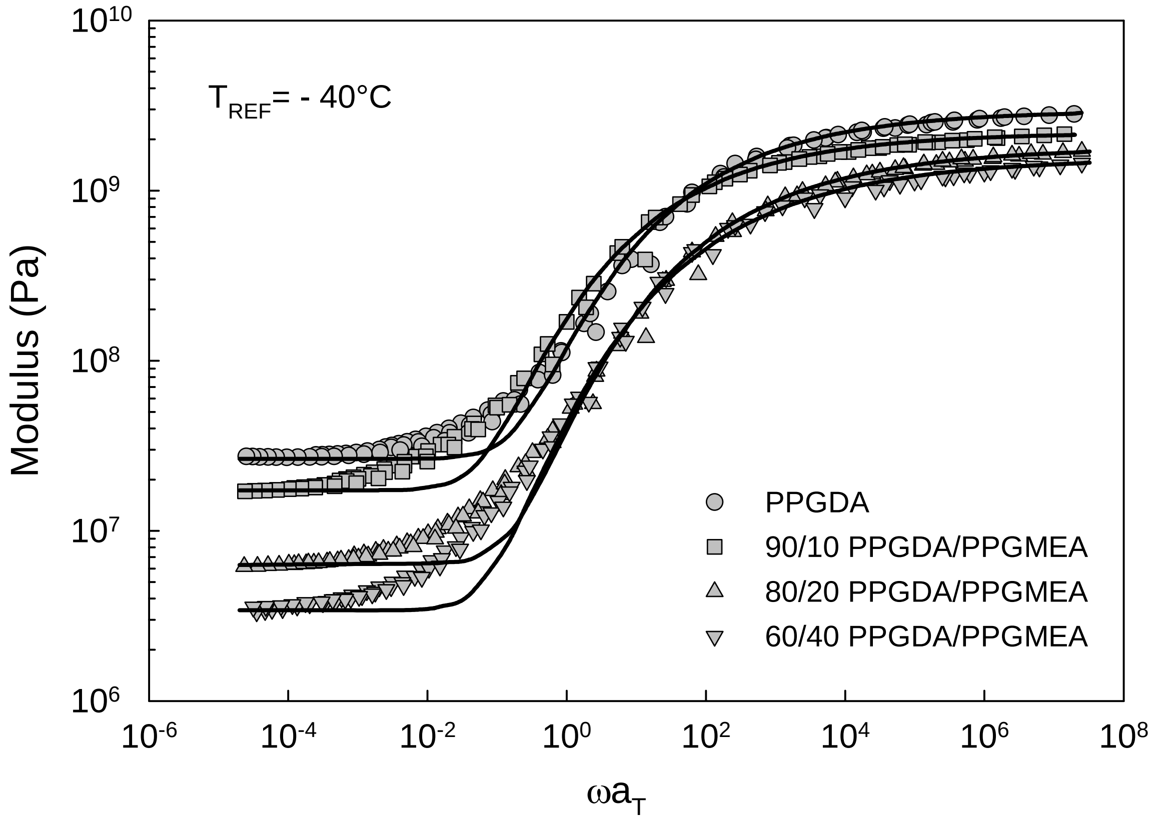

Figure 4.26: Time-temperature master curves for PPGDA/PPGMEA copolymer networks; T_{REF} = –40°C. Solid curves are KWW best fits.

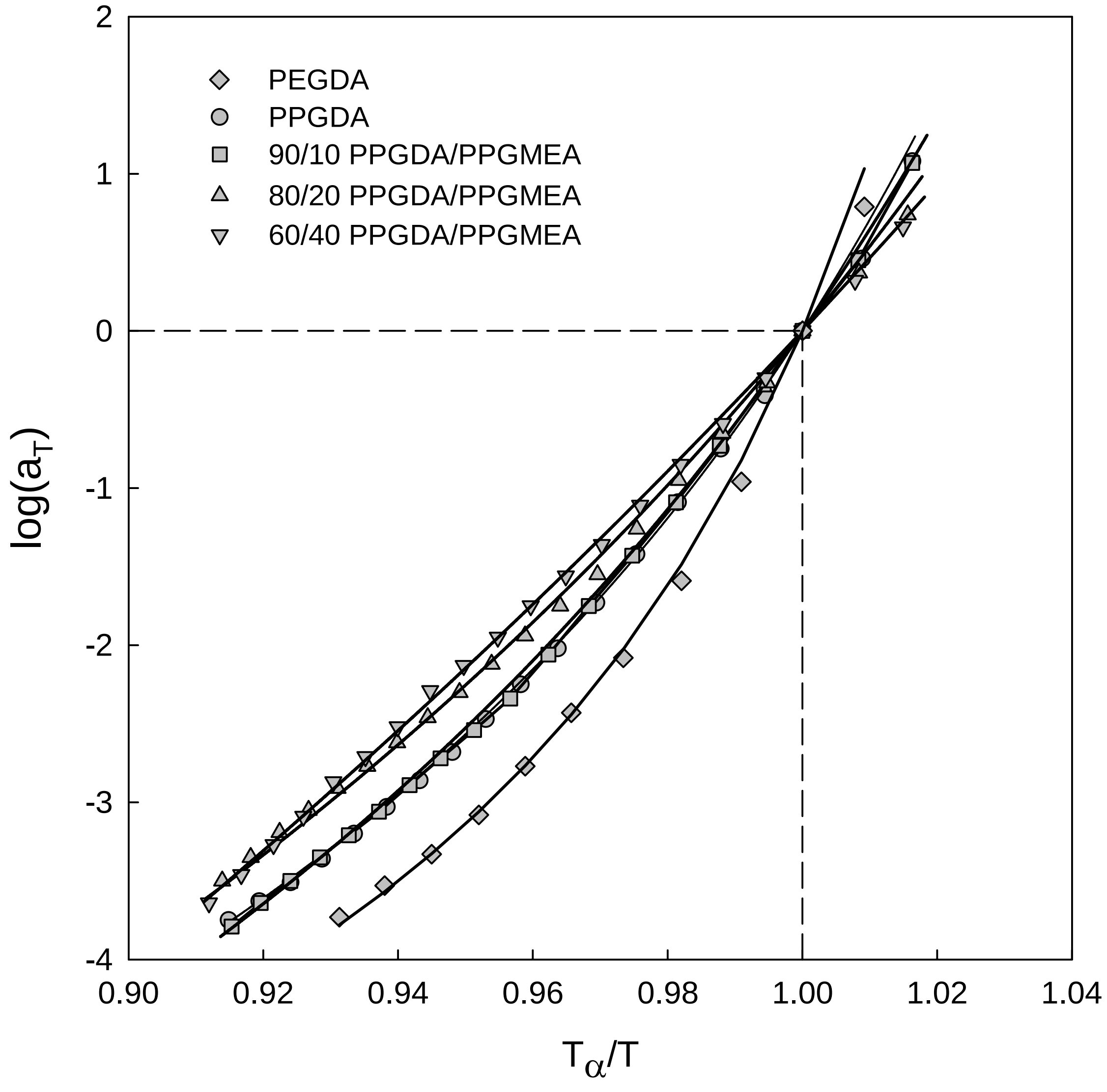

Figure 4.27: Cooperativity plots (log(a_T) versus T_α/T) for PPGDA/PPGMEA copolymer networks. Solid curves are WLF fits.

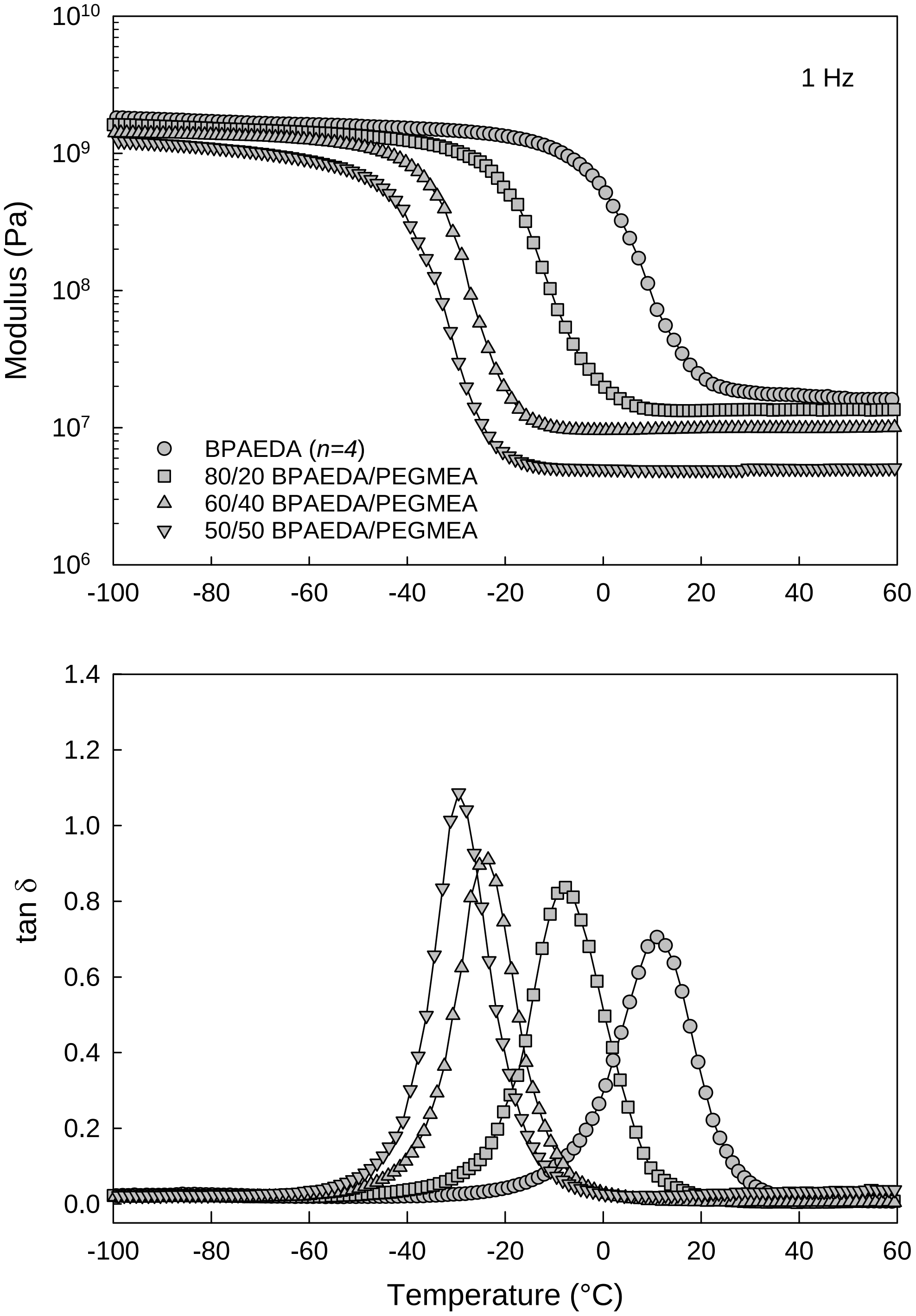

Figure 4.28: Dynamic mechanical properties (*E'*; *tanδ*) versus temperature for BPAEDA/PEGMEA copolymer networks. Frequency of 1 Hz; heating rate of 1°C/min.

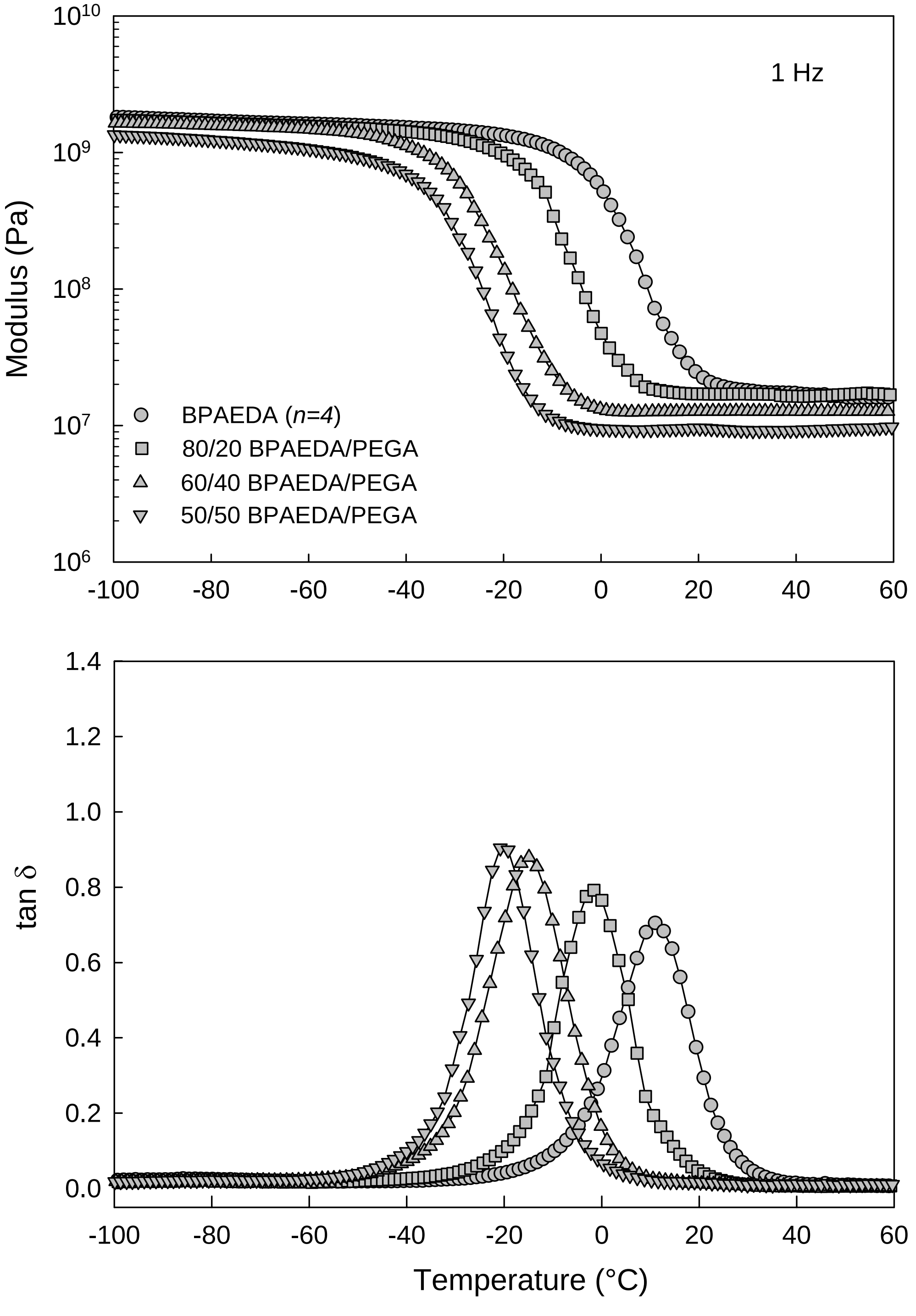

Figure 4.29: Dynamic mechanical properties (E'; $tan\delta$) versus temperature for BPAEDA/PEGA copolymer networks. Frequency of 1 Hz; heating rate of 1°C/min.

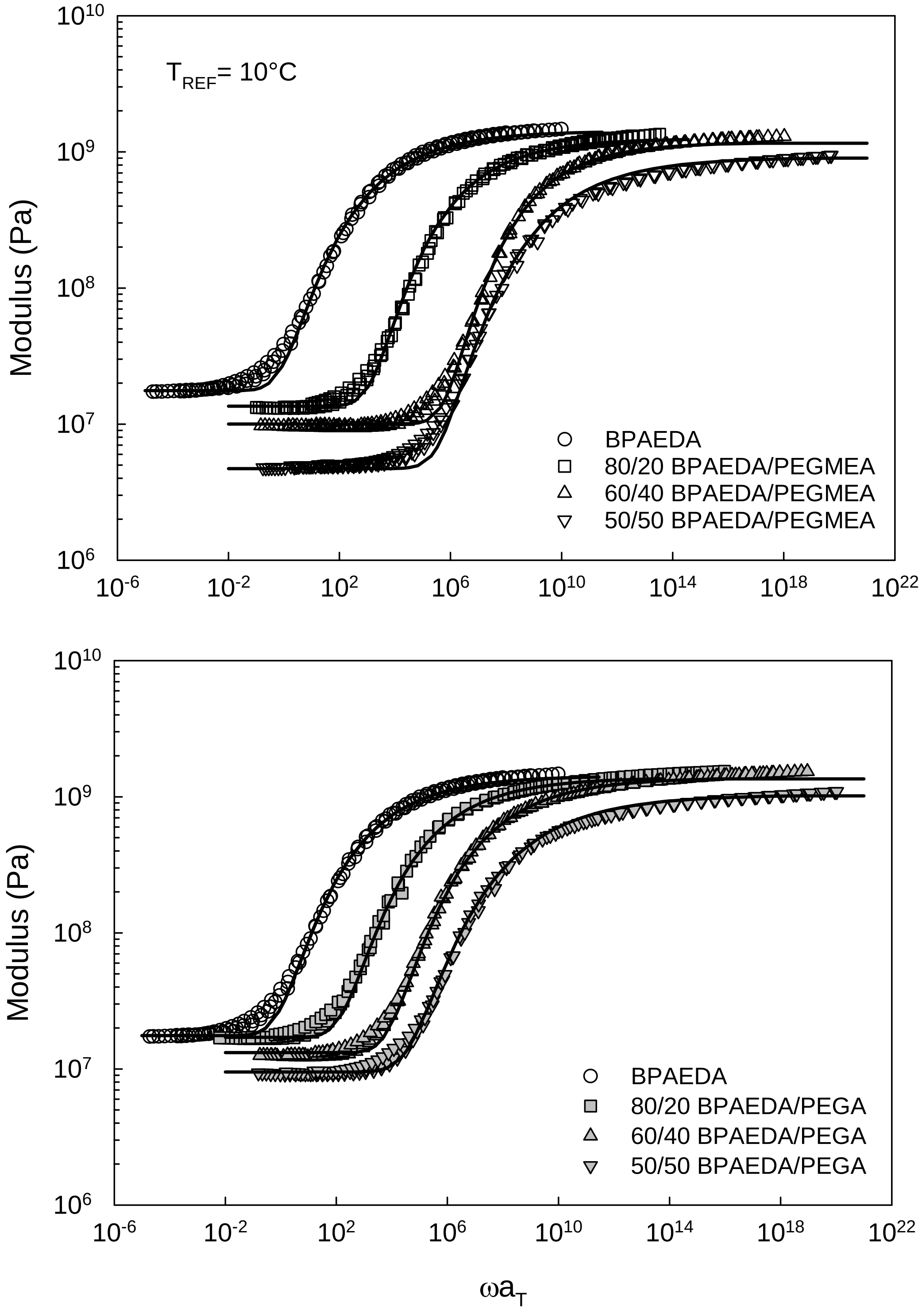

Figure 4.30: Time-temperature master curves for BPAEDA copolymer networks; T_{REF} = 10°C. Solid curves are KWW best fits.

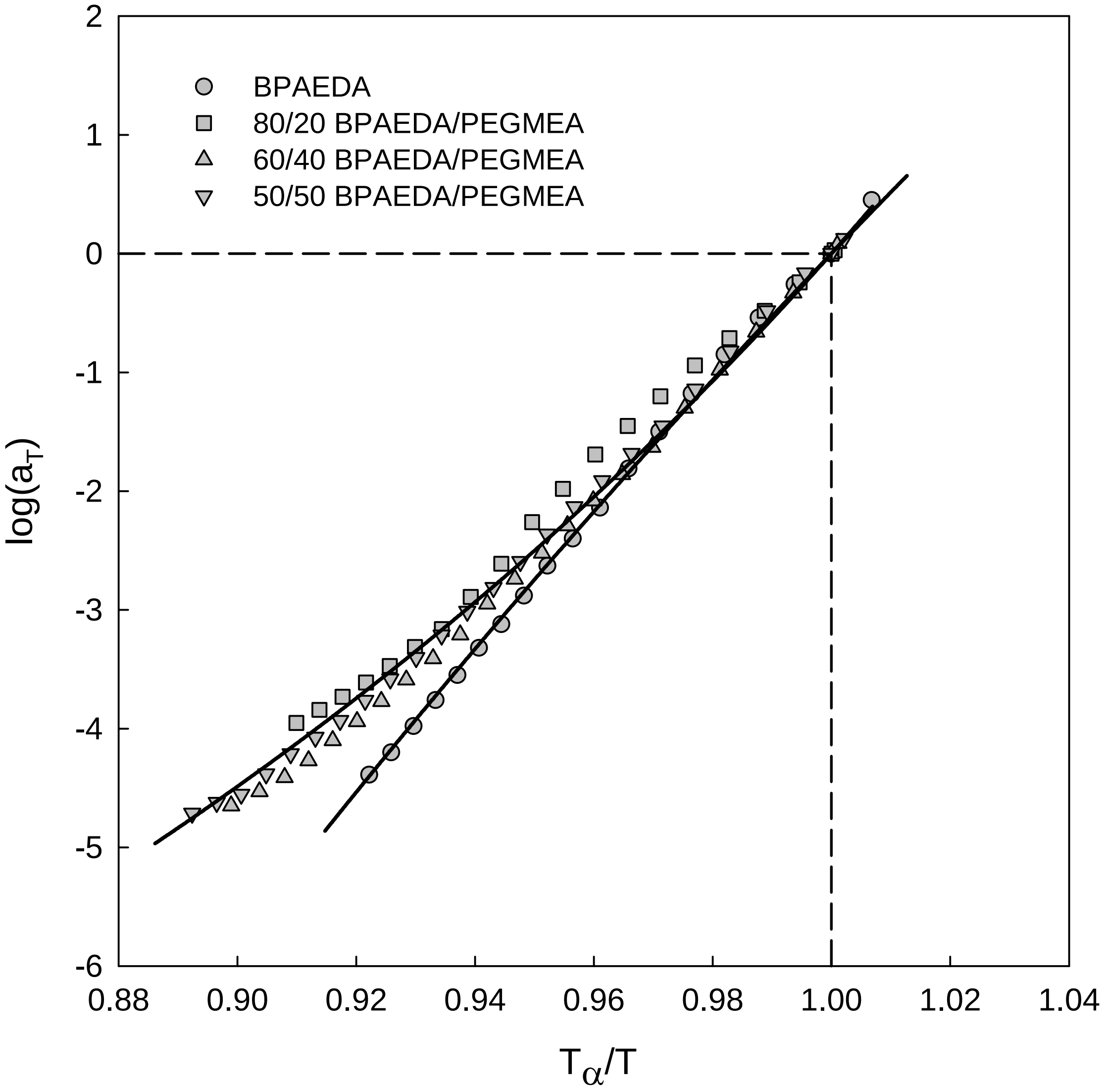

Figure 4.31: Cooperativity plots (log(a_T) versus T_α/T) for BPAEDA/PEGMEA copolymer networks. Solid curves are WLF fits.

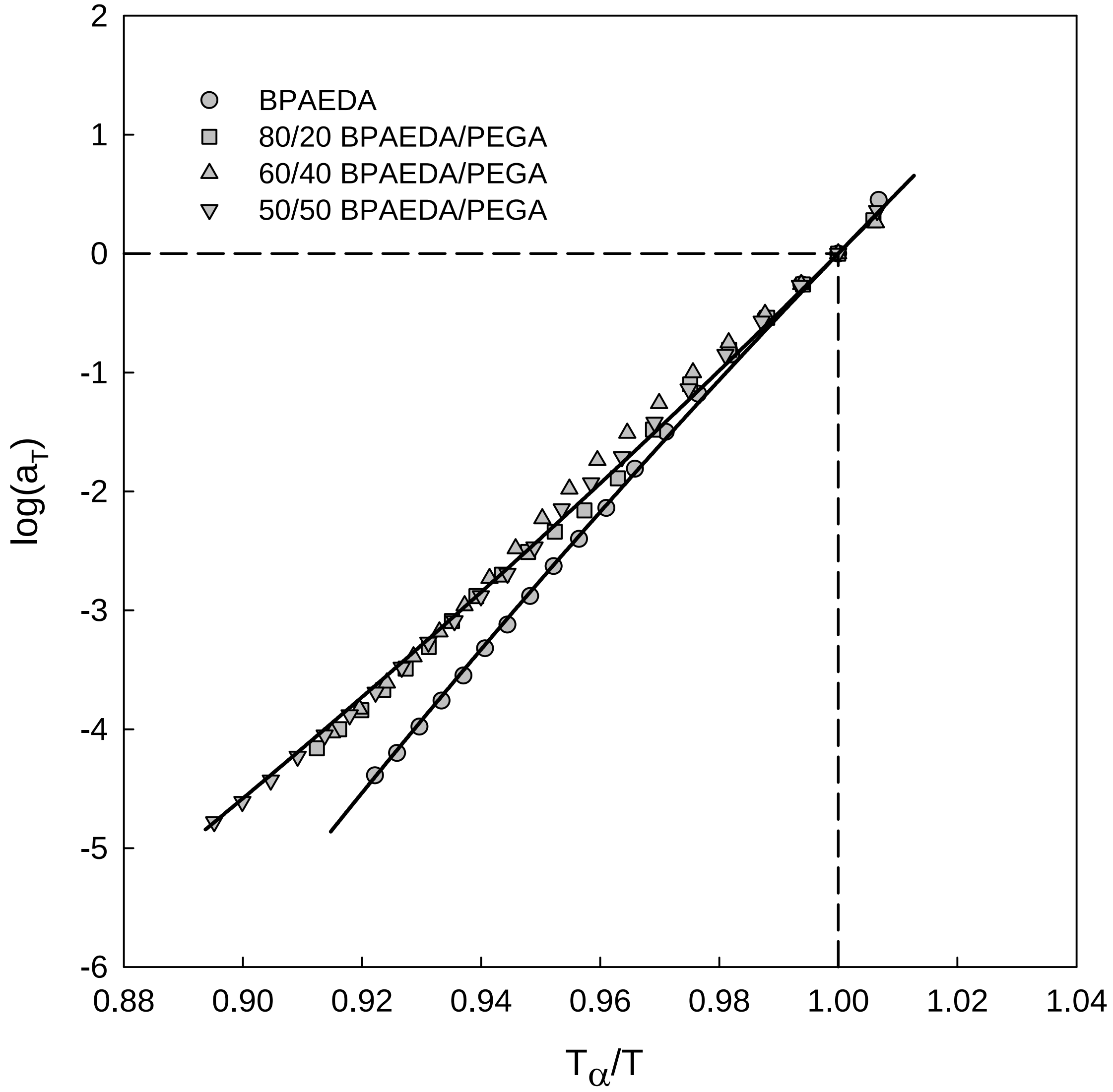

Figure 4.32: Cooperativity plots (log(a_T) versus T_α/T) for BPAEDA/PEGA copolymer networks. Solid curves are WLF fits.

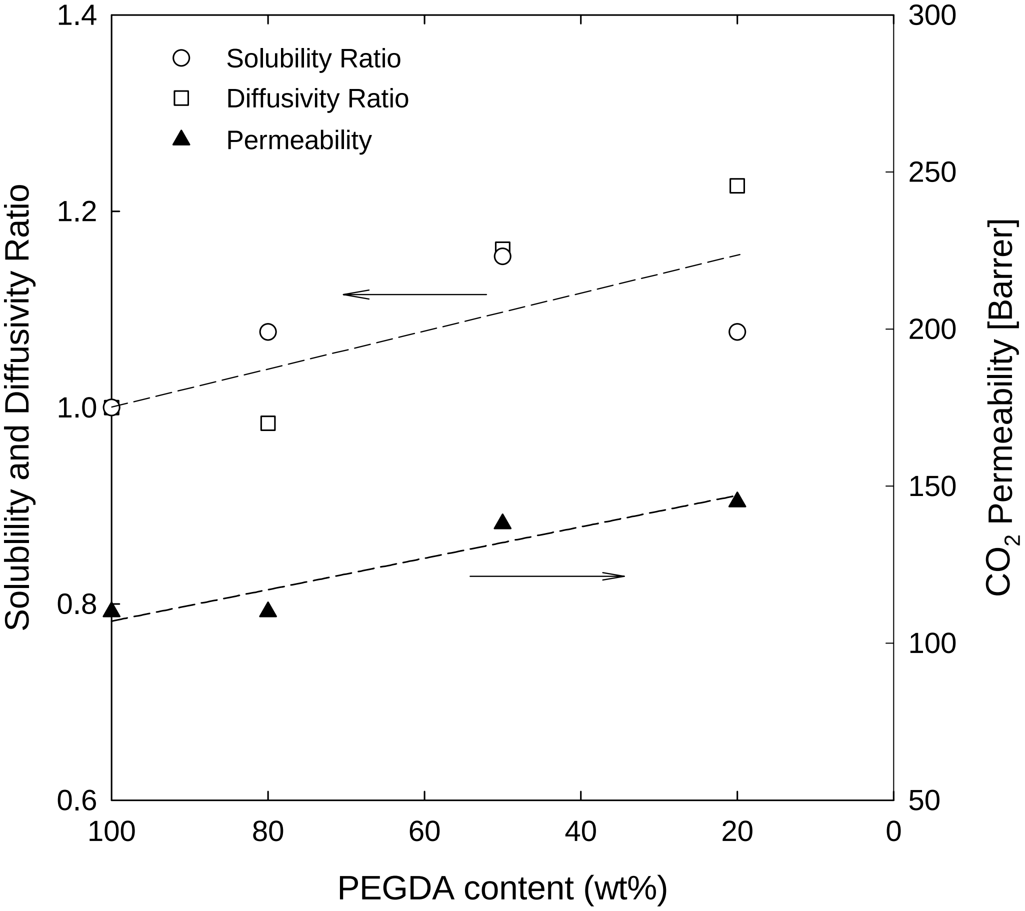

Figure 4.33: CO_2 transport properties determined at 35°C and infinite dilution for PEGDA/water networks. Solubility, diffusivity ratios defined relative to values for 100% PEGDA (*n=14*): S = 1.3 cm^3(STP)/(cm^3-atm), D = 6.2 x 10^{-7} cm^2/s.[115]

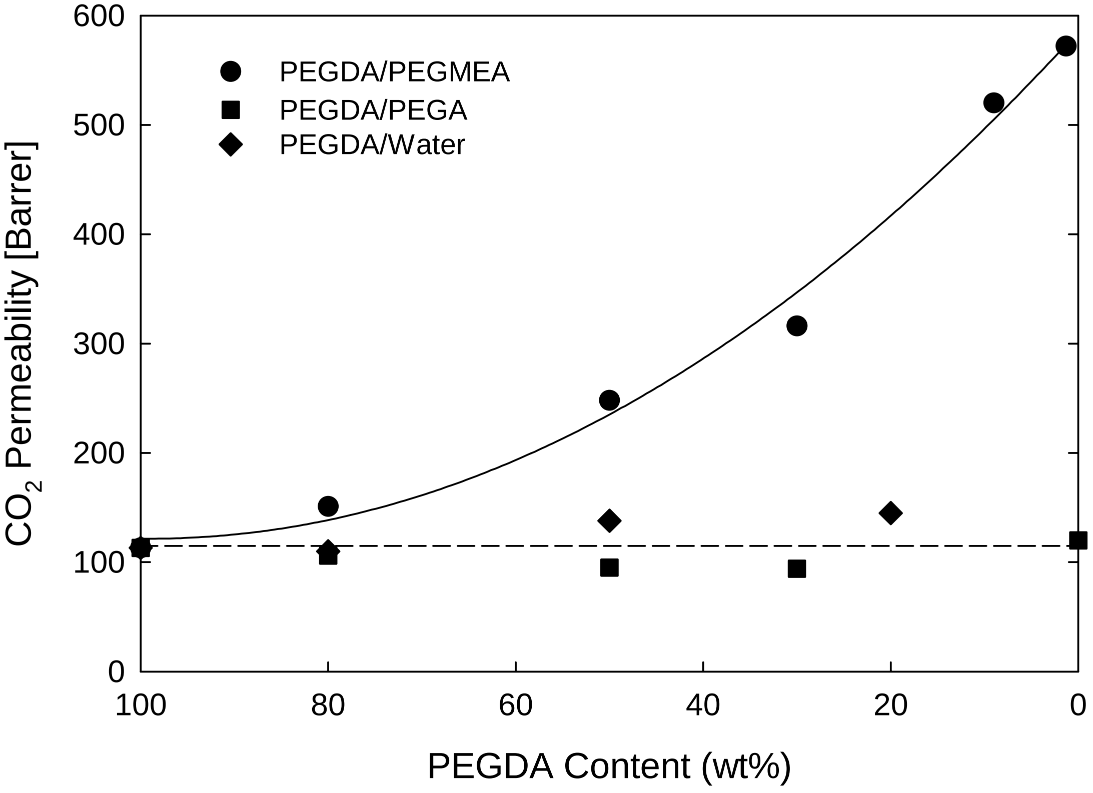

Figure 4.34: CO_2 permeability (Barrer) determined at 35°C and infinite dilution for PEGDA networks.[115,124] 1 Barrer = 10^{-10}cm^3(STP) cm/(cm^{2}s cm-Hg).

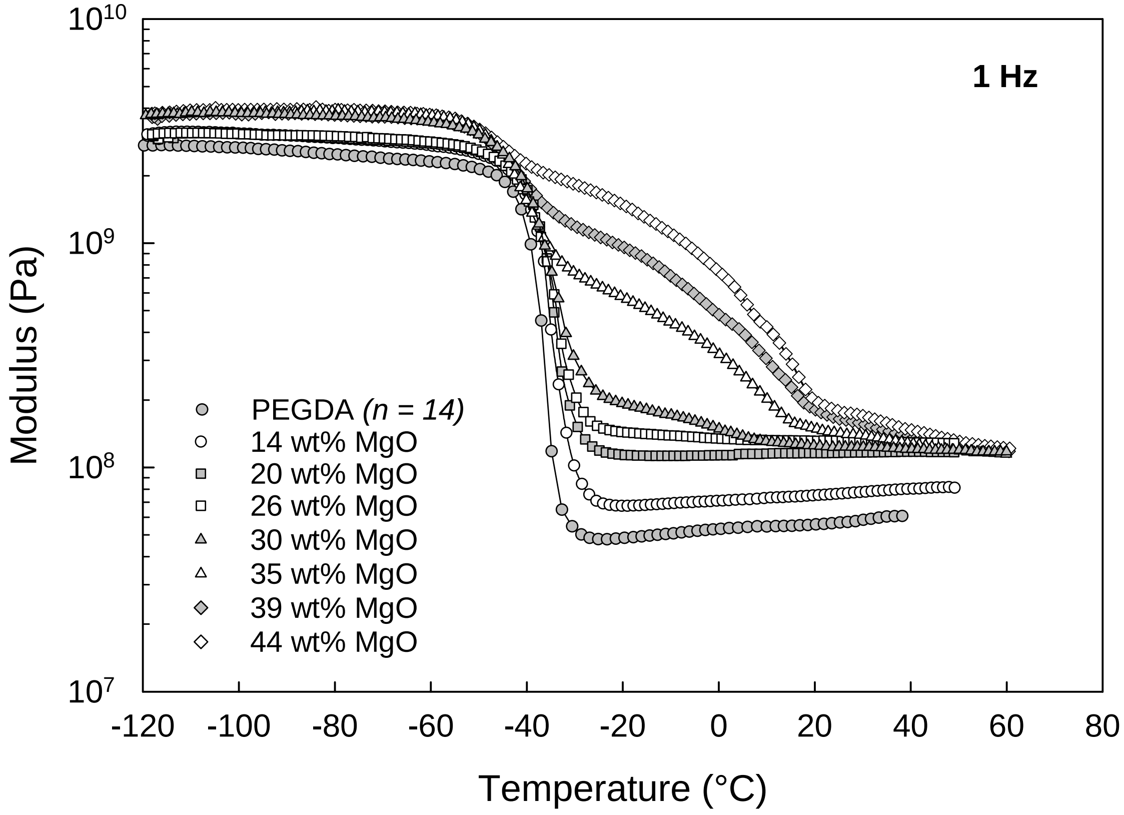

Figure 4.35: Dynamic mechanical storage modulus (*E′*) versus temperature for PEGDA networks with varying MgO (wt%) loading. Frequency of 1 Hz; heating rate of 1°C/min.

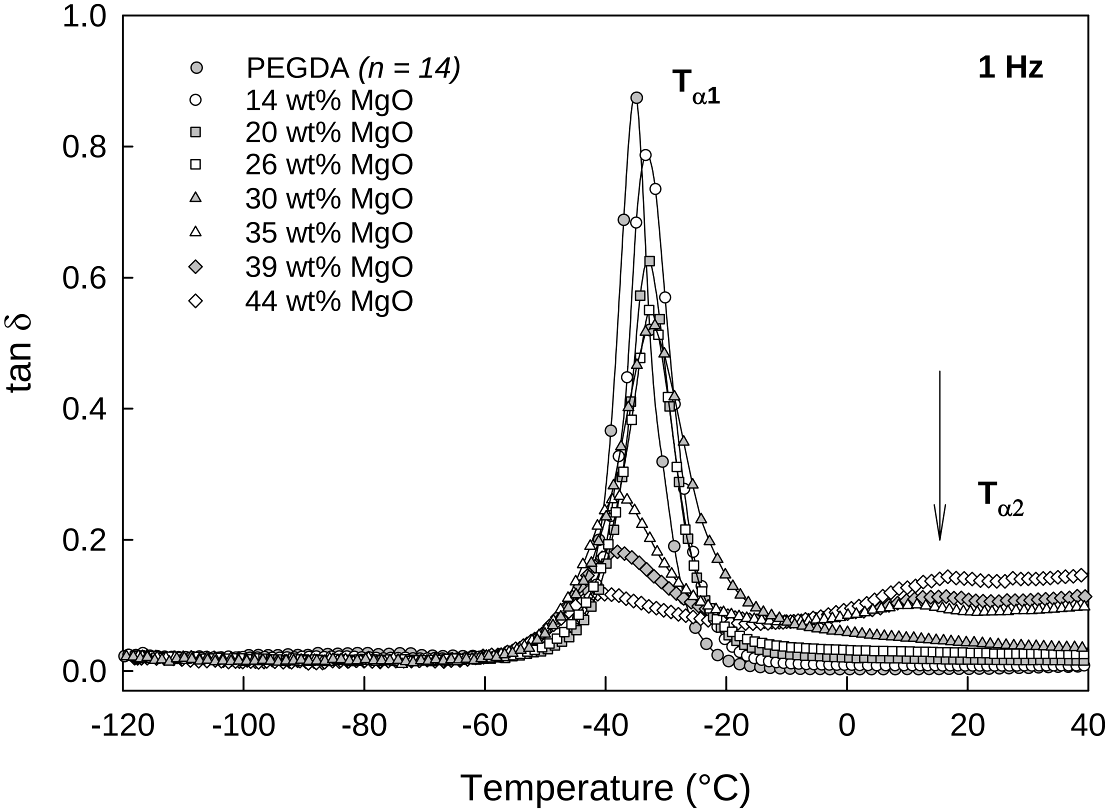

Figure 4.36: Dynamic mechanical loss factor (*tanδ*) versus temperature for PEGDA networks with varying MgO (wt%) loading. Frequency of 1 Hz; heating rate of 1°C/min.

Copyright © Sumod Kalakkunnath 2007

Chapter Five

Molecular Dynamics of Crosslinked Poly(ethylene glycol) Networks by Broadband Dielectric Spectroscopy

This chapter is based on work published as:

(i) S. Kalakkunnath, D.S. Kalika, H. Lin, R. D. Raharjo, B.D. Freeman, *"Molecular Relaxation in Cross-Linked Poly(ethylene glycol) and Poly(propylene glycol) Diacrylate Networks by Dielectric Spectroscopy"*, Polymer, **48(2)**, 579-589 (2007). Copyright 2006 Elsevier Ltd.

(ii) S. Kalakkunnath, D.S. Kalika, H. Lin, R. D. Raharjo, B.D. Freeman, *"Molecular Dynamics of Poly(ethylene glycol) and Poly(propylene glycol) Copolymer Networks by Broadband Dielectric Spectroscopy"*, Macromolecules, **40(8)**, 2773-2781. Copyright 2007 American Chemical Society.

5.1 INTRODUCTION

The dynamic relaxation properties of crosslinked polymer networks are highly sensitive to network composition and polymer chain architecture. Changes in backbone structure, crosslink density, or the introduction of pendant groups or branches can have a dramatic effect on the characteristics of the cooperative segmental motions associated with the glass transition, as well as on the more localized processes observed below T_g. Broadband dielectric spectroscopy provides a sensitive and non-intrusive means by which to probe motional relaxations in polymeric solids over a wide range of temperature and timescale. Dielectric spectroscopy relies on the presence of permanent dipole groups along the polymer chain contour as a probe for the detection of molecular reorientation (*i.e.*, polarization) in the presence of an alternating electric field. The primary advantage of BDS is the exceptionally wide range of frequencies that can be accessed: commercial instruments provide for measurement from as low as 10^{-5} Hz to 10^{7} Hz, and an overall range of up to 18 decades can be achieved by a combination of experimental configurations.[130,131] Dielectric spectroscopy has been used to investigate relaxations in a variety of polymeric materials including semi-crystalline polymers and blends.[132] This tool can also be effectively used to characterize polymer networks, as it can be applied to monitor the evolution of network formation in situ,[133,134] as well as to elucidate polymer chain motions in the fully-cured material. A distinguishing feature of BDS is the ability to successfully capture the low intensity, sub-glass relaxation behavior via probing of the constituent dipole groups, a characteristic unavailable in complementary techniques like dynamic mechanical analysis.

In the present chapter, the dielectric relaxation characteristics of amorphous polymer networks prepared by the photopolymerization of poly(ethylene glycol) diacrylate [PEGDA], poly(propylene glycol) diacrylate [PPGDA] and bisphenol A ethoxylate diacrylate [BPAEDA] crosslinkers, previously characterized by dynamic mechanical analysis (see Chapter 4), are discussed. Further, the crosslink density of these networks has been varied by the inclusion of mono-functional acrylate in the prepolymerization reaction mixture. Specifically, the dielectric relaxation characteristics of a select series of UV-polymerized rubbery copolymer networks have been studied: PEGDA copolymerized with poly(ethylene glycol) methyl ether acrylate [PEGMEA], poly(ethylene glycol) acrylate [PEGA] and diethylene glycol ethyl ether acrylate [DGEEA]; PPGDA copolymerized with poly(propylene glycol) methyl ether acrylate [PPGMEA]; and BPAEDA copolymerized with PEGMEA and PEGA. Details regarding the monomers and their corresponding network structure were presented in Sections 2.2 and 4.1.

A number of studies have examined the influence of crosslinking and related structural modifications on the segmental relaxation properties of polymer networks: dynamic mechanical analysis and dielectric spectroscopy have been used to assess the effect of varying crosslink density on the glass transition temperature and corresponding time-temperature characteristics of the glass-rubber relaxation.[24-31,33] In general, the presence of high levels of crosslinking in polymeric networks results in a restriction of segmental mobility in the vicinity of the crosslink junctions that reduces the conformational freedom of the polymer chains, often leading to an increase in the measured glass transition temperature and inhomogeneous broadening of the glass-rubber relaxation.[29,30,113] This broadening reflects the range of relaxation environments experienced by the responding dipoles and the local constraint imposed by the presence of the crosslinks. As will be demonstrated for the non-crystalline networks studied here, the constraints that are present in the PEGDA crosslinked polymers lead to dielectric relaxation characteristics that are in many respects analogous to features encountered upon the relaxation of constrained amorphous segments in crystalline PEO,[121] as well as amorphous PEO confined at the nanometer scale in intercalated nanocomposites.[135,136] For the PEGDA/PEGMEA and PEGDA/PEGA series, the molecular weights of the acrylate co-monomers were intentionally chosen so as to maintain an approximately constant EO content in the networks while simultaneously inserting relatively long, flexible PEG branches into the network architecture; this approach facilitates the interpretation of changes in network dielectric response independent of variations in overall composition. The PEGDA/DGEEA and PPGDA/PPGMEA series, by contrast, have comparatively short (n = 2) pendant groups positioned along the network backbone, and encompass variations in chemical composition with varying co-monomer content. The BPAEDA networks introduce an additional variation to the network structure via the inclusion of a bulky bisphenol A segment along the crosslinker. The measurement of dielectric response for these families of materials provides useful insights as to the effect of crosslinking and associated constraints on their sub-glass and glass-rubber relaxation characteristics, and how variations in crosslinking influence the static and dynamic properties of the networks.

5.2 EXPERIMENTAL

5.2.1 Materials

Poly(ethylene glycol) diacrylate [PEGDA; Mol.Wt. = 700 g/mol], poly(propylene glycol) diacrylate [PPGDA; Mol.Wt. = 900 g/mol] and bisphenol A ethoxylate diacrylate [BPAEDA; Mol.Wt. = 688 g/mol] crosslinkers were obtained from Aldrich Chemical Company (Milwaukee, WI), along with poly(ethylene glycol) methyl ether acrylate [PEGMEA; Mol.Wt. = 460 g/mol], poly(ethylene glycol) ether acrylate [PEGA; Mol.Wt. = 380 g/mol], di(ethylene glycol) ethyl ether acrylate [DGEEA; Mol.Wt. = 188 g/mol] and poly(propylene glycol) methyl ether acrylate [PPGMEA; Mol.Wt. = 202 g/mol]. 1-hydroxyl-cyclohexyl phenyl ketone [HCPK] initiator was also purchased from Aldrich. All reagents were used as received.

The molecular weights of the diacrylate crosslinkers and mono-functional acrylates were characterized using proton nuclear magnetic resonance (^{1}H NMR) and fast atom bombardment mass spectrometry (FAB-MS) in order to verify the values provided by the supplier; complete details of these characterizations have been reported previously.**[115]** The number-averaged molecular weight for each reactant is indicated by the value of the monomeric repeat, *n*, as discussed in Section 4.2. For all reactants, FAB-MS measurements indicated a narrow distribution of molecular weight (polydispersity index < 1.10). All ^{1}H NMR and FAB-MS measurements were completed at the University of Texas at Austin.

5.2.2 Polymer film preparation

Crosslinked polymer films were prepared by UV photopolymerization. For the 100% diacrylate (*i.e.,* PEGDA, PPGDA or BPAEDA) films, a prepolymer solution comprised of the liquid crosslinker and 0.1 wt% HCPK initiator was prepared. For the copolymer series, the appropriate crosslinker and acrylate co-monomer (*i.e.*, PEGMEA, PEGA, DGEEA or PPGMEA) were blended in the desired ratio with the initiator. The mixture was sandwiched between two quartz plates which were separated by spacers to control film thickness, and polymerized by exposure to 312 nm UV light in a UV Crosslinker (Model FB-UVXL-1000, Fisher Scientific) for 90 seconds at 3 mW/cm^2. The solid films obtained by this process were three dimensional networks and contained a negligible amount of low molecular weight polymer (*i.e.*, sol) that was not bound to the network. In order to remove any residual sol or unreacted crosslinker, the films were washed with toluene in a Soxhlet extractor (Chemglass) for 1 day. Film thickness for the crosslinked networks was approximately 350 μm; the precise thickness for each film was measured using a digital micrometer readable to ± 1 μm.

The extent of the polymerization reaction in the crosslinked polymer films was determined using FTIR-ATR spectroscopy (Nexus 470 spectrometer from Thermo Nicolet, Madison, WI). The reaction of the acrylate double bonds during polymerization leads to a decrease in the intensity of sharp peaks at 810 cm^{-1} (ascribed to the twisting vibration of the acrylic CH_2=CH bond), at 1410 cm^{-1} (deformation of the CH_2=CH bond) and at 1190 cm^{-1} (acrylic C=O bond).[117,137] For all three crosslinkers, FTIR-ATR spectra showed essentially complete disappearance of the characteristic double bond peaks, indicating that the reaction conversion was close to 100%. All FTIR-ATR measurements were completed at the University of Texas at Austin.

PEO films were obtained by solution casting according to the method detailed in a previous study.[17] PEO powder (3 wt%) was dissolved in distilled water and cast into flat-bottomed Petri dishes. The incipient films were covered in order to control the rate of drying, and were allowed to dry slowly under ambient conditions until a uniform film was obtained. All films were then held under vacuum at room temperature until further characterization. The thickness of the PEO films was ~ 500 μm. Crystallinity in the films was evaluated using differential scanning calorimetry (Perkin-Elmer DSC-7): sample size was approximately 10 mg, and a heating rate of 10°C/min was used.

5.2.3 Dielectric Relaxation Spectroscopy

Dielectric spectroscopy measurements were performed using the Novocontrol Concept 40 broadband dielectric spectrometer (Hundsangen, Germany). In order to ensure the integrity of electrical contact during measurement, concentric silver electrodes (33 mm diameter) were vacuum evaporated on each polymer sample using a VEECO thermal evaporation system. Samples were then mounted between gold platens and positioned in the Novocontrol Quatro Cryosystem. All samples were rigorously dried under vacuum prior to measurement and sample mounting procedures were designed to minimize exposure to ambient moisture. Dielectric constant (ε') and loss (ε'') were recorded in the frequency domain (0.1 Hz to 1.0 MHz) at discrete temperatures from -150°C to 100°C.

5.3 RESULTS AND DISCUSSION

5.3.1 Properties of crosslinked PEGDA, PPGDA and PEO films

UV photopolymerization of the PEGDA and PPGDA diacrylate crosslinkers, as described above, results in amorphous, rubbery polymer networks with essentially 100% conversion of the diacrylate end groups as confirmed by FTIR-ATR. An idealized schematic of the PEGDA network is shown in Figure 2.1. Characteristics of the cross-linked networks as determined by calorimetry, dynamic mechanical analysis and density measurement are reported in Chapter 4. In these fully-reacted networks, the effective crosslink density (and average molecular weight between crosslinks, M_c) is established by the molecular weight of the diacrylate prepolymer: for PEGDA (n = 14), M_c = 688 gm/mol, while for PPGDA (n = 12), M_c = 768 gm/mol. Both networks display very similar glass transition temperatures, but the density of the crosslinked PPGDA [XLPPGDA] is approximately 10% lower than that of crosslinked PEGDA [XLPEGDA]. This difference in bulk density is reflected in the estimation of fractional free volume (FFV) for the two networks, with FFV = 0.160 for XLPPGDA, and FFV = 0.118 for XLPEGDA. Details on the determination of FFV for the networks are provided in previous studies.[115,138]

PEO films prepared by solution casting were characterized using DSC, and showed properties close to those previously reported by Lin and Freeman.[17] For the samples studied here, DSC thermograms indicated a melting peak temperature of 68°C, and a percentage crystallinity of ~ 80 wt% based on the 100% crystal heat of fusion reported by Wunderlich.[139]

5.3.2 Dielectric results for XLPEGDA, XLPPGDA, PEO films

Dielectric results for the crosslinked film based on 100% PEGDA are shown in **Figure 5.1** as dielectric constant (ε') and dielectric loss (ε'') vs. temperature at frequencies ranging from 10 Hz to 0.5 MHz. An expanded plot of dielectric loss at frequencies of 0.1, 1, and 10 Hz is also provided for the sub-glass region (see inset). The data show two apparent dipolar relaxation processes with increasing temperature as evidenced by the overlapping, incremental increases in dielectric constant and corresponding peaks in dielectric loss. These processes are designated as the β and α relaxations, respectively, with the higher-temperature α relaxation corresponding to the large-scale segmental motions associated with the glass transition. In the sub-glass region, lower-frequency measurements show that the β relaxation is comprised of two distinct processes, which are designated as the β_1 (lower-temperature) and β_2 (higher-temperature) relaxations, respectively. The strong increase in dielectric loss at low frequencies and high temperatures (*i.e.*, above the glass transition) reflects the onset of conduction associated with the transport of mobile charge carriers in the rubbery amorphous matrix.[99]

Figures 5.2 to **5.4** show three-dimensional relaxation contour maps for XLPEGDA, XLPPGDA, and crystalline PEO. In each case, the data are plotted as dielectric loss vs. temperature vs. frequency. For all three materials, two distinct relaxation processes were observed in the sub-glass region (designated as β_1 and β_2); these relaxations merge with increasing frequency, with the combined β process eventually merging with the (glass-rubber) α relaxation at the highest frequencies measured. The influence of conduction is evident on the far left of each plot, as dielectric loss increases strongly with temperature. Conduction effects are especially prominent in the PEO sample as the presence of internal crystal boundaries results in local charge blocking and an additional contribution to the overall polarization (Maxwell-Wagner-Sillars (MWS) polarization).

In order to interpret the dielectric results for the crosslinked networks, it is useful to examine previous reports of dielectric relaxation properties for the appropriate uncrosslinked analogs, *i.e.*, PEO and poly (propylene oxide) [PPO]. Earlier studies on the dielectric and dynamic mechanical relaxation of PEO indicate a total of three relaxation processes:[120,140-144] a high-temperature local process originating in the crystalline phase, a cooperative segmental process occurring in non-crystalline regions and usually correlated with the glass transition, and a local low-temperature twisting process, also associated with the non-crystalline phase. Various labeling conventions have been adopted for these motional processes, with the high-temperature crystalline process typically designated as the α (or α_c) process, and the glass transition and local sub-glass processes designated as β and γ, respectively.[67,96] Recent broadband dielectric measurements reported by Jin *et al.* reveal an additional local process situated between the β and γ relaxations, designated γ'.[121] Based on the characteristics of the relaxation, Jin and coworkers proposed that the distinct γ' process corresponds to segmental motions occurring in the crystal-amorphous order-disorder transition region, in the vicinity of crystal lamellar surface. For the PEO studies reported here (see Figure 5.4), two sub-glass relaxations are also clearly seen, with the intermediate transition designated as the β_2 relaxation according to the labeling convention adopted for the XLPEGDA and XLPPGDA networks. The position of the β_2 relaxation in these PEO data is virtually the same as that reported by Jin *et al.* Notably, both of the amorphous crosslinked networks also show an intermediate (β_2) relaxation. The origin of this relaxation in the networks, and its relation to the process observed in crystalline PEO, is discussed below.

The dielectric relaxation characteristics of amorphous poly(propylene glycol) and poly(propylene oxide) in the glassy and liquid states have been studied by a number of investigators.[145-153] PPO displays two dielectric relaxation processes in the vicinity of T_g: a fast (lower-temperature) process reflecting the segmental motions associated with the glass-rubber transition, and a slow (higher-temperature) process corresponding to normal mode reorientations owing to the presence of a cumulative dipole moment along the polymer chain. These relaxations are designated as the α and α' (or α_N) processes, respectively. In the glassy state, two sub-glass relaxations are detected, designated as the γ and β processes.[148] In the PPO polymer, the lower-temperature γ relaxation is only observed at temperatures below -150°C. A number of dielectric studies have examined the influence of molecular weight on the characteristics of the normal mode motions, as well as on the relationship between the β and α relaxations.[146,149,151,152] For low-molecular weight PPG oligomers, the β and α relaxations overlap to a significant degree, and a distinct β relaxation is difficult to distinguish. At higher (*i.e.*, polymeric) molecular weights, the sub-glass relaxation shifts to shorter relaxation times relative to the α process, and a more distinct β peak emerges. In all cases, however, the intensity of the β process remains at least one order of magnitude below that of the glass-rubber relaxation. Comparison of the β and α peaks for XLPPGDA (Figure 5.3) reveals a similar result with respect to relaxation intensity.

For all three materials examined (XLPEGDA, XLPPGDA, PEO), there is considerable overlap of the dielectric relaxations in the sub-glass region. In order to objectively establish the characteristics of each individual process, the data were fit in the frequency domain according to a dual Havriliak-Negami (HN) model:[42,154]

$$\varepsilon^* = \varepsilon' - i\varepsilon'' = \varepsilon_{U_1} + \sum_{k=1}^{2}\left[\frac{\Delta\varepsilon_k}{\left(1+(i\omega\tau_{HN_k})^{a_k}\right)^{b_k}}\right] \qquad [5.1]$$

where ε_R and ε_U represent the relaxed ($\omega \to 0$) and unrelaxed ($\omega \to \infty$) values of the dielectric constant for each individual relaxation, $\omega = 2\pi f$ is the frequency, τ_{HN} is the relaxation time for each process, and a and b represent the broadening and skewing parameters, respectively. All curve fits reported here were obtained using the WinFIT software package provided with the Novocontrol dielectric spectrometer. For the sub-glass relaxations (β_1 and β_2), it was observed that satisfactory fits to the dielectric dispersion could be obtained with the skewing parameter (*b*) set equal to 1 in all cases; this corresponds to the symmetric Cole-Cole form of equation 5.1.[98]

A representative dual-HN curve fit for XLPEGDA in the β relaxation region is shown in **Figure 5.5**. The data are plotted as dielectric loss vs. frequency at a measurement temperature of -78°C. When plotted on this basis, the lower-temperature β_1 relaxation appears on the right side, and the higher-temperature β_2 relaxation appears on the left; the individual relaxation fits are indicated by the dashed lines. Dielectric loss data and corresponding HN fits for the entire dual-relaxation region are plotted in **Figure 5.6**. Across this range, the overall relaxation intensity is observed to increase with increasing temperature, and the relaxations eventually merge at higher temperatures. In the case of XLPEGDA, deconvolution of the two relaxations could be reasonably accomplished at temperatures up to -62°C. At the higher temperatures shown in Figure 5.6, the influence of the glass-rubber (α) relaxation appears at low frequencies.

A comparison of the sub-glass dielectric relaxation response for XLPEGDA, XLPPGDA and PEO (-78°C) is shown in **Figure 5.7**. For each of the three polymers, overlapping β_1 and β_2 relaxations are observed. The peak positions (and corresponding relaxation times) associated with these transitions are nearly the same in all three materials. When comparing the dielectric relaxation intensity associated with these polymers, it is necessary to consider the composition of each material, as well as its morphology. In crosslinked PEGDA, the network is 100% amorphous (as confirmed previously by DSC and X-ray[115]), in contrast to PEO, which is ~ 80% crystalline. For sub-glass relaxations that originate in non-crystalline regions of the PEO polymer, a significant fraction of the PEO segments will be incapable of responding to the applied alternating field, and thus will not contribute to the measured dielectric response. In addition, the presence of (—COO—) ester groups at the crosslink junctions in XLPEGDA and XLPPGDA increases the overall concentration of dipoles as compared to PEO or PPO, with the potential to thereby increase the net dielectric intensity of the observed relaxations.

Examination of the sub-glass relaxation response for XLPEGDA vs. PEO in Figure 5.7 shows approximately one order of magnitude lower dielectric relaxation intensity for crystalline PEO, as compared to XLPEGDA. As discussed above, this difference is attributable largely to the high fraction crystallinity in the PEO polymer, as well as the potential additional contribution of the ester dipoles present in the XLPEGDA network. However, the respective β_1 and β_2 relaxation times ($\tau_{MAX} = [2\pi f_{MAX}]^{-1}$) are virtually identical for both XLPEGDA and PEO, so these motional processes could very well have the same or similar molecular origin.

Comparison of the sub-glass relaxations for XLPEGDA vs. XLPPGDA in Figure 5.7 shows that the relaxation intensity for XLPPGDA is much lower than that observed for XLPEGDA (see also Figure 5.2). The intensity of a particular dielectric relaxation depends on a number of factors, perhaps most fundamentally on the concentration of dipoles available that could potentially reorient in response to an applied alternating field. An accounting of the differences in molar mass and density for the two crosslinked networks indicates that the number of ether linkages in the XLPPGDA network is 70% the number present in the XLPEGDA network, and that the XLPPGDA network contains 81% the number of —COO— groups present in XLPEGDA. Clearly, these values are not sufficient to explain the observed difference in sub-glass relaxation intensity for the two networks. In addition to differences in dipolar concentration, structural factors will influence the measured dielectric intensity, as chain conformation constraints and possible dipolar cancellations typically lead to relaxation intensities that are well below what would be expected based on a full and uncorrelated dipolar response. The relatively low intensity of the sub-glass relaxation in XLPPGDA is consistent with the observed dielectric response in PPO.[148,151,152] Apparently, the presence of the dipolar ester units in the XLPPGDA network does not alter this qualitative result, either when considering the relative intensity of the β and α relaxations in XLPPGDA, or when comparing the sub-glass relaxation intensities in XLPPGDA vs. XLPEGDA.

The application of dual HN curve fits across the sub-glass region provides for the determination of dielectric relaxation intensity ($\Delta\varepsilon = \varepsilon_R - \varepsilon_U$), relaxation time ($\tau_{HN}$), and broadening parameter (a) for the individual β_1 and β_2 relaxations. **Figure 5.8** shows the results for XLPEGDA, XLPPGDA, and PEO. For the β_1 process, relaxation intensity is nearly independent of temperature, while for the β_2 process, $\Delta\varepsilon$ increases with temperature for XLPEGDA. Examination of the broadening parameter as a function of temperature reveals opposing trends for the β_1 and β_2 relaxations in all three materials. For the β_1 process, the symmetric dispersion is observed to narrow with increasing temperature (*i.e.*, the value of the broadening parameter increases). This result, which reflects a narrower distribution of relaxation times with increasing thermal energy, is consistent with the trend observed for both sub-glass and glass-rubber transitions in many common polymers.[155] For the β_2 process, however, the relaxation is observed to broaden with increasing temperature. This behavior, while unusual, has been reported previously for the γ' process in crystalline PEO, a relaxation that was assigned to localized motions originating in the crystal-amorphous order-disorder transition region. Jin *et al.*[121] speculated that the observed broadening of the γ' relaxation in PEO was the result of "environmental asymmetry" between the amorphous phase, which becomes more mobile with increasing temperature, and the crystalline phase, which remains immobile. Consequently, the responding dipoles located in the order-disorder transition region experience a more heterogeneous relaxation environment at higher temperatures, leading to a broader dispersion.

The time-temperature characteristics for the β_1 and β_2 relaxations are presented in an Arrhenius plot of log(f_{MAX}) vs. 1000/T(K) in **Figure 5.9**. For the symmetric sub-glass processes, f_{MAX} was determined directly from the individual HN curve fits. Both the β_1 and β_2 transitions show a linear, Arrhenius relationship which is indicative of a local relaxation process; this behavior is typical of sub-glass relaxations in amorphous and semi-crystalline polymers.[67,132] The positions of the β_1 and β_2 relaxations in the crystalline PEO sample are virtually identical to those reported previously (re: γ and γ' processes, respectively[121]). The apparent activation energies (E_A) of the individual relaxations are reflected in the slope of the data for each material. For the β_1 relaxation, XLPEGDA displays an activation energy of 41 kJ/mol, as compared to 32 kJ/mol for the comparable process in PEO. In XLPPGDA, the β_1 activation energy is also 32 kJ/mol. This value is nearly the same as values reported in the literature for the sub-glass relaxation in PPO polymer;[151,152] relaxation data for PPO reported by Leon *et al.*[151] are included in Figure 5.7 for comparison purposes. For the β_2 relaxation, the time-temperature relation for all three materials can be described by a single activation energy, $E_A = 65$ kJ/mol.

Examination of the dielectric contour plots in Figures 5.2 to 5.4, as well as the time-temperature results in Figure 5.9, establishes the similarity in sub-glass relaxation behavior for PEO, XLPEGDA, and XLPPGDA. In all three cases, an intermediate "fast" relaxation process (β_2) is observed with a corresponding relaxation time that is much shorter than that associated with the glass transition. As discussed above, dielectric studies completed by Jin *et al.* on PEO show this same intermediate relaxation, the origin of which was assigned to non-cooperative motions in the vicinity of the crystal-amorphous interface.[121] It was suggested that the fast process corresponds to a subset of segmental motions that, owing to the confinement imposed by the crystalline lamellae, assume a more localized character. The resulting dipolar relaxation process, which encompasses motions of lesser cooperativity, appears at lower temperature (*i.e.*, shorter relaxation time) and with an Arrhenius time-temperature profile more characteristic of a local relaxation. An analogy was drawn between the behavior observed in bulk PEO and the response of amorphous PEO chains confined between inorganic layers in an intercalated nanocomposite.[135,136] In a recent publication, Elmahdy and co-workers report the emergence of an intermediate "fast" process in PEO/Silicate nanocomposites; the intensity of this process, which displays local Arrhenius character, correlates with the amount of PEO confined within the intercalated galleries.[136] It is conceivable that a comparable mechanism is operative in the XLPEGDA and XLPPGDA networks, with the constraint imposed by the crosslink junctions extending along the contour of the PEGDA or PPGDA bridging groups (see Figure 2.1). This constraint could potentially be responsible for the β_2 process encountered in the networks, in the same way that the constraint experienced by the polymer chain segments in the vicinity of the crystal surface leads to the observed fast process in PEO.

In the glass transition region, the dielectric spectra show overlap of the β and α relaxation processes, as well as the influence of conduction (see Figures 5.2 to 5.4). HN analysis was performed across the frequency domain in the vicinity of T_g in order to deconvolute the individual dipolar relaxation processes, and to remove the influence of conduction. The governing expression in this region is as follows:

$$\varepsilon^* = \varepsilon' - i\varepsilon'' = \varepsilon_{U_1} + \sum_{k=1}^{2}\left[\frac{\Delta\varepsilon_k}{\left(1+(i\omega\tau_{HN_k})^{a_k}\right)^{b_k}}\right] - i\left(\frac{\sigma_0}{\varepsilon_0\omega}\right)^N \qquad [5.2]$$

where σ_0 is the conductivity and ε_0 is the vacuum permittivity. For a pure conduction process, N assumes a value of 1.[99]

Dielectric loss data and corresponding HN curve fits for XLPEGDA in the glass transition region are plotted in **Figure 5.10**. The data are shown with the conduction contribution subtracted according to equation 5.2. For all temperatures examined, the conduction contribution could be satisfactorily described with a value of N = 1; *i.e.*, ε''_{cond} varied consistently with ω^{-1}. The data, and corresponding HN fits, display a strong overlap of the β and α relaxations in this temperature range. The relaxation times (τ_{MAX}) associated with the individual peak maxima were determined from the HN best-fit parameters according to the following equation:[99]

$$\tau_{MAX} = \tau_{HN}\left[\frac{\sin(\frac{\pi ab}{2+2b})}{\sin(\frac{\pi a}{2+2b})}\right]^{1/a} \qquad [3.19]$$

For the merged sub-glass relaxation (β_1 + β_2), the skewing parameter (b) was taken as equal to 1, so that $\tau^{\beta}_{MAX} = \tau^{\beta}_{HN}$. The frequency maxima for the separated α relaxation process, $f_{MAX} = [2\pi\tau_{MAX}]^{-1}$, were the basis for the data points plotted in Figure 5.9 (XLPEGDA and XLPPGDA). In the case of PEO, the combined influence of MWS polarization and the strong overlap of the α and β relaxations made it impossible to reliably separate the data into their constituent dispersions. As a result, the values plotted in Figure 5.9 for PEO correspond to f_{MAX} for the merged $\alpha + \beta$ process, after correction for conduction.

Dielectric loss data for XLPPGDA in the α relaxation region are shown in **Figure 5.11**. Since the β relaxation process in this network is very weak as compared to the α process, the spectra for XLPPGDA could be fit across the range using a single HN function, with the corresponding curves as shown. The small influence of the β process, evident at high frequencies for the lower-temperature curves shown in Figure 5.11, was removed by eliminating those points during the HN fit procedure. The resulting f_{MAX} values, derived from the HN fits and equation 3.19, are plotted in Figure 5.9.

Examination of the α relaxation results for XLPEGDA and XLPPGDA in Figure 5.9 show the relaxations offset to higher temperatures as compared to the experimental values for PEO and literature values for PPO,[151] respectively; the positive offset for both networks is presumably the result of constraints imposed by network connectivity on the cooperative motions inherent to the α process. The non-Arrhenius time-temperature characteristics of the α relaxation are almost the same for both networks and can be described in the vicinity of T_g by the Williams-Landel-Ferry (WLF) equation (see solid curves in Figure 5.9).[38] The near coincidence of the data points for XLPEGDA and XLPPGDA in Figure 5.9 indicates a similar apparent activation energy or dynamic fragility associated with the underlying segmental motions occurring in both networks.[43,122] This result may reflect a trade-off between structural differences in the two networks, and their inherent free volume. While the motions in XLPEGDA would presumably encompass segments that are fairly smooth and compact,[44] the fractional free volume available for such motions is relatively low. By contrast, reorientations encompassing the $–CH_3$ pendant group present in the XLPPGDA repeat unit would arguably require greater cooperativity, but motions involving this segment occur in a network with higher FFV. The net result appears to be time-temperature α relaxation characteristics that are nearly indistinguishable for these two particular networks.

A concise format for the comparison of dispersion characteristics (*i.e.*, relaxation intensity, shape) in XLPEGDA and XLPPGDA is the Cole-Cole plot. Cole-Cole plots of ε'' vs. ε' at -34°C are shown in **Figure 5.12**. For XLPEGDA, the α and β relaxations are broken into their constituent curves according to the HN fits. For the α process, the high-frequency, asymmetric broadening associated with the HN form is observed, with a corresponding value of the skewing parameter, $b = 0.54$. A similar value was obtained for XLPPGDA, also at -34°C. The merged sub-glass process is very prominent in XLPEGDA, while it appears only as a small shoulder in the XLPPGDA dispersion. Based on the data available for PPO, this latter result is perhaps not unexpected, as the sub-glass relaxation observed in the PPO polymer is quite weak relative to the glass transition.[148,151,152] However, if the "β_2" portion of the merged sub-glass process can be attributed to some subset of segmental motions that become faster and less cooperative as a result of confinement effects, it is somewhat surprising that the β process does not appear more prominently in the results for the XLPPGDA network. This is particularly noteworthy given that the network includes strongly dipolar ester linkages located at the crosslink junctions, moieties that could amplify the measured intensity of any segmental reorientations originating in the vicinity of the crosslinks. Apparently, while the constraint in XLPPGDA is sufficient to produce a measurable "fast" relaxation, the underlying motions associated with the β_2 process remain limited or strongly coupled, such that only a weak dispersion is detected.

In the case of XLPEGDA, review of the curves in Figure 5.7 indicates a considerably stronger β_2 process compared to either XLPPGDA or PEO, both in absolute terms and on the basis of the relative intensities of the β_2 vs. β_1 peaks. The enhancement of the β_2 process in XLPEGDA as compared to PEO may reflect an additional contribution by the network ester groups to the relaxation intensity associated with the "fast" segmental process, a process that would most likely be sensitive to the character of the crosslink junctions and the degree of constraint that they impose. This added dipolar response could provide some explanation for the relative strength of the merged β process as shown in Figure 5.12. It is difficult to draw a definitive conclusion in this regard, however, given the very different relaxation environment present in the amorphous XLPEGDA network, as compared to crystalline PEO.

5.3.3 Properties of PEGDA and PPGDA copolymers

UV photopolymerization of the PEGDA/PEGMEA, PEGDA/PEGA, PEGDA/DGEEA and PPGDA/PPGMEA prepolymerization mixtures led to the formation of amorphous rubbery polymer networks with essentially 100% conversion of the acrylate and diacrylate end groups as verified by FTIR-ATR. The calorimetric glass transition temperatures (T_g) and fractional free volume values associated with each network series have been reported previously (see Chapter 4). The copolymerization of PEGDA with either PEGMEA (n = 8) or PEGA (n = 7) leads to a progressive reduction in T_g, with the effect appearing more strongly in the PEGDA/PEGMEA copolymers. There is a distinct contrast in the fractional free volume trends associated with the two series: FFV in the PEGDA/PEGMEA copolymers increases with increasing co-monomer (*i.e.*, branch) content, while FFV in the PEGDA/PEGA series decreases with co-monomer content, possibly due to the formation of hydrogen bonds involving the –OH terminal group present on the PEGA monomer. This difference in free volume characteristics appears to be a decisive factor in the resulting gas permeability properties of the networks. For the PEGDA/DGEEA copolymers, the T_g of the PEGDA network shows a modest decrease upon inclusion of the short DGEEA groups, and the FFV trend is similar to the PEGDA/PEGMEA copolymers. However, for the PPGDA/PPGMEA series, T_g is independent of copolymer composition, with the short PPGMEA branches having little apparent influence on the glass transition properties of the high free volume PPGDA networks. Also, FFV in the PPGDA networks increases strongly with co-monomer content, and this increase is reflected in systematically higher permeability values.[138]

5.3.4 Dielectric results for PEGDA/PEGMEA, PEGDA/PEGA copolymers

Dielectric measurements for the PEGDA/PEGMEA and PEGDA/PEGA copolymer networks reveal three motional transitions with increasing temperature, and these have been labeled as the β_1, β_2, and α relaxations, respectively. A representative contour plot for the PEGDA/PEGMEA copolymer series is shown in **Figure 5.13** (50/50 PEGDA/PEGMEA network composition), with dielectric loss (ε'') plotted vs. temperature vs. frequency. The observed sub-glass processes merge into a single relaxation with increasing frequency, and the combined (β) process eventually merges with the (glass-rubber) α process at the highest frequencies measured. The increase in dielectric loss at low frequency and high temperature (*i.e.*, on the far left side of Figure 5.13) reflects the onset of conduction in the rubbery amorphous matrix.[99]

Isochronal plots of dielectric constant (ε') and loss (ε'') for the various PEGDA/PEGMEA and PEGDA/PEGA specimens at 95 kHz are shown in **Figures 5.14** and **5.15**, respectively. In each case, the influence of conduction on dielectric loss was subtracted by fitting the loss-temperature data to an empirical Arrhenius function over the region where the conduction contribution dominates the response. For both series, the chemical composition of the films remains virtually unchanged with variations in monomer content, and this is reflected by the invariance of the low-temperature, "unrelaxed" value of the dielectric constant. Across the PEGDA/PEGMEA series, a negative shift in the α-relaxation (glass-rubber) peak temperature is observed with increasing acrylate content that is consistent with the previously reported DSC and dynamic mechanical (DMA) results, while for the PEGDA/PEGA series, the dielectric peak temperature at 95 kHz is nearly independent of composition. In both cases, there is a net increase in the dielectric relaxation intensity with increasing acrylate content (*i.e.*, decreasing crosslink density). Within the PEGDA/PEGA series, a small reversal in the intensity-composition trend is observed for the 30/70 PEGDA/PEGA specimen.

Dielectric loss curves for the PEGDA/PEGMEA copolymers across the sub-glass transition region are shown in **Figure 5.16**; the data are plotted as ε'' vs. temperature at a frequency of 1Hz. The curves reveal a strong sensitivity of the β_2 relaxation intensity to copolymer composition. Increasing the amount of PEGMEA co-monomer in the prepolymerization reaction mixture leads to a marked decrease in β_2 relaxation intensity for the resulting copolymer films. This outcome suggests that as the PEGMEA branch content increases, and the corresponding crosslink density decreases, the overall constraint imposed by the crosslink junctions is diminished. Consequently, a smaller portion of the responding segments contribute to the "fast" β_2 process.

Dielectric loss (ε'') for the PEGDA/PEGMEA series is plotted versus frequency in **Figure 5.17**; the selected temperature (-78°C) corresponds to the mid-range of the sub-glass transitions. The curves in Figure 5.17 are the result of the dual HN fits. Once again, the sensitivity of the β_2 relaxation to PEGMEA branch content and degree of crosslinking is evident, with the intensity of the β_2 relaxation decreasing with increasing co-monomer content. As the constraint imposed by the crosslink junctions is loosened, fewer segments assume the restricted conformations associated with the β_2 process. With less local confinement, some portion of the segments originally associated with the β_2 process in the fully crosslinked (*i.e.*, 100% PEGDA) network adopt a conformation closer to that of the amorphous bulk, leading to a less intense β_2 relaxation.

The HN parameters for the PEGDA/PEGMEA series are plotted in **Figure 5.18** (relaxation intensity; $\Delta\varepsilon = \varepsilon_R - \varepsilon_U$) and **Figure 5.19** (breadth), respectively. For both the β_1 and β_2 processes, the relaxation intensity increases with temperature (see Figure 5.18). Increasing the co-monomer content leads to a decrease in $\Delta\varepsilon$ for both dispersions, but the drop in intensity is much more pronounced for the β_2 relaxation, as discussed above. Examination of Figure 5.19 reveals a progressive narrowing of the β_1 process as indicated by the increase in broadening parameter, which reflects a tighter distribution of relaxation times with increasing thermal energy. The β_2 process, however, shows an overall broadening with increasing temperature that appears to be characteristic of this constrained relaxation. It is notable that as the PEGMEA content in the networks is reduced, this effect becomes weaker (see trend lines in Figure 5.19), a result that is consistent with the reduction in crosslink constraint at higher levels of co-monomer incorporation.

The sub-glass relaxation results for the PEGDA/PEGA copolymer series are presented in **Figure 5.20** (ε'' versus frequency at -78°C). Across this series of specimens, the influence of copolymer composition on relaxation intensity is not as strong as in the PEGDA/PEGMEA samples. For the PEGDA/PEGA copolymers, the introduction of PEGA branches leads to a reduction in FFV, possibly due to the formation of hydrogen bonds involving the –OH groups located at the ends of the PEGA segments. While the incorporation of the PEGA co-monomer produces a decrease in overall crosslink density in the networks, the potential for interactions involving the branch ends results in the persistence of a significant degree of motional constraint. Accordingly, only a modest decrease in the intensity of the β_2 relaxation with co-monomer content is observed for the PEGDA/PEGA series of copolymers.

The time-temperature characteristics of the β_1 and β_2 dispersions in PEGDA/PEGMEA and PEGDA/PEGA are presented via Arrhenius plots of log(f_{MAX}) vs. 1000/T(K) in **Figure 5.21**. For the symmetric sub-glass processes, f_{MAX} was determined directly from the individual HN curve fits, with $f_{MAX} = [2\pi\tau_{MAX}]^{-1}$. Both the β_1 and β_2 relaxations display a linear, Arrhenius time-temperature relationship that is consistent with a local relaxation process. The positions of the β_1 and β_2 relaxations are nearly independent of copolymer composition, with a slightly greater spread in the data evident across the PEGDA/PEGMEA series. For the PEGDA/PEGA copolymers, the apparent activation energies (E_A) associated with the β_1 and β_2 processes are essentially the same as previously reported for the 100% XLPEGDA network: $E_A(\beta_1)$ = 41 kJ/mol, and $E_A(\beta_2)$ = 65 kJ/mol (see Section 5.3.2). In the PEGDA/PEGMEA polymers, the activation energy for the β_1 process ranges from 41 kJ/mol (100% PEGDA) to 33 kJ/mol (30/70 PEGDA/PEGMEA). The activation energy for the β_2 process is approximately constant at 65 kJ/mol.

Dielectric loss data (-30°C) and corresponding HN curve fits for the PEGDA/PEGMEA and PEGDA/PEGA copolymer series are plotted versus frequency in **Figures 5.22** and **5.23**, respectively. The data are shown with the conduction contribution removed according to equation 5.2: for all specimens, the conduction exponent N ~ 1, which is consistent with an ideal conduction process in the amorphous networks.[99]

Examination of the PEGDA/PEGMEA glass-rubber (α) relaxation in Figure 5.22 indicates a strong shift in the relaxation maximum to higher frequencies (*i.e.*, shorter relaxation times) that is consistent with the observed negative offset in T_g with increasing PEGMEA content (see Table 4.3). At lower crosslinker contents, there is extensive overlap between the relaxations owing to the shift in the α relaxation to higher frequencies. For the 30/70 PEGDA/PEGMEA specimen, a very broad relaxation curve is obtained at -30°C. PEGDA/PEGMEA networks with high levels of PEGMEA content and correspondingly low crosslink densities have a tendency to crystallize. Previous DMA scans on the 30/70 PEGDA/PEGMEA network, for example, display cold crystallization just above T_g (see Figure 4.12); a small degree of cold crystallization has also been detected in DSC scans on lightly crosslinked PEGDA/PEGMEA networks.[124] It is feasible that a small amount of crystallinity is present in the 30/70 PEGDA/PEGMEA specimen examined via dielectric spectroscopy, evolving either during the initial cooling of the specimen, or possibly as cold crystallization in the course of measurements just above T_g. The presence of crystallinity would be expected to subject the responding chains segments to additional constraint, shifting the glass transition to higher temperatures (*i.e.*, lower frequencies) and broadening the relaxation.[132] Both effects appear to be evident in the 30/70 PEGDA/PEGMEA dispersion recorded at -30°C.

The dielectric loss curves for the PEGDA/PEGA series (-30°C; see Figure 5.23) show a somewhat clearer separation between the α and β relaxations across the series of copolymer specimens: in this case, the position of the α relaxation is less sensitive to composition, resulting in a lower degree of α-β overlap at higher PEGA co-monomer content. The intensity of both the α and β dispersions increases with increasing PEGA, although this trend reverses for the 30/70 copolymer (*i.e.*, intensities for the 30/70 PEGDA/PEGA sample are lower than those for the 50/50 network). This behavior may reflect competing structural factors that influence the net dielectric response. Although the overall chemical constitution of the PEGDA networks remains constant across each series, decreasing crosslink density correlates with an increase in the measured dielectric intensity, most likely due to increased mobility of the (−COO−) ester linkages located at the crosslink junctions. However, in the case of the 30/70 PEGDA/PEGA sample, the large number of −OH terminated PEGA branches, and the potential formation of hydrogen bonds involving these terminal groups, may be responsible for a decrease in dipolar mobility as compared to the 50/50 PEGDA/PEGA copolymer. The result, as seen in Figure 5.23, is a net reduction in dielectric intensity, driven primarily by a decrease in the strength of the α relaxation response.

The peak maxima associated with the α and β relaxations were determined across a range of temperatures in the vicinity of the glass transition (-14°C to -50°C, depending on composition). The results for the α relaxation are plotted as $f_{MAX} = [2\pi\tau_{MAX}]^{-1}$ versus reciprocal temperature in Figure 5.21, where τ_{MAX} was determined from the individual HN curve fits according to equation 3.19. For the PEGDA/PEGMEA and PEGDA/PEGA series, the α relaxation displays time-temperature characteristics that are consistent with a cooperative reorientation response, and which can be described by the Williams-Landel-Ferry (WLF) relation (see solid curves in Figure 5.21).[38] In both cases, the relative position of the relaxation curves, which shift to higher values of reciprocal temperature with decreasing crosslinker content, are consistent with the glass transition results measured by DMA and DSC (see Table 4.3). The offset in the curves is more pronounced for the PEGDA/PEGMEA polymers, in direct correspondence to the data presented in Table 4.3.

5.3.5 Dielectric results for PEGDA/DGEEA copolymers

PEGDA/DGEEA copolymers are diverse in nature as compared to the PEGDA copolymers discussed earlier, owing to the relatively short length of the pendant group and varying chemical composition with monomer content. However, dielectric measurements for the PEGDA/DGEEA copolymer networks indicate an overall relaxation trend similar to the above-mentioned PEGDA copolymers. A representative contour plot (see **Figure 5.24**) of dielectric loss (ε'') vs. temperature vs. frequency for the

60/40 PEGDA/DGEEA copolymer composition exhibits two sub-glass (β_1 and β_2) transitions that initially merge together and eventually join the glass-rubber (α) relaxation at higher frequencies. The appearance of the β_1 and β_2 transitions over the same temperature and frequency range as observed for the other PEGDA copolymers suggests that the origin for these motional transitions remains unchanged.

Dielectric loss (ε'') versus frequency data for the PEGDA/DGEEA series at -78°C are shown in **Figure 5.25**; the solid lines are dual HN curve fits. The intensity of the β_2 relaxation decreases strongly with increasing DGEEA monomer content; this trend was also observed for the PEGMEA series (see Figure 5.17). The result reflects a reduction in the overall constraint imposed by the crosslink junctions with increasing branch content and corresponding decrease in the effective crosslink density. However, a reversal in the trend is observed for the PEGDA/DGEEA copolymer containing the highest DGEEA content (*i.e.*, 50/50 PEGDA/DGEEA, see Figure 5.25). This behavior suggests that as the DGEEA content is increased beyond a certain level, the increasing overall dipolar content (via increase in the carbonyl linkages) leads to a net increase in the intensity of the β_2 relaxation. A similar, more pronounced effect has been observed in dielectric relaxation studies conducted on PEGDA networks prepared with shorter branch, –OH terminated acrylate monomer.[126] The insertion of –OH groups adds to the dipoles associated with the constrained regions, resulting in an amplified dielectric response for the β_2 relaxation.

The sub-glass HN parameters for the PEGDA/DGEEA series are plotted as relaxation intensity ($\Delta\varepsilon$) and breadth versus temperature in **Figures 5.26** and **5.27**, respectively. $\Delta\varepsilon$ for both dispersions decreases with increasing amounts of the co-monomer, the effect being more pronounced for the β_2 transition, as noted above. The broadening parameter (see Figure 5.27) follows a trend similar to the PEGDA/PEGMEA series of networks, with higher DGEEA content resulting in a successive narrowing of the β_1 relaxation accompanied by a characteristic broadening of the constrained β_2 transition. Here again, the degree of broadening for the β_2 transition decreases with the co-monomer content, reflecting a reduction in the effective crosslink constraint with decreasing crosslink density (see trend lines in Figure 5.27).

The time-temperature characteristics of both the glass-rubber (α) and sub-glass (β_1 and β_2) dispersions are reported via Arrhenius plots of log(f_{MAX}) vs. 1000/T(K) in **Figure 5.28**. The sub-glass relaxations follow a linear, Arrhenius time-temperature relationship, as expected for a local relaxation process. The positions of both the β_1 and β_2 relaxations seem to be influenced by the copolymer composition, with the spread in data more pronounced for the β_2 transition. The apparent activation energies (E_A) evaluated for both sub-glass processes remain essentially the same as that observed for 100% XLPEGDA: $E_A(\beta_1)$ ranges from 41 kJ/mol (100% PEGDA) to 39 kJ/mol (50/50 PEGDA/DGEEA), with $E_A(\beta_2)$ varying from 65 kJ/mol to 58 kJ/mol. The glass-rubber (α) dispersion was successfully described via the WLF equation,[38] consistent with the response of a large-scale, cooperative relaxation (see solid curves in Figure 5.28). The curves show a modest positive offset to higher values of reciprocal temperature with decreasing crosslinker content. This is consistent with the observed decrease in T_g determined via DMA and DSC scans (see Table 4.5).

Dielectric loss data for the PEGDA/DGEEA series at -30°C are plotted versus frequency in **Figure 5.29**. The solid curves represent the HN curve fits after conduction removal, as per the method described in the previous section. Examination of the PEGDA/DGEEA glass-rubber (α) relaxation in Figure 5.29 reveals a modest shift in the relaxation maximum to higher frequencies, consistent with the corresponding decrease in T_g with increasing DGEEA. The intensity of the α relaxation increases strongly with increasing DGEEA content, a trend that is most likely driven by the increased population of (−COO−) ester linkages at higher levels of DGEEA copolymerization. The overlapping β relaxation displays a sharp drop in intensity for the 80/20 PEGDA/DGEEA copolymer, followed by an increase for higher co-monomer contents. This behavior may reflect competing effects due to the increase in dipolar content via increase in the carbonyl linkages, as well as a correspondingly less restrictive motional environment in the vicinity of the crosslink junctions.

5.3.6 Dielectric results for PPGDA/PPGMEA copolymers

The PPGDA/PPGMEA rubbery copolymer networks, based on the monomers shown in Figures 3.1 and 3.2, differ from the PEGDA series in a number of respects: (i), the 100% crosslinked network, XLPPGDA, encompasses a much higher degree of fractional free volume as compared to XLPEGDA; (ii) the PPGMEA co-monomer molecular weight is relatively low, such that much shorter pendant branches (n = 2) are inserted into the network; and (iii) the introduction of PPGMEA co-monomer to the reaction mixture results in a change in the chemical composition of the network, with increasing PPGMEA content leading to an increase in the relative population of (−COO−) linkages. Isochronal plots (120 kHz) of dielectric constant and loss for the PPGDA/PPGMEA specimens are shown in **Figure 5.30**. Increasing amounts of PPGMEA in the copolymers leads to an increase in the intrinsic polarizability of the networks, as manifested by an increase in the low-temperature value of the dielectric constant, ε_U (see Figure 5.30(a)). The dielectric loss data display a weak sub-glass (β) relaxation, and the intensity of the glass-rubber (α) relaxation increases systematically with increasing PPGMEA content owing to both an increase in the number of (−COO−) ester moieties present in the network, as well as a likely increase in dipolar mobility with increasing fractional free volume. However, there is little variation in the dielectric peak temperature associated with the glass transition; a similar result was obtained in the course of calorimetric and dynamic mechanical measurements on this system.[138]

Figure 5.31 shows dielectric loss plotted versus frequency for the PPGDA/PPGMEA series in the sub-glass transition range (-78°C). For XLPPGDA and the PPGDA-based copolymers, the intensities of the sub-glass transitions are much weaker than those encountered in PEGDA, and this is consistent with the character of the sub-glass process observed in uncrosslinked PPO polymer; [148,151,152] see the discussion in Section 5.3.2. Two distinct sub-glass transitions are evident in the PPGDA copolymer networks, with the position of the β_2 process quite close to the “fast” relaxations observed in XLPEGDA and PEO. The β_2 relaxation in XLPPGDA and its copolymers likely has the same underlying origin as the β_2 process observed in the PEGDA copolymers, and would presumably display a comparable sensitivity to copolymer composition and the corresponding degree of constraint imposed by the network junctions. Examination of Figure 5.31 reveals that the relative intensity of the β_2 process is diminished with decreasing crosslinker content, in a manner similar to that observed for the PEGDA/PEGMEA and PEGDA/PEGA series: as the overall network structure is loosened, fewer segments adopt conformations that contribute to the "fast" relaxation response. Unfortunately, the strong degree of overlap between the β_1 and β_2 dispersions makes it difficult to reliably determine the HN broadening parameters associated with the individual relaxations at lower PPGDA content. However, for the 100% XLPPGDA network, the HN broadening parameter for the β_2 relaxation displays the same trend with temperature that was observed for PEO and the PEGDA copolymers, and which is consistent with the β_2 process originating at the constrained crosslink junctions (see Figure 5.8).

Owing to the relatively weak intensity of the sub-glass processes in the PPGDA/PPGMEA copolymers, the dielectric spectra for these materials can be fit in the range of the glass transition using a single HN function. Representative dielectric loss data (-30°C) and the corresponding HN curve fits for these polymers are plotted versus frequency in **Figure 5.32**. HN best-fits in the glass transition region were used to establish the value of τ_{MAX} for each copolymer as a function of temperature. The time-temperature characteristics of the PPGDA/PPGMEA networks can be compared by the construction of cooperativity or fragility plots, which are normalized Arrhenius plots wherein relaxation time (τ_{MAX}/τ_α) is plotted versus reciprocal temperature (T_α/T).[29,43] In this context, T_α is the glass transition temperature, and τ_α is the relaxation time associated with T_α. For the dielectric measurements reported here, the convention adopted defines T_α as the transition temperature associated with a value of the relaxation time, $\tau_\alpha = 1$ sec. The cooperativity plots for XLPPGDA and its copolymers are presented in **Figure 5.33**, wherein the solid curves correspond to WLF fits to the data. The apparent activation energy for the individual networks can be determined by evaluating the slope of each data curve at $T = T_\alpha$. For the 100% PPGDA network, an apparent activation $E_A = 310$ kJ/mol is obtained from the dielectric data, which is very close to the value determined from DMA measurements where T_α was assigned to the dynamic mechanical peak temperature at 1 Hz. Across the PPGDA/PPGMEA copolymer series, a progressive decrease in apparent activation energy is observed with decreasing crosslink density: this trend is consistent with previous DMA results for the PEGDA and PPGDA copolymers (see Chapter 4), and has been reported in the literature for other crosslinked homopolymer systems.[25,29,30] For the PPGDA/PPGMEA dielectric data reported here, an apparent activation energy E_A = 280 kJ/mol is obtained for the 80/20 copolymer composition, and an E_A value of 250 kJ/mol is obtained for the 50/50, 30/70 and 9/91 PPGDA/PPGMEA copolymers. The introduction of PPGMEA into the network leads to a reduction in the cooperativity inherent to the glass transition with decreasing effective crosslink density. The net impact of copolymerization with the acrylate co-monomer is an overall increase in fractional free volume and a decrease in the degree of constraint imposed by the crosslink junctions, such that less segmental cooperation is required across the glass-rubber relaxation.

5.3.7 Properties of crosslinked BPAEDA and copolymers

UV photopolymerization of BPAEDA crosslinker and copolymer mixtures with PEGMEA and PEGA monomers led to highly crosslinked amorphous networks with essentially complete acrylate conversion, as verified by FTIR-ATR studies. The 100% BPAEDA [XLBPAEDA] network has a lower value of molecular weight between crosslinks (M_c = 634 g/mol) as compared to XLPEGDA (M_c = 688 g/mol), resulting in a somewhat more constrained network. Also, the presence of shorter lengths of ethylene oxide (EO) segments (8, as compared to 14 in PEGDA), along with bulky phenyl rings within the bridging group, reduces the overall chain mobility. This manifests itself via a relatively high T_g for the XLBPAEDA network in comparison to XLPEGDA, as verified by DMA and DSC scans (see Tables 4.3 and 4.7). Introduction of flexible PEGMEA or PEGA chains into the BPAEDA network results in a substantial decrease in T_g for both the BPAEDA/PEGMEA and BPAEDA/PEGA series. The BPAEDA/PEGA series tends to show higher T_g values as compared to the BPAEDA/PEGMEA copolymer networks, possibly due to the –OH terminal group on PEGA resulting in additional hydrogen bonding (see Table 4.7).

5.3.8 Dielectric results for crosslinked BPAEDA and copolymers

Dielectric results for the XLBPAEDA network are shown in a three-dimensional contour plot of dielectric loss (ε'') vs. temperature vs. frequency in **Figure 5.34**. Similar to the 100% PEGDA network (see Figure 5.2), the XLBPAEDA network exhibits three motional transitions: two local sub-glass (β_1 and β_2) dispersions and the glass-rubber (α) relaxation. The influence of conduction is stronger within the XLBPAEDA network, and it overlaps with the α relaxation at higher temperatures and lower frequencies.

A plot of dielectric loss (ε'') versus frequency in the sub-glass transition region for XLBPAEDA is shown in **Figure 5.35**; the solid curves represent dual HN fits. Both β_1 and β_2 dispersions show an increase in intensity with temperature, along with a progressive merging of the two relaxations. For XLBPAEDA, the two relaxations can be reasonably deconvoluted to as high as -54°C. At the lower frequencies and higher temperatures, the dielectric loss data shows an upward trend, indicating the emergence of the cooperative, glass-rubber (α) relaxation.

Dielectric results for the BPAEDA/PEGMEA and BPAEDA/PEGA copolymers are plotted as dielectric constant (ε') and dielectric loss (ε'') versus temperature in **Figures 5.36** and **5.37**, respectively; the loss data were corrected for conduction via an Arrhenius function applied over the conduction dominant region. The position of the loss maxima (*i.e.*, α relaxation peak temperatures) for both series exhibits a significant negative shift with increasing acrylate content, a trend consistent with prior DMA and DSC studies (see Table 4.7). Increasing the co-monomer content reduces the effective crosslink density of the XLBPAEDA network, and this is manifested in a corresponding increase in the dielectric relaxation intensity (see Figures 5.36 and 5.37).

Figures 5.38 and **5.39** present dielectric loss data in the sub-glass region (-70°C) for the BPAEDA/PEGMEA and BPAEDA/PEGA copolymer series, respectively. In both cases, examination of the β_2 dispersion intensity reveals an initial drop, followed by an increase in the relaxation intensity with increasing acrylate content. This trend is in contradiction to that observed for the model PEGDA copolymer systems (see Figures 5.17 and 5.20). However, the behavior is consistent with copolymer networks that vary in chemical constitution upon inclusion of acrylate monomers with short branches; for example, as observed for the PEGDA/DGEEA series (see Figure 5.25). The upward trend in the β_2 peak intensity is more pronounced and appears at lower branch concentrations for the BPAEDA/PEGA series as compared to BPAEDA/PEGMEA; see **Figure 5.40**. This can be attributed to the presence of the –OH terminal group on the PEGA monomer, resulting in additional dipolar content and a stronger net response.

5.4 CONCLUSIONS

The relaxation characteristics of amorphous homopolymer networks based on the UV photopolymerization of PEGDA and PPGDA crosslinkers have been investigated using broadband dielectric spectroscopy. These polymers, and related copolymer networks, display high CO_2 permeability and favorable CO_2/light gas selectivity, and have been identified as promising membrane materials for the separation of mixtures comprised of CO_2 and light gases such as H_2 or CH_4. Dielectric measurements on the XLPEGDA and XLPPGDA networks reveal the emergence of a "fast", non-cooperative segmental relaxation located intermediate to the sub-glass and glass-rubber processes traditionally reported for PEO and PPO. This fast process appears to be analogous to an intermediate relaxation detected previously in crystalline PEO,[121] a result that was confirmed by independent experimental studies on PEO films. In the case of PEO, it was proposed by Jin *et al.* that the fast process was the result of segmental constraint in the crystal-amorphous transition region. Owing to the limited conformational freedom of the polymer chain segments in this region, a more localized, largely non-cooperative process emerges, apparently as a subset of the cooperative segmental motions that constitute the glass transition. The dielectric relaxation characteristics of XLPEGDA and XLPPGDA are similar in many respects to those encountered in PEO, suggesting that a comparable constraint or confinement mechanism could be responsible for the detection of a fast segmental relaxation process in the crosslinked networks. The appearance of this additional process may be a general phenomenon in systems with a sufficient level of chemical or physical constraint, as it is observed in the amorphous XLPEGDA and XLPPGDA crosslinked networks, crystalline PEO, and in dielectric studies on PEO nanocomposites.

Similar dielectric relaxation studies have been undertaken to investigate the relaxation characteristics of amorphous copolymer networks based on the PEGDA and PPGDA crosslinkers. The glass-rubber and sub-glass relaxation processes in these networks are sensitive to the details of the network architecture, including branch length and the nature and character of the branch end groups. For the PEGDA-based networks, the inclusion of acrylate co-monomer in the prepolymerization reaction mixture and corresponding insertion of flexible branch groups in the resulting crosslinked networks led to a decrease in the measured glass-rubber relaxation temperature and an overall increase in dielectric relaxation intensity with reduced crosslink density. In both the PEGDA- and PPGDA-based networks, the intermediate (β_2) sub-glass relaxation was observed, and was attributed to a subset of non-cooperative segmental reorientations originating in the vicinity of the crosslink junctions. The measured intensity of the β_2 process decreased with increasing co-monomer content owing to a loosening of the constraint imposed by the network junctions at lower effective crosslink density. A characteristic broadening of the β_2 relaxation was observed with increasing temperature that reflected the contrasting mobility of the flexible and constrained regions of the network; this distinctive broadening behavior was less pronounced in the copolymers containing lower degrees of crosslinking. Also, a reversed trend was observed in the measured intensity of the β_2 relaxation for the short-branched PEGDA/DGEEA series, an effect that can be attributed to increased overall dipolar carbonyl content at higher levels of acrylate co-monomer. For the short-branched PPGDA networks, dielectric relaxation intensity increased strongly with co-monomer content across the glass transition region owing to the increase in the number of (–COO–) ester dipoles present along the network backbone. Normalized cooperativity plots indicated a progressive decrease in the dynamic fragility of the networks (*i.e.*, lower apparent activation energy with decreased crosslink density), a result that was consistent with previous dynamic mechanical studies.

Dielectric relaxation measurements have been performed on crosslinked BPAEDA and copolymer networks with PEGMEA and PEGA co-monomers. These networks experience a higher T_g as compared to the PEGDA-based networks owing to a shorter and bulkier bridging group. The copolymer networks exhibit a significant drop in T_g with increasing co-monomer content as a result of the inherent flexibility of the PEGMEA and PEGA species. Similar to the short branched DGEEA networks, the measured intensity of the β_2 relaxation for the BPAEDA copolymer networks exhibits an increase with increasing acrylate content. The effect is more pronounced for the –OH terminated PEGA copolymer series where additional dipolar content further amplifies the dielectric response.

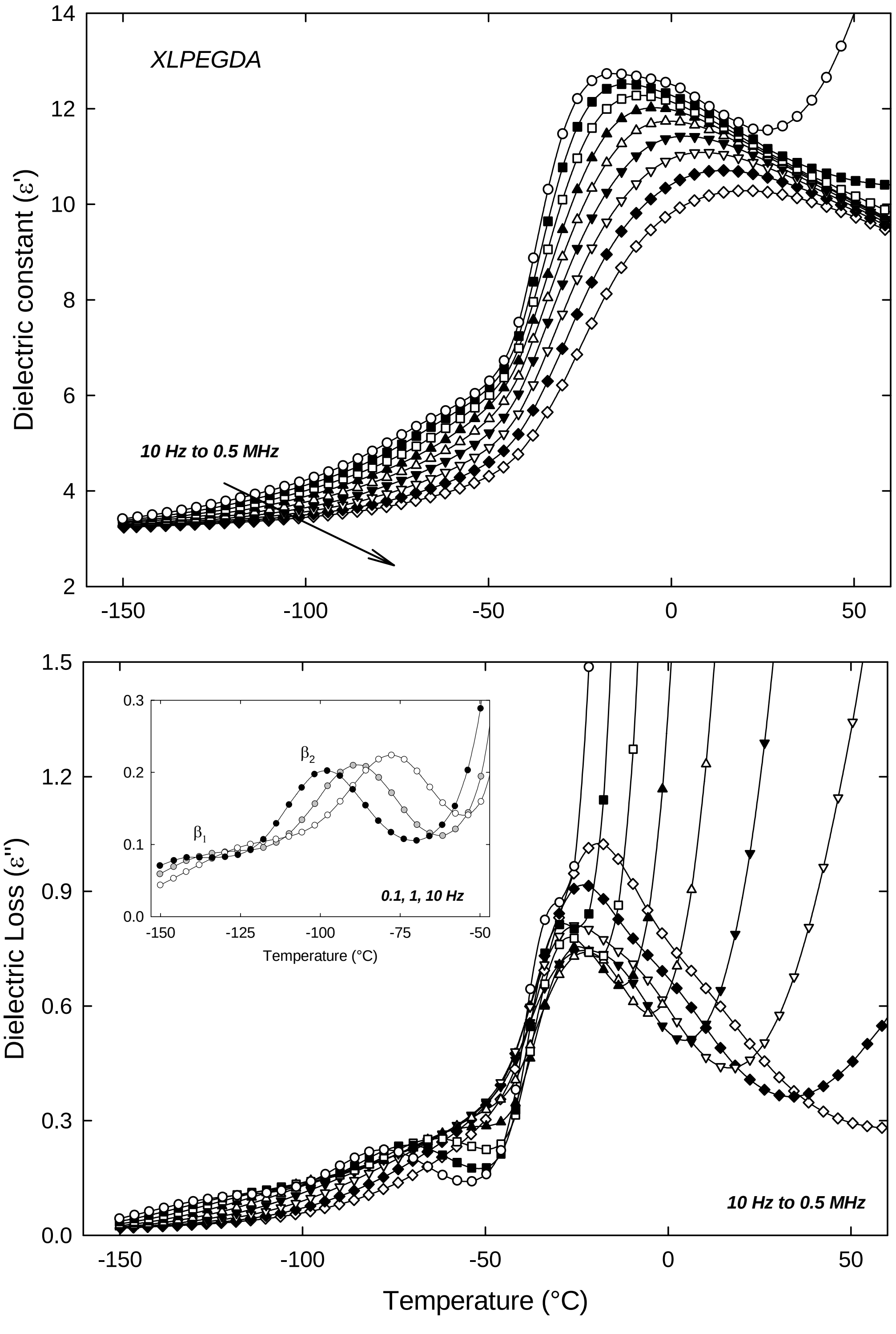

Figure 5.1: Dielectric constant (ε') and loss (ε'') vs. temperature for XLPEGDA; selected frequencies from 10 Hz to 0.5 MHz. *Inset*: expanded view of dielectric loss across the sub-glass region at 0.1, 1, and 10 Hz.

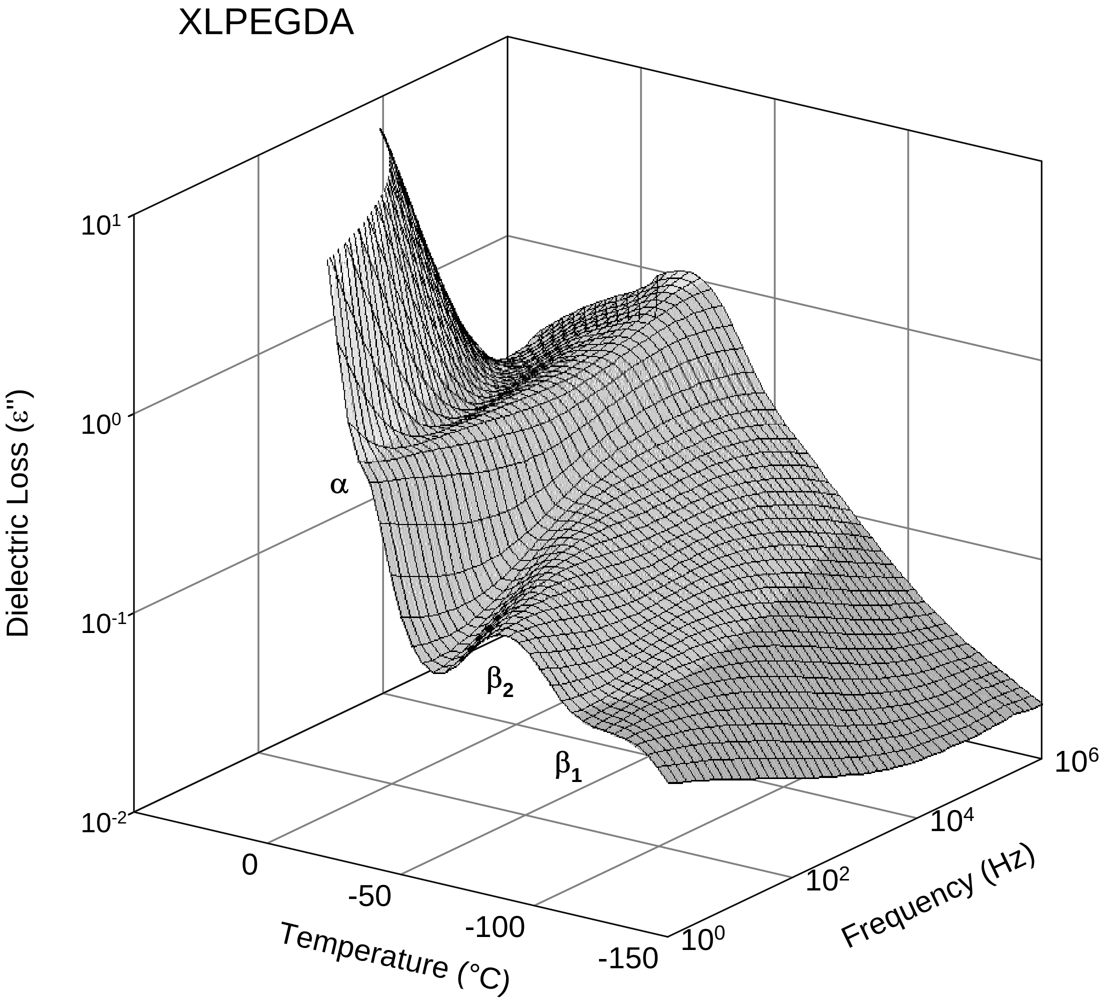

Figure 5.2: Contour plot of dielectric loss (ε'') vs. temperature (°C) vs. frequency (Hz) for XLPEGDA network.

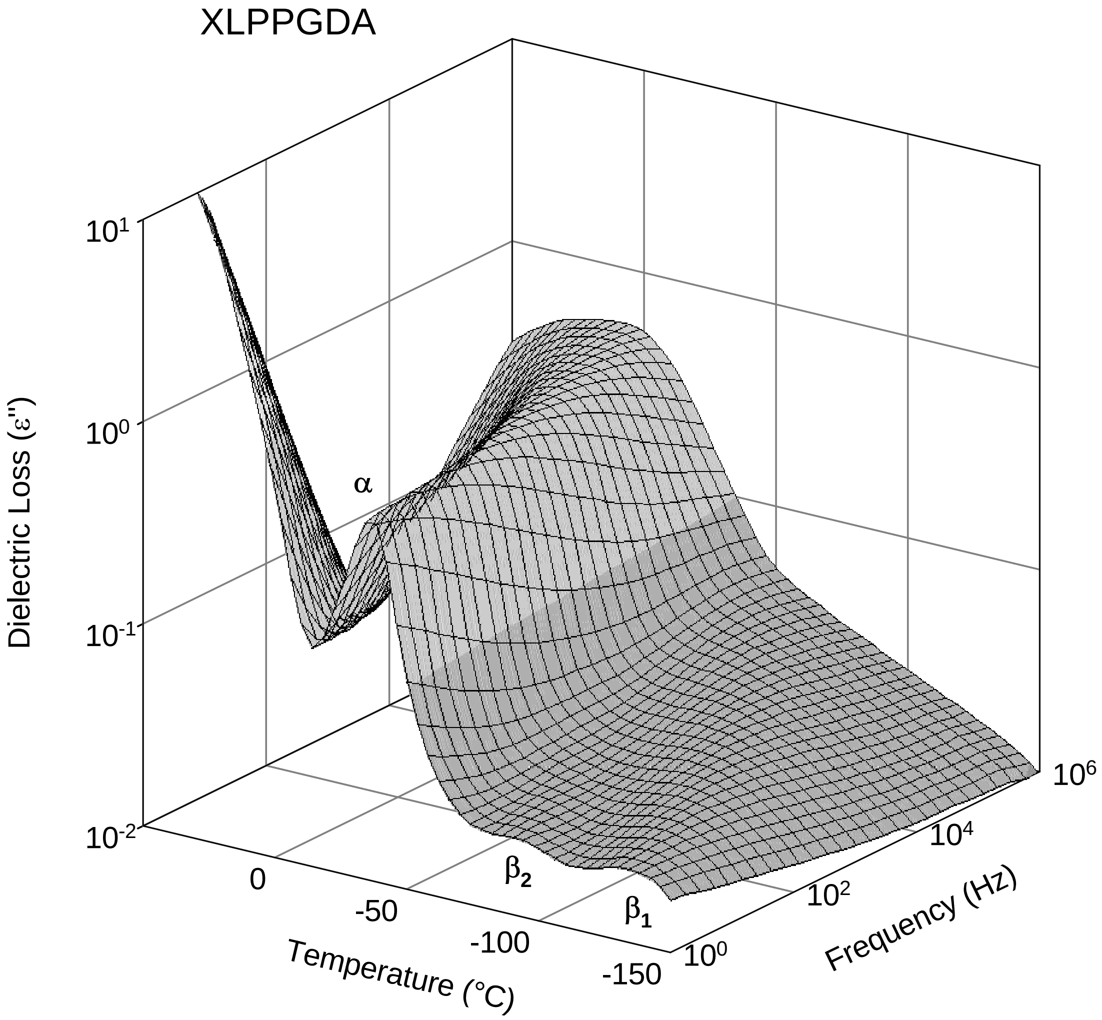

Figure 5.3: Contour plot of dielectric loss (ε'') vs. temperature (°C) vs. frequency (Hz) for XLPPGDA network.

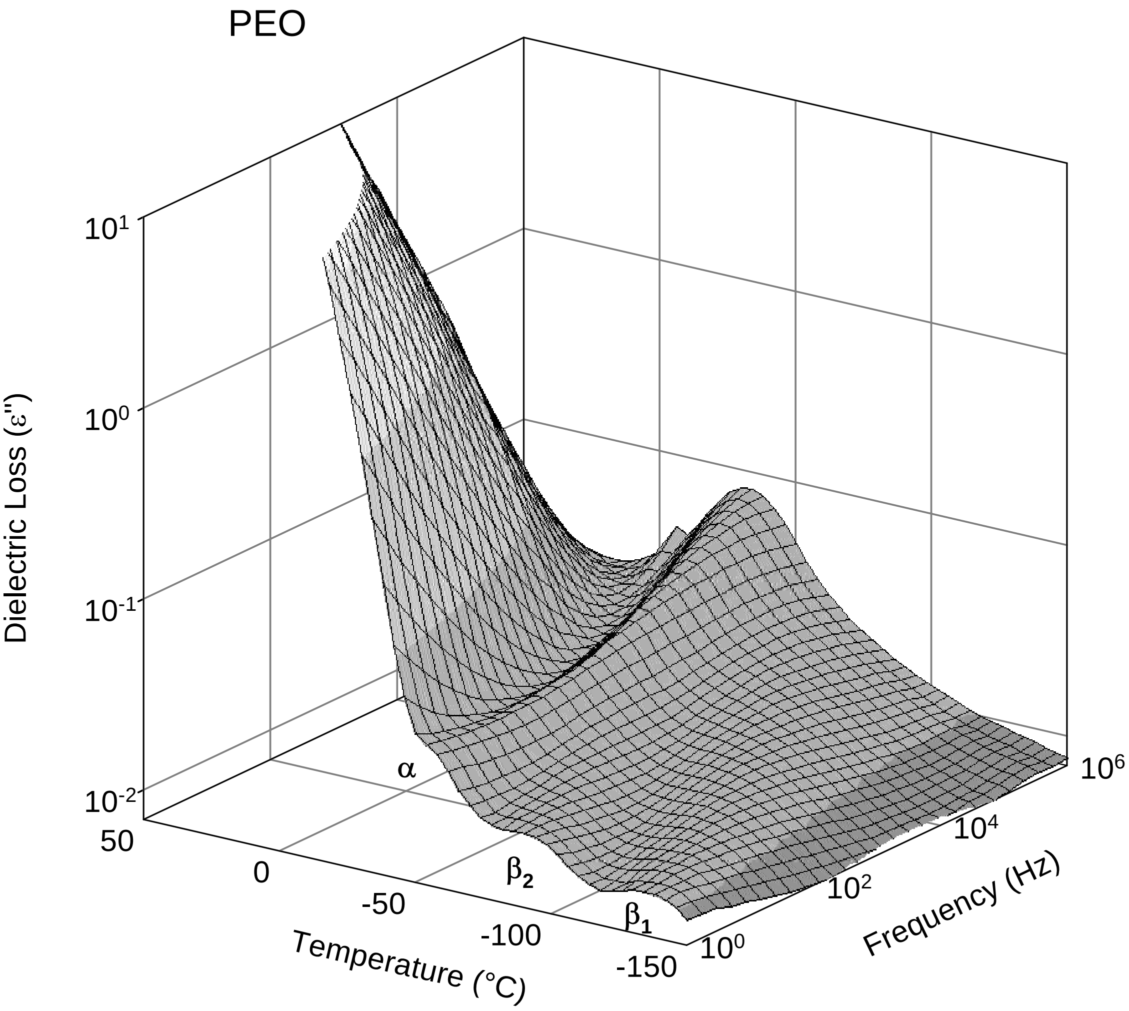

Figure 5.4: Contour plot of dielectric loss (ε'') vs. temperature (°C) vs. frequency (Hz) for PEO network.

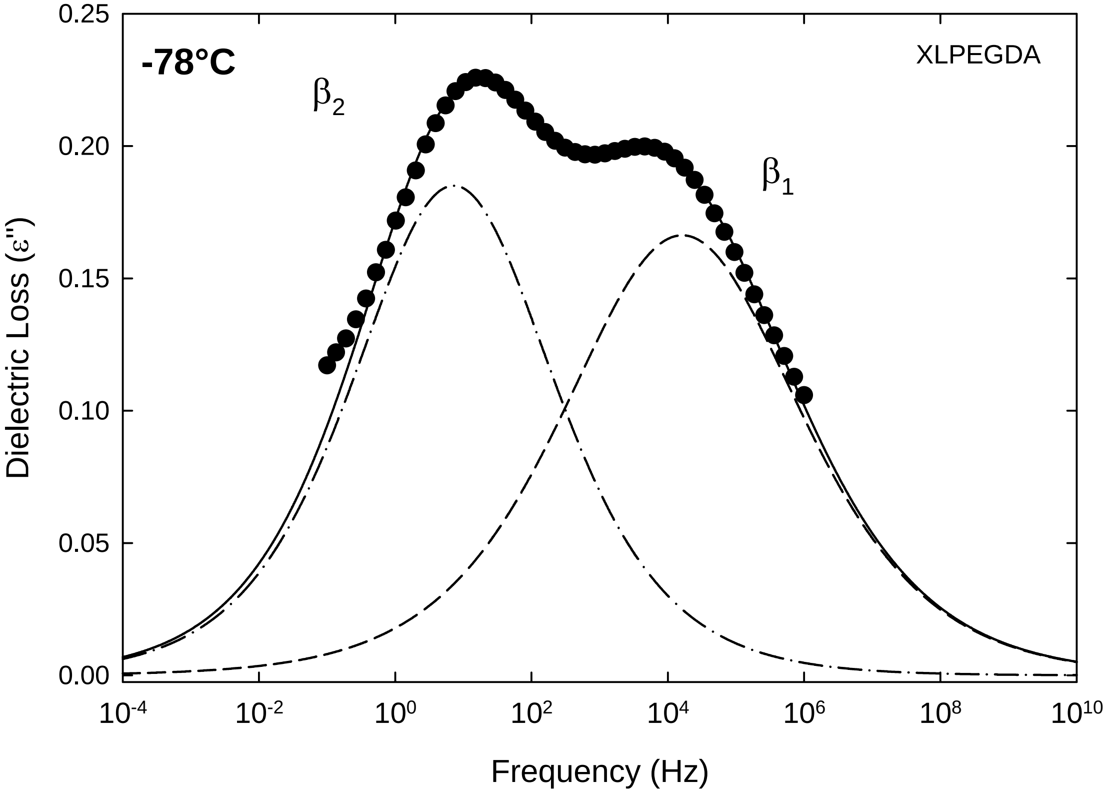

Figure 5.5: Dielectric loss (ε'') vs. frequency (Hz) for XLPEGDA at -78°C. Solid curve is dual HN fit; dashed curves are individual HN fits for the β_1 and β_2 relaxations.

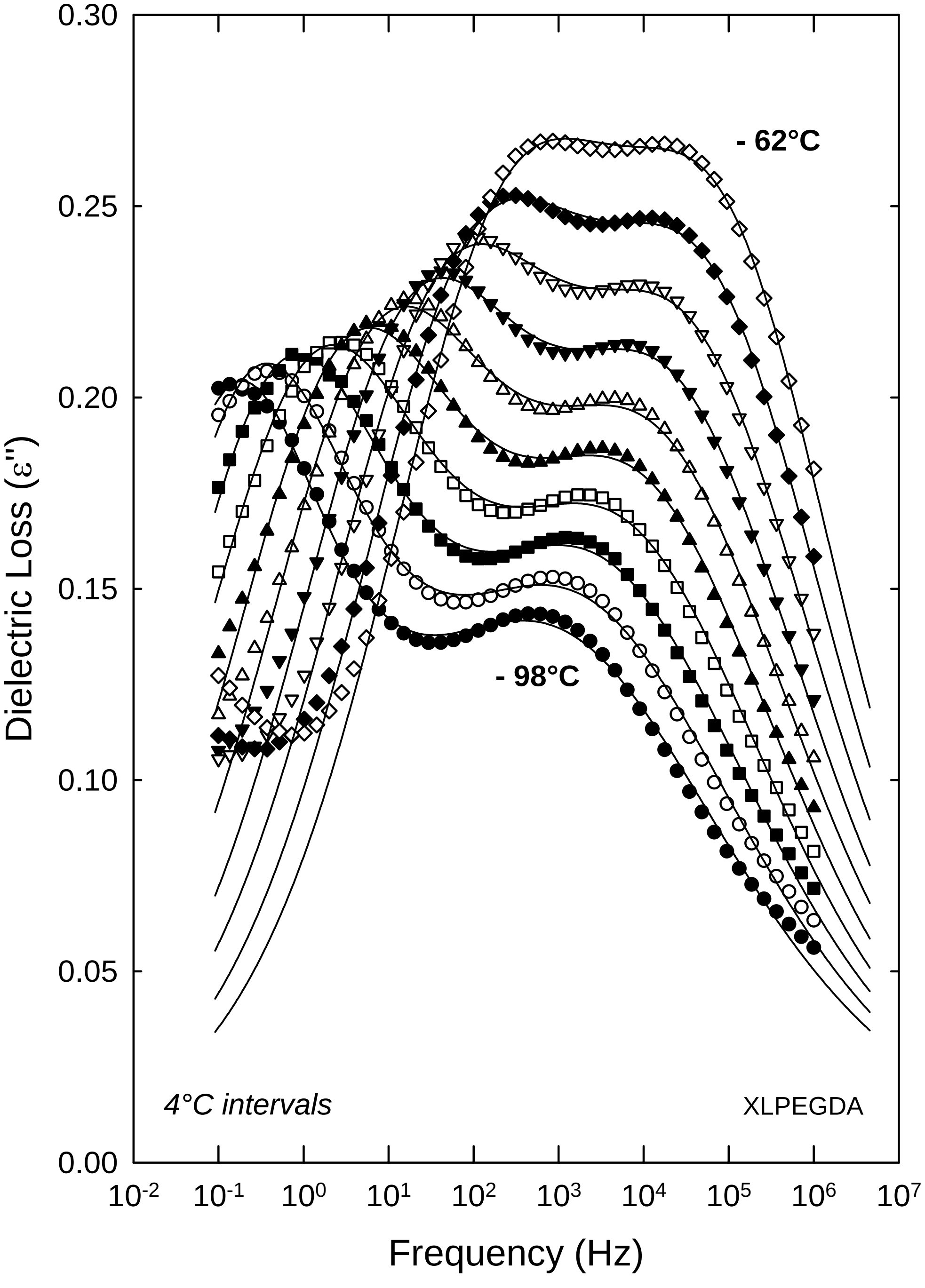

Figure 5.6: Dielectric loss (ε'') vs. frequency (Hz) for XLPEGDA; temperatures from -98°C to -62°C at 4°C intervals. Solid curves are dual HN fits.

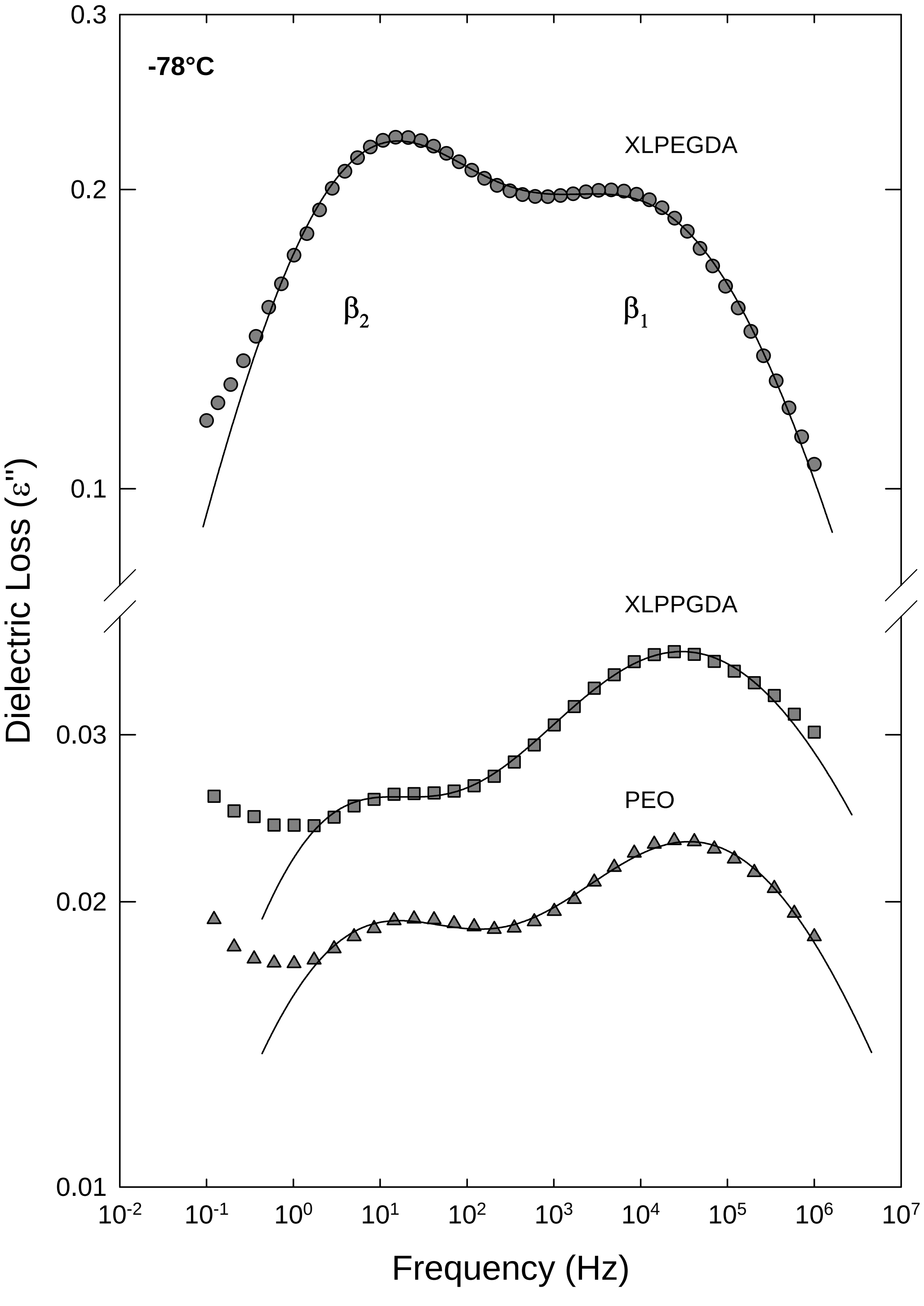

Figure 5.7: Dielectric loss (ε'') vs. frequency (Hz) for XLPEGDA, XLPPGDA and PEO at -78°C. Solid curves are dual HN fits.

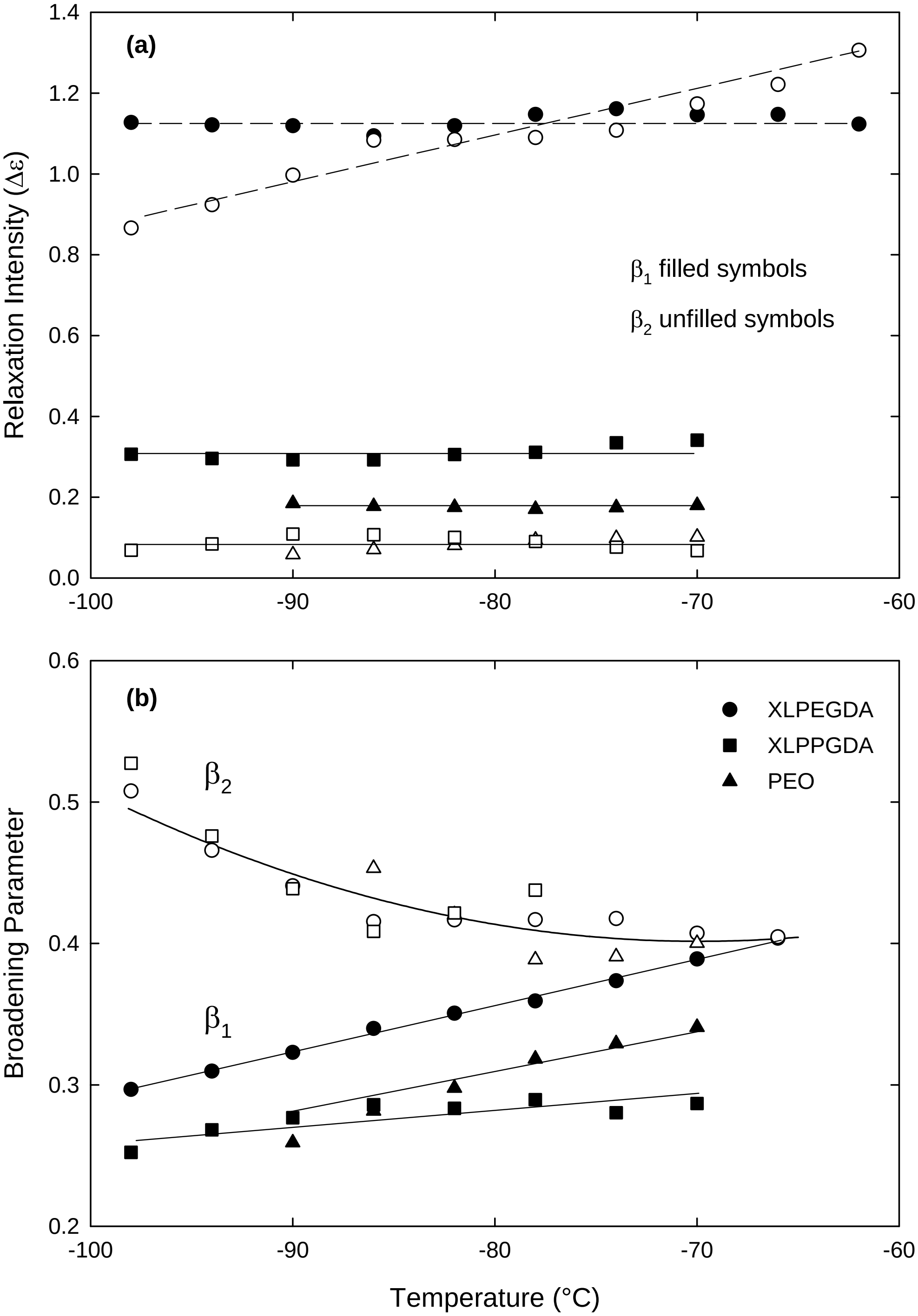

Figure 5.8: HN curve fit parameters for XLPEGDA, XLPPGDA and PEO vs. temperature (°C). (a) relaxation intensity; (b) HN broadening parameter.

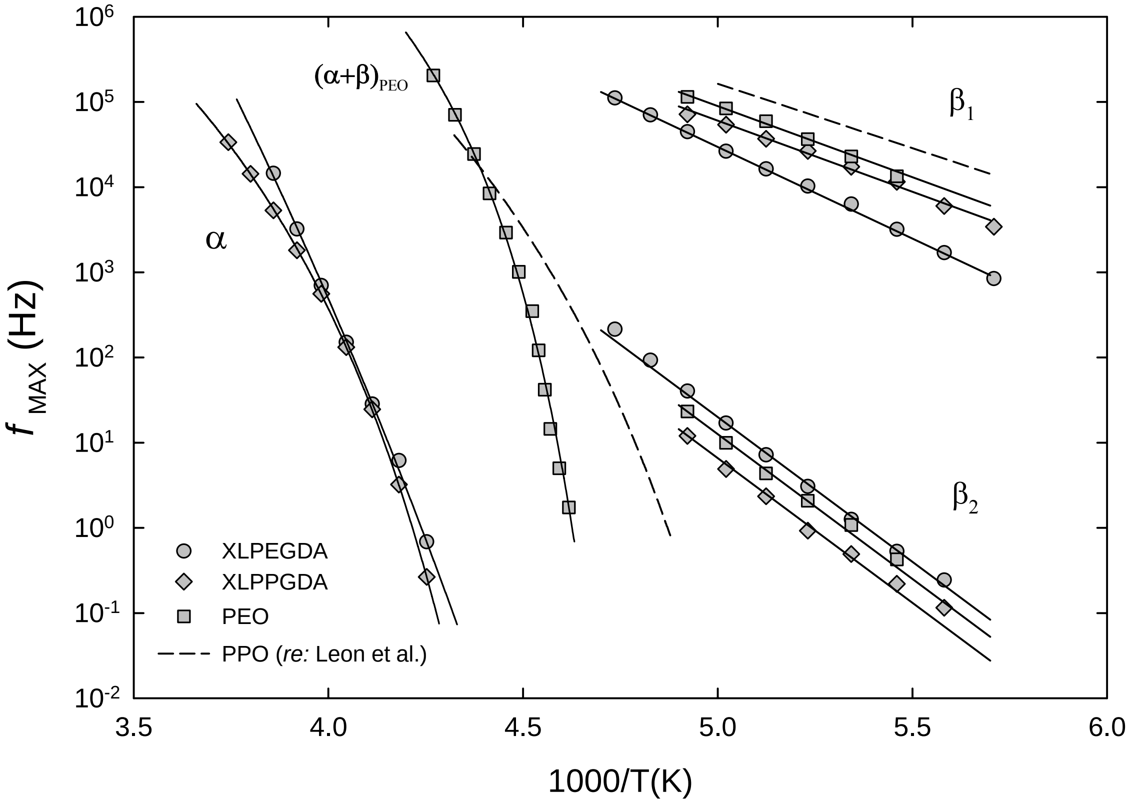

Figure 5.9: Arrhenius plot of f_{MAX} (Hz) vs. 1000/T(K) for XLPEGDA, XLPPGDA and PEO. Dashed lines correspond to data for PPO polymer (see ref. 151).

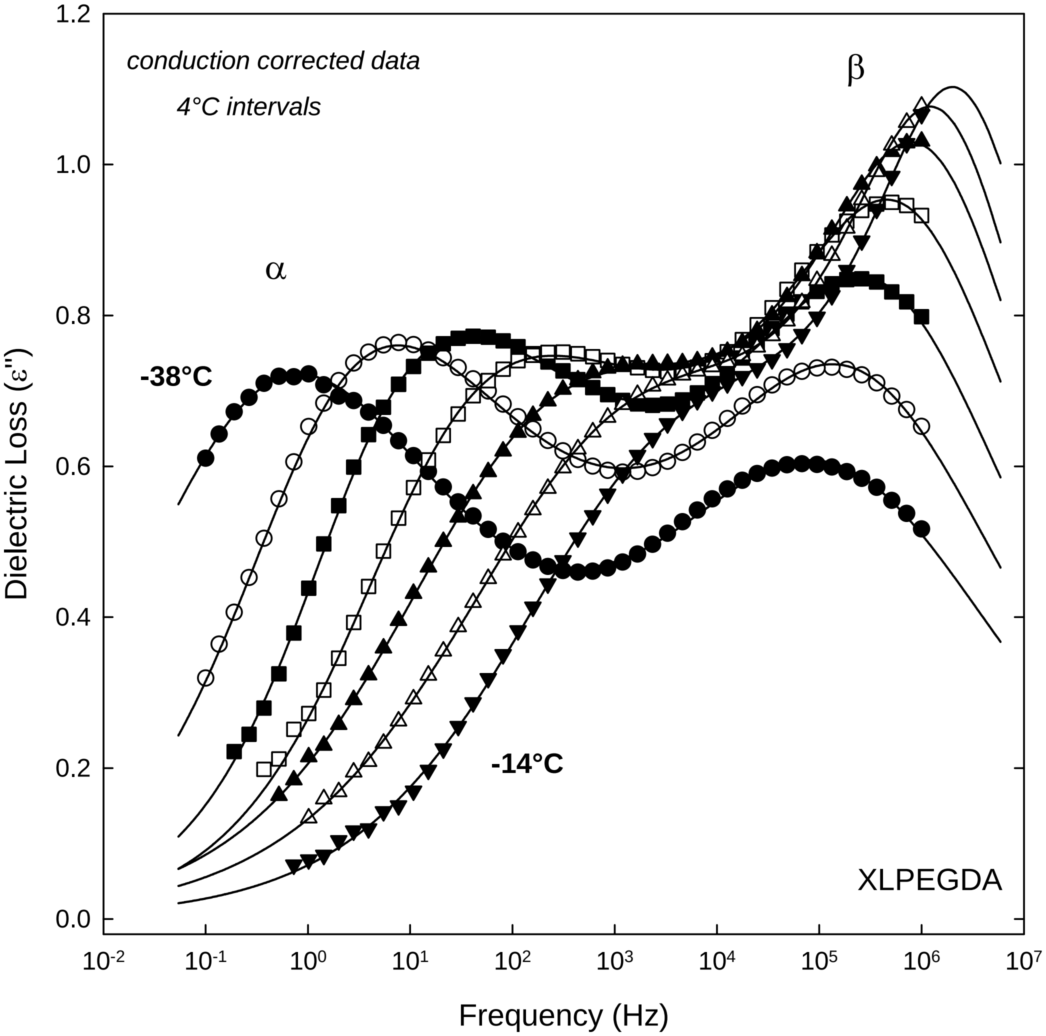

Figure 5.10: Dielectric loss (ε'') vs. frequency (Hz) for XLPEGDA; temperatures from -38°C to -14°C at 4°C intervals. Data are corrected for conduction contribution according to equation 5.2. Solid curves are dual HN fits.

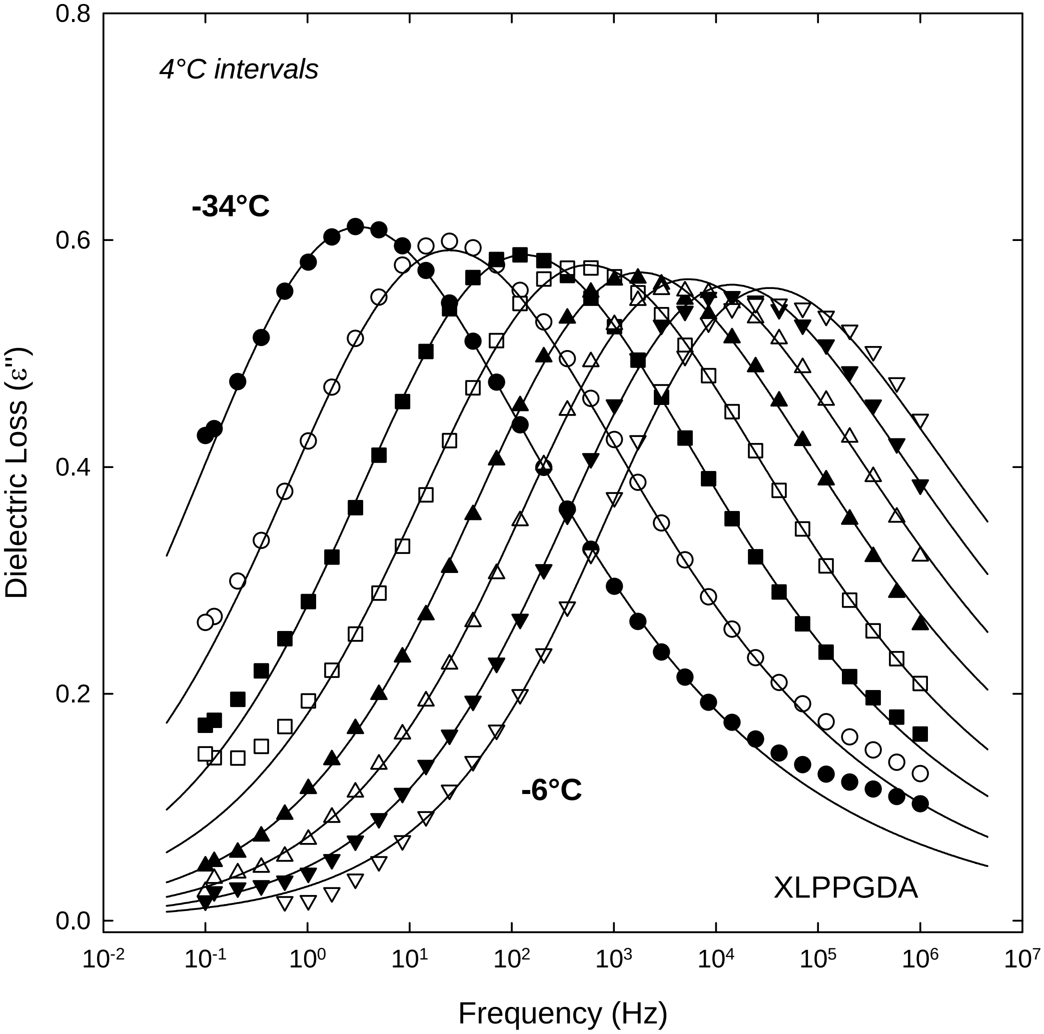

Figure 5.11: Dielectric loss (ε'') vs. frequency (Hz) for XLPPGDA; temperatures from -34°C to -6°C at 4°C intervals. Solid curves are HN fits.

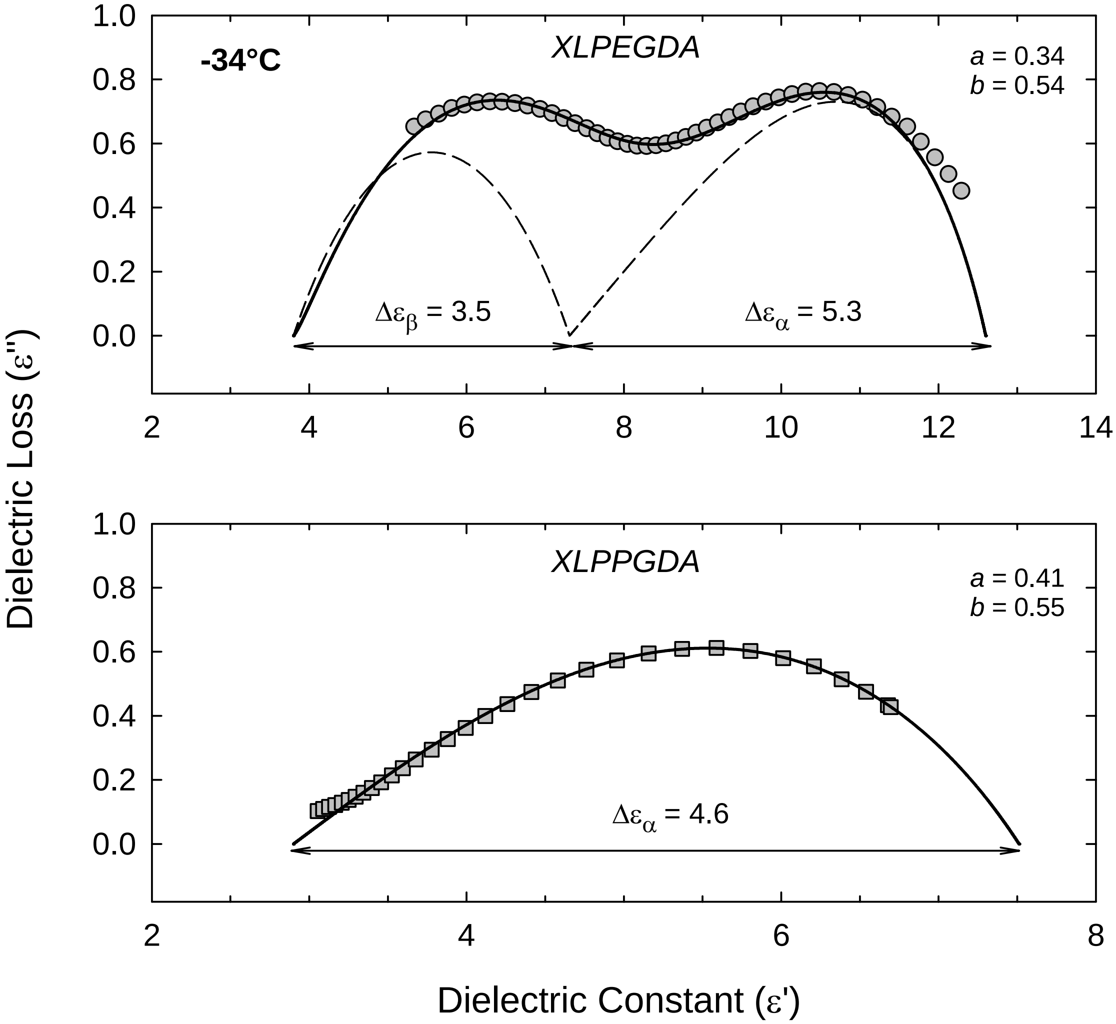

Figure 5.12: Cole-Cole plots of dielectric loss (ε'') vs. dielectric constant (ε') for XLPEGDA and XLPPGDA at -34°C. Solid curve is HN best fit. HN fit parameters (*a*,*b*) for the glass-rubber relaxation are as indicated.

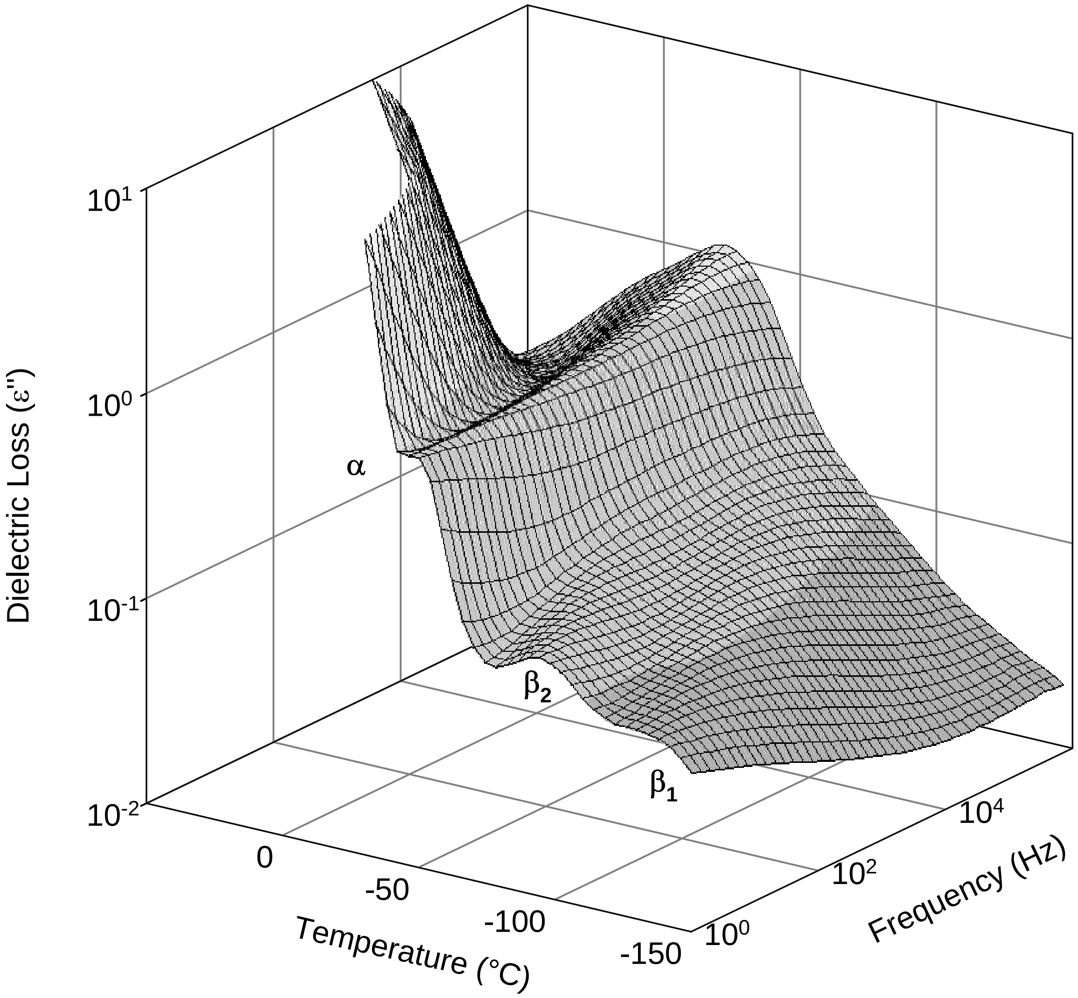

Figure 5.13: Contour plot of dielectric loss (ε'') vs. temperature (°C) vs. frequency (Hz) for 50/50 (wt%) PEGDA/PEGMEA network.

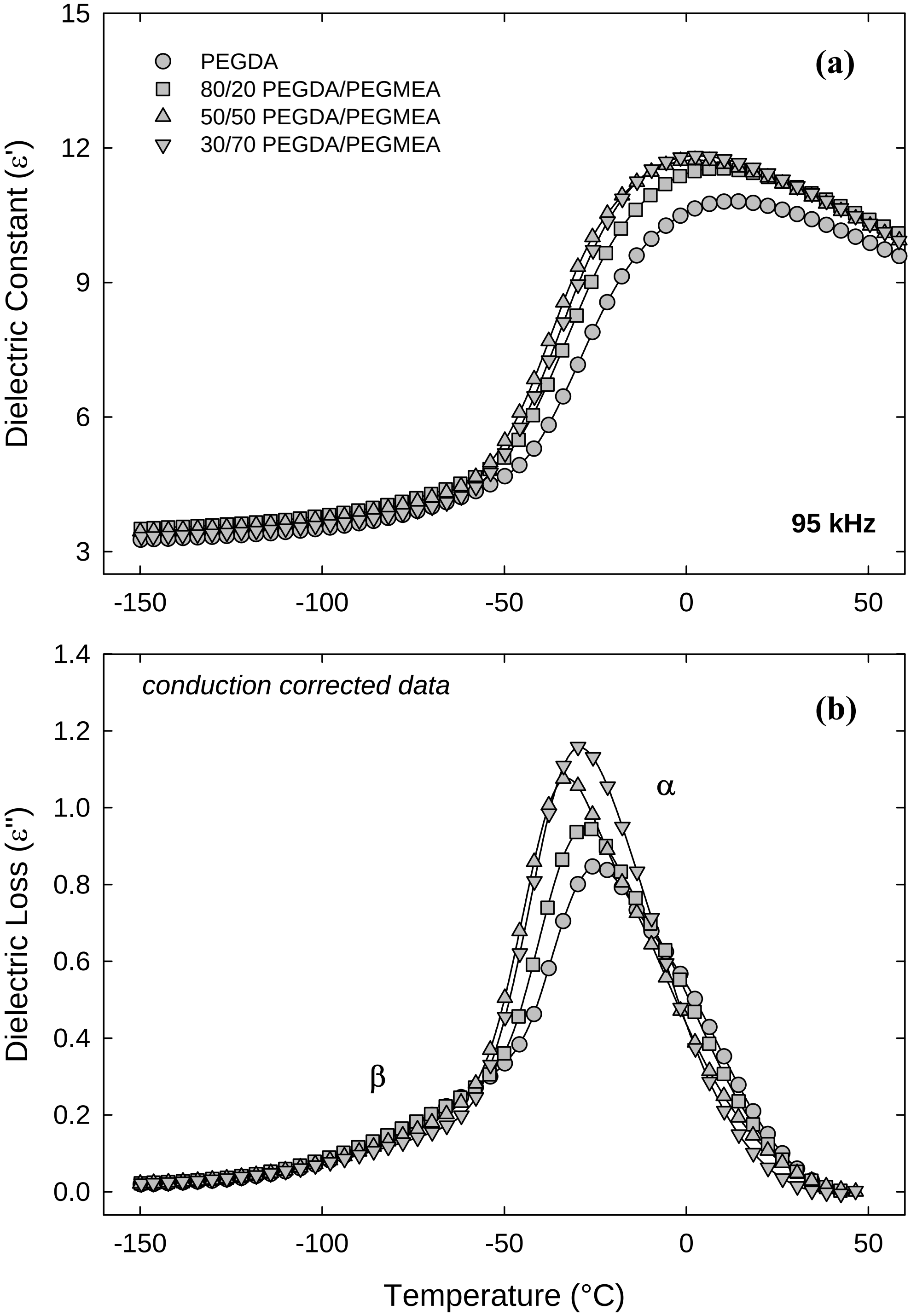

Figure 5.14: Dielectric properties of PEGDA/PEGMEA copolymer networks: (a) dielectric constant (ε'); (b) dielectric loss (ε'') vs. temperature. Frequency of 95 kHz. Dielectric loss data corrected for conduction.

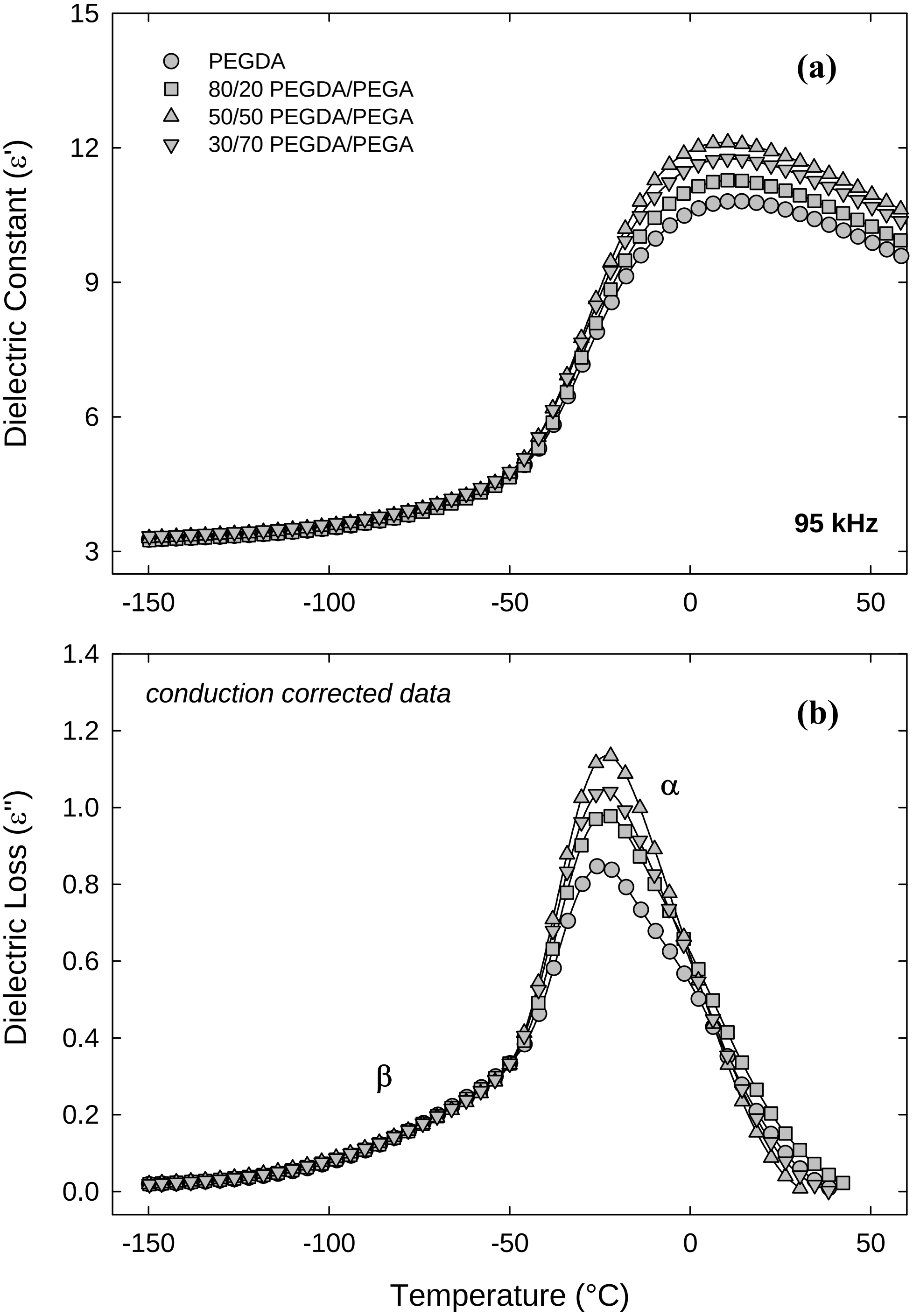

Figure 5.15: Dielectric properties of PEGDA/PEGA copolymer networks: (a) dielectric constant (ε'); (b) dielectric loss (ε'') vs. temperature. Frequency of 95 kHz. Dielectric loss data corrected for conduction.

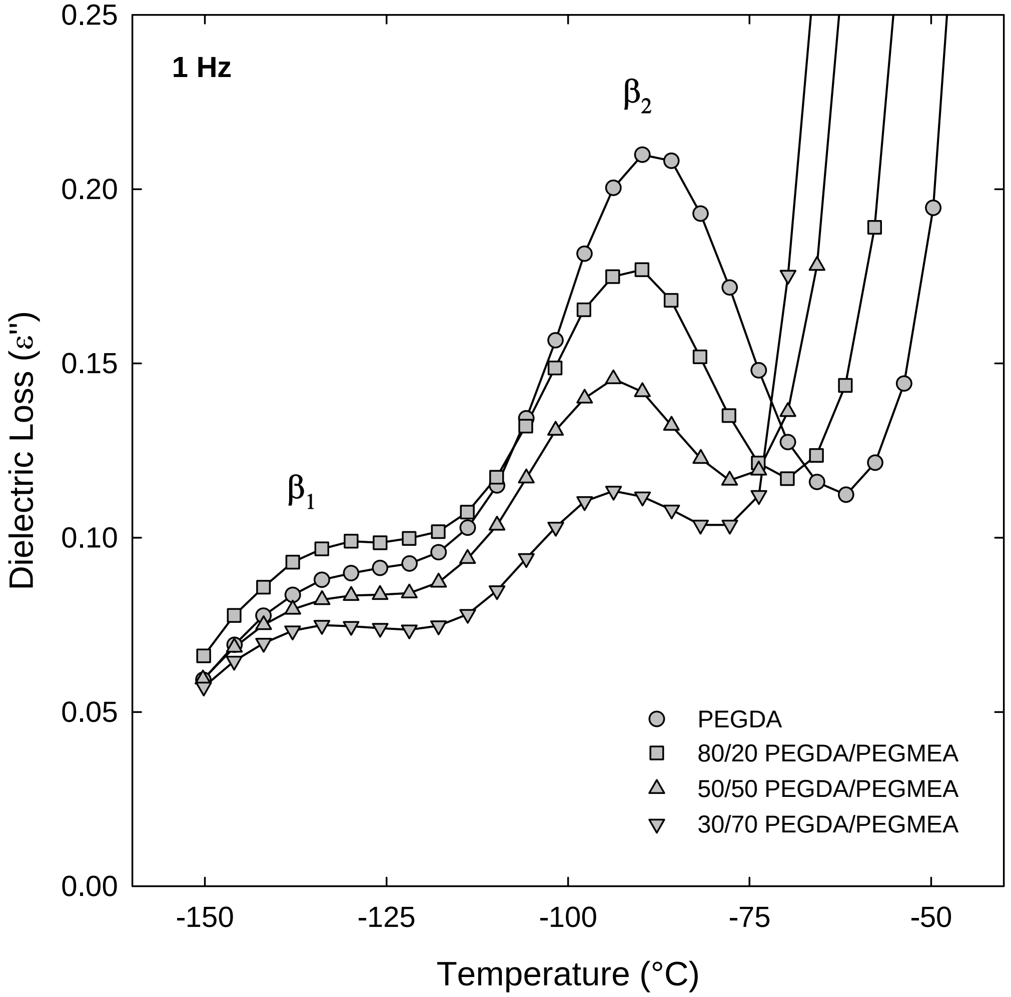

Figure 5.16: Dielectric loss (ε'') vs. temperature for PEGDA/PEGMEA copolymer networks across the sub-glass transition region. Frequency of 1 Hz.

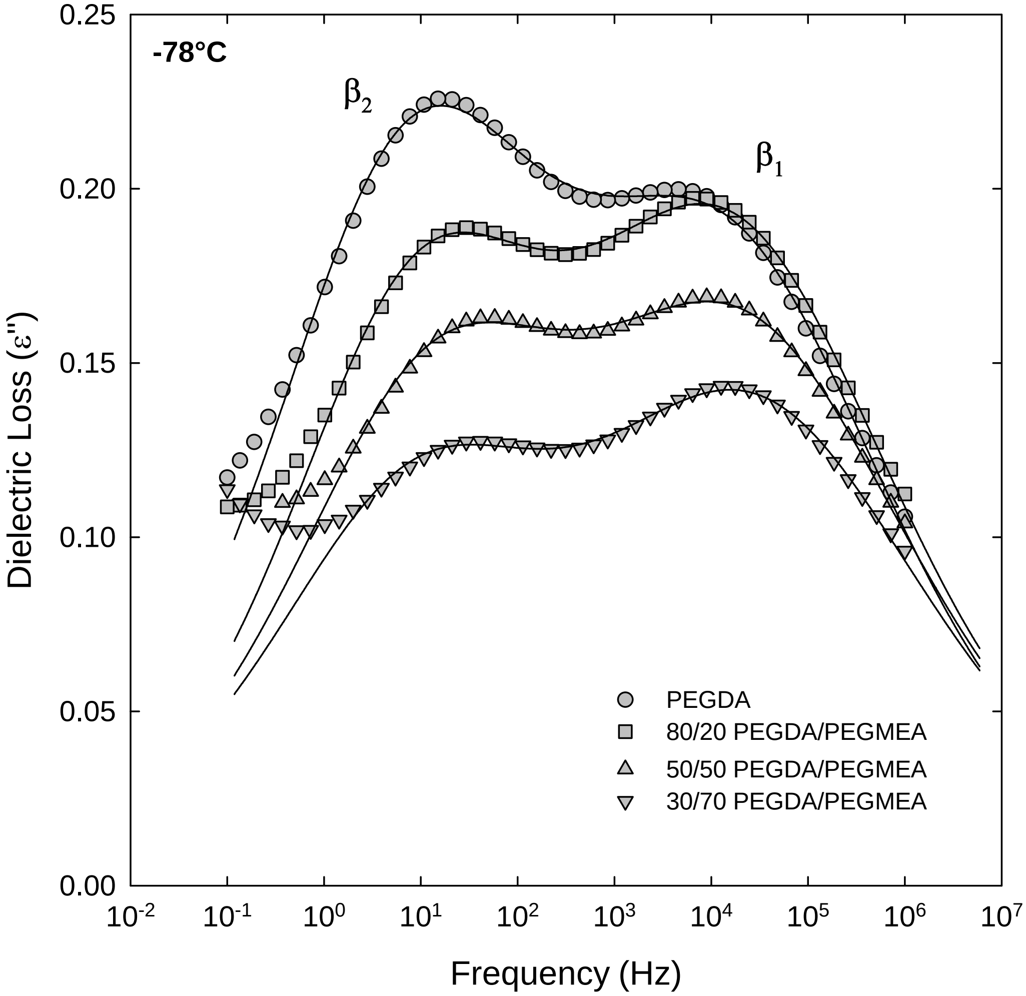

Figure 5.17: Dielectric loss (ε'') vs. frequency for PEGDA/PEGMEA copolymer networks at -78°C. Solid curves are dual HN fits.

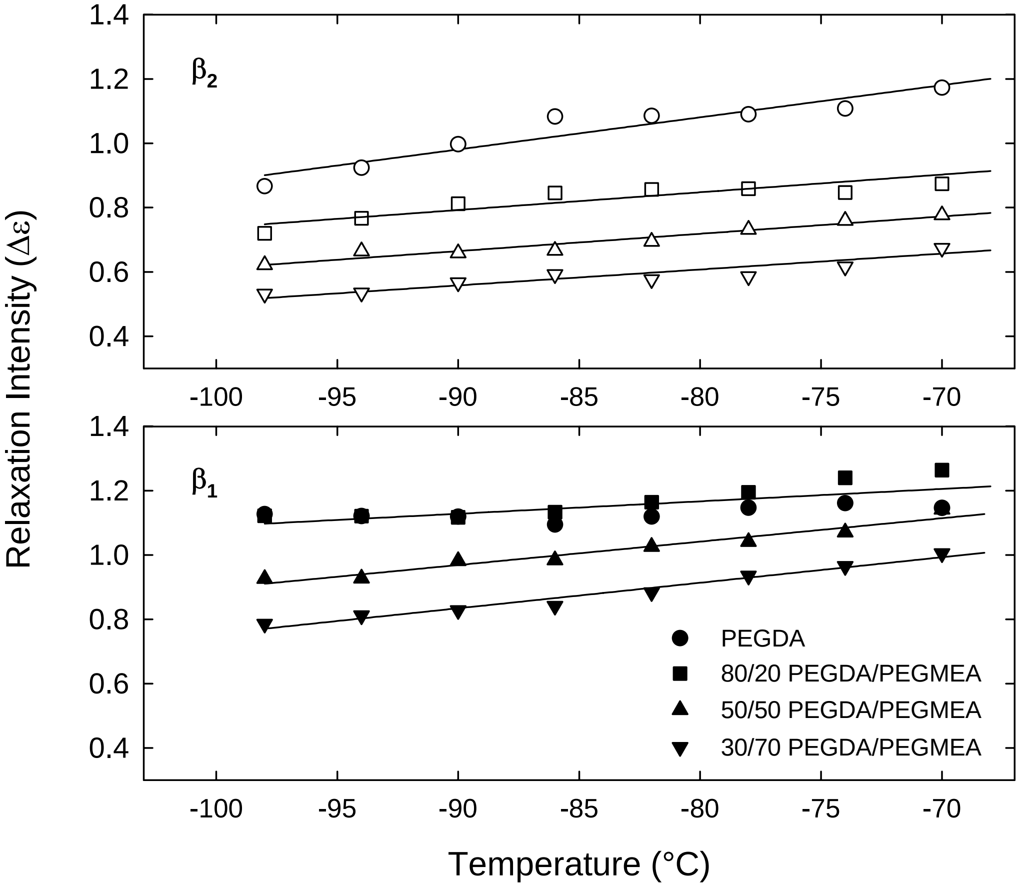

Figure 5.18: Dielectric relaxation intensity ($\Delta\varepsilon$; determined from HN fits) vs. temperature for PEGDA/PEGMEA copolymer networks. β_1 and β_2 sub-glass transitions.

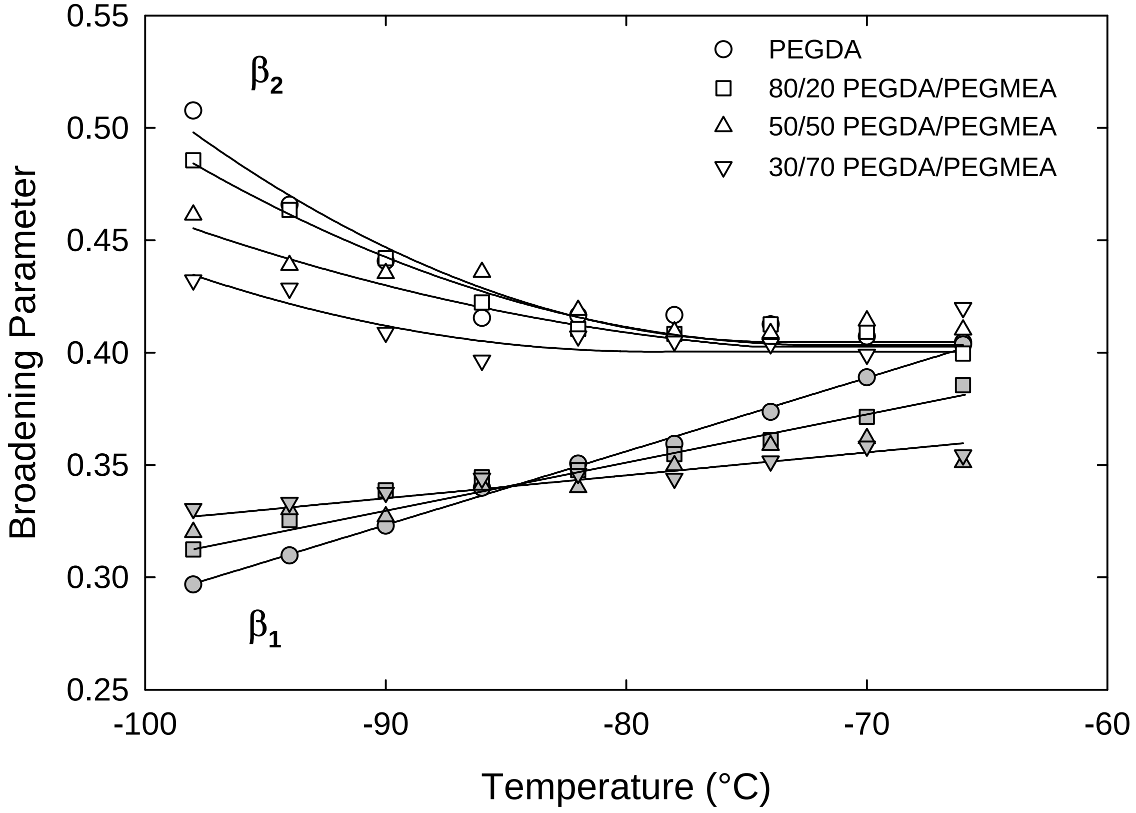

Figure 5.19: Havriliak-Negami [HN] broadening parameter vs. temperature for PEGDA/PEGMEA copolymer networks. β_1 and β_2 sub-glass transitions.

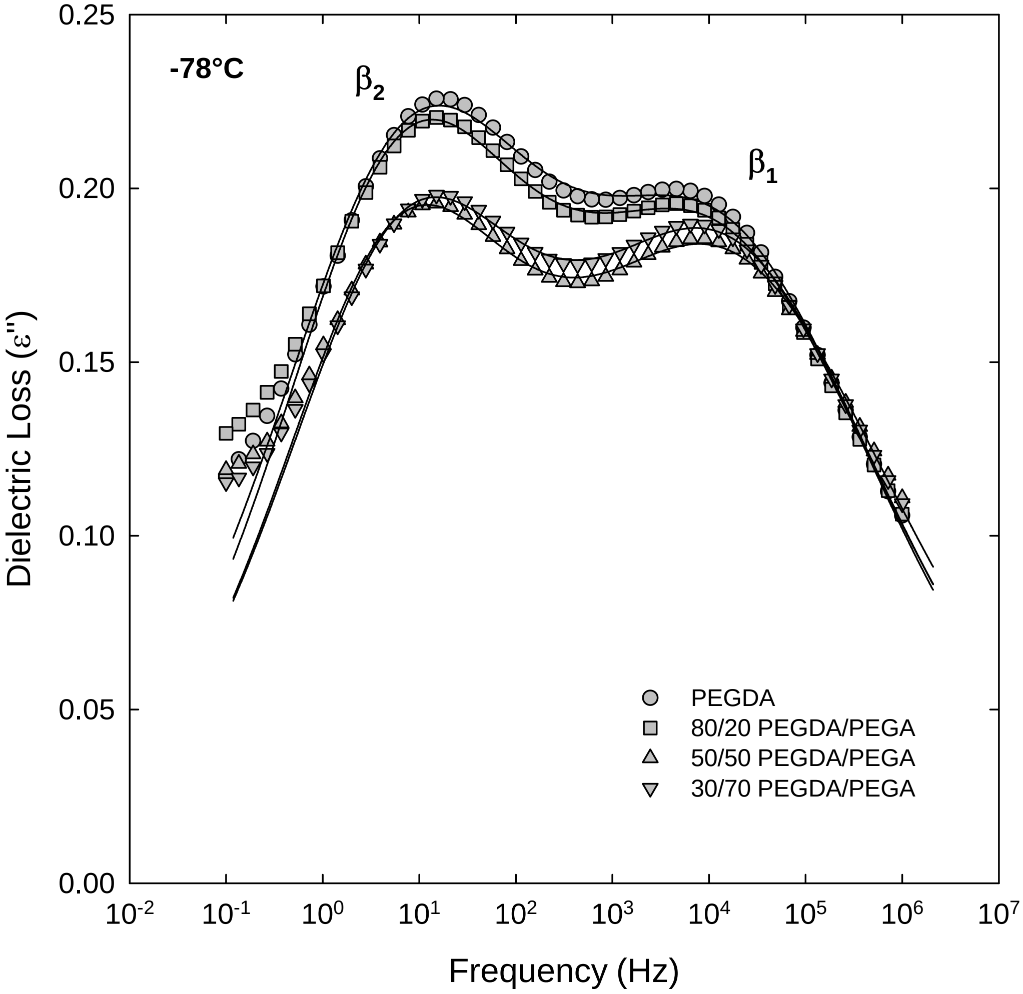

Figure 5.20: Dielectric loss (ε'') vs. frequency for PEGDA/PEGA copolymer networks at -78°C. Solid curves are dual HN fits.

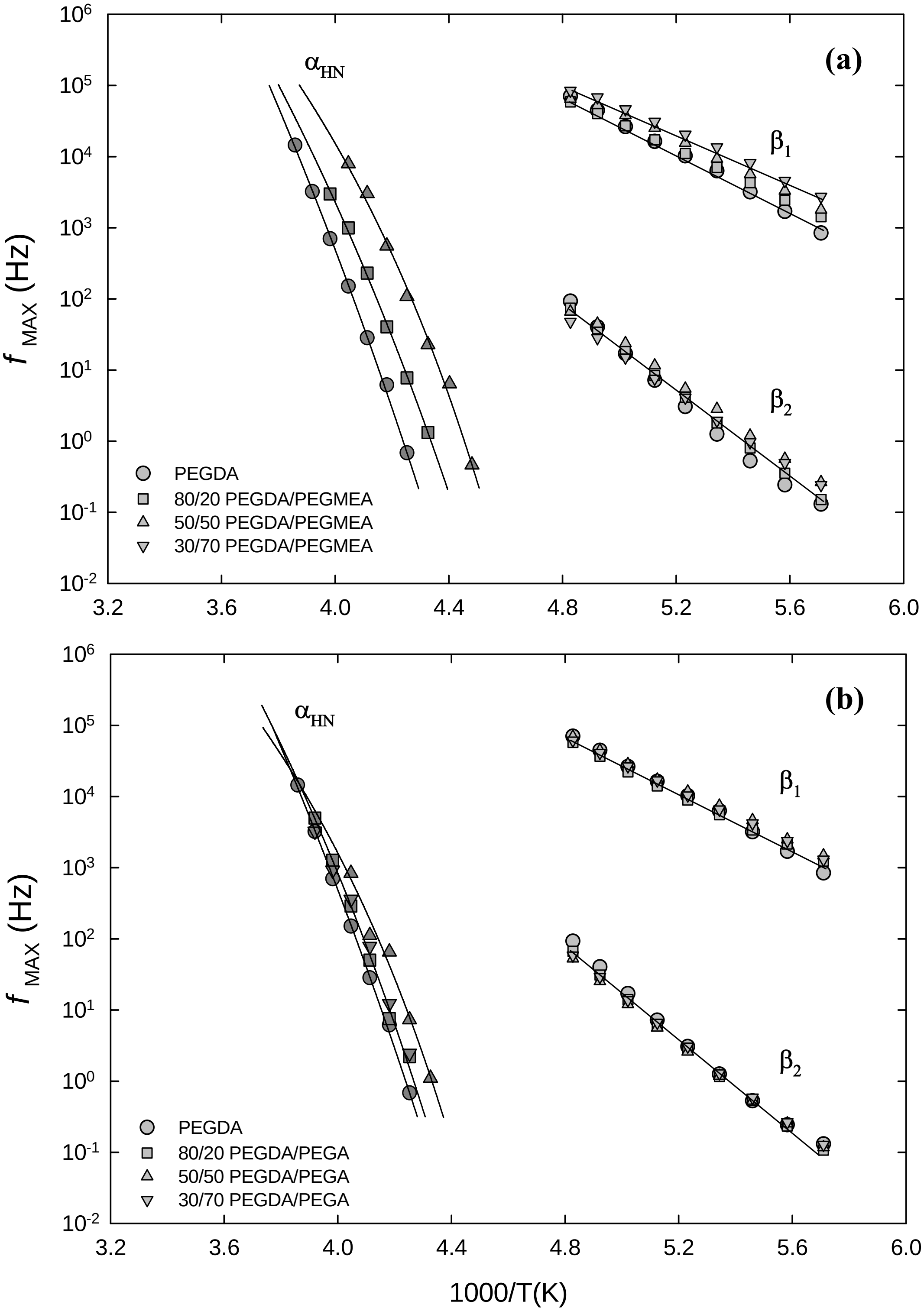

Figure 5.21: Arrhenius plot of f_{MAX} (Hz) vs. 1000/T(K): (a) PEGDA/PEGMEA copolymer networks; (b) PEGDA/PEGA copolymer networks.

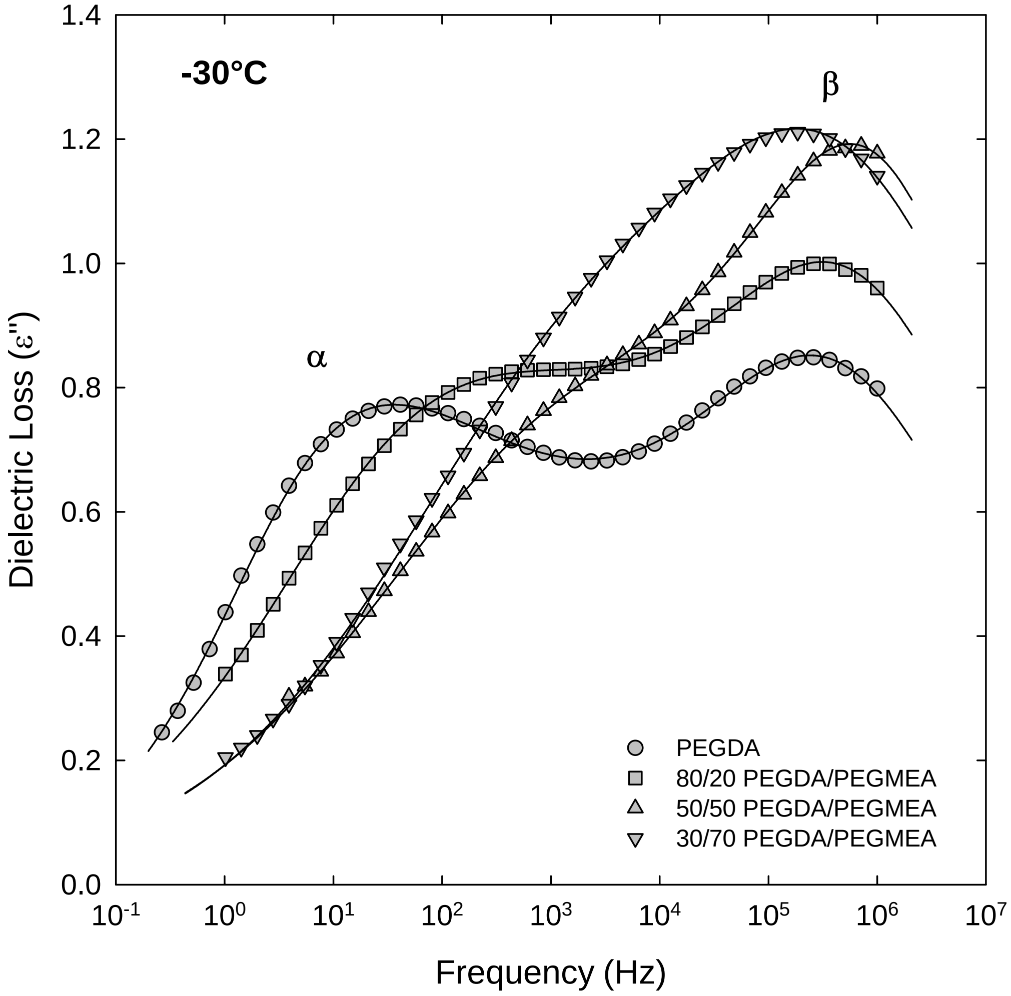

Figure 5.22: Dielectric loss (ε'') vs. frequency for PEGDA/PEGMEA copolymer networks at -30°C. Data are corrected for conduction contribution according to Equation 5.2. Solid curves are dual HN fits.

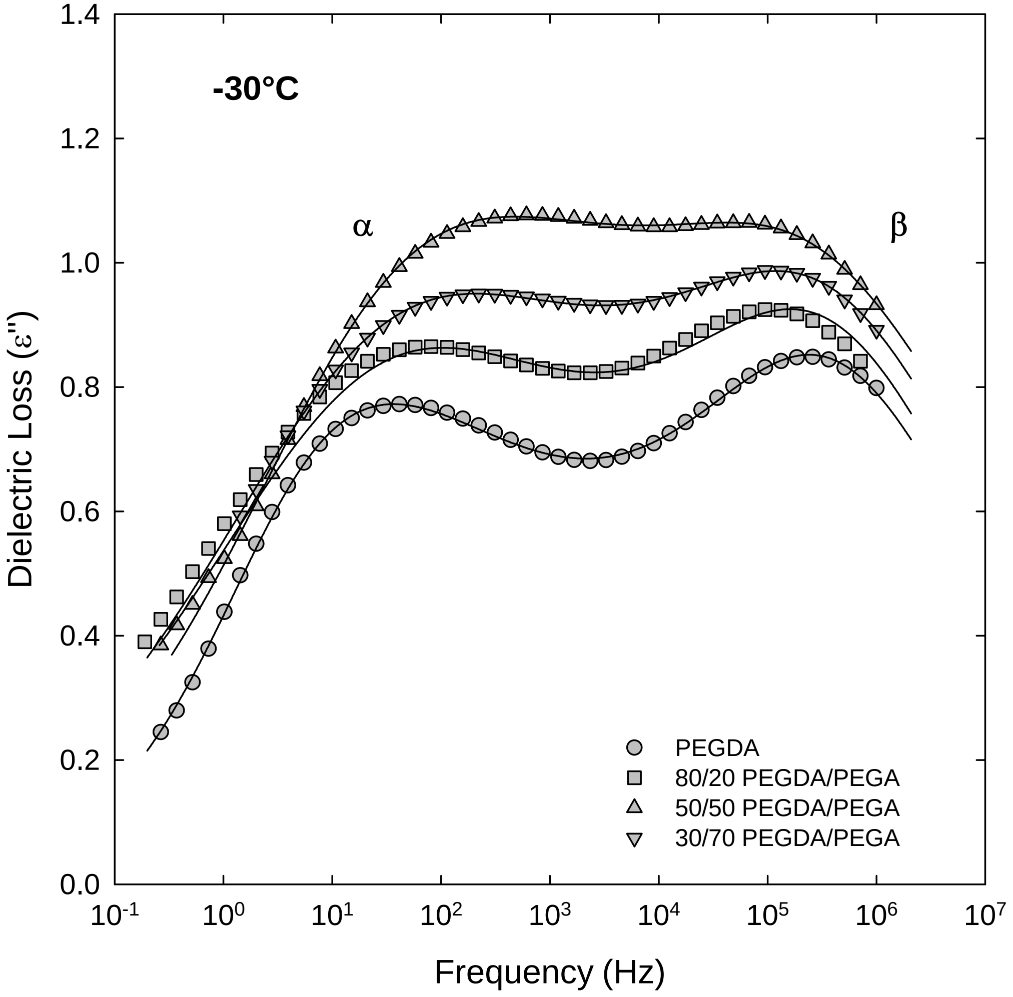

Figure 5.23: Dielectric loss (ε'') vs. frequency for PEGDA/PEGA copolymer networks at -30°C. Data are corrected for conduction contribution according to Equation 5.2. Solid curves are dual HN fits.

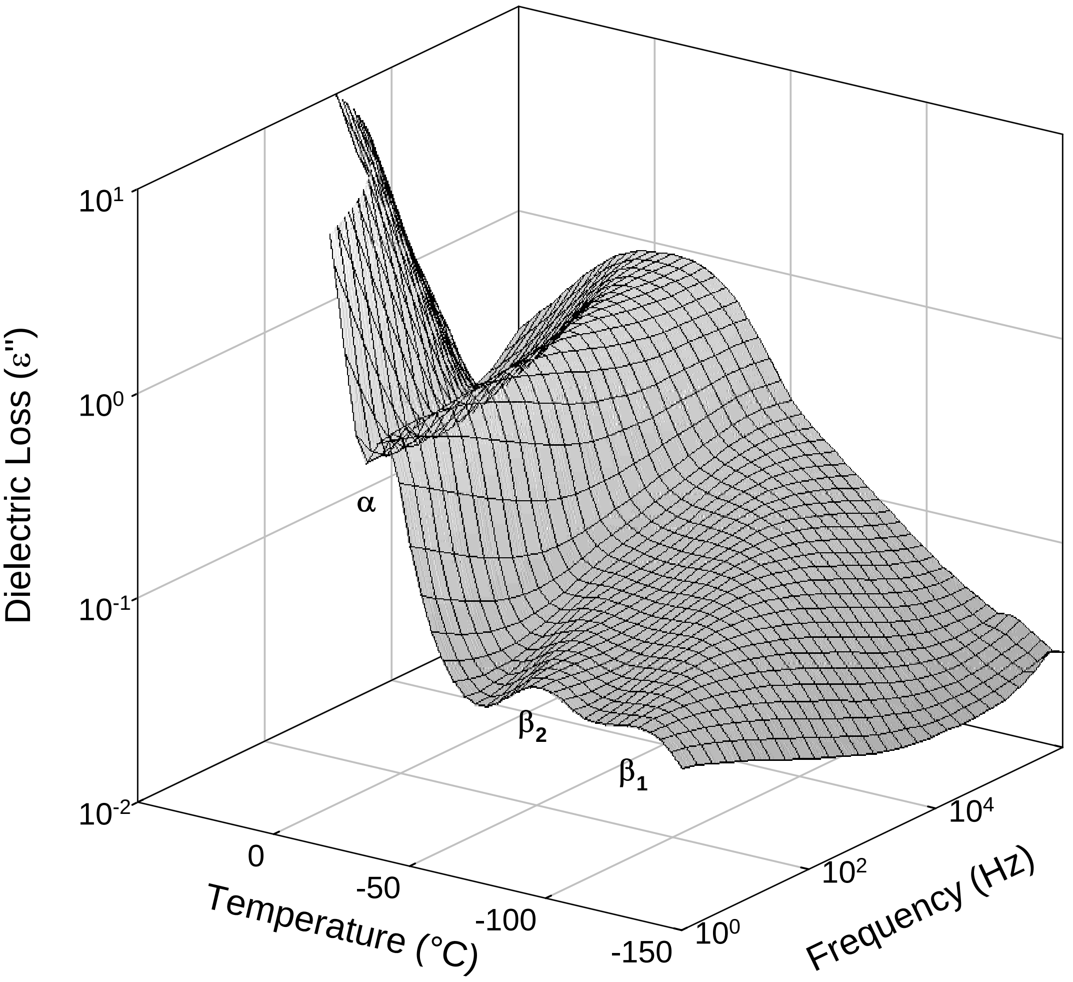

Figure 5.24: Contour plot of dielectric loss (ε'') vs. temperature (°C) vs. frequency (Hz) for 60/40 (wt%) PEGDA/DGEEA copolymer network.

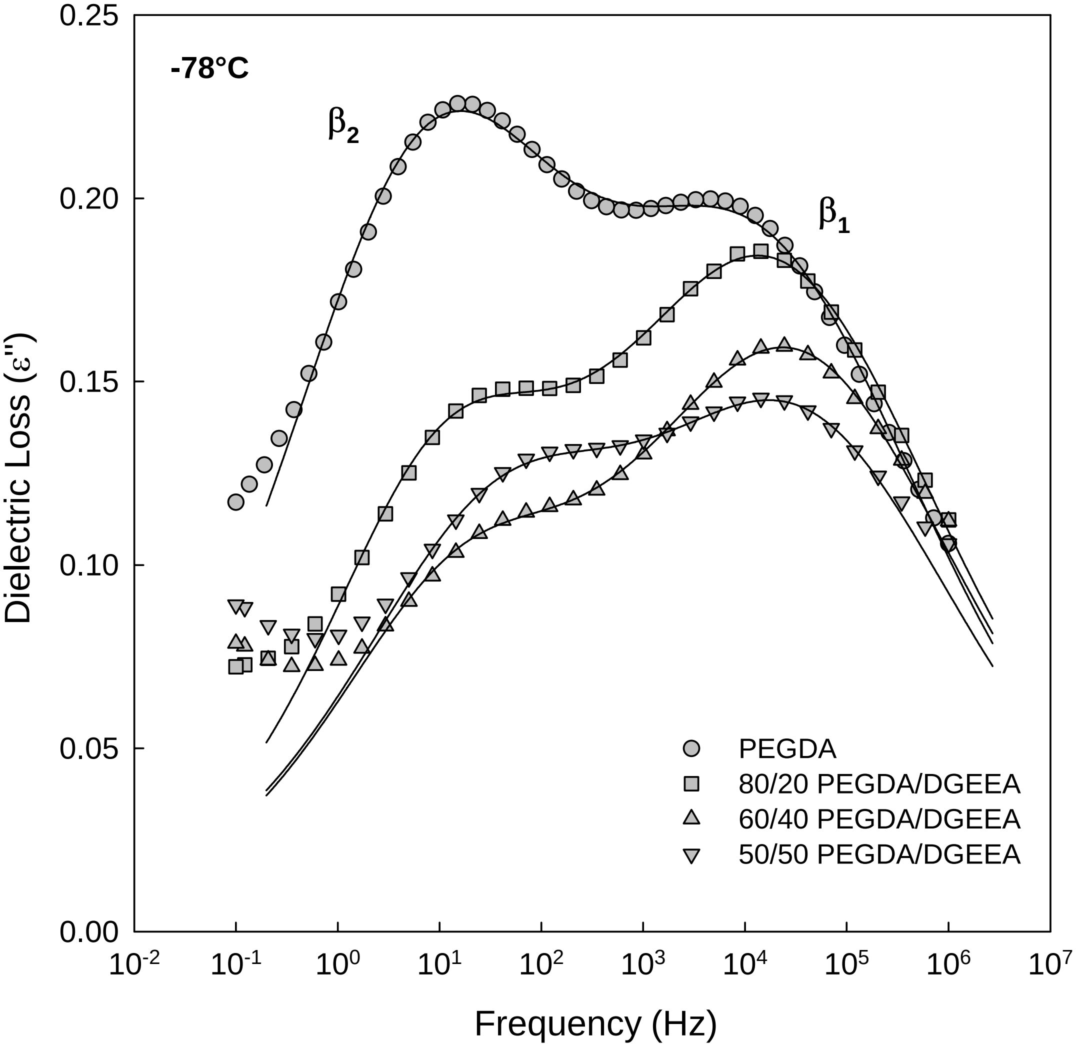

Figure 5.25: Dielectric loss (ε'') vs. frequency for PEGDA/DGEEA copolymer networks at -78°C. Solid curves are dual HN fits.

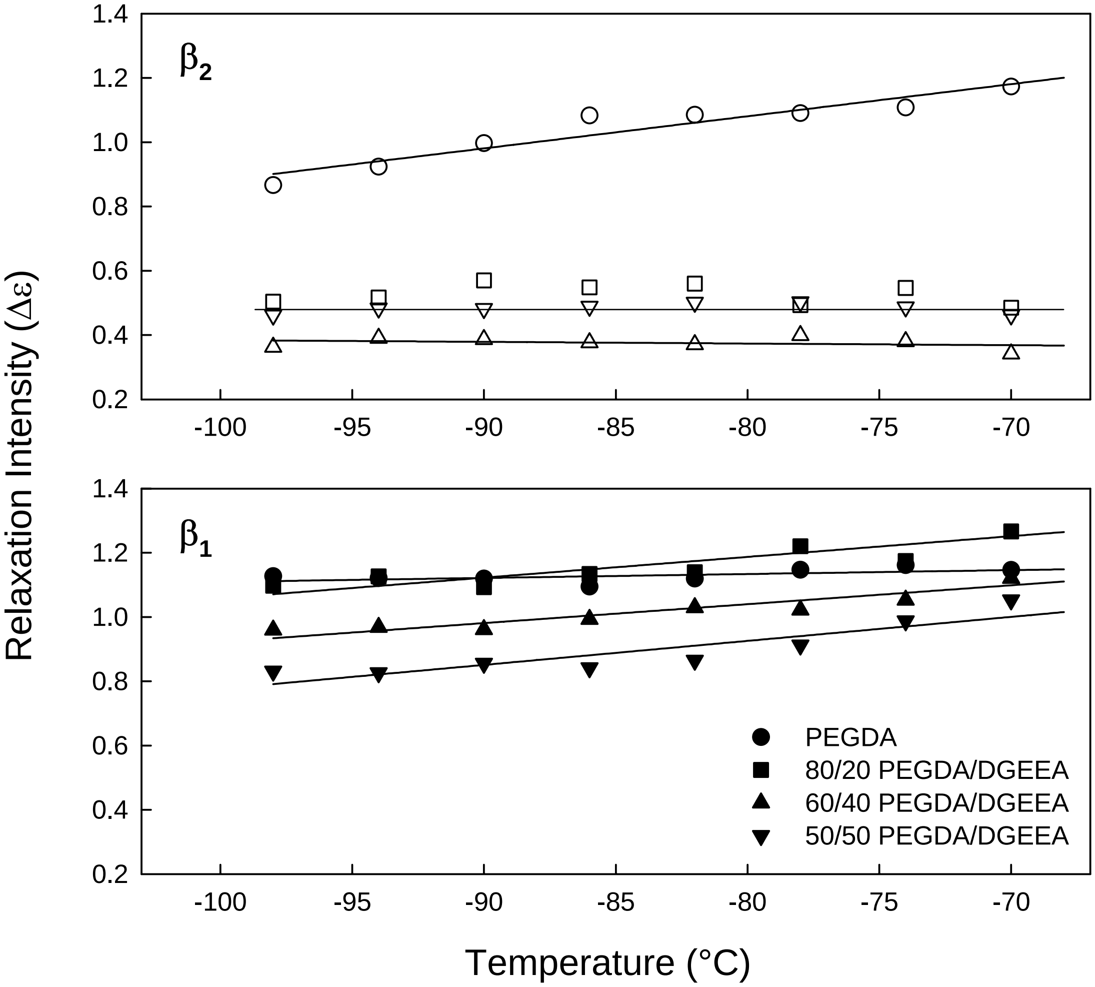

Figure 5.26: Dielectric relaxation intensity (*Δε*; determined from HN fits) vs. temperature for PEGDA/DGEEA copolymer networks. β_1 and β_2 sub-glass transitions.

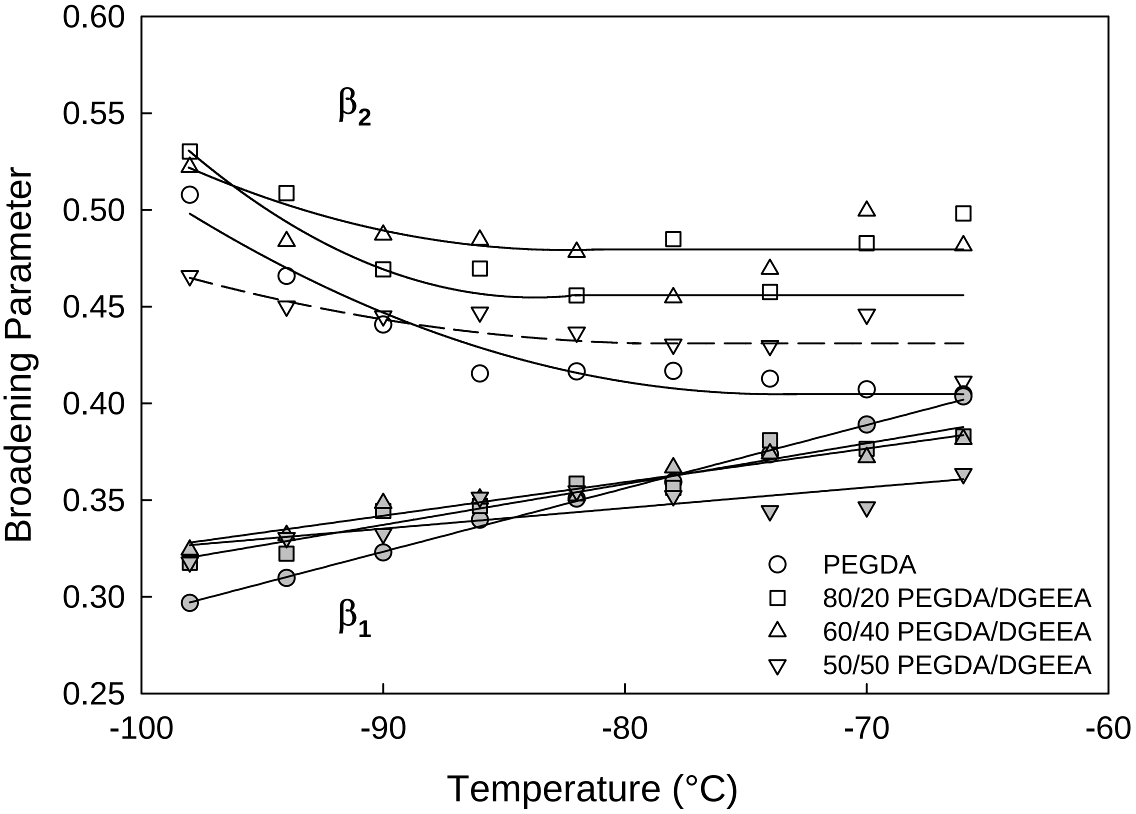

Figure 5.27: Havriliak-Negami [HN] broadening parameter vs. temperature for PEGDA/DGEEA copolymer networks. β_1 and β_2 sub-glass transitions.

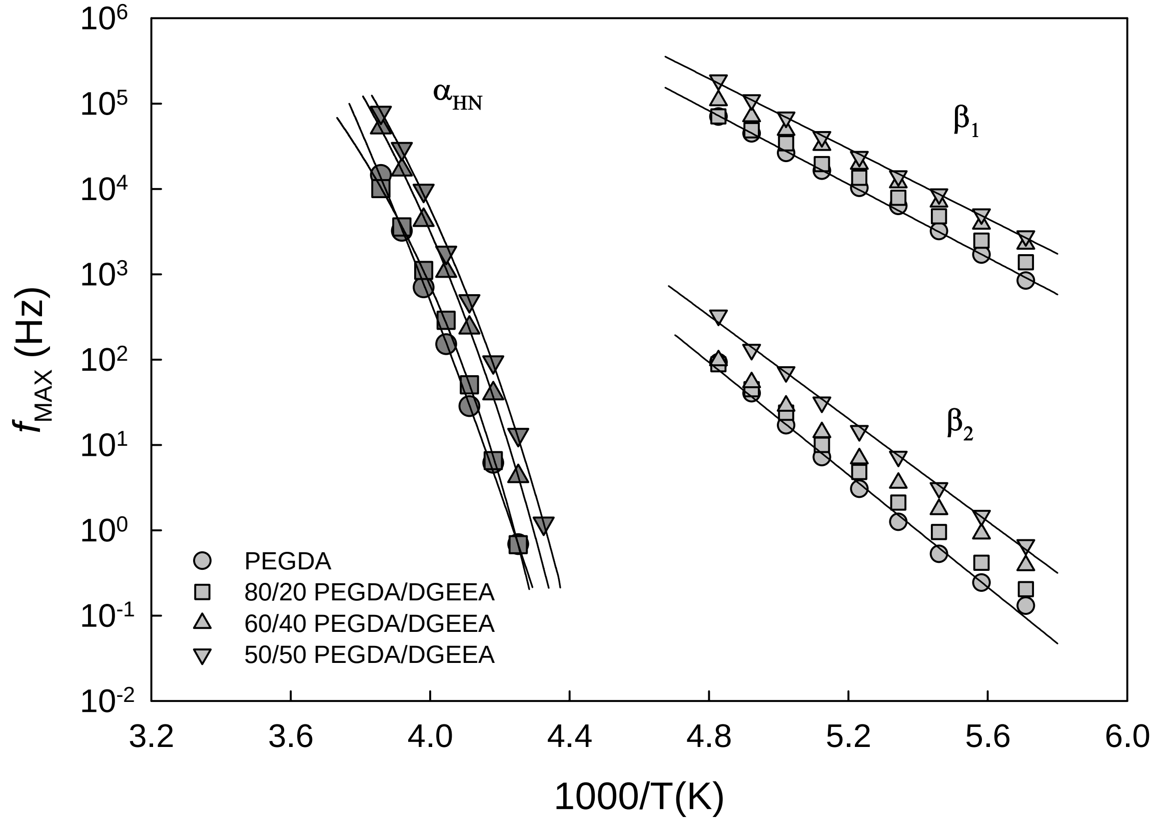

Figure 5.28: Arrhenius plot of f_{MAX} (Hz) vs. 1000/T(K) for PEGDA/DGEEA copolymer networks.

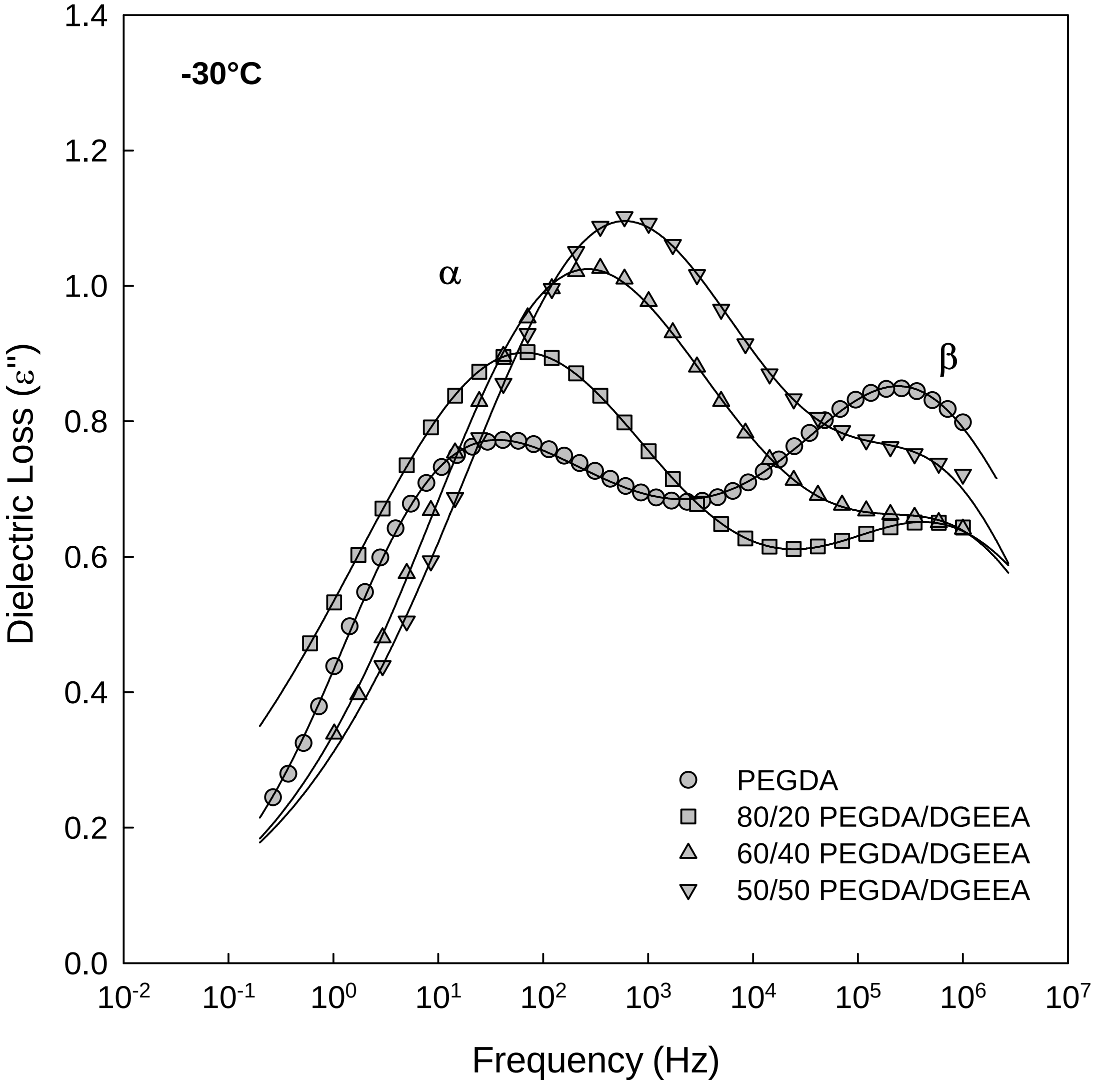

Figure 5.29: Dielectric loss (ε'') vs. frequency for PEGDA/DGEEA copolymer networks at -30°C. Solid curves are dual HN fits.

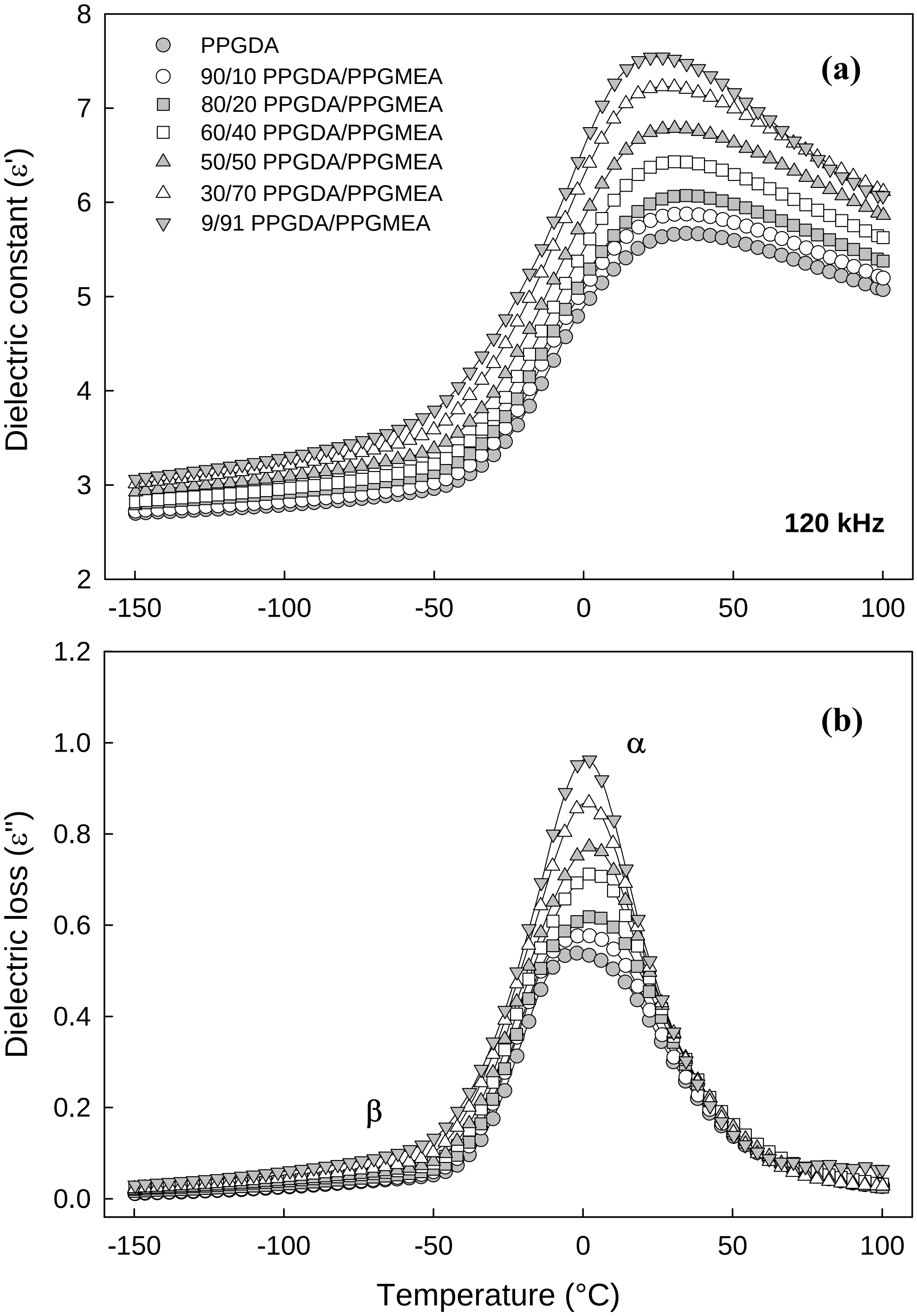

Figure 5.30: Dielectric properties of PPGDA/PPGMEA copolymer networks: (a) dielectric constant (ε'); (b) dielectric loss (ε'') vs. temperature. Frequency of 120 kHz.

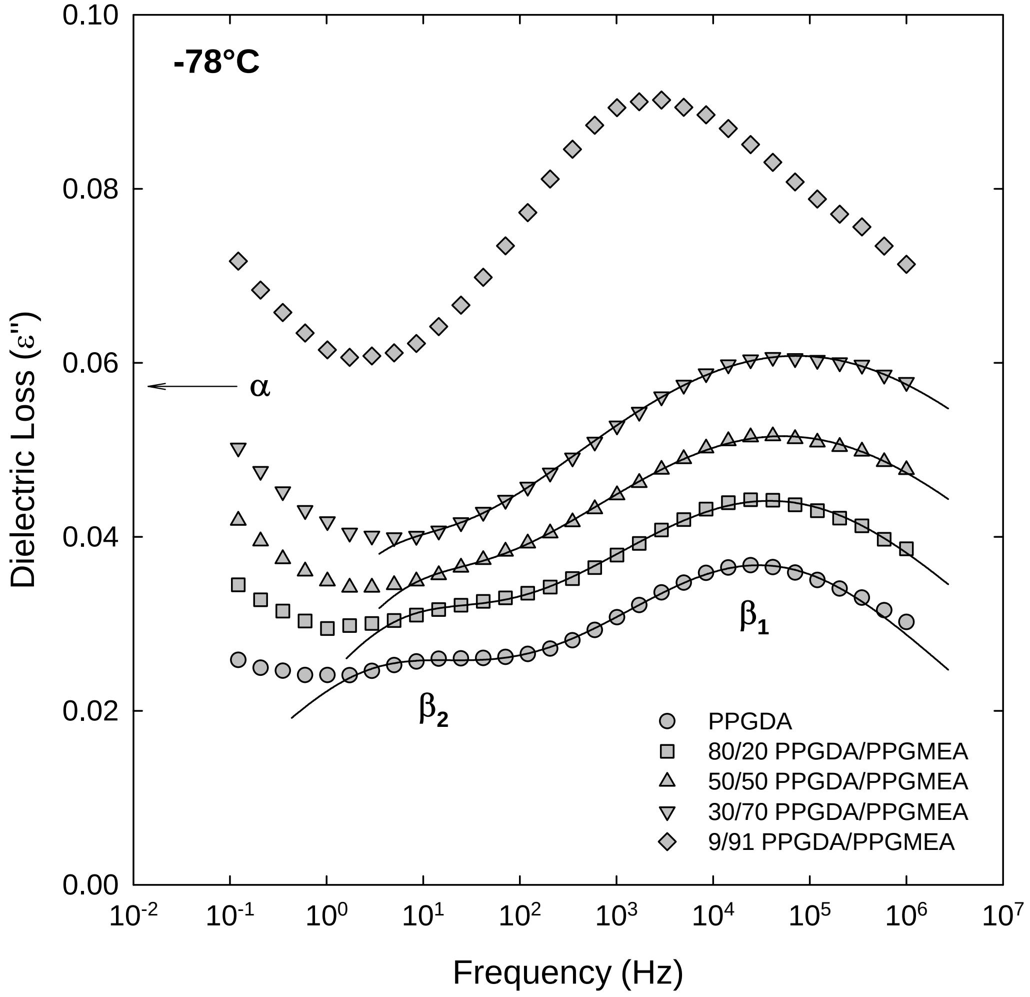

Figure 5.31: Dielectric loss (ε'') vs. frequency for PPGDA/PPGMEA copolymer networks at -78°C. Solid curves are dual HN fits.

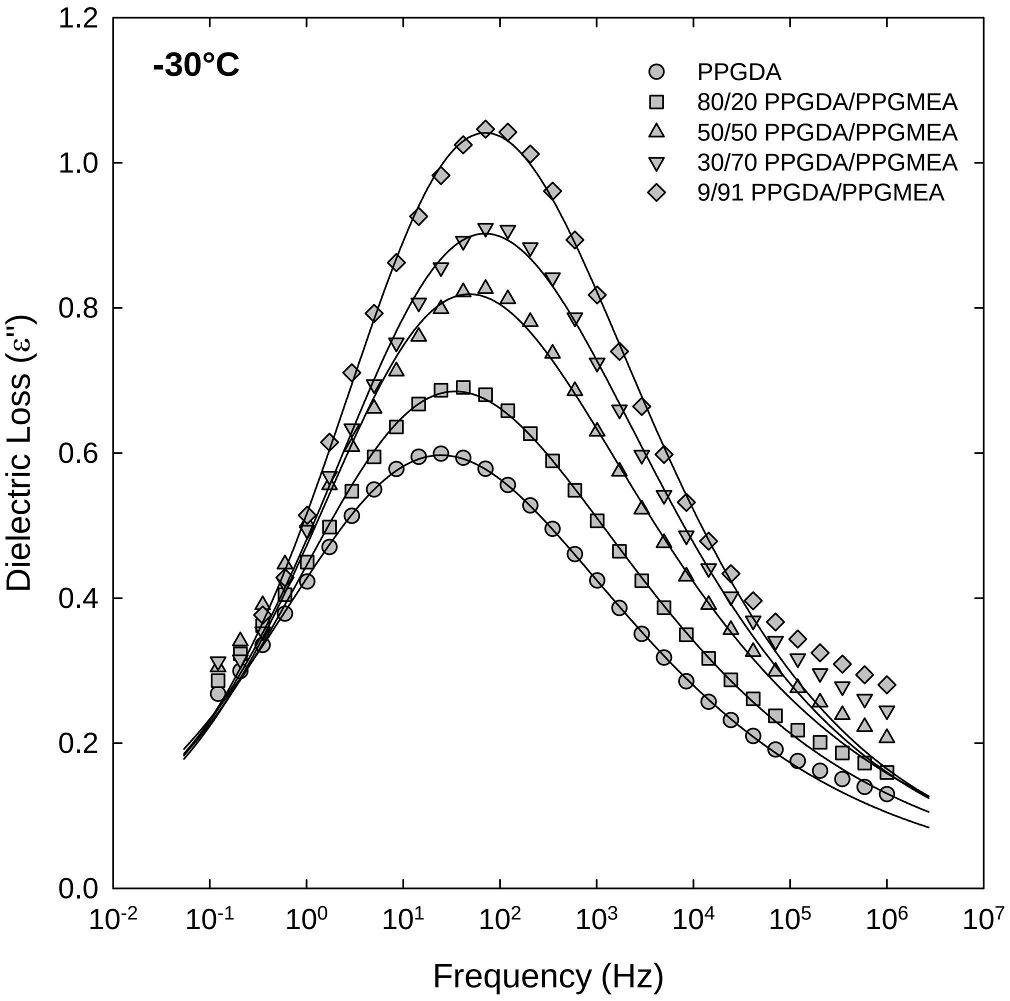

Figure 5.32: Dielectric loss (ε'') vs. frequency for PPGDA/PPGMEA copolymer networks at -30°C. Solid curves are dual HN fits.

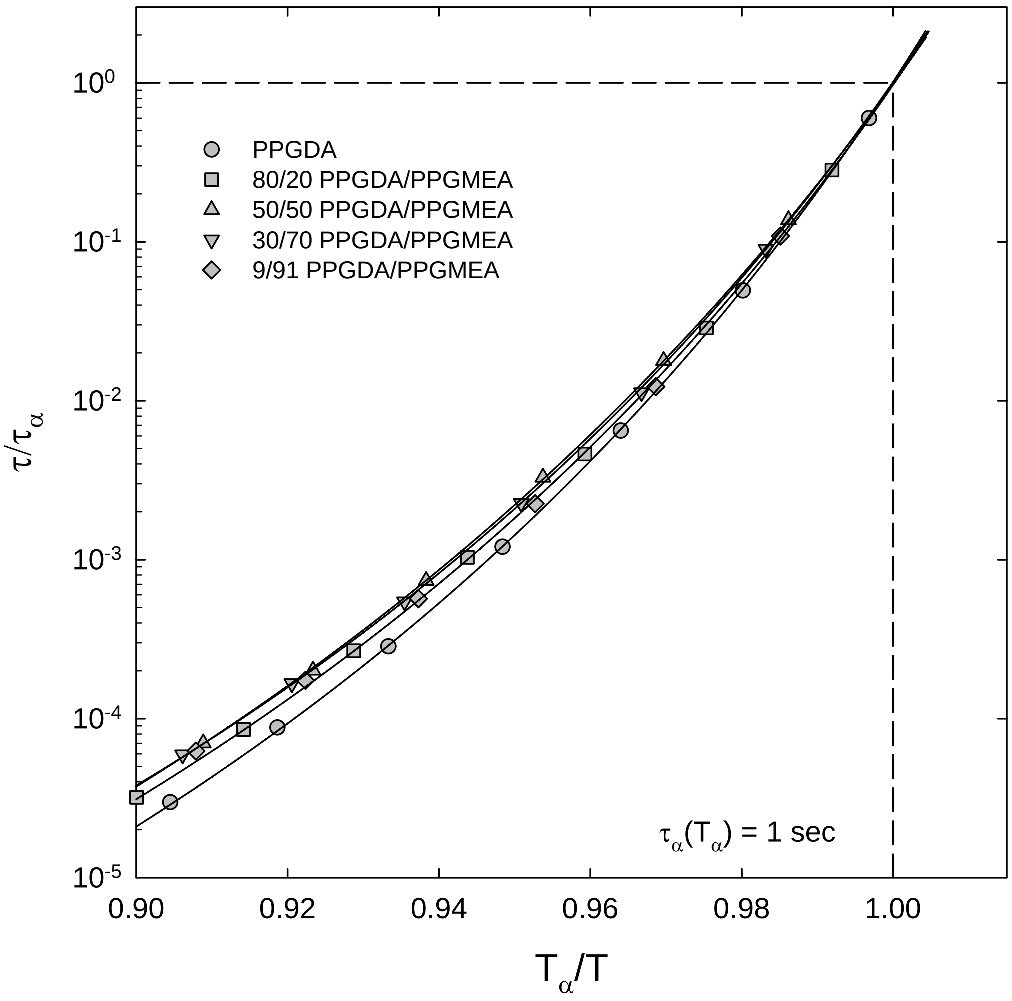

Figure 5.33: Cooperativity plots of τ/τ_α vs. T_α/T for PPGDA/PPGMEA copolymer networks. Solid curves are WLF fits.

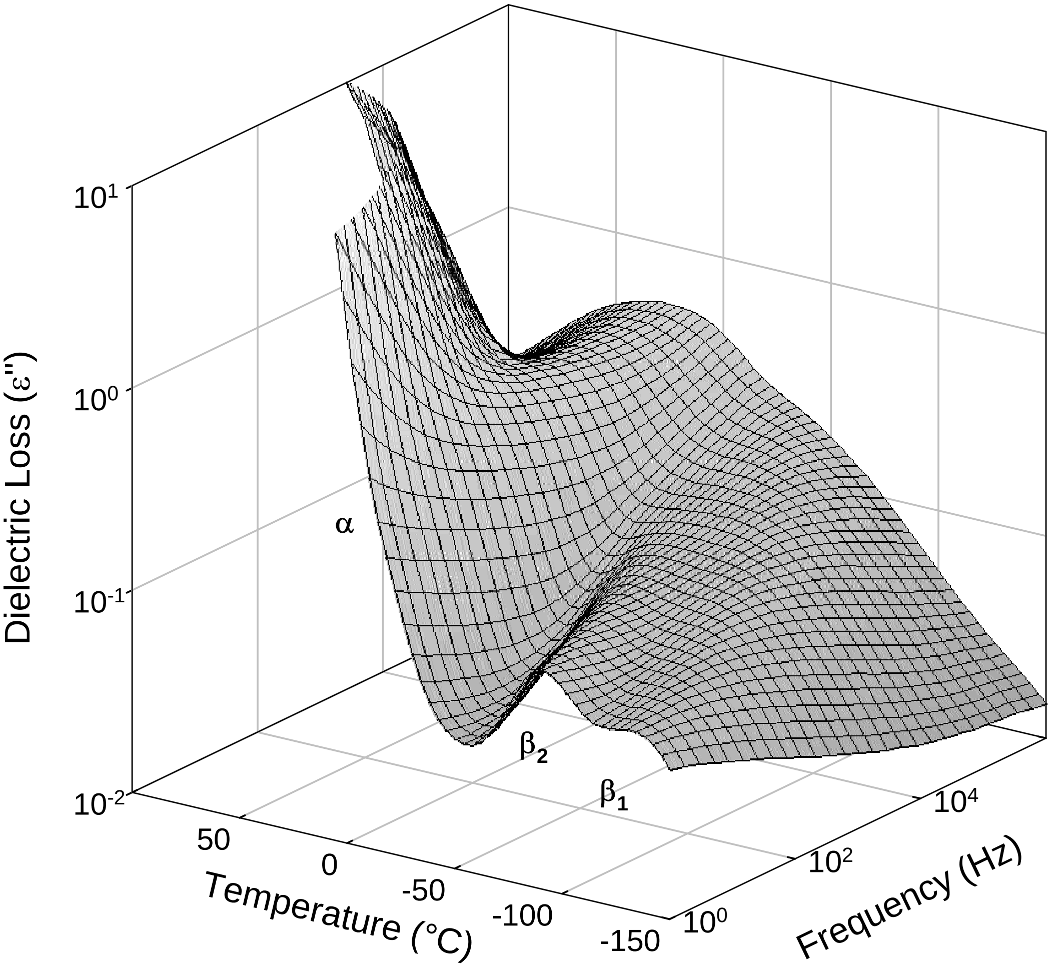

Figure 5.34: Contour plot of dielectric loss (ε'') vs. temperature (°C) vs. frequency (Hz) for XLBPAEDA network.

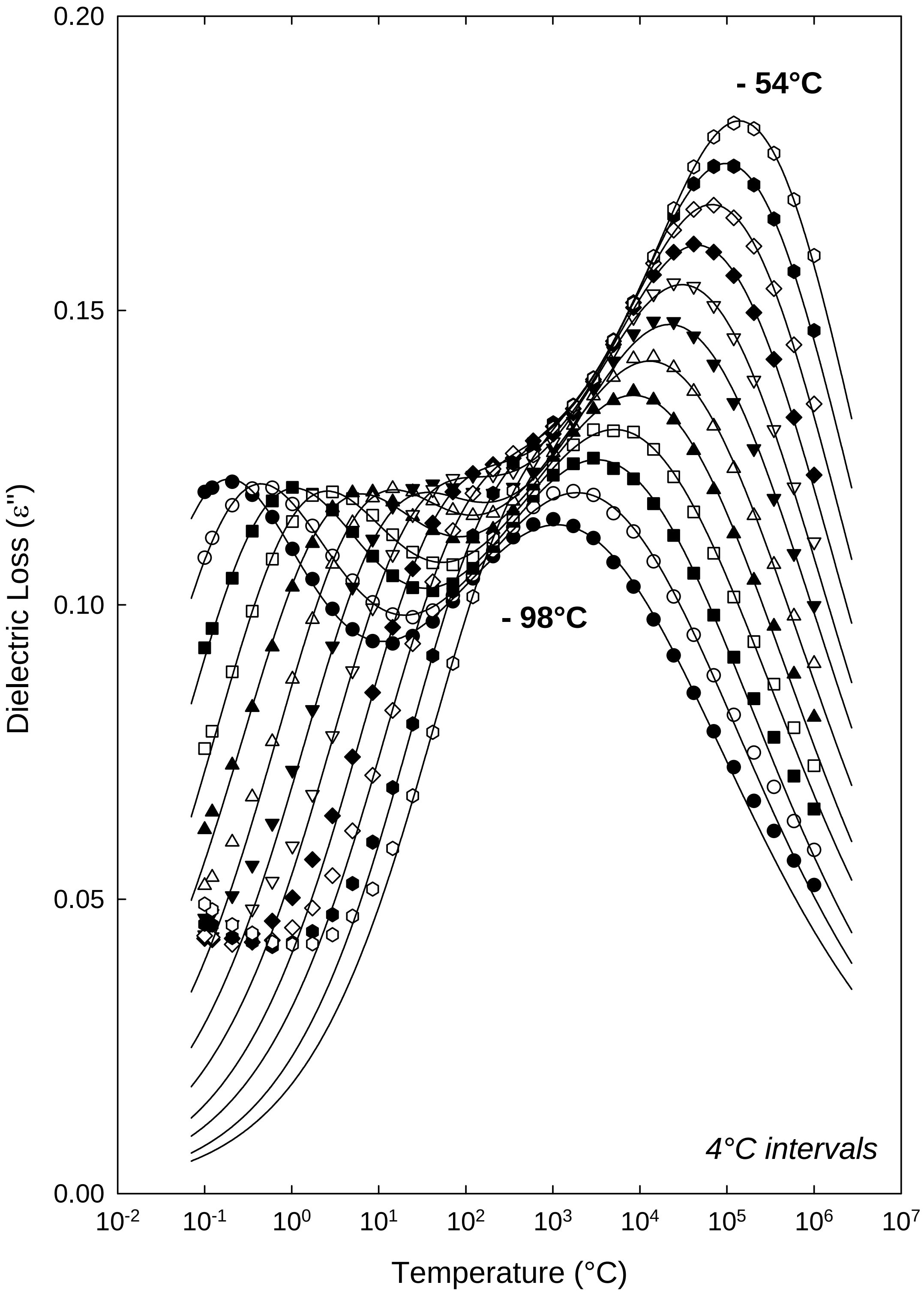

Figure 5.35: Dielectric loss (ε'') vs. frequency (Hz) for XLBPAEDA; temperatures from -98°C to -54°C at 4°C intervals. Solid curves are dual HN fits.

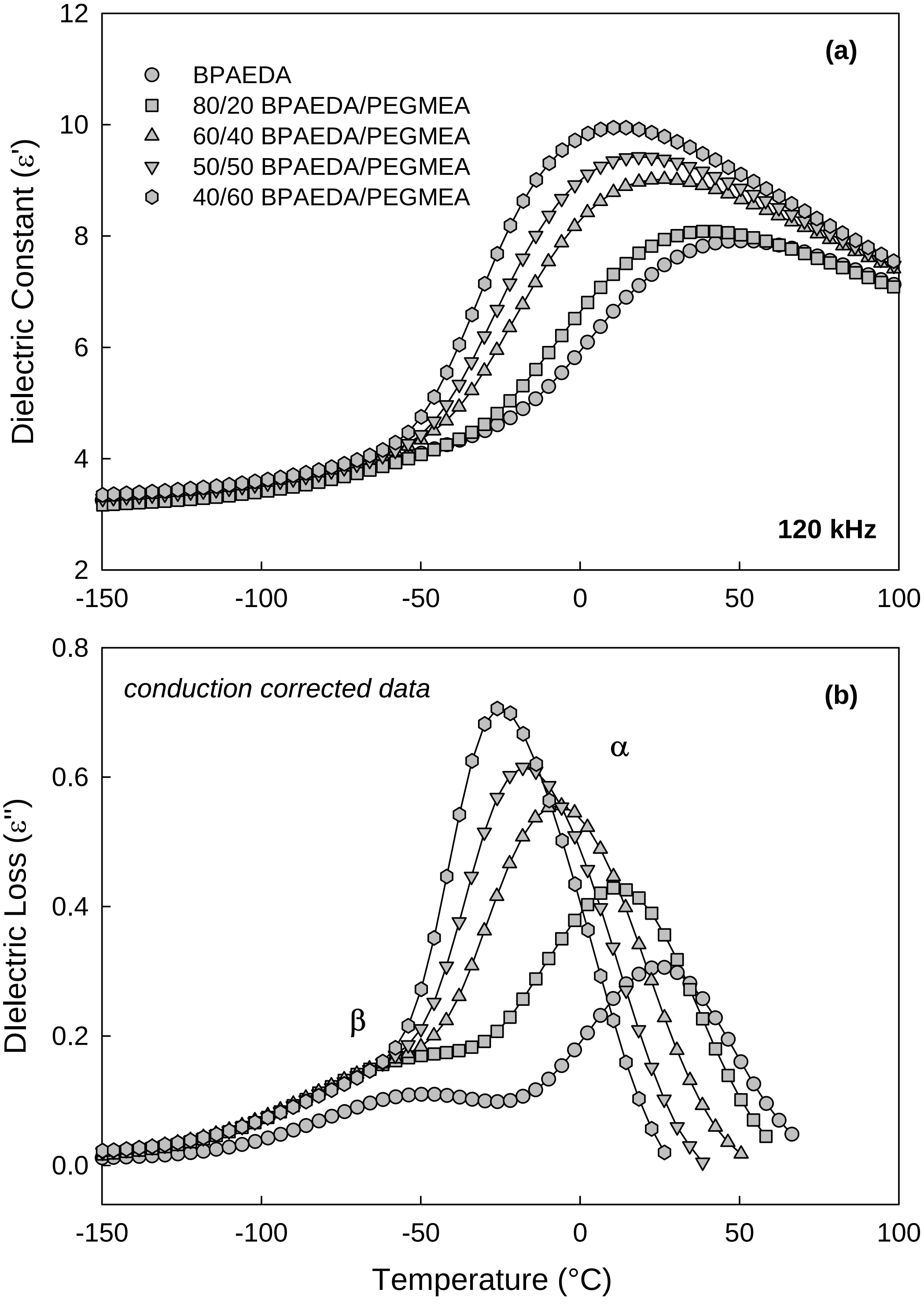

Figure 5.36: Dielectric properties of BPAEDA/PEGMEA copolymer networks: (a) dielectric constant (*ε*′); (b) dielectric loss (*ε*′′) vs. temperature. Frequency of 120 kHz. Dielectric loss data corrected for conduction.

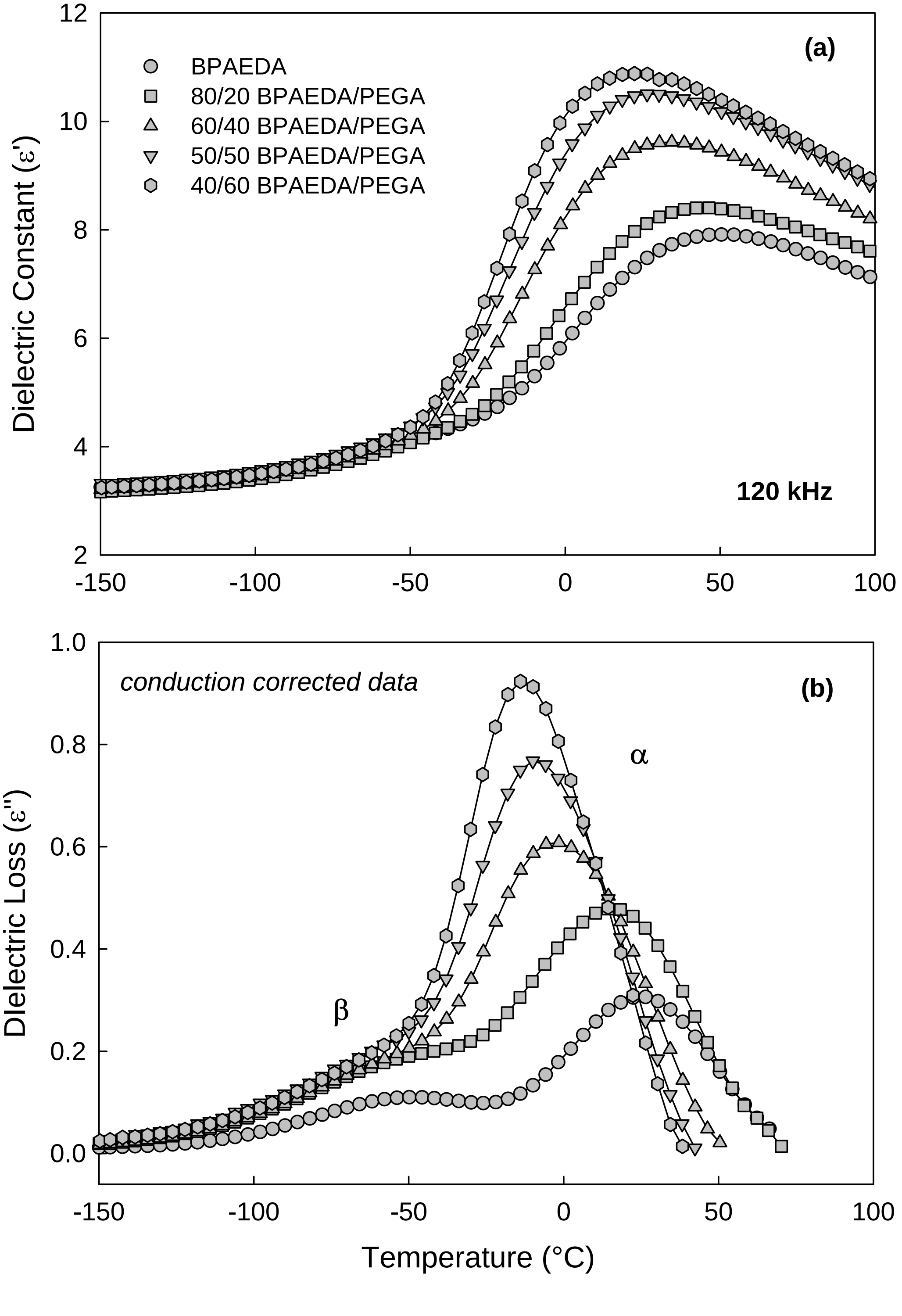

Figure 5.37: Dielectric properties of BPAEDA/PEGA copolymer networks: (a) dielectric constant (ε'); (b) dielectric loss (ε'') vs. temperature. Frequency of 120 kHz. Dielectric loss data corrected for conduction.

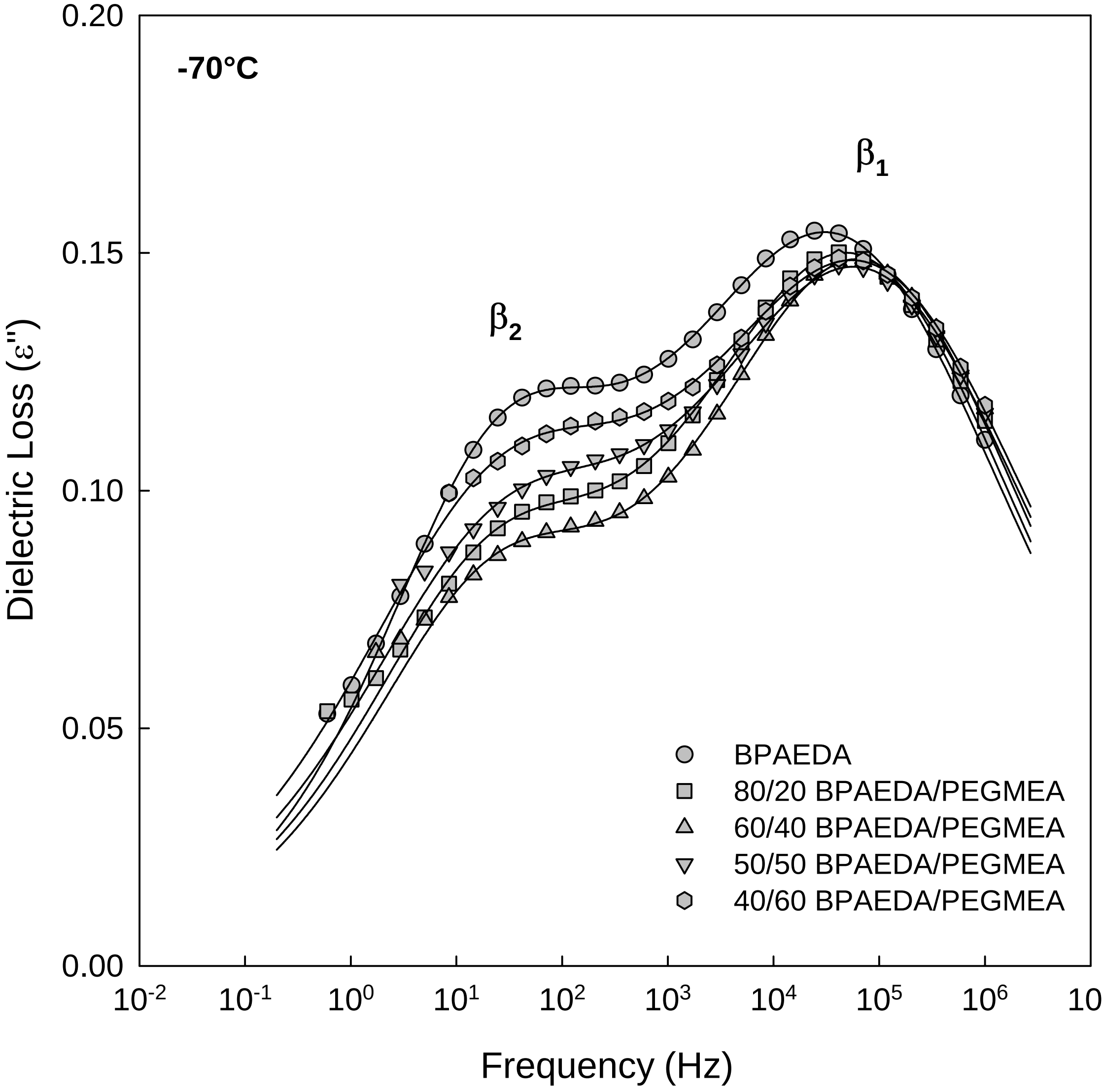

Figure 5.38: Dielectric loss (ε'') vs. frequency for BPAEDA/PEGMEA copolymer networks at -70°C. Solid curves are dual HN fits.

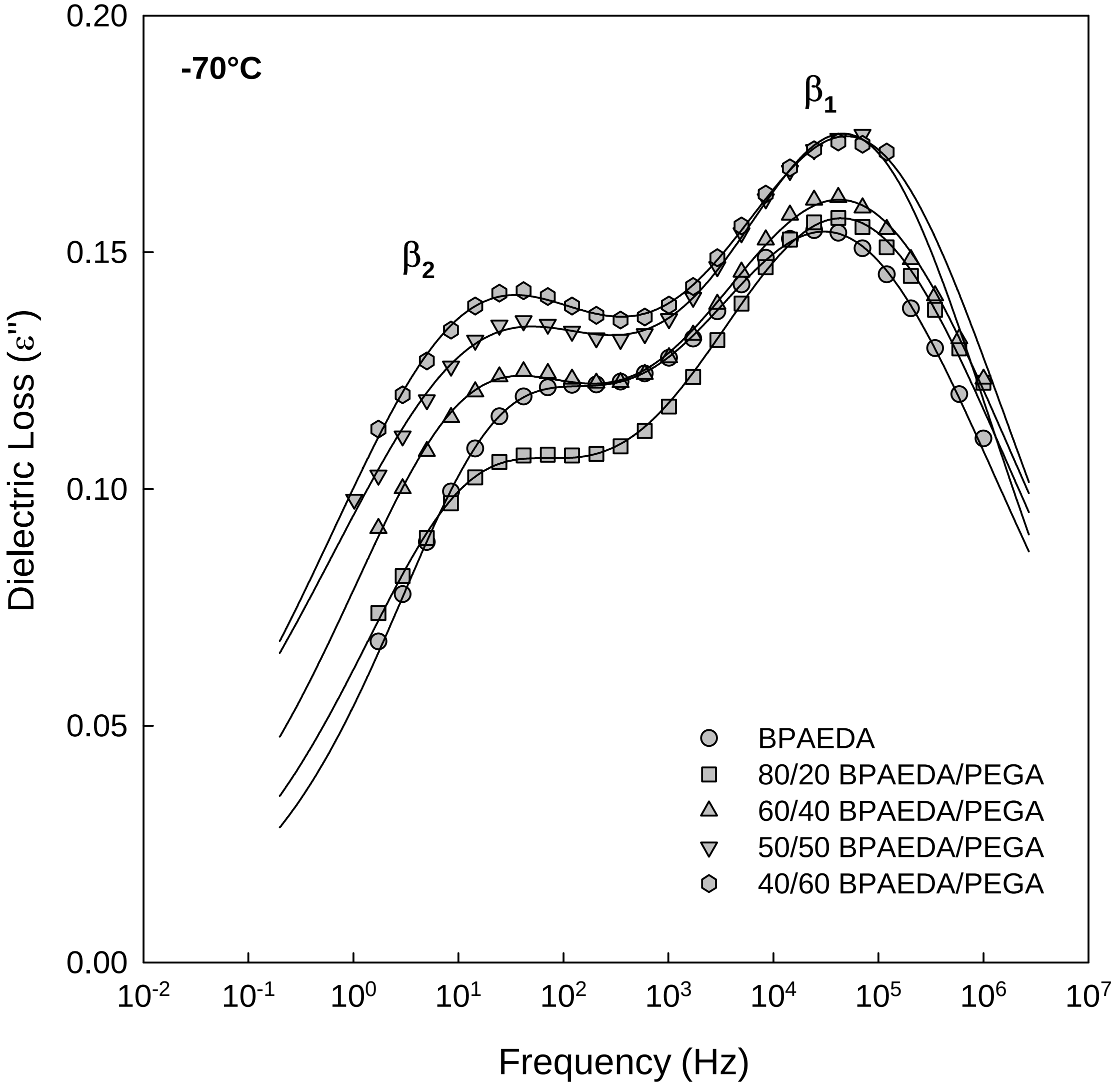

Figure 5.39: Dielectric loss (ε'') vs. frequency for BPAEDA/PEGA copolymer networks at -70°C. Solid curves are dual HN fits.

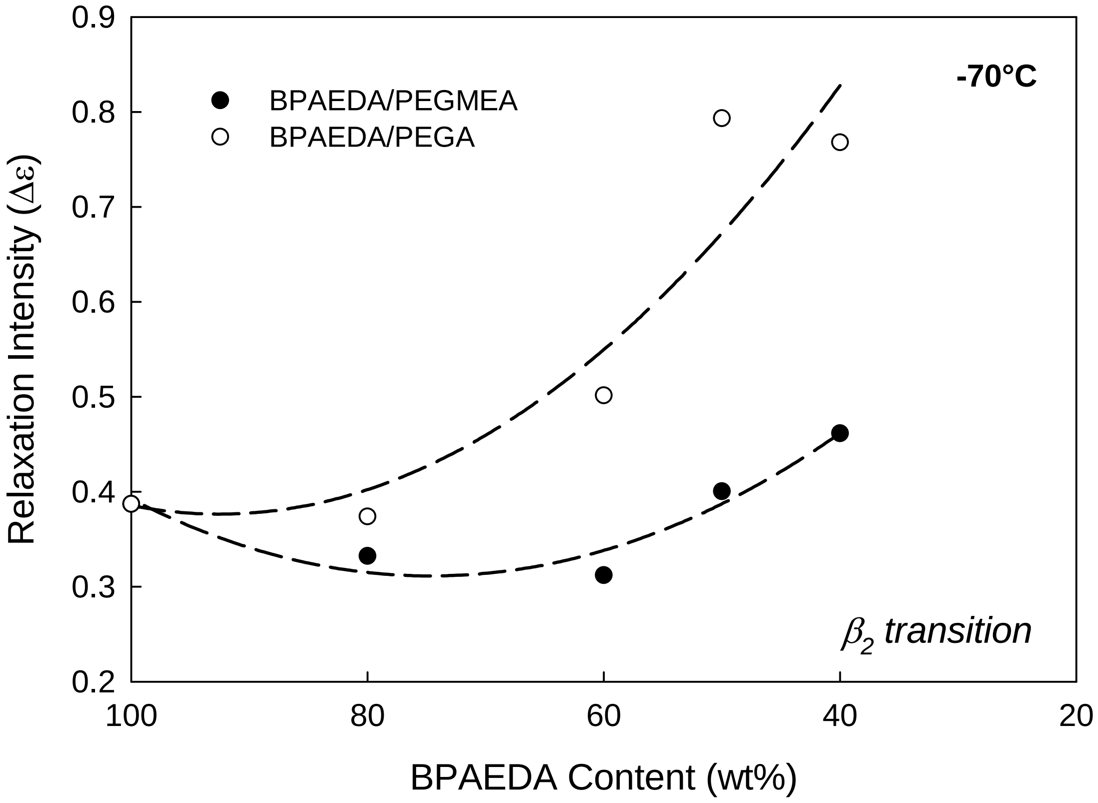

Figure 5.40: Dielectric relaxation intensity ($\Delta\varepsilon$; determined from HN fits) vs. BPAEDA content (wt%) for BPAEDA/PEGMEA and BPAEDA/PEGA copolymer networks. β_2 sub-glass transition at -70°C.

Copyright © Sumod Kalakkunnath 2007

Chapter Six

Thermal Characterization of Poly(trimethylene terephthalate)

This chapter is based on work published as: S. Kalakkunnath and D.S. Kalika, "*Dynamic Mechanical and Dielectric Relaxation Characteristics of poly(trimethylene terephthalate)*", Polymer, **47(20)**, 7085-7094 (2006). Copyright 2006 Elsevier Ltd.

6.1 INTRODUCTION

Poly(trimethylene) terephthalate (PTT), a semicrystalline aromatic polyester, is an emerging member of the terephthalate polyester family prepared by the polycondensation of terephthalic acid (TPA) and 1,3-propane diol (PDO). Until recently, PTT production was not viable at a commercial scale due to the lack of a low cost method to manufacture PDO. Shell Chemical Company overcame this problem in the mid-1990s and launched the first commercial resin, CORTERRA® PTT. DuPont has subsequently introduced a competing PTT resin, SORONA 3GT®, employing a fermentation process to produce PDO from a renewable source, *i.e.*, sugars obtained from corn biomass. The success of these resins has made PTT an attractive alternative to its predecessors, polyethylene terephthalate (PET) and polybutylene terephthalate (PBT), and has stimulated further interest in fundamental characterization of its material properties and their correlation to performance. Current commercial applications of PTT are mainly in the field of textile and fiber products, with increasing use of PTT in structural materials.[156-158]

Previous studies have explored in detail the crystal structure[159-162] of PTT, its thermal properties,[92,163-166] crystallization kinetics[167-175] and thermal stability[176-180]. The thermal and relaxation characteristics exhibited by PTT are those typically observed in semiflexible polymers of low to medium crystallinity and lie intermediate to the properties of PET and PBT.[69,79,81,83,88,132,181-183] PTT encompasses the good dimensional stability and stiffness found in PET along with the excellent processability seen in PBT. The kinked molecular conformation, shown by PTT renders it more elastic and less rigid as compared to PET and PBT (see Figure 2.7). Pyda *et al.*[92] have reported an equilibrium melting temperature of 237°C for PTT with a corresponding 100% crystalline heat of fusion equal to 30 kJ mol^{-1}. Even under aggressive quenching conditions, PTT exhibits a residual weight fraction crystallinity of approximately 14% with a calorimetric glass transition temperature (T_g) of 42°C. Introduction of further crystallinity via thermal annealing leads to a positive offset of nearly 15°C in T_g as compared to the quenched sample which can be attributed to the constrained relaxation environment imposed by the crystals.[92]

The morphology of PTT is similar to PET in that it contains a sizeable rigid amorphous phase fraction (RAP): a portion of the amorphous phase that remains frozen above T_g and relaxes with increasing temperature. The amount of rigid amorphous phase is a function of prior crystallization history, with heat capacity studies indicating RAP fractions as large as 33% in cold crystallized samples.[163] The prominent RAP fraction in PTT, which has been related to a number of macroscopic properties in other semicrystalline thermoplastics (*e.g.*, fracture toughness and barrier performance), may be a reflection of its distinctive three-linkage backbone structure.

The main focus of this work is to elucidate the glass transition characteristics of PTT as a function of processing history via dynamic thermal analysis techniques; *i.e.*, dynamic mechanical analysis and broadband dielectric spectroscopy. Experiments were conducted on samples obtained by direct quenching in liquid N_2, as well as for various isothermally melt crystallized samples prepared with controlled thermal history. Complementary calorimetric and X-ray measurements were performed to ascertain the sample morphology. The influence of crystallinity on the glass-rubber relaxation and the characteristics of the rigid amorphous phase fraction were studied in detail.

6.2 EXPERIMENTAL

PTT resin was obtained in pellet form (CORTERRA^{TM} PTT 200) through the courtesy of Shell Chemical Company, Houston, TX. The as-received pellets were dried at 90°C under vacuum for 24 hours, and then stored over desiccant at room temperature until further use. Compression molding was used to prepare film of 0.25 to 0.5 mm thickness in a Carver melt press with the polymer being held in the melt at 260°C for approximately 5 minutes during molding. Quenched specimens were obtained by transferring the incipient films directly from the melt press to an enclosed bath of liquid nitrogen, and the resulting samples were stored under refrigeration at 4°C to minimize potential aging effects. Isothermally melt crystallized films were prepared by transferring the polymer from the melt press to a second, adjacent press held at the desired crystallization temperature ranging from 160°C to 200°C. An annealing time of one hour was sufficient for full crystallization of the samples, as confirmed by calorimetry. The melt crystallized films were subsequently held under vacuum at room temperature prior to measurement.

A Perkin-Elmer DSC-7 differential scanning calorimeter was used to conduct calorimetric studies on the quenched and isothermally-crystallized films. Transition temperatures and melting enthalpy were calibrated using indium and zinc standards. A sapphire (Al_2O_3) reference was used for the calibration of heat capacity in the vicinity of the glass transition temperature;[109] determination of heat capacity was accomplished according to the method detailed by Wunderlich (see detailed analysis in Section 3.4).[108] All DSC scans were performed at a heating rate of 10°C min^{-1}, with a sample size of 10 mg.

Wide-angle X-ray scattering (WAXS) was employed for the investigation of crystal structure in the quenched and selected melt crystallized films. Samples were examined using a Siemens 5000 diffractometer with Cu K_α radiation (λ = 1.5406Å) at room temperature. Data were recorded across a range of scattering angles (2θ) from 5 to 50° at a scan rate of 2°min^{-1} and a data interval of 0.02°.

Dynamic mechanical analysis (DMA) was performed using a Polymer Laboratories dynamic mechanical thermal analyzer operating in single cantilever bending geometry; the polymer films had a thickness of 0.50 mm. Storage modulus (E') and loss tangent ($tan\delta$) were recorded at a heating rate of 1°C min^{-1} with test frequencies in the range of 0.1 to 10 Hz; all measurements were carried out under inert (N_2) atmosphere.

Dielectric spectroscopy measurements were conducted using the Novocontrol Concept 40 broadband dielectric spectrometer (Hundsangen, Germany). Concentric silver electrodes were vacuum evaporated on the crystallized samples using a VEECO thermal evaporation system. For the quenched PTT films, electrodes were deposited at room temperature using silver paint (SPI Inc., West Chester, PA). Samples were mounted between gold platens and positioned in the Novocontrol Quatro Cryosystem; sample thickness was 0.25 mm in all cases. Dielectric constant (ε') and loss (ε'') were recorded in the frequency domain (0.1 Hz to 1.0 MHz) at discrete temperatures from -150°C to 150°C.

6.3 RESULTS AND DISCUSSION

6.3.1 Calorimetric and X-ray analysis

DSC heating sweeps for the quenched and isothermally melt-crystallized PTT sample films are reported in **Figure 6.1**. The quenched film shows a glass transition centered at 44°C, followed by a sharp cold crystallization exotherm (67°C) and melting at 227°C. In the isothermally melt-crystallized samples, the glass transition is shifted to ~ 54°C, with T_g displaying virtually no dependence on prior crystallization temperature. An expanded view of the DSC curves in the vicinity of the glass transition is shown in **Figure 6.2**.

The DSC heating sweeps for the melt crystallized PTT samples show a characteristic double-melting behavior, with a lower temperature melting peak positioned approximately 10°C above the isothermal annealing temperature, followed by an apparent crystal re-organization process and second melting peak at ~ 227°C. Multiple melting behavior has been reported for a wide range of flexible and semiflexible crystalline polymers and is typically attributed to the existence of distinct crystal lamellar populations, or the onset of crystal melting and ongoing re-crystallization during the DSC heating scan itself. In a detailed analysis presented by Srimoaon *et al.*,[166] multiple melting phenomena in PTT were attributed primarily to simultaneous melting and re-crystallization over the course of the DSC scan. This conclusion is consistent with the form of the curves shown in Figure 6.1, wherein the position of the higher-temperature melting peak (T_m = 227°C) is independent of prior isothermal crystallization temperature and reflects the conditions of re-organization during the DSC heating sweep.

In addition to the "double-melting" peaks described above, a small endothermic melting feature is evident in the DSC scans at 100°C for all of the semicrystalline specimens. This peak, with a corresponding enthalpy of ~ 0.2 kJ mol^{-1}, appears to reflect a small amount of additional crystallization that occurs in the samples when they are removed from the melt press and allowed to cool to room temperature after isothermal annealing.

Isothermal crystallization studies were performed to assess the kinetics of PTT crystallization for various melt crystallization conditions. PTT films (~10 mg) were melted in crimped DSC pans at 260°C for 10 min to remove any prior thermal history. The samples were then quenched in the DSC at approximately 80°C/min to the desired crystallization temperature. The samples were held at the corresponding temperature for 1 hr, and the results recorded as heat flow versus time as shown in **Figure 6.3**. The polymer exhibited a rapid crystallization behavior, with the sample held at the highest crystallization temperature (T_c = 200°C) achieving full crystallization in ~ 20 mins. Thus, the selected annealing time of 1h was found to be sufficient to ensure complete crystallization for all samples tested.

The enthalpy associated with each calorimetric event was determined in order to establish the net heat of fusion (ΔH_F). Pyda *et al.*[92] have reported a ΔH_F value of 30 kJ/mol for 100% crystalline PTT at 510 K. This value can be corrected to the apparent melting temperature of the semicrystalline samples using the following equations:[184]

$$\Delta H_F(T_1) = \Delta H_F(T_2) - \int_{T_1}^{T_2} \Delta C_p dT \qquad [6.1]$$

$$\Delta C_p = C_p^L - C_p^S \qquad [6.2]$$

where C_p^L is the heat capacity of PTT in the completely liquid phase (above T_m), and C_p^S is the corresponding heat capacity in the solid phase (below T_g). From the data provided by Pyda,[92] the following expressions apply for C_p (J/mol K):

$$C_p^L = 211.6 + 0.434T(K) \qquad [6.3]$$

$$C_p^S = 28.9 + 0.679T(K) \qquad [6.4]$$

The corresponding weight fraction crystallinity present in the individual PTT samples was then calculated using the equation:

$$W_C = \frac{\Delta H_F(sample, T_m)}{\Delta H_F^{100\%}(T_m)} \qquad [6.5]$$

For the liquid nitrogen quenched film, comparison of the crystallization and melting peaks in the DSC sweep indicates the presence of 13 wt% residual crystallinity in the original sample, which is very close to the value reported by Pyda.[92] This appears to be the minimum level of crystallinity captured in this commercial PTT resin, even under aggressive quenching conditions. Complementary studies involving the melting and direct liquid nitrogen quenching of PTT samples held in sealed aluminum DSC pans showed similar levels of residual crystallinity. For the isothermally melt-crystallized films, the weight fraction crystallinity across the various samples was $W_C = 0.30 \pm 0.02$, with no systematic variation in crystallinity evident as a function of prior crystallization temperature.

The presence of crystallinity in semiflexible polymers typically leads to a positive offset in T_g owing to the constraining influence of the crystals on the large scale segmental motions inherent to the glass-rubber transition. This behavior has been observed in a number of polymers for which wholly amorphous specimens can be obtained by rapid quenching to the glassy state; *e.g.,* PET, [69,185] poly (phenylene sulfide) [PPS],[88,183] and poly (ether ether ketone) [PEEK].[79,81,182] The measured offset in the glass transition temperature is usually in the range of 10 to 15°C. A similar result is observed for the quenched and melt crystallized PTT samples examined here ($\Delta T = +\ 10°C$), even though the quenched PTT resin could not be captured in the 100% amorphous state. In addition to its influence on T_g, the presence of crystallinity often results in a disproportionate decrease in the intensity of the glass transition, as measured by the step change in heat capacity, $\Delta C_p(T_g)$. The disproportionate decrease in ΔC_p for crystalline samples as compared to a wholly amorphous specimen can be quantified using a three-phase morphological model that includes a separate rigid amorphous phase fraction, *i.e.,* a portion of the non-crystalline material that remains "rigid" at the glass transition and thus does not contribute to the observed increase in heat capacity observed at T_g. The mobile amorphous phase fraction (W_{MA}) is defined as:

$$W_{MA} = \frac{\Delta C_p^{sc}(T_g)}{\Delta C_p^{A}(T_g)} \qquad [6.6]$$

where ΔC_p^{SC} corresponds to the measured heat capacity increment for the semicrystalline sample (calculation procedure in Section 3.4.3), and ΔC_p^{A} corresponds to the heat capacity increment for the wholly amorphous material evaluated at T_g using equations 6.2-6.4. It then follows that the rigid amorphous phase fraction can be determined by difference:

$$W_{RAP} = 1 - W_{MA} - W_C \qquad [6.7]$$

In **Figure 6.4**, $\Delta C_p(T_g)$ for the various crystallized PTT samples is plotted versus the value of the net heat of fusion (ΔH_F) following the approach presented in reference 92. The dashed line reflects the limit for a strictly two phase model, where the intensity of the glass transition is directly proportional to the amount of non-crystalline phase present in the sample; the limiting values for ΔC_p and ΔH_F are the result of extrapolations reported by Pyda and co-workers.[92] Data points that fall below the dashed line correspond to samples wherein the intensity of the glass transition is less than what would be anticipated according to a strictly two phase response, and thus can be interpreted using a three phase model that includes a separate rigid amorphous phase fraction. For the thermally crystallized samples investigated here, the data are clustered well below the two-phase limit, suggesting the existence of a sizeable amount of RAP material, with W_{RAP} in the range of 0.30 to 0.40. There does not appear to be any clear correlation between RAP fraction and crystallization temperature for this particular group of samples. The corresponding RAP values are comparable to W_{RAP} fractions for PTT reported by Hong *et.al.*,[165] where phase fraction determinations were based on both DSC and small angle X-ray studies.

The crystallinity characteristics of the PTT films were also examined by wide angle X-ray scattering (WAXS) measurements. **Figure 6.5** shows diffraction patterns for the quenched film, and a representative melt crystallized film prepared at T_c = 180°C. The diffraction pattern for the quenched film is essentially featureless, suggesting that the minimal crystallinity (W_C = 0.13) present in the quenched specimen cannot be differentiated from the amorphous halo. Thus, WAXS does not provide any additional information regarding the amount or character of the residual crystallinity present in the quenched film. The melt crystallized specimen, however, shows a distinct diffraction pattern that closely matches WAXS results reported in the literature:[161,162] the Miller indices included in Figure 6.5 correspond to a triclinic unit cell, with dimensions as reported in ref. 162.

6.3.2 Dynamic Mechanical Analysis

Dynamic mechanical heating scans were performed on quenched PTT films and isothermally melt crystallized specimens. Results for a quenched film are shown in **Figure 6.6**. The sample displays two distinct mechanical relaxation processes: a sub-glass process (designated as the β relaxation), centered at -70°C (1 Hz; see inset in Figure

6.6), followed by the glass transition (α relaxation), with an onset temperature of approximately 50°C. The glass-rubber relaxation results in a dramatic decrease in the storage modulus (E') of the quenched sample accompanied by a sharp peak in $tan\delta$ (loss factor) which is typical for an amorphous polymer. The onset of cold crystallization during the dynamic mechanical heating sweep leads to a recovery in the modulus, followed by additional (broader) relaxation of the semicrystalline specimen above 80°C (refer to Figure 6.6).

The origin of sub-glass relaxations in poly(*n*-methylene terephathalates) has been the subject of considerable interest. Early dynamic mechanical measurements across a series of such polyesters with $n = 2$ (PET) up to $n = 10$ indicated a complex character for the observed β relaxation, which appeared to encompass at least two superimposed loss processes.[186] More recent studies on the secondary relaxation behavior of PTT have similarly indicated overlapping mechanical relaxations across the sub-glass range.[187,188] Maxwell and co-workers performed ^{13}C and deuterium NMR studies,[189] as well as dynamic mechanical and dielectric measurements,[190] in order to elucidate the underlying sub-glass molecular motions in amorphous PET. A comparison of their dielectric and dynamic mechanical data indicated that the dielectric (β) peak was the result of a single relaxation process, while the dynamic mechanical peak encompassed two apparent motional processes. The dielectric relaxation, which corresponds to the low-temperature side of the dynamic mechanical peak, was assigned to localized motion of the carbonyl groups. The high-temperature side of the dynamic mechanical peak was the result of (dielectrically inactive) phenyl ring motions, as corroborated by NMR. Similar behavior is observed for our PTT specimens: a direct comparison of the dynamic mechanical and dielectric results for quenched PTT is provided in the section on dielectric spectroscopy, below.

Dynamic mechanical data for a representative melt crystallized PTT specimen (T_c = 160°C) are presented in **Figure 6.7**. In the crystallized PTT sample, the glass-rubber (α) relaxation is much broader than that observed in the quenched film, and reflects the heterogeneous character of the relaxation environment in the semicrystalline material.

Time-temperature superposition[38] was used to construct a modulus-frequency master curve for crystalline PTT in the vicinity of the glass transition: a reference temperature of 80°C was selected, which corresponds to the position of the dynamic mechanical tanδ peak at a frequency of 1 Hz. The result for the T_c = 160°C sample is shown in **Figure 6.8**, where the data are plotted as storage modulus versus ωa_T, where ω is the applied test frequency ($\omega = 2\pi f$, with f expressed in Hz) and a_T is the dimensionless shift factor. The inset to Figure 6.8 shows the shift factor plotted as a function of temperature: the a_T data display a temperature dependence consistent with the WLF (Williams-Landel-Ferry) relation.[38]

The glass-rubber relaxation in crystalline PTT could be satisfactorily described using the Kohlrausch-Williams-Watts (KWW) "stretched exponential" relaxation time distribution function:

$$\phi(t) = \exp[-(t/\tau_o)^{\beta}] \qquad [2.9]$$

where τ_o is the observed relaxation time and β is the distribution parameter. β ranges from 0 to 1, with values close to unity corresponding to a narrow, single relaxation time (Debye) response. Lower values of β reflect increased intermolecular coupling, as well as inhomogeneous relaxation broadening owing to the presence of physical or chemical crosslinks. Series approximations reported by Williams *et al.* express modulus and loss for the KWW model in the frequency domain:[39] the best-fit relaxation curve based on these equations is shown in Figure 6.8. A distribution parameter value (β) of 0.14 was obtained for isothermally melt crystallized PTT prepared at 160°C.

Dynamic mechanical results for the various melt crystallized PTT samples are compared across the glass transition region in **Figure 6.9**. As discussed above, the thermal histories imposed in this study (*i.e.*, isothermal melt crystallization at temperatures ranging from 160°C to 200°C) produced only minimal differences in the bulk crystallinity of the resulting materials. Similarly, the dynamic mechanical *tanδ* curves for these specimens show very little variation as a function of crystallization condition, with relaxation peak temperature and intensity nearly invariant for the different films. For samples crystallized at lower temperatures (160°C and 170°C), the relaxation appears to be somewhat broader, especially on the high-temperature side of the relaxation peak. This suggests a broader distribution of relaxation environments in these samples, and may reflect poorer crystal organization owing to the deep quench intervals experienced by the films during preparation.

6.3.3 Broadband Dielectric Spectroscopy

Dielectric results for quenched PTT are plotted in **Figure 6.10** as dielectric constant (ε') and loss (ε'') versus temperature at selected frequencies from 0.1 Hz to 1 MHz. The data show a broad low temperature relaxation (β relaxation), and then a sharp increase in permittivity that corresponds to large scale dipolar mobilization at the glass transition (α relaxation). The glass transition is followed by an abrupt, frequency-independent decrease in dielectric constant that reflects the onset of cold crystallization in the quenched specimen and the corresponding immobilization and/or constraint of some fraction of the responding dipoles with increased bulk crystallinity. The presence of cold crystallinity leads to a positive offset in the nominal glass transition temperature of the test specimen, as well as a broadening of the glass-rubber relaxation. The completion of the offset glass transition process at higher temperatures (> 70°C) is evident as a gradual increase in ε', and as a broad high temperature shoulder in ε''. Similar features in dielectric constant and loss have been reported for quenched PET,[69] PPS[87,90] and PEEK.[79,85,87]

Dielectric results for isothermally melt crystallized PTT (T_c = 170°C) are reported in **Figure 6.11**. In this case, two distinct incremental increases in dielectric constant are evident, corresponding to the sub-glass (β) and glass-rubber (α) relaxations; the features of the glass transition are not complicated by the effects of additional crystallization during measurement. The dielectric loss peak at the glass transition is considerably broadened as compared to the quenched sample, as the polymer chains experience a much wider spectrum of segmental relaxation environments. The observed increase in dielectric constant and loss at lower test frequencies and higher temperatures corresponds to the onset of Maxwell-Wagner-Sillars (MWS) interfacial polarization owing to the accumulation of mobile charge carriers at the interfaces between the crystal and amorphous phases.[99]

The dielectric dispersions for both the glass-rubber and sub-glass relaxations were analyzed according to the Havriliak-Negami (HN) modification of the single relaxation time Debye expression:[42,154]

$$\varepsilon^* = \varepsilon_U + \frac{\varepsilon_R - \varepsilon_U}{[1 + (i\omega\tau_{HN})^a]^b} \qquad [2.10]$$

where ε_R and ε_U represent the relaxed ($\omega \to 0$) and unrelaxed ($\omega \to \infty$) values of the dielectric constant, $\omega = 2\pi f$ is the frequency, τ_{HN} is the central relaxation time, and a and b represent the broadening and skewing parameters, respectively. All (HN) curve fits reported here were performed using the WinFit software program provided with the Novocontrol dielectric instrument.

Dielectric loss data are plotted as a function of frequency for quenched PTT in **Figure 6.12**. Across the glass transition region, there is a narrow temperature range (44°C to 56°C) for which satisfactory HN curve fits can be obtained without the influence cold crystallization. Results for a representative melt crystallized sample (T_c = 170°C) are provided in **Figure 6.13**. In each case (α and β relaxations, respectively), the loss data in the frequency domain were fit with a single HN function. The HN curve fits were used to establish the frequency associated with the maximum in dielectric loss (f_{MAX}), and the dielectric relaxation intensity ($\Delta\varepsilon = \varepsilon_R - \varepsilon_U$) as a function of temperature.

The time-temperature characteristics for the α and β relaxations are presented as an Arrhenius plot of log (f_{MAX}) versus 1000/$T(K)$ in **Figure 6.14**, with data corresponding to the quenched sample and selected melt crystallized films. For the β relaxation, the localized motions, which are presumably associated with reorientation of carbonyl groups, follow a linear Arrhenius relation which is typical of sub-glass relaxations in polymers.[67] The position of the β relaxation is nearly independent of sample morphology (*i.e.*, quenched versus melt crystallized samples), reflecting the localized character of the dipolar reorientations. The apparent activation energy (E_A) determined from the slope of the dielectric Arrhenius plot is 54 kJ mol^{-1} for the quenched sample, which is close to values reported for both PET[72,75] and PBT[191]. The results for the dielectric α relaxation in Figure 6.14 clearly reflect the positive offset in glass transition temperature that is observed with the presence of melt crystallinity in the PTT samples. Over the range of frequencies investigated, the data for both the quenched and crystallized films can be described by a single activation energy; E_A = 485 kJ mol^{-1}.

Examination of the dielectric and DMA data for quenched PTT shows that the sub-glass dynamic mechanical loss peak is offset to higher temperatures relative to the dielectric β relaxation (re: Figure 6.14). A direct comparison of the $tan\delta$ curves for quenched PTT at a frequency of 1 Hz is provided in **Figure 6.15**. As discussed above, previous dielectric and dynamic mechanical studies on PET have suggested that the sub-glass dielectric relaxation corresponds to a single (lower temperature) process that reflects motion of the carbonyl groups, while the dynamic mechanical peak encompass two processes; *i.e.*, carbonyl motions, as well as (higher temperature) phenyl ring flips.[190] The PTT $tan\delta$ curves shown in Figure 6.15 are consistent with this scenario, with the dielectric probe sensitive to only a subset of the local motions that comprise the overall sub-glass relaxation response.

The HN curve fits reported in Figures 6.12 and 6.13 were used to establish the dielectric relaxation intensities for the α and β relaxations as a function of temperature and thermal history. **Figure 6.16** reports $\Delta\varepsilon$ versus temperature for quenched and melt crystallized PTT. Comparison of $\Delta\varepsilon$ for the β relaxation indicates an overall decrease in relaxation intensity of 25% for the melt crystallized samples relative to the quenched film, which is consistent with the measured increase in bulk crystallinity, W_C, from 0.13 to 0.30. Previous studies on PET samples encompassing a wide range of crystallinity indicated that the intensity of the sub-glass relaxation varies directly with the fraction amorphous phase present in the samples, which implies that the localized sub-glass motions that occur in the amorphous regions are unperturbed by the presence of the crystallites.[69,74]

The PTT results presented here indicate a similar behavior, although the range of crystallinities encompassed by the PTT samples is not sufficient to establish a definitive relationship between dielectric relaxation intensity and fraction crystallinity.

The PTT dielectric relaxation intensity across the α relaxation is a strong function of temperature for both the quenched and melt crystallized materials; see Figure 6.16. In quenched PTT, dielectric relaxation intensity for the glass transition can be determined across a relatively narrow range of measurement temperatures prior to the onset of cold crystallization. Over this range, $\Delta\varepsilon$ decreases steadily with temperature in a manner that has been reported for a number of similar polymers; *e.g.*, PET,[69] PPS[87,90] and PEEK[79,85]. For the melt crystallized PTT samples, the dielectric relaxation intensity is reduced substantially below that which might be expected based on a strictly two-phase morphological model wherein only those chain segments incorporated into the crystalline phase are held immobile in the range between T_g and crystal melting. This again suggests the presence of a sizeable rigid amorphous phase fraction in these samples, with the constraining influence of the crystals extending well into the amorphous phase. The comparison of dielectric relaxation intensity for the semicrystalline samples ($\Delta\varepsilon^{SC}$) relative to the value for a wholly amorphous specimen ($\Delta\varepsilon^{A}$) provides an alternate route for the determination of mobile amorphous phase fraction, W_{MA}. However, the calculation is complicated by a number of factors, including the availability of an experimental value for a 100% amorphous PTT sample, as well as the strong temperature dependence of $\Delta\varepsilon$ observed for the both the quenched and crystallized materials; this issue is addressed in detail for PEEK in reference 79. Using a quenched sample value for $\Delta\varepsilon$ equal to 2.7 (and adjusting for residual crystallinity), the mobile amorphous phase fraction for isothermally crystallized PTT is calculated to be $W_{MA} \sim 0.45$ at 70°C. This corresponds to a rigid amorphous phase fraction, $W_{RAP} = 0.25$.

At temperatures above T_g, the dielectric relaxation intensity measured for the melt-crystallized samples increases strongly with temperature. This behavior, which has been observed to varying extents in the other polymers cited above, may reflect a gradual mobilization of the rigid amorphous phase with increasing temperature, as well as a reduction in local dipolar correlation of the ester groups. The extent of dipolar correlation is typically expressed via the Onsager-Kirkwood correlation factor, g,[67,192] which accounts for the influence of intra- and inter-molecular correlations on the response of the individual constituent dipoles, and can reflect local dipolar cancellations as well as spatial restrictions to dipolar orientation.[193] In PTT, the increase in $\Delta\varepsilon$ with temperature above T_g appears to be exceptionally strong, and may reflect not only the progressive mobilization of “rigid amorphous” segments in the crystal-amorphous interphase, but also the disruption of local dipolar cancellations owing to an increase in overall conformational mobility, thus leading to a larger net dipolar response.

6.4 CONCLUSIONS

The thermal and dynamic relaxation characteristics of quenched and melt crystallized poly(trimethylene terephthalate) have been investigated. Quenching PTT from the melt state into liquid N_2 resulted in films with a residual crystalline fraction, $W_C = 0.13$; fully-amorphous samples could not be obtained for the PTT resin examined in this study. Isothermal melt crystallization at temperatures ranging from 160 to 200°C led to a bulk crystallinity of ~ 0.30, independent of crystallization temperature. The presence of melt crystallinity led to a positive offset in the glass transition temperature ($\Delta T = 10$°C), and calorimetry measurements revealed the existence of a sizeable rigid amorphous phase fraction in the melt crystallized samples. Dynamic mechanical analysis and broadband dielectric spectroscopy were used to study the sub-glass and glass-rubber relaxation characteristics of quenched and crystalline PTT. The relaxation properties of PTT were consistent with the behavior reported for other semiflexible polymers such as PET, PPS and PEEK. The sub-glass (β) relaxation in PTT was largely unperturbed by the presence of crystallinity. Comparison of the dynamic mechanical and dielectric sub-glass relaxations suggested that the dielectric response reflected a lower-temperature subset of the motions that were encompassed in the broader, more complex mechanical relaxation. For the glass-rubber (α) relaxation, dielectric measurements showed a strong influence of crystallinity on the resulting dielectric relaxation intensity, again consistent with the presence of a significant amount of rigid amorphous material in the melt crystallized specimens. The strong increase in measured relaxation intensity with temperature above T_g suggested a gradual mobilization of the rigid amorphous phase, as well as an overall loss of dipolar correlation.

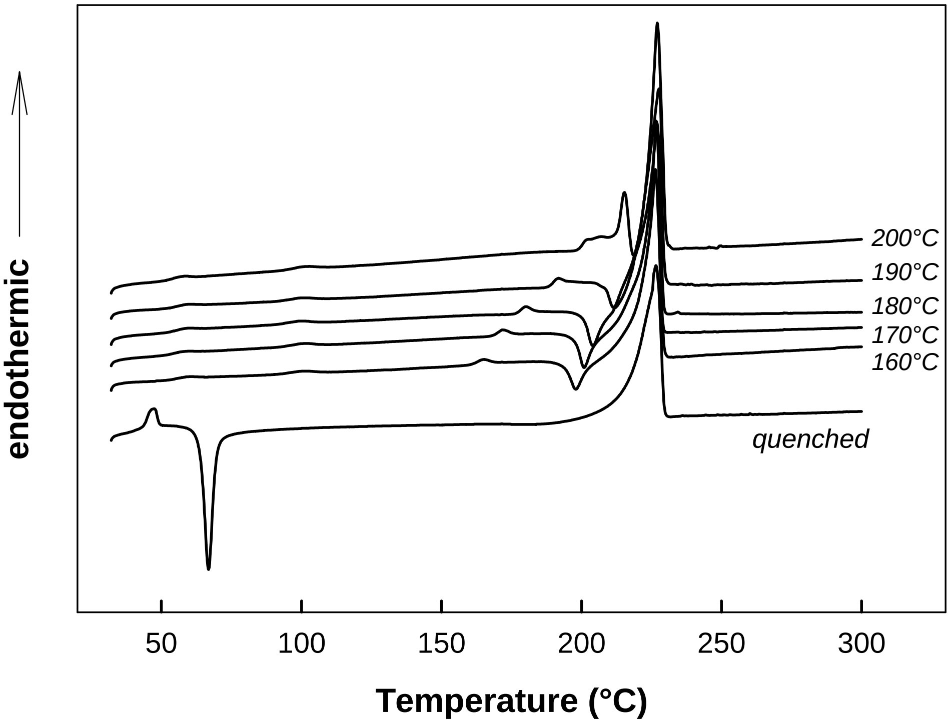

Figure 6.1: DSC heating sweeps (10°C min^{-1}) for quenched and isothermally melt crystallized PTT.

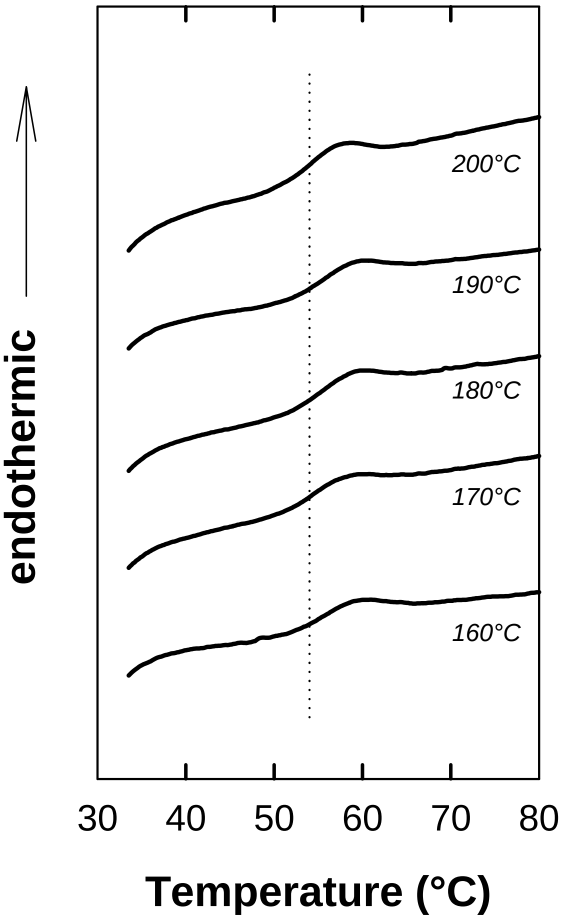

Figure 6.2: DSC heating sweeps (10°C min^{-1}) for isothermally melt crystallized PTT: expanded view of glass transition region.

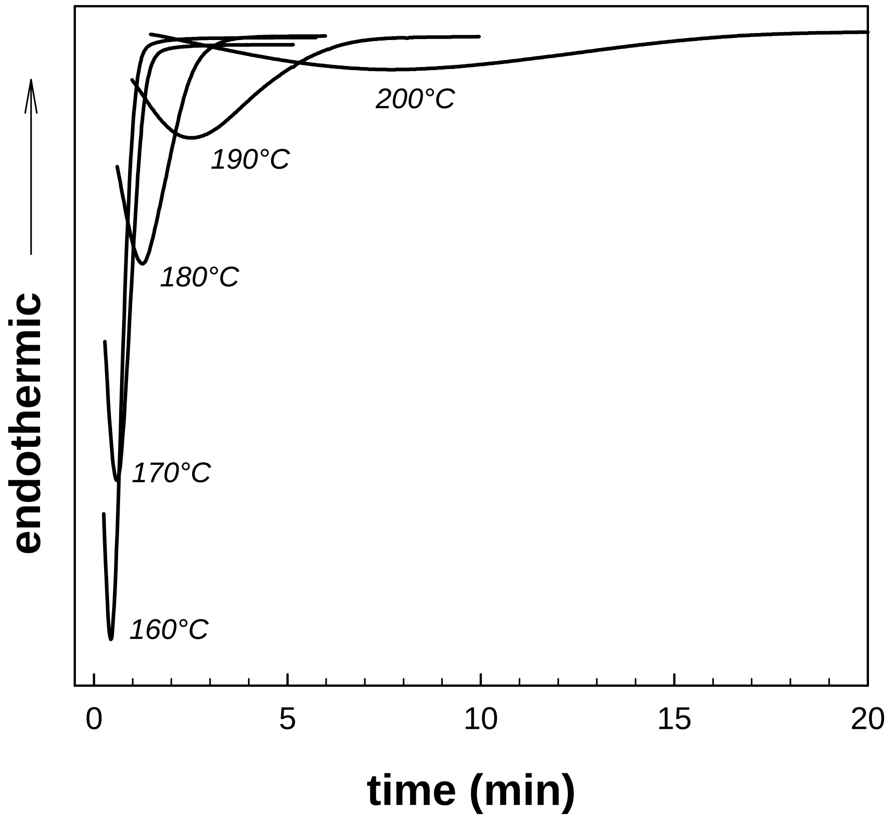

Figure 6.3: DSC heating sweeps (10°C min^{-1}) for isothermally melt crystallized PTT plotted versus time. Samples quenched from melt (260°C) at 80°C/min.

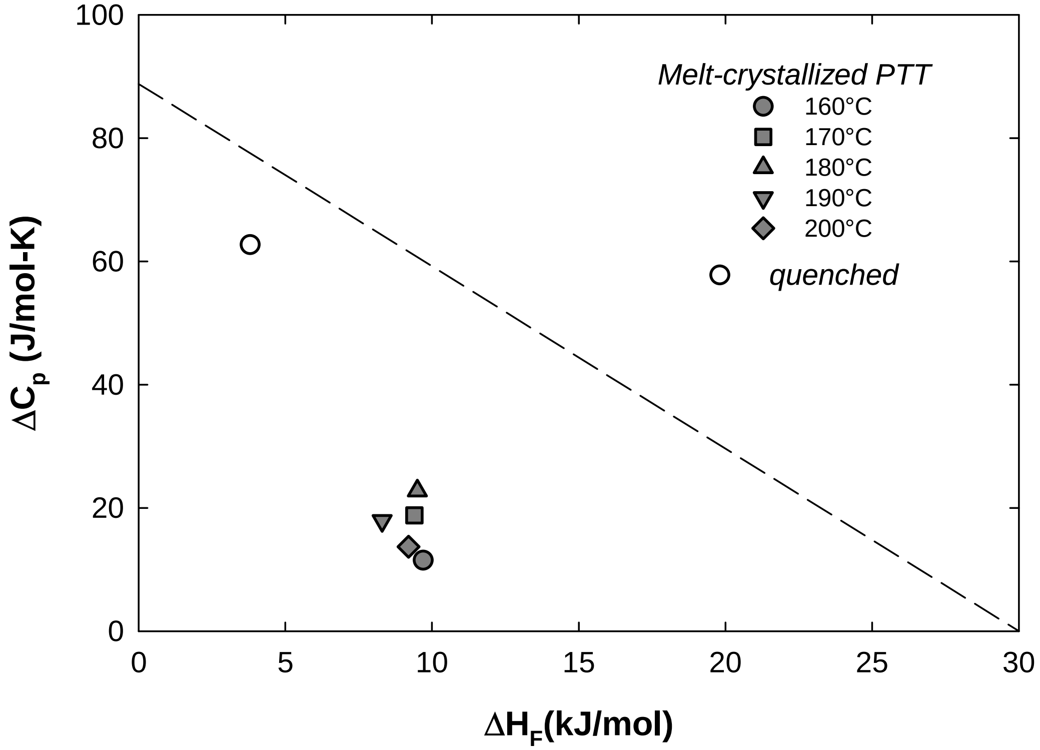

Figure 6.4: Incremental increase in heat capacity ($\Delta C_p(T_g)$; J/mol-K) versus net heat of fusion (ΔH_F; kJ/mol) for melt crystallized PTT.

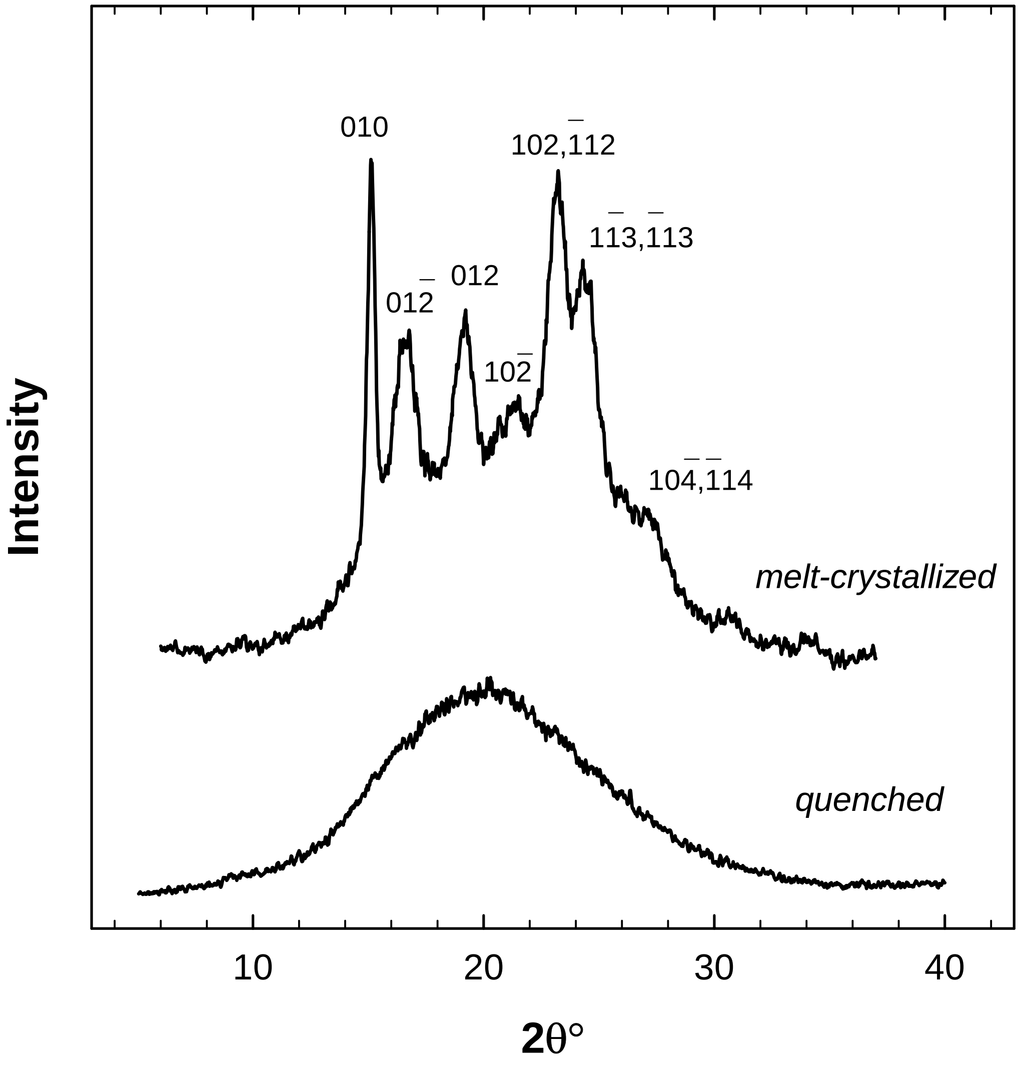

Figure 6.5: Wide-angle X-ray diffraction patterns (intensity versus *2θ*) for quenched and melt crystallized (T_c = 180°C) PTT; Cu K_α radiation, λ = 1.5406Å. Indexing of diffraction peaks as per reference 162.

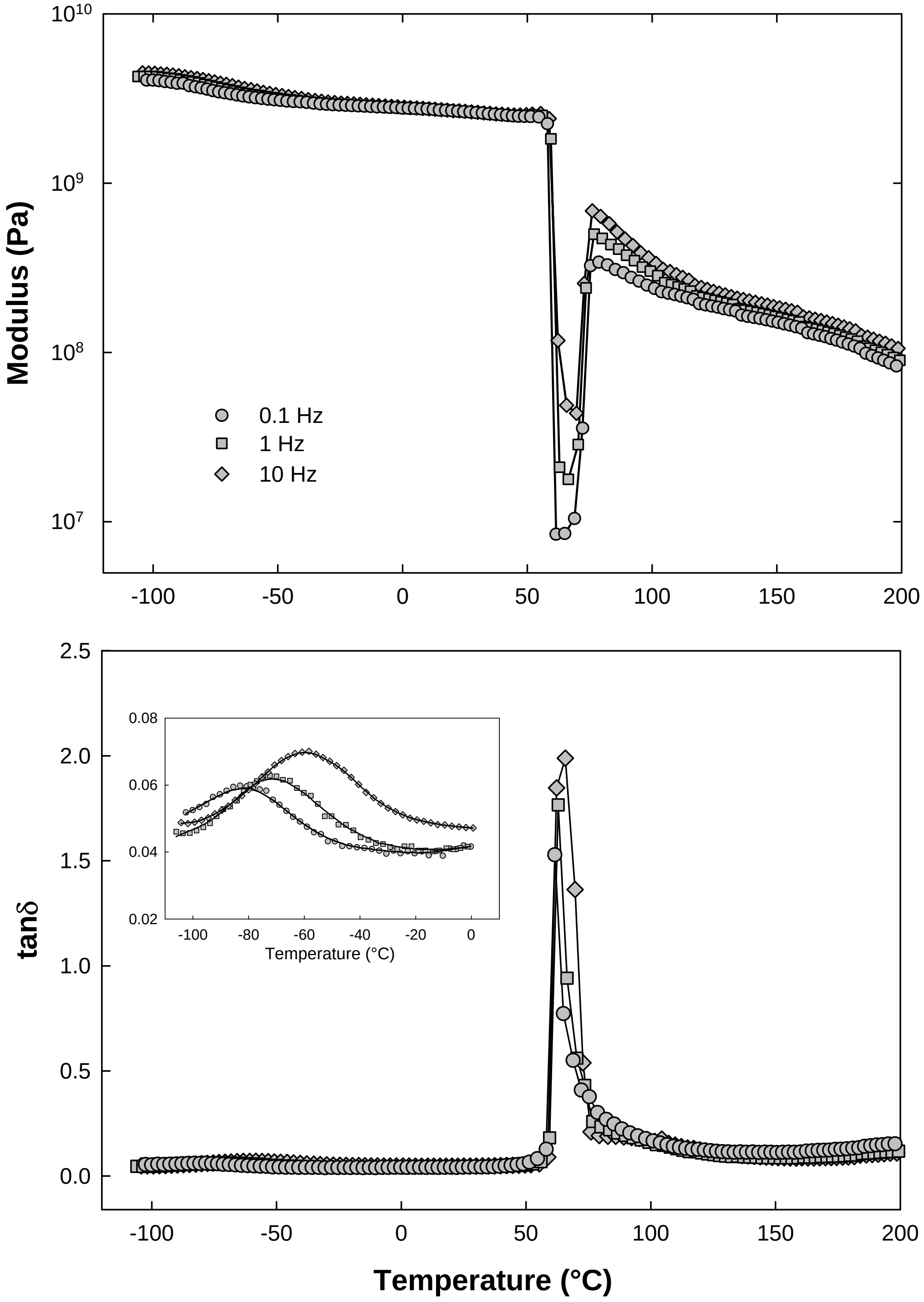

Figure 6.6: Dynamic mechanical storage modulus (*E′*; Pa) and loss factor (*tanδ*) versus temperature for quenched PTT; heating rate of 1°C min^{-1}. *Inset: tanδ* versus temperature for sub-glass (*β*) transition region.

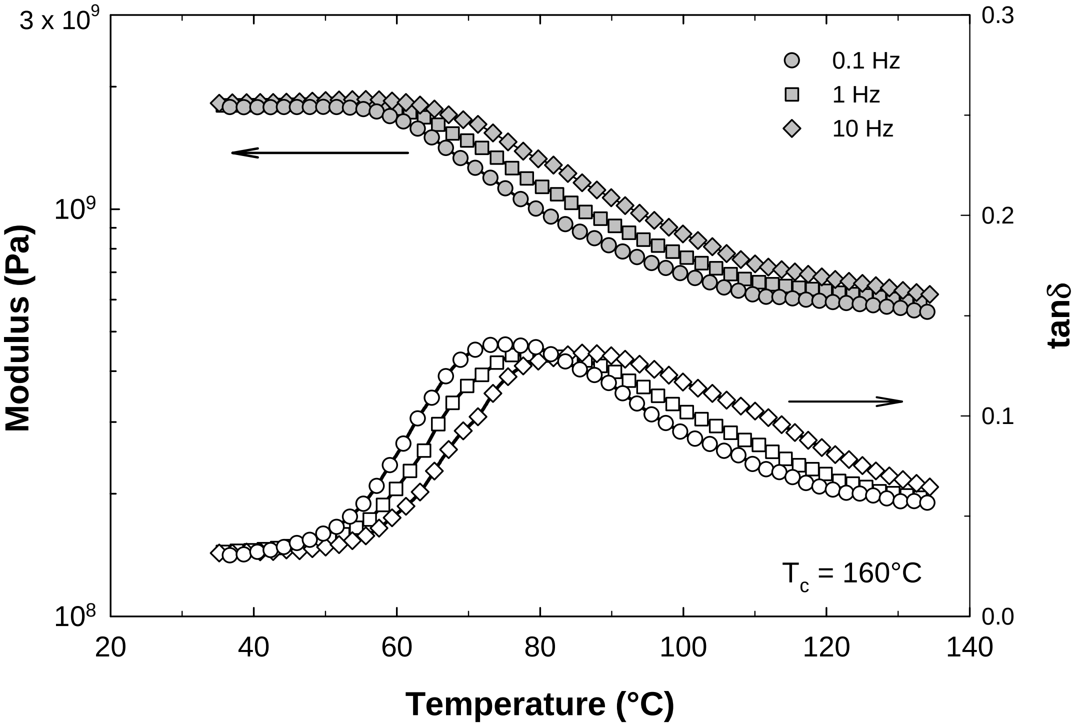

Figure 6.7: Dynamic mechanical storage modulus (filled symbols) and loss factor (*tan*δ) (empty symbols) versus temperature for melt crystallized (T_c = 160°C) PTT; heating rate of 1°C min^{-1}.

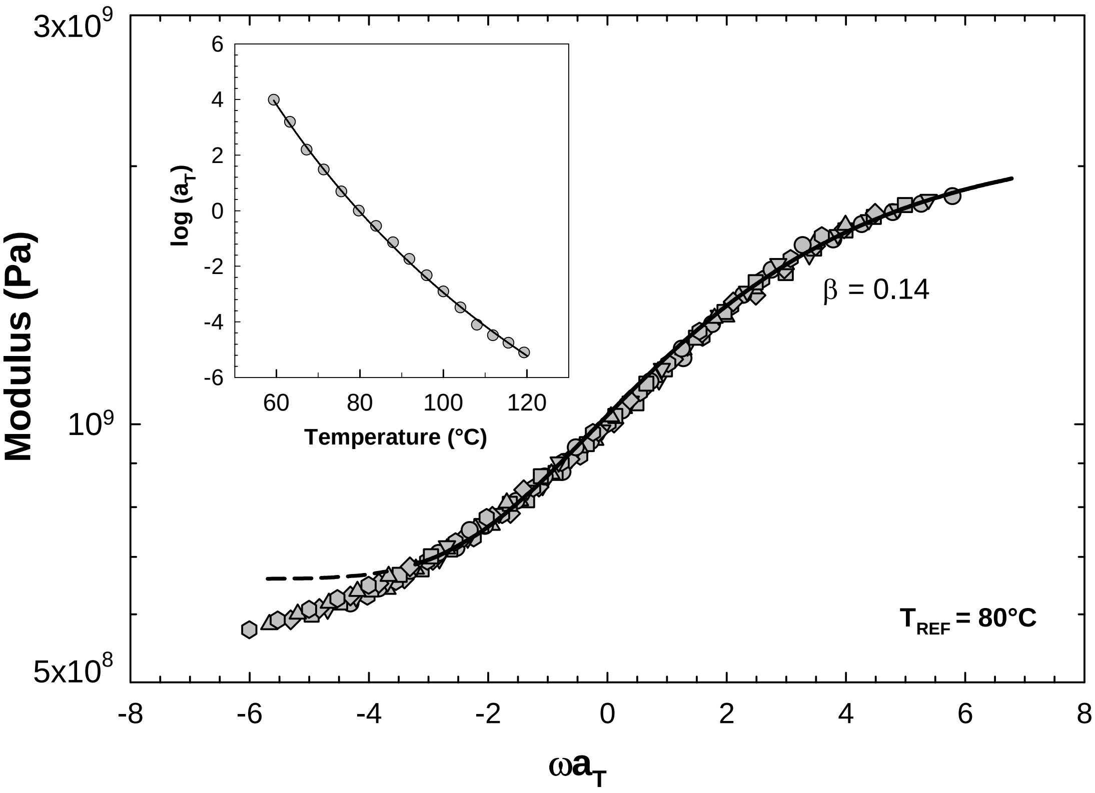

Figure 6.8: Time-temperature master curve for melt crystallized (T_c = 160°C) PTT; T_{REF} = 80°C. Solid curve is KWW best-fit. *Inset:* time-temperature shift factor (a_T) versus temperature.

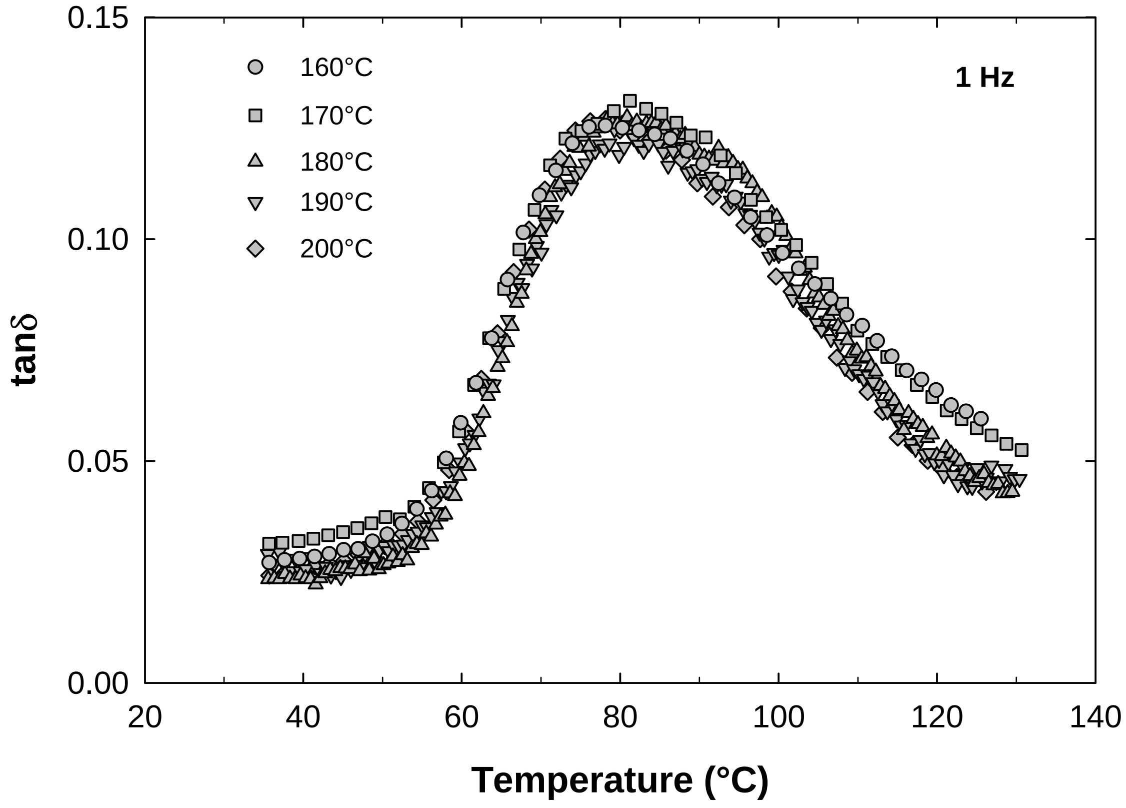

Figure 6.9: Dynamic mechanical *tanδ* versus temperature for melt crystallized PTT. Frequency of 1 Hz; heating rate of 1°C min^{-1}.

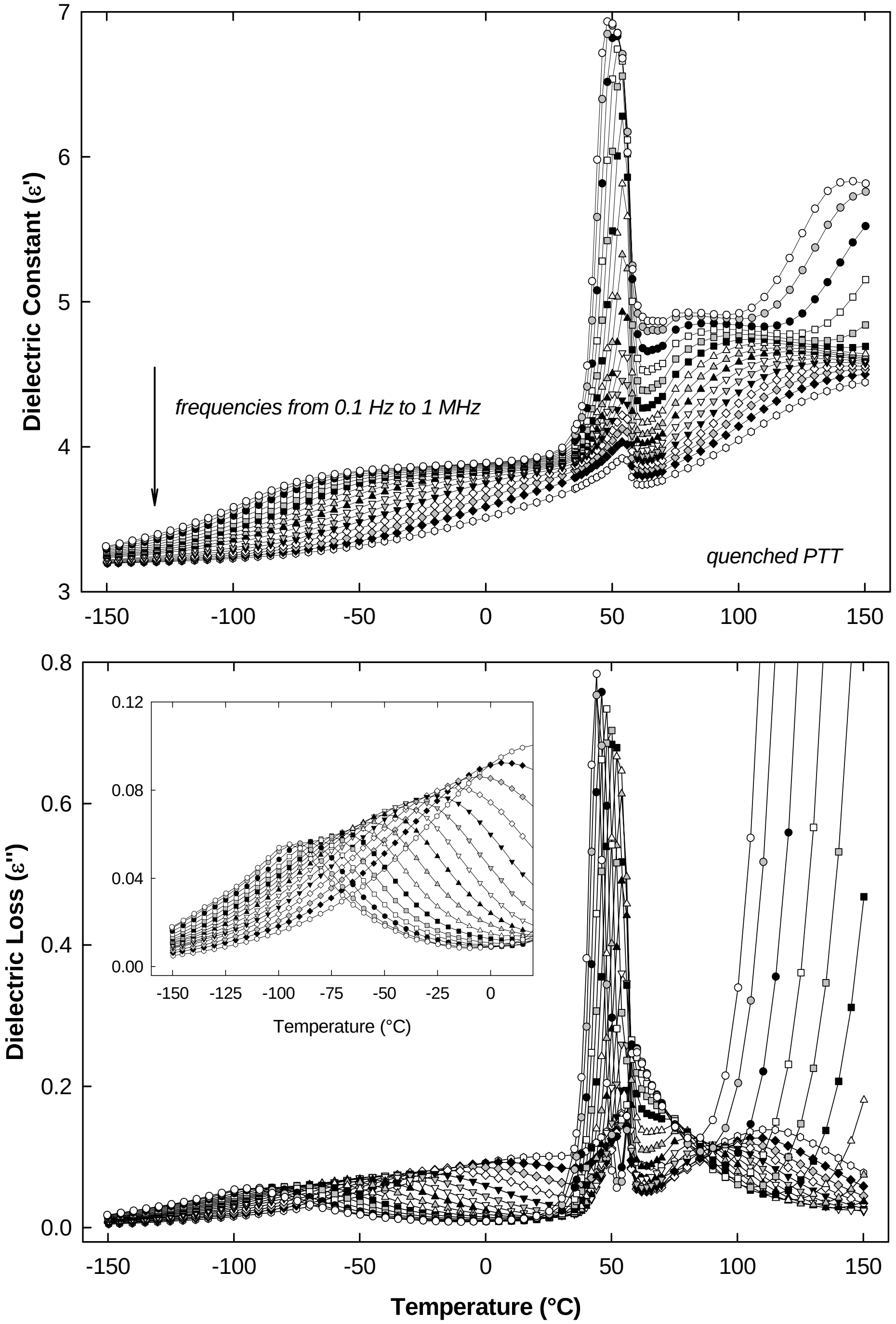

Figure 6.10: Dielectric constant (ε') and loss (ε'') versus temperature for quenched PTT; selected frequencies from 0.1 Hz to 1 MHz. *Inset:* expanded view of dielectric loss across the sub-glass transition region.

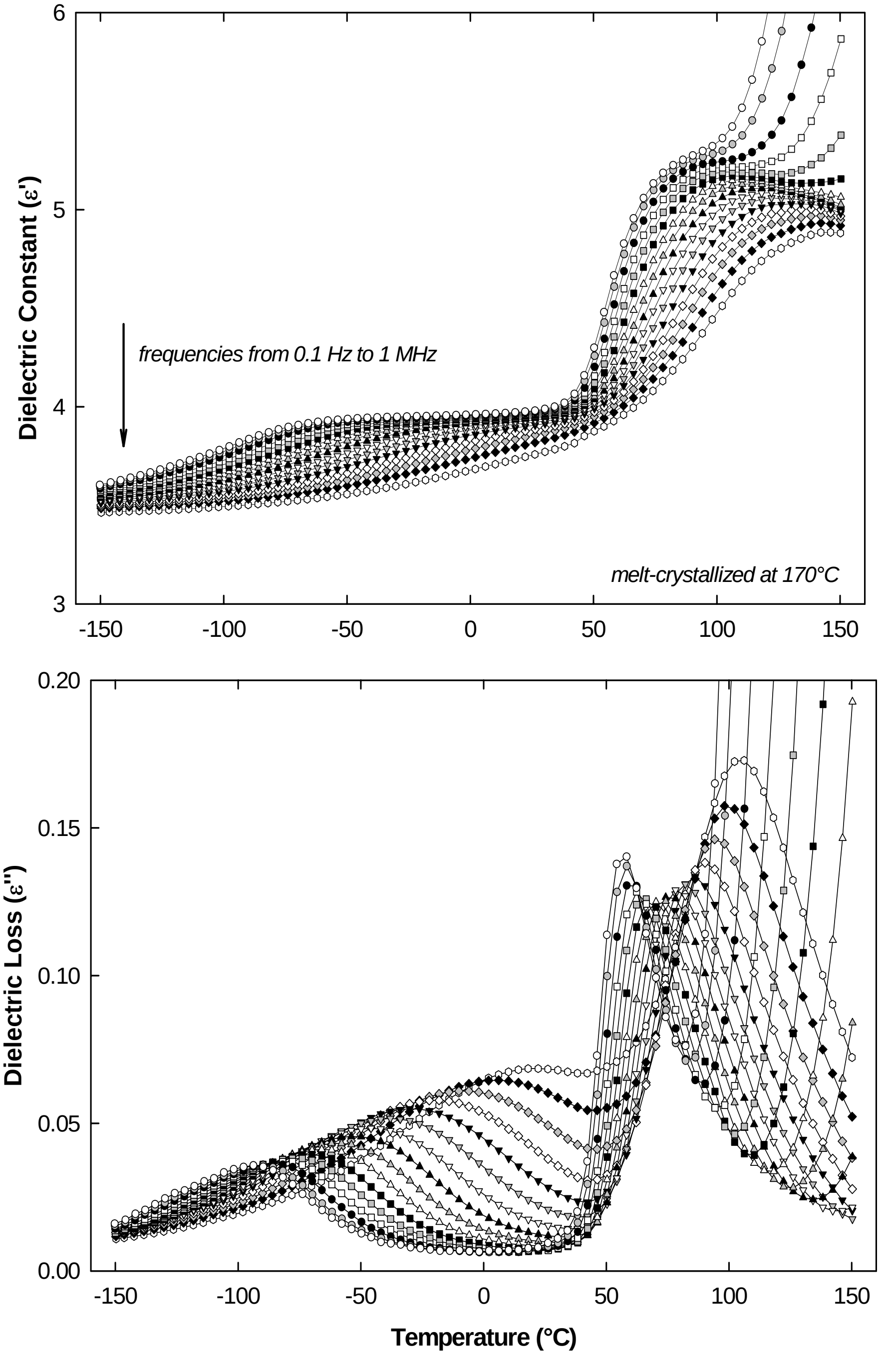

Figure 6.11: Dielectric constant (ε') and loss (ε'') versus temperature for melt crystallized (T_c = 170°C) PTT; selected frequencies from 0.1 Hz to 1 MHz.

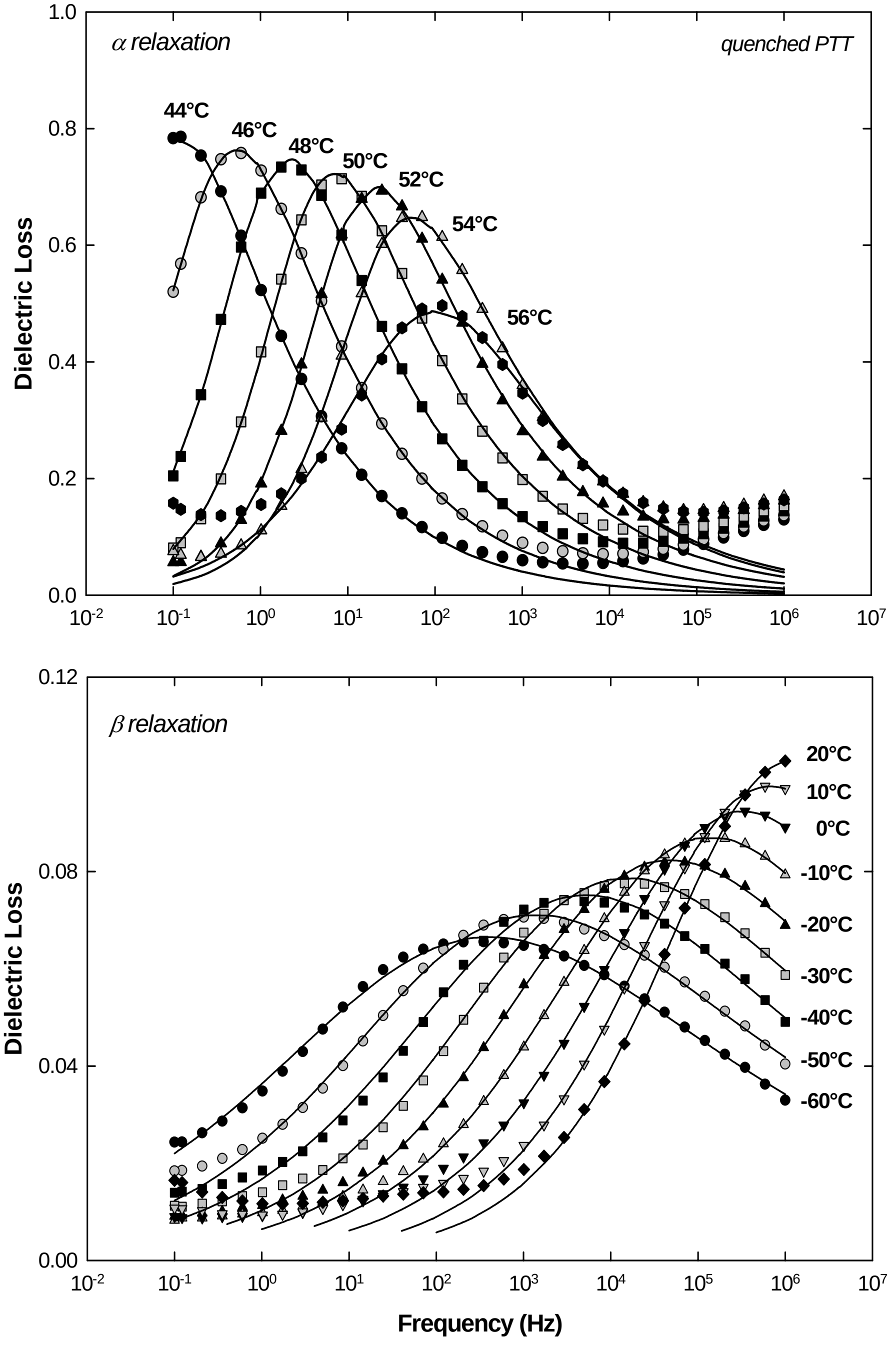

Figure 6.12: Dielectric loss (ε'') versus frequency for quenched PTT across the glass-rubber (α) and sub-glass (β) relaxation regions. Solid curves are Havriliak-Negami best fits.

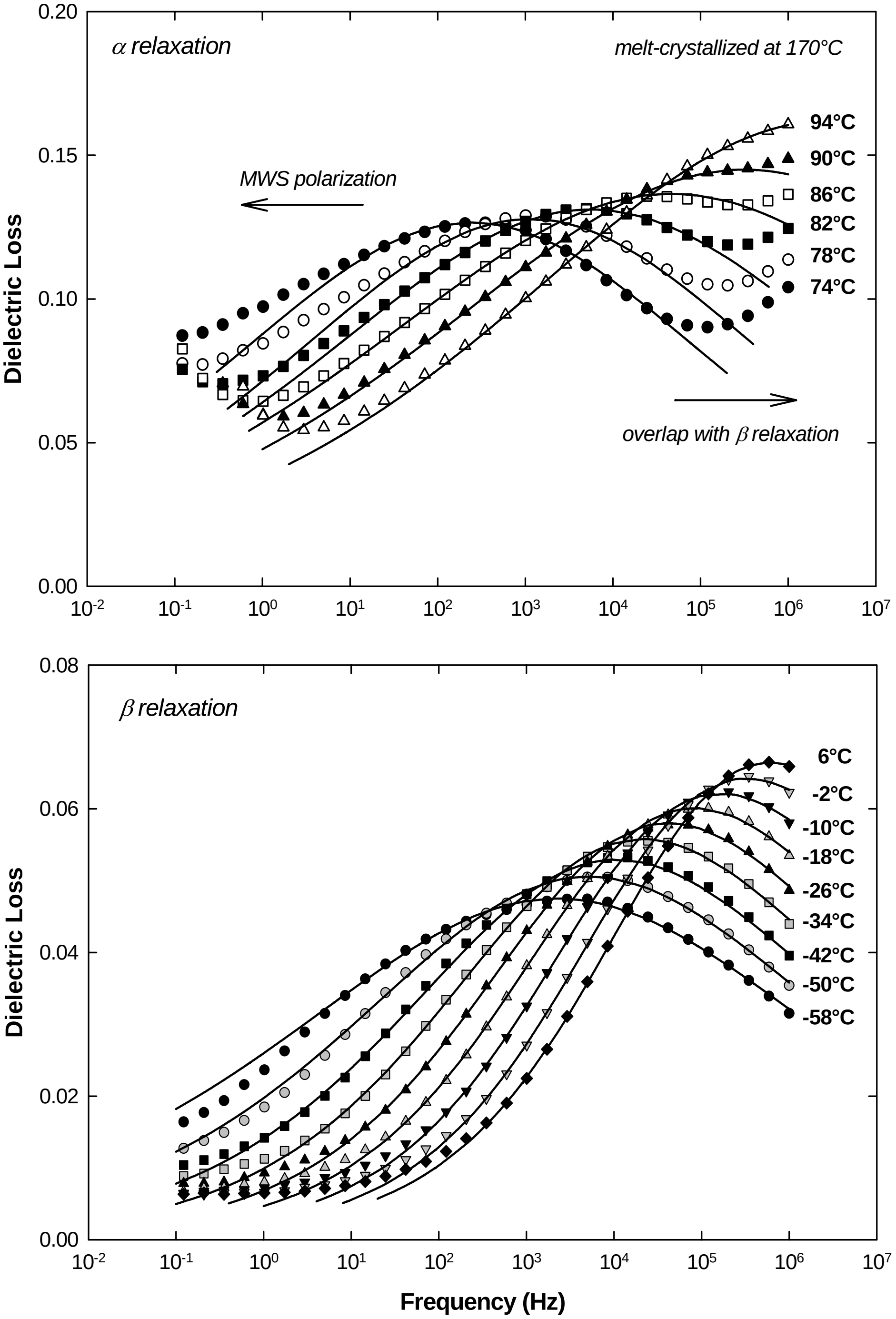

Figure 6.13: Dielectric loss (ε'') versus frequency for melt crystallized (T_c = 170°C) PTT across the glass-rubber (α) and sub-glass (β) relaxation regions. Solid curves are Havriliak-Negami best fits.

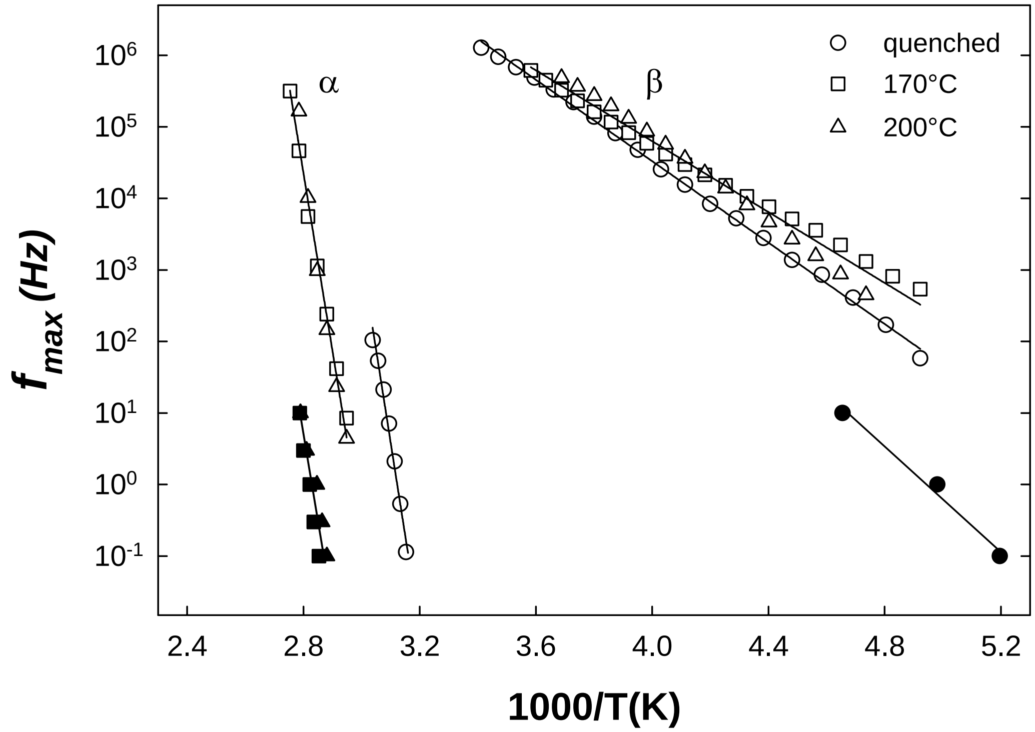

Figure 6.14: Arrhenius plot of f_{MAX} (Hz) versus 1000/T(K) for quenched and melt crystallized PTT. (○) quenched; (□) T_c = 170°C; (△) T_c = 200°C. Empty symbols: dielectric results. Filled symbols: dynamic mechanical results.

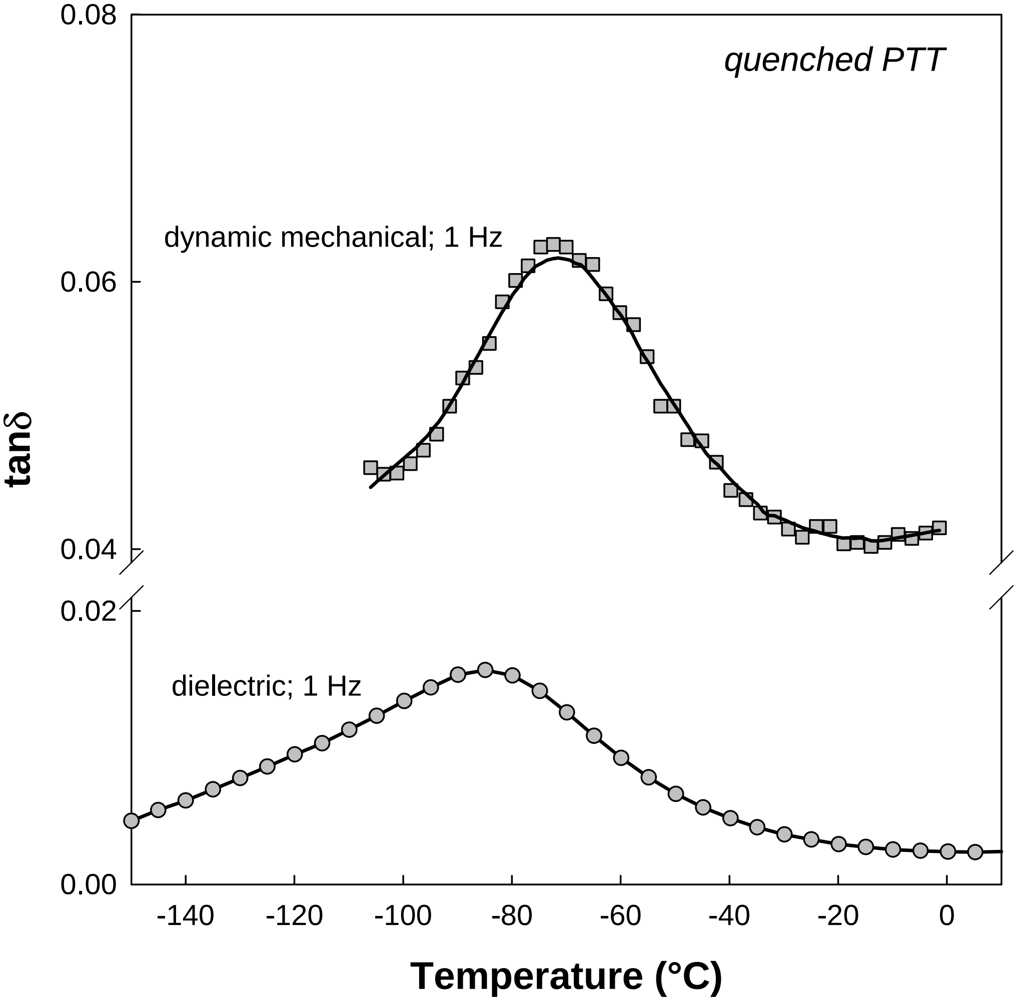

Figure 6.15: Comparison of *tanδ* versus temperature curves for quenched PTT; 1 Hz.

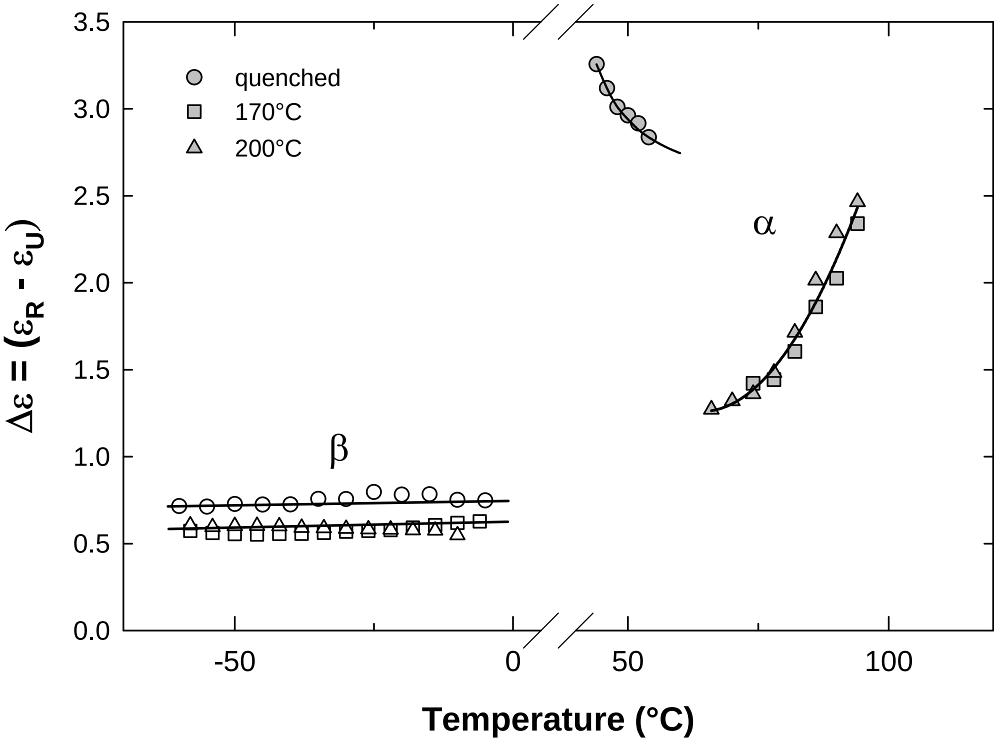

Figure 6.16: Dielectric relaxation intensity ($\Delta\varepsilon = \varepsilon_R - \varepsilon_U$) versus temperature for quenched and melt crystallized PTT; sub-glass (β) and glass-rubber (α) relaxations.

Copyright © Sumod Kalakkunnath 2007

Chapter Seven

Conclusions

The molecular dynamics of rubbery PEG-based crosslinked networks and semicrystalline poly(trimethylene terephthalate) (PTT) have been investigated in detail using dynamic mechanical and dielectric techniques. For the rubbery networks, fundamental relations have been established between polymer composition, network architecture, and dynamic relaxation characteristics, as well as their correlation to gas transport properties. In the case of PTT, calorimetric and X-ray methods, in concert with dynamic thermal analysis, have been used to elucidate the influence of sample processing history on resultant semicrystalline morphology.

The significant accomplishments and key findings of this work are summarized below:

> A detailed viscoelastic characterization has been performed on model PEGDA networks via dynamic mechanical analysis. PEGDA/water networks showed a systematic decrease in effective crosslink density with increasing water content in the prepolymerization reaction mixture. For these networks, a narrowing of the glass-rubber relaxation along with a progressive decrease in fragility was observed with decreasing crosslink density, but there was little variation in the measured glass transition temperature or fractional free volume. Gas permeation measurements indicated only a very modest variation in gas transport properties despite the sizeable variation in apparent crosslink density achieved in these materials. This result suggests that the controlling structural factor for gas transport in the networks is not crosslink density alone, and that attempts to correlate gas transport to network structure must necessarily consider the broader relationships between crosslink density, segmental mobility, and fractional free volume.

Copolymerization of PEGDA with appropriate amounts of acrylate monomers, PEGMEA and PEGA, resulted in copolymer networks with varying crosslink density, but similar chemical composition. For both series, the introduction of the acrylate co-monomer led to a decrease in the measured glass transition temperature, as well as a systematic reduction in crosslink density as reflected in the rubbery modulus of the network. KWW curve fits to time-temperature modulus master curves indicated a narrowing of the glass-rubber relaxation with reduced crosslink density that correlated with a decrease in fragility, suggesting that a more homogeneous, less cooperative relaxation environment is present in the copolymer networks. The influence of the copolymer branches was more pronounced in the PEGDA/PEGMEA series, which displayed a larger variation in glass transition temperature and fractional free volume upon changes in PEGDA content. A contrast was also evident in the gas transport properties of the two network series, with the PEGDA/PEGMEA membranes displaying favorable variations in permeability and selectivity over the range of copolymer compositions examined. These studies revealed the sensitivity of the membrane properties to relatively minor structural variations, such as changes in branch end group.

PEGDA/MgO nanocomposites posed an interesting morphological variation as manifested in the emergence of a second, higher-temperature T_g which was attributed to confined polymer chains experiencing restricted mobility in the vicinity of the particle surfaces.

A detailed dielectric investigation revealed the existence of two sub-glass relaxations (β_1 and β_2) in the PEGDA crosslinked networks. The “fast” β_2 relaxation, which was positioned intermediate to the β_1 and glass-rubber (α) processes, was attributed to a subset of non-cooperative segmental reorientations originating in the vicinity of the crosslink junctions. The limited conformational freedom of the polymer chain segments in this region led to the emergence of a more localized, largely non-cooperative process, a behavior consistent with that encountered in crystalline PEO and amorphous PEO located within the confined regions of polymer nanocomposites.

Dynamic relaxation studies performed on crosslinked BPAEDA indicated a significantly higher T_g as compared to PEGDA owing to a lower molecular weight between crosslinks and the presence of the bulky, bisphenol A segment along the crosslinker bridging group. Copolymerization of BPAEDA with either PEGMEA or PEGDA led to a strong decrease in T_g with co-monomer content as a result of the inherent flexibility of the PEGMEA and PEGA chains. The substantial structural difference between the crosslinker and the acrylate monomers produced a greater overall relaxation heterogeneity that was manifested in a gradual broadening of the glass transition despite decreasing crosslink density. The BPAEDA copolymer networks displayed an increase in the measured dielectric intensity with increasing acrylate content, the effect being more pronounced for the –OH terminated PEGA copolymer series, where additional dipolar content amplified the dielectric response.

The thermal and dynamic relaxation characteristics of quenched and melt crystallized poly(trimethylene terephthalate) (PTT) have also been investigated. Quenching PTT from the melt state into liquid N_2 resulted in films with a residual crystalline fraction, $W_C = 0.13$; fully-amorphous samples could not be obtained for the PTT resin examined in this study. The presence of melt crystallinity led to a positive offset in the glass transition temperature ($\Delta T = 10°C$), and calorimetry measurements revealed the existence of a sizeable rigid amorphous phase fraction in the melt crystallized samples. Dynamic mechanical analysis and broadband dielectric spectroscopy were used to study the sub-glass and glass-rubber relaxation characteristics of quenched and crystalline PTT; the relaxation properties of PTT were consistent with the behavior reported for other semiflexible polymers such as PET, PPS and PEEK. The sub-glass (β) relaxation in PTT was largely unperturbed by the presence of crystallinity. Comparison of the dynamic mechanical and dielectric sub-glass relaxations suggested that the dielectric response reflected a lower-temperature subset of the motions that were encompassed in the broader, more complex mechanical relaxation. For the glass-rubber (α) relaxation, dielectric measurements showed a strong influence of crystallinity on the resulting dielectric relaxation intensity, again consistent with the presence of a significant amount of rigid amorphous material in the melt crystallized specimens. The observed increase in measured relaxation intensity with temperature above T_g suggested a gradual mobilization of the rigid amorphous phase, as well as an overall loss of dipolar correlation.

Copyright © Sumod Kalakkunnath 2007

References

(1) Baker, R. W. *Membrane Technology and Applications, 2nd edition*; John Wiley and Sons: New York, **2004**.

(2) Ghosal, K.; Freeman, B. D. *Polymers for Advanced Technologies* **1994**, 5, 673-697.

(3) Cohen, M. H.; Turnbull, D. *Journal of Chemical Physics* **1959**, 31, 1164 -1169.

(4) Fujita, H. *Fortschr. Hochpolymer. Forsch.* **1961**, 3, 1-47.

(5) Lee, W. M. *Polymer Engineering and Science* **1980**, 20, 65-69.

(6) Van Krevelen, D. W. *Properties of Polymers: Their Correlation with Chemical Structure, Their Numerical Estimation and Prediction from Additive Group Contributions*; Elsevier: Amsterdam, **1990**.

(7) Koros, W. J.; Fleming, G. K. *Journal of Membrane Science* **1993**, 83, 1-80.

(8) Petropoulos, J. H. "Mechanisms and Theories for Sorption and Diffusion of Gases in Polymers" In *Polymeric Gas Separation Membranes*; Paul, D. R.; Yampolskii, Y. P., eds.; CRC Press: Boca Raton, FL, **1994**; pp 17-81.

(9) Freeman, B. D.; Pinnau, I. *Trends in Polymer Science* **1997**, 5, 167-173.

(10) Zolandz, R. R.; Fleming, G. K. "Gas Permeation" In *Membrane Handbook*; Ho, W. S. W.; Sirkar, K. K., eds.; Van Nostrand Reinhold: New York, **1992**; pp 17-101.

(11) Merkel, T. C.; Bondar, V. I.; Nagai, K.; Freeman, B. D.; Pinnau, I. *Journal of Polymer Science, Part B: Polymer Physics* **2000**, 38, 415 - 434.

(12) Koros, W. J. *Journal of Polymer Science, Part B: Polymer Physics* **1985**, 23, 1611-1628.

(13) Bondar, V. I.; Freeman, B. D.; Pinnau, I. *Journal of Polymer Science, Part B: Polymer Physics* **1999**, 37, 2463-2475.

(14) Hirayama, Y.; Kase, Y.; Tanihara, N.; Sumiyama, Y.; Kusuki, Y.; K. Haraya. *Journal of Membrane Science* **1999**, 160, 87-99.

(15) Bondar, V. I.; Freeman, B. D.; Pinnau, I. *Journal of Polymer Science, Part B: Polymer Physics* **2000**, 38, 2051-2062.

(16) Patel, N. P.; Miller, A. C.; Spontak, R. J. *Advanced Materials* **2003**, 15, 729-733.

(17) Lin, H.; Freeman, B. D. *Journal of Membrane Science* **2004**, 239, 105-117.

(18) Lin, H.; Freeman, B. D. *Journal of Molecular Structure* **2005**, 739, 57-74.

(19) Graham, N. B. In *Hydrogels in Medicine and Pharmacy, Volume 2*; Peppas, N. A., ed.; CRC Press: Boca Raton, **1987**; Vol. 2, pp 95-113.

(20) Priola, A.; Gozzelino, G.; Ferrero, F.; Malucelli, G. *Polymer* **1993**, 34, 3653-3657.

(21) Baker, J. P.; Hong, L. H.; Blanch, H. W.; Prausnitz, J. M. *Macromolecules* **1994**, 27, 1446 -1454.

(22) Okay, O.; Kurz, M.; Lutz, K.; Funke, W. *Macromolecules* **1995**, 28, 2728-2737.

(23) Kizilay, M.; Okay, O. *Macromolecules* **2003**, 36, 6856-6862.

(24) Litvinov, V. M.; Dias, A. A. *Macromolecules* **2001**, 34, 4051-4060.

(25) Alves, N. M.; Gomez Ribelles, J. L.; Gomez Tejedor, J. A.; Mano, J. F. *Macromolecules* **2004**, 37, 3735-3744.

(26) Kannurpatti, A. R.; Anderson, K. J.; Anseth, J. W.; Bowman, C. N. *Journal of Polymer Science, Part B: Polymer Physics* **1997**, 35, 2297-2307.
(27) Kannurpatti, A. R.; Anseth, J. W.; Bowman, C. N. *Polymer* **1998**, 39, 2507-2513.
(28) Kannurpatti, A. R.; Bowman, C. N. *Macromolecules* **1998**, 31, 3311-3316.
(29) Roland, C. M. *Macromolecules* **1994**, 27, 4242-4247.
(30) Schroeder, M. J.; Roland, C. M. *Macromolecules* **2002**, 35, 2676-2681.
(31) Glatz-Reichenbach, J. K. W.; Sorriero, L. J.; Fitzgerald, J. J. *Macromolecules* **1994**, 27, 1338-1343.
(32) Yu Kramarenko, V.; Ezquerra, T. A.; Sics, I.; Balta-Calleja, F. J.; Privalko, V. P. *Journal of Chemical Physics* **2000**, 113, 447-452.
(33) Fitz, B. D.; Mijovic, J. *Macromolecules* **1999**, 32, 3518-3527.
(34) Flory, P. J. *Principles of Polymer Chemistry*; Cornell University Press: Ithaca, NY, **1953**.
(35) Treloar, L. R. G. *The Physics of Rubber Elasticity, 3rd ed.*; Oxford University Press: New York, **1975**.
(36) Mark, J. E. *Rubber Chemistry and Technology* **1982**, 55, 762-768.
(37) Hill, L. W. *Progress in Organic Coatings* **1997**, 31, 235-243.
(38) Ferry, J. D. *Viscoelastic Properties of Polymers, 3rd ed.*; John Wiley and Sons: New York, **1980**.
(39) Williams, G.; Watts, D. C.; Dev, S. B.; North, A. M. *Transactions of the Faraday Society* **1971**, 67, 1323-1335.
(40) Ngai, K. L.; White, C. T. *Physical Review B: Condensed Matter and Materials Physics* **1979**, 20, 2475-2486.
(41) Ngai, K. L.; Rajagopal, A. K.; Teitler, S. *Journal of Chemical Physics* **1988**, 88, 5086-5094.
(42) Havriliak, S.; Negami, S. *Journal of Polymer Science, Polymer Symposia* **1966**, 14, 99-103.
(43) Angell, C. A. *Journal of Non-Crystalline Solids* **1991**, 131-133, 13-31.
(44) Ngai, K. L.; Roland, C. M. *Macromolecules* **1993**, 26, 6824-6830.
(45) Hall, C. K.; Helfand, E. *Journal of Chemical Physics* **1982**, 77, 3275-3282.
(46) Schönhals, A.; Schlosser, E. *Colloid and Polymer Science* **1989**, 267, 125 -132.
(47) Merkel, T. C.; Freeman, B. D.; Spontak, R. J.; He, Z.; Pinnau, I.; Meakin, P.; Hill, A. J. *Science* **2002**, 296, 519-522.
(48) Bansal, A.; Yang, H.; Li, C.; Cho, K.; Benicewicz, B. C.; Kumar, S. K.; Schadler, L. S. *Nature Materials* **2005**, 4, 693-698.
(49) Fragiadakis, D.; Pissis, P.; Bokobza, L. *Polymer* **2005**, 46, 6001-6008.
(50) Ash, B. J.; Siegel, R. W.; Schadler, L. S. *Journal of Polymer Science, Part B: Polymer Physics* **2004**, 42, 4371-4383.
(51) Barrer, R. M. In *Diffusion in Polymers*; Crank, J.; Park, G. S., eds.; Academic Press: New York, **1968**; pp 165-217.
(52) Maxwell, C. *Treatise on Electricity and Magnetism*; Oxford University Press: London, **1873**; Vol. 1.
(53) Barrer, R. M.; Barrie, J. A.; Raman, N. K. *Polymer* **1962**, 3, 605-614.
(54) Merkel, T. C.; Freeman, B. D.; Spontak, R. J.; He, Z.; Pinnau, I.; Meakin, P.; Hill, A. J. *Chemistry of Materials* **2003**, 15, 109-123.

(55) Merkel, T. C.; He, Z.; Pinnau, I.; Freeman, B. D.; Meakin, P.; Hill, A. J. *Macromolecules* **2003**, 36, 6844-6855.

(56) Matteucci, S. T.; Lin, H.; Kusuma, V.; Freeman, B. D.; Kalakkunnath, S.; Kalika, D. S.; Hill, A. J.; Mayo, S. "*Permeability Enhancement in Nanoparticle Filled Polymeric Membranes*", AIChE Annual Meeting, San Francisco, **2006**.

(57) Nielsen, L. E.; Landel, R. F. *Mechanical Properties of Polymers and Composites, 2nd ed.*; Marcel Dekker: New York, **1994**.

(58) Yim, A.; Chahal, R. S.; St. Pierre, L. E. *Journal of Colloid and Interface Science* **1973**, 43, 583-590.

(59) Reid, C. G.; Greenberg, A. R. *Journal of Applied Polymer Science* **1990**, 39, 995-1014.

(60) Tsagaropoulos, G.; Eisenberg, A. *Macromolecules* **1995**, 28, 396-398.

(61) Tsagaropoulos, G.; Eisenberg, A. *Macromolecules* **1995**, 28, 6067-6077.

(62) Arrighi, V.; McEwen, I. J.; Qian, H.; Prieto, M. B. S. *Polymer* **2003**, 44, 6259-6266.

(63) Ellison, C. J.; Mundra, M. K.; Torkelson, J. M. *Macromolecules* **2005**, 38, 1767-1778.

(64) Boyd, R. H. *Polymer* **1985**, 26, 323-347.

(65) Reddish, W. *Transactions of the Faraday Society* **1950**, 46, 459-475.

(66) Ishida, Y.; Yamafugi, K.; Ito, H.; Takayanagi, M. *Kolloid-Zeitschrift* **1962**, 184, 97-108.

(67) McCrum, N. G.; Read, B. E.; Williams, G. *Anelastic and Dielectric Effects in Polymeric Solids*; John Wiley and Sons: London, **1967**.

(68) Sawada, K.; Ishida, Y. *Journal of Polymer Science, Part B: Polymer Physics* **1975**, 13, 2247-2250.

(69) Coburn, J. C.; Boyd, R. H. *Macromolecules* **1986**, 19, 2238-2245.

(70) Schick, C.; Nedbal, J. *Progress in Colloid and Polymer Science* **1988**, 78, 9 -12.

(71) Schlosser, E.; Schoenhals, A. *Colloid and Polymer Science* **1989**, 267, 963-969.

(72) Tatsumi, T.; Eiko, I.; Hayakawa, R. *Journal of Polymer Science, Part B: Polymer Physics* **1992**, 30, 701-706.

(73) Ezquerra, T. A.; Balta-Calleja, F. J.; Zachmann, H. G. *Polymer* **1994**, 35, 2600-2606.

(74) Dobbertin, J.; Hensel, A.; Schick, C. *Journal of Thermal Analysis* **1996**, 47, 1027-1040.

(75) Pop, T.; Iordache, D.; Jonas, A. *Microelectronic Engineering* **1997**, 33, 377-384.

(76) Cheng, S. Z. D.; Cao, M. Y.; Wunderlich, B. *Macromolecules* **1986**, 19, 1868-1876.

(77) Ahlborn, K. *Cryogenics* **1988**, 28, 234-239.

(78) David, L.; Etienne, S. *Macromolecules* **1992**, 25, 4302-4308.

(79) Kalika, D. S.; Krishnaswamy, R. K. *Macromolecules* **1993**, 26, 4252-4261.

(80) Jonas, A.; Legras, R. *Macromolecules* **1993**, 26, 813-824.

(81) Krishnaswamy, R. K.; Kalika, D. S. *Polymer* **1994**, 35, 1157-1165.

(82) Kalika, D. S.; Nickell, J. C.; Krishnaswamy, R. K.; Barton, B. F. *Journal of Polymer Science, Part B: Polymer Physics* **1994**, 32, 759-770.

(83) Kalika, D. S.; Krishnaswamy, R. K. In *Polymeric Materials Encyclopedia*; Salamone, J. C., ed.; CRC Press: Boca Raton, FL, **1996**.

(84) Kalika, D. S.; Gibson, D. G.; Quiram, D. J.; Register, R. A. *Journal of Polymer Science, Part B: Polymer Physics* **1998**, 36, 65-73.

(85) Huo, P.; Cebe, P. *Macromolecules* **1992**, 25, 902-909.

(86) Gardner, K. H.; Hsiao, B. S.; Matheson, R. R., Jr.; Wood, B. A. *Polymer* **1992**, 33, 2483-2495.

(87) Krishnaswamy, R. K.; Kalika, D. S. *Polymer* **1996**, 37, 1915-1923.

(88) Wu, S. S.; Kalika, D. S.; Lamonte, R. R.; Makhija, S. *Journal of Macromolecular Science, Physics* **1996**, B35, 157-178.

(89) Kalika, D. S.; Wu, S. S.; Lamonte, R. R.; Makhija, S. *Journal of Macromolecular Science, Physics* **1996**, B35, 179-197.

(90) Huo, P.; Cebe, P. *Journal of Polymer Science, Part B: Polymer Physics* **1992**, 30, 239-250.

(91) "*COTERRA® PTT: What is CORTERRA® Polymer?*" Shell Chemicals, http://www.shellchemicals.com/corterra/1,1098,280,00.html

(92) Pyda, M.; Boller, A.; Grebowicz, J.; Chuah, H.; Lebedev, B. V.; Wunderlich, B. *Journal of Polymer Science, Part B: Polymer Physics* **1998**, 36, 2499-2511.

(93) Ward, I. M. *Mechanical Properties of Solid Polymers, 2nd ed.*; Wiley-Interscience: London, **1983**.

(94) Gradin, P.; Howgate, P. G.; Selden, R. "Dynamic Mechanical Properties" In *Comprehensive Polymer Science Volume II: Polymer Properties*; Allen, G., ed.; Pergamon Press: New York, **1989**.

(95) Instruction Manual, *Polymer Laboratories - Dynamic Mechanical Thermal Analyser*.

(96) Hedvig, P. *Dielectric Spectroscopy of Polymers*; John Wiley and Sons: New York, **1977**.

(97) Williams, G. "Dielectric Properties" In *Comprehensive Polymer Science, Volume II: Polymer Properties*; Allen, G., ed.; Pergamon Press: New York, **1989**.

(98) Cole, K. S.; Cole, R. H. *Journal of Chemical Physics* **1941**, 9, 341-351.

(99) Schönhals, A.; Kremer, F. "Analysis of Dielectric Spectra" In *Broadband Dielectric Spectroscopy*; Kremer, F.; Schönhals, A., eds.; Springer-Verlag: New York, **2003**; pp 59-98.

(100) Davidson, D. W.; Cole, R. H. *Journal of Chemical Physics* **1950**, 18, 1417.

(101) Debye, P. *Polar Molecules*; Chemical Catalog Company: New York, **1929**.

(102) Onsager, L. *Journal of American Chemical Society* **1936**, 58, 1486-1493.

(103) Kirkwood, J. G. *Journal of Chemical Physics* **1939**, 7, 911-919.

(104) Fröhlich, H. *Theory of Dielectrics*; Oxford University Press: Oxford, **1949**.

(105) Instruction Manual, *Novocontrol GmbH - Broadband Dielectric Spectrometer*, **2004**.

(106) Instruction Manual, *Perkin Elmer - DSC 7: Differential Scanning Calorimetry*.

(107) Richardson, M. J. "Thermal Analysis" In *Comprehensive Polymer Science, Volume I: Polymer Characterization*; Allen, G., ed.; Pergamon Press: New York, **1989**.

(108) Wunderlich, B. *Thermal Analysis*; Academic Press: San Diego, **1990**.

(109) Furukawa, G. T.; Douglas, T. B.; McCoskey, R. E.; Ginnings, D. C. *Journal of Research of the National Bureau of Standards* **1956**, 57, 67-82.

(110) Cullity, B. D. *Elements of X-ray Diffraction*; Addison-Wesley Publishing Company: Massachusetts, **1978**.

(111) Baker, R. W. *Membrane Technology and Applications, 2nd ed.*; John Wiley and Sons: New York, **2004**.

(112) Ngai, K. L.; Roland, C. M. *Macromolecules* **1994**, 27, 2454-2459.

(113) Roland, C. M.; Ngai, K. L.; Plazek, D. J. *Computational and Theoretical Polymer Science* **1997**, 7, 133-137.

(114) Huang, D.; McKenna, G. B. *Journal of Chemical Physics* **2001**, 114, 5621-5630.

(115) Lin, H.; Kai, T.; Freeman, B. D.; Kalakkunnath, S.; Kalika, D. S. *Macromolecules* **2005**, 38, 8381-8393.

(116) Decker, C.; Moussa, K. *Journal of Applied Polymer Science* **1987**, 34, 1603-1618.

(117) Colthup, N. B.; Daly, L. H.; Wiberley, S. E. *Introduction to Infrared and Raman Spectroscopy*; Academic Press: New York, **1975**.

(118) Ravi, N.; Mitra, A.; Hamilton, P.; Horkay, F. *Journal of Polymer Science, Part B: Polymer Physics* **2002**, 40, 2677-2684.

(119) Decker, C. *Macromolecular Rapid Communications* **2002**, 23, 1067-1093.

(120) Ishida, Y.; Matsuo, M.; Takayanagi, M. *Journal of Polymer Science, Part B: Polymer Letters* **1965**, 3, 321-324.

(121) Jin, X.; Zhang, S.; Runt, J. *Polymer* **2002**, 43, 6247-6254.

(122) Bohmer, R.; Ngai, K. L.; Angell, C. A.; Plazek, D. J. *Journal of Chemical Physics* **1993**, 99, 4201-4209.

(123) Roland, C. M.; Santangelo, P. G.; Ngai, K. L. *Journal of Chemical Physics* **1999**, 111, 5593-5598.

(124) Lin, H.; Van Wagner, E.; Swinnea, J. S.; Freeman, B. D.; Pas, S. J.; Hill, A. J.; Kalakkunnath, S.; Kalika, D. S. *Journal of Membrane Science* **2006**, 276, 145-161.

(125) Sperling, L. H. *Introduction to Physical Polymer Science, 4th ed.*; Wiley Interscience: New York, **2005**.

(126) Borns, M. A.; Freeman, B. D.; Kalika, D. S. "*Reverse-Selective Membrane Networks for the Purification of CO_2 Gas Mixtures*", AIChE Annual Meeting, San Francisco, **2006**.

(127) Patel, N. P.; Aberg, C. M.; Sanchez, A. M.; Capracotta, M. D.; Martin, J. D.; Spontak, R. J. *Polymer* **2004**, 45, 5941-5950.

(128) Schwarzl, F. R.; Bree, H. W.; Nederveen, C. J.; Schwippert, G. A.; Struik, L. C. E.; Van der Wal, C. W. *Rheologica Acta* **1966**, 5, 270-275.

(129) Matteucci, S. T.; Lin, H.; Freeman, B. D.; Kusuma, V.; Jose-Yacaman, M.; Kalakkunnath, S.; Kalika, D. S.; Hill, A. J. "*Permeability Enhancement in Nanoparticle Filled Polymeric Membranes*", AIChE Annual Meeting, Cincinnati, **2005**.

(130) Kremer, F.; Arndt, M. "Broadband Dielectric Measurement Techniques" In *Dielectric Spectroscopy of Polymeric Materials: Fundamentals and Applications*; Runt, J. P.; Fitzgerald, J. J., eds.; American Chemical Society: Washington, **1997**; pp 67-79.

(131) Kremer, F.; Schönhals, A. "Broadband Dielectric Measurement Techniques" In *Broadband Dielectric Spectroscopy*; Kremer, F.; Schonhals, A., eds.; Springer-Verlag: Berlin, **2003**; pp 35-57.

(132) Kalika, D. S. "Dielectric Spectroscopy of Crystalline Polymers and Blends" In *Handbook of Low and High Dielectric Constant Materials and Their Applications, Volume 1*; Nalwa, H. S., ed.; Academic Press: New York, **1999**; pp 275-327.
(133) Kranbuehl, D. E. "Dielectric Monitoring of Polymerization and Cure" In *Dielectric Spectroscopy of Polymeric Materials*; Runt, J. P.; Fitzgerald, J. J., eds.; ACS Books: Washington, D.C., **1997**; pp 303-328.
(134) Mijovic, J. "Dielectric Spectropscopy of Reactive Network-Forming Polymers" In *Broadband Dielectric Spectroscopy*; Kremer, F.; Schönhals, A., eds.; Springer-Verlag: Berlin, **2003**; pp 349-384.
(135) Vaia, R. A.; Sauer, B. B.; Tse, O. K.; Giannelis, E. P. *Journal of Polymer Science, Part B: Polymer Physics* **1997**, 35, 59-67.
(136) Elmahdy, M. M.; Chrissopoulou, K.; Afratis, A.; Floudas, G.; Anastasiadis, S. *Macromolecules* **2006**, 39, 5170-5173.
(137) Decker, C.; Moussa, K. J. *Journal of Applied Polymer Science* **1987**, 34, 1603-1618.
(138) Raharjo, R. D.; Lin, H.; Sanders, D. F.; Freeman, B. D.; Kalakkunnath, S.; Kalika, D. S. *Journal of Membrane Science* **2006**, 283, 253-265.
(139) Wunderlich, B. *Macromolecular Physics, Vol. 3, Crystal Melting*; Academic Press: New York, **1980**.
(140) Connor, T. M.; Read, B. E.; Williams, G. *Journal of Applied Chemistry* **1964**, 14, 74-80.
(141) Porter, C. H.; Boyd, R. H. *Macromolecules* **1971**, 4, 589-594.
(142) Se, K.; Adachi, K.; Kotaka, T. *Polymer Journal* **1981**, 13, 1009-1017.
(143) Wintersgill, M. C.; Fontanella, J. J.; Welcher, P. J.; Andeen, C. G. *Journal of Applied Physics* **1985**, 58, 2875-2878.
(144) Fanggao, C.; Saunders, G. A.; Lambson, E. F.; Hampton, R. N.; Carini, G.; Di Marco, G.; Lanza, M. *Journal of Polymer Science, Part B: Polymer Physics* **1996**, 34, 425-433.
(145) Williams, G. *Transactions of the Faraday Society* **1965**, 61, 1564-1577.
(146) Beevers, M. S.; Elliott, D. A.; Williams, G. *Polymer* **1980**, 21, 13-20.
(147) Varadarajan, K.; Boyer, R. F. *Polymer* **1982**, 23, 314-317.
(148) Johari, G. P. *Polymer* **1986**, 27, 866-870.
(149) Schlosser, E.; Schoenhals, A. *Progress in Colloid and Polymer Science* **1993**, 91, 158-161.
(150) Ichikawa, K.; MacKnight, W. J.; Nozaki, R.; Bose, T. K.; Yagihara, S. *Polymer* **1994**, 35, 1166-1170.
(151) Leon, C.; Ngai, K. L.; Roland, C. M. *Journal of Chemical Physics* **1999**, 110, 11585-11591.
(152) Mattsson, J.; Bergman, R.; Jacobsson, P.; Borjesson, L. *Physics Review Letters* **2003**, 90, 0757021-0757024.
(153) Roland, C. M.; Psurek, T.; Pawlus, S.; Paluch, M. *Journal of Polymer Science, Part B: Polymer Physics* **2003**, 41, 3047-3052.
(154) Havriliak, S.; Havriliak, S. J. *Dielectric and Mechanical Relaxation in Materials*; Hanser: Cincinnati, **1997**.

(155) Schönhals, A. "Dielectric Properties of Amorphous Polymers" In *Dielectric Spectroscopy of Polymeric Materials: Fundamentals and Applications*; Runt, J. P.; Fitzgerald, J. J., eds.; American Chemical Society: Washington, **1997**; pp 81-106.
(156) Leaversuch, R. "*Thermoplastic Polyesters: It's a Good Time to Know Them Better*", Plastics Technology, **June 2004**, http://www.ptonline.com/articles/200406fa1.html
(157) "*CORTERRA polytrimethylene terephthalate: What is CORTERRA® polymer?*" Shell Chemicals, http://www.shellchemicals.com/corterra/1,1098,280,00.html
(158) "*Sorona® Literature*", DuPont Company, **2004**, http://www2.dupont.com/Sorona/en_US/index.html
(159) Poulin-Dandurand, S.; Pérez, S.; Revol, J. F.; Brisse, F. *Polymer* **1979**, 20, 419-426.
(160) Desborough, I. J.; Hall, I. H.; Neisser, J. Z. *Polymer* **1979**, 20, 545-552.
(161) Ho, R.-M.; Ke, K.-Z.; Chen, M. *Macromolecules* **2000**, 33, 7529-7537.
(162) Wang, B.; Li, C. Y.; Hanzlicek, J.; Cheng, S. Z. D.; Geil, P. H.; Grebowicz, J.; Ho, R.-M. *Polymer* **2001**, 42, 7171-7180.
(163) Pyda, M.; Wunderlich, B. *Journal of Polymer Science, Part B: Polymer Physics* **2000**, 38, 622-631.
(164) Chung, W.-T.; Yeh, W.-J.; Hong, P.-D. *Journal of Applied Polymer Science* **2002**, 83, 2426-2433.
(165) Hong, P.-D.; Chuang, W.-T.; Yeh, W.-J.; Lin, T.-L. *Polymer* **2002**, 43, 6879-6886.
(166) Srimoaon, P.; Dangseeyun, N.; Supaphol, P. *European Polymer Journal* **2004**, 40, 599-608.
(167) Huang, J.-M.; Chang, F.-C. *Journal of Polymer Science, Part B: Polymer Physics* **2000**, 38, 934-941.
(168) Chuah, H. H. *Polymer Engineering and Science* **2001**, 41, 308-313.
(169) Hong, P.-D.; Chung, W.-T.; Hsu, C.-F. *Polymer* **2002**, 43, 3335-3343.
(170) Supaphol, P.; Dangseeyun, N.; Srimoaon, P.; Nithitanakul, M. *Thermochimica Acta* **2003**, 406, 207-220.
(171) Dangseeyun, N.; Srimoaon, P.; Supaphol, P.; Nithitanakul, M. *Thermochimica Acta* **2004**, 409, 63-77.
(172) Supaphol, P.; Apiwanthanakorn, N. *Journal of Polymer Science, Part B: Polymer Physics* **2004**, 42, 4151-4163.
(173) Xue, M.-L.; Sheng, J.; Yu, Y.-L.; Chuah, H. H. *European Polymer Journal* **2004**, 40, 811-818.
(174) Zhang, J. *Journal of Applied Polymer Science* **2004**, 93, 590-601.
(175) Sahay, S. S.; Krishnan, K. *Thermochimica Acta* **2005**, 430, 23-29.
(176) Wang, X.-S.; Li, X.-G.; Yan, D. *Polymer Degradation and Stability* **2000**, 69, 361-372.
(177) Wang, X.-S.; Li, X.-G.; Yan, D. *Polymer Testing* **2001**, 20, 491-502.
(178) Wang, X.-S.; Li, X.-G.; Yan, D. *Journal of Applied Polymer Science* **2002**, 84, 1600-1608.
(179) Ramiro, J.; Eguiazabal, J. I.; Nazabal, J. *Journal of Applied Polymer Science* **2002**, 86, 2775-2780.
(180) Kelsey, D. R.; Kiibler, K. S.; Tutunjian, P. N. *Polymer* **2005**, 46, 8937-8946.
(181) Boyd, R. H. *Polymer* **1985**, 26, 323-347.

(182) Cheng, S. Z. D.; Cao, M.-Y.; Wunderlich, B. *Macromolecules* **1986**, 19, 1868-1876.

(183) Cheng, S. Z. D.; Wu, Z. Q.; Wunderlich, B. *Macromolecules* **1987**, 20, 2802-2810.

(184) Kong, Y.; Hay, J. N. *Polymer* **2002**, 43, 3873-3878.

(185) Ilers, K. H.; Breuer, H. *Journal of Colloid Science* **1963**, 18, 1-31.

(186) Farrow, G.; Macintosh, J.; Ward, I. M. *Makromolekulare Chemie* **1960**, 38, 147-158.

(187) Gonzalez, C. C.; Perena, J. M.; Bello, A. *Journal of Polymer Science, Part B: Polymer Physics* **1988**, 26, 1397-1408.

(188) MacKintosh, A. R.; Liggat, J. J. *Journal of Applied Polymer Science* **2004**, 92, 2791-2796.

(189) Maxwell, A. S.; Ward, I. M.; Laupretre, F.; Monnerie, L. *Polymer* **1998**, 39, 6835-6849.

(190) Maxwell, A. S.; Monnerie, L.; Ward, I. M. *Polymer* **1998**, 39, 6851-6859.

(191) Pratt, G. J.; Smith, M. J. A. *Journal of Materials Science* **1990**, 25, 477-481.

(192) Schönhals, A.; Kremer, F. "Theory of dielectric relaxation" In *Broadband Dielectric Spectroscopy*; Kremer, F.; Schönhals, A., eds.; Springer-Verlag: New York, **2003**; pp 1-33.

(193) Boyd, R. H.; Liu, F. "Dielectric spectroscopy of semicrystalline polymers" In *Dielectric Spectroscopy of Polymeric Materials*; Runt, J. P.; Fitzgerald, J. J., eds.; American Chemical Society: Washington, DC, **1997**; pp 107-136.

Table of Nomenclature

A	Aea of the capacitor (m^2)
A	Constant in Arrhenius equation
A_D	Pe-exponential factor
C	Capacitance (Farads)
C_1	Constant used in WLF model
C_2	Constant used in WLF model (K)
C_2	Concentration of gas A sorbed on the upstream side of the polymer (cm^3(STP)/cm^3 polymer)
C_0	Capacitance across two plates in vacuum (Farads)
Cp^{cal}	Calibration standard heat capacity (cal/gm°C)
Cp^{Rubber}	Sample heat capacity in rubbery phase (cal/gm°C)
Cp^{Solid}	Sample heat capacity in solid (glassy) phase (cal/gm°C)
C_S	External stray capacitance (Farads)
C_{edge}	Edge compensation capacitance (Farads)
D	Dielectric displacement (V/m)
$D(t)$	Time-dependent dielectric displacement (V/m)
D_A	Effective diffusivity (cm^2/s)
D_{eff}	Effective diffusivity in filled polymer phase (cm^2/s)
D_p	Effective diffusivity in pure polymer phase (cm^2/s)
E	Elastic modulus (Pa)
E	Electric field strength (V/m)
$E(t)$	Time-dependent electric field strength (V/m)
E_A	Apparent activation energy (kJ/mol)
E_R	Storage modulus in the rubbery plateau region (Pa)
E^*	Complex modulus (Pa)
E_1	In-phase (elastic) component of the complex modulus (Pa)
E_2	Out of-phase (viscous) component of the complex modulus (Pa)
FFV	Fractional free volume
ΔH_F	Heat of fusion (kJ/mol)

N	Number of dipoles per unit volume
N_A	Steady-state flux of a gas A (cm^3(STP)/cm^2s)
M_c	Molecular weight between crosslinks (g/mol)
P_A	Permeability of a gas A (Barrer; 1 barrer = $10^{-10}$$cm^3$(STP) cm/($cm^2$ s cm-Hg))
P_{eff}	Permeability in filled polymer phase (Barrer)
P_p	Permeability in pure polymer phase (Barrer)
Q	Magnitude of charge on each plate of the capacitor (Coulombs)
R	Universal gas constant (J/mol K)
S_A	Apparent solubility coefficient (cm^3(STP)/(cm^3 atm))
S_f	Solubility of the filler phase (cm^3(STP)/(cm^3 atm))
S_p	Solubility of the pure polymer phase (cm^3(STP)/(cm^3 atm))
T_c	Crystallization temperature (°C)
T_g	Glass transition temperature (°C)
T_m	Melting peak temperature (°C)
T_{REF}	Arbitrary reference temperature (°C)
V	Potential difference across the capacitor plates (Volts)
V	Specific volume of the polymer (cm^3/g)
V_0	Specific occupied volume at 0 K (cm^3/g)
W_C	Weight fraction crystallinity
W_{MA}	Weight fraction of mobile amorphous phase
W_{RAP}	Weight fraction of rigid amorphous phase
a	Havriliak-Negami broadening parameter
a_{cal}	Heat flow amplitude of the calibration standard (mW)
a_r	Heat flow amplitude of the reference (mW)
a_s	Heat flow amplitude of the sample (mW)
a_T	Shift factor
b	Havriliak-Negami skewing parameter
d	Spacing between the two plates in a parallel-plate capacitor (m)
d	Characteristic lattice spacing per Bragg's Law (Å)

e	Strain
$e(t)$	Time-dependent strain
de/dt	Strain rate (s^{-1})
f	Applied frequency (Hz)
g	Kirkwood correlation factor
k	Boltzmann constant
k	Proportionality constant
l	Membrane thickness (cm)
m	Fragility index
m_c	Mass of calibration standard (mg)
m_s	Mass of sample of interest (mg)
p_1	Permeate side (low) partial pressure of gas A (atm)
p_2	Feed side (high) partial pressure of gas A (atm)
q	Heating rate employed in DSC instrument (°C/min)
$\alpha(t)$	Exponential decay function
β	KWW distribution parameter
δ	Phase angle of complex response (radians)
ε^*	Complex dielectric constant
ε_S	Static dielectric constant
ε_R	Relaxed dielectric constant (Dielectric constant as $\omega \rightarrow 0$)
ε_U	Unrelaxed dielectric constant (Dielectric constant as $\omega \rightarrow \infty$)
ε_0	Permittivity of vacuum
ε'	Real part of the complex dielectric constant (permittivity)
ε''	Imaginary part of the complex dielectric constant (dielectric loss)
$\phi(t)$	Relaxation time distribution function
ϕ_f	Volume fraction of the filler particles
ϕ_p	Volume fraction of the pure polymer phase
η	Viscosity (Pa s)
λ	Incident wavelength (Å)

μ_0	Permanent dipole moment of the relaxing unit when surrounded by vacuum
θ	Scattering angle (radians)
ρ_p	Bulk polymer density (g/cm^3)
σ	Stress (Pa)
σ	Charge density (Coulombs/m^2)
$\sigma(t)$	Time-dependent stress (Pa)
σ_0	Conductivity (Siemens/cm)
τ	Tortuosity factor
τ_0	Single relaxation time constant (s)
τ_{HN}	Relaxation time constant as predicted by the Havriliak-Negami model (s)
τ_{MAX}	Relaxation time constant corresponding to the dielectric loss maximum (s)
τ_{REF}	Relaxation time constant at reference temperature (s)
υ_e	Effective number of crosslinks per unit volume (mol/cm^3)
ω	Angular frequency (radians/sec)
ω_{exp}	Experimental Angular frequency (radians/sec)
ω_{MC}	Angular frequency pertaining to the generated master curve (radians/sec)

VITA

Date of birth:	Place of birth:
11th May, 1981	Mumbai, India

Education:

Bachelors in Chemical Engineering (May, 2002)
Mumbai University Institute of Chemical Technology
(formerly known as UDCT)
University of Mumbai, India

Honors:

Kentucky Opportunity Fellowship, University of Kentucky, 2004-05.

Commonwealth Research Award, University of Kentucky, 2006-07.

2nd place award, poster session, Eastern Regional Chemical & Materials Engineering Graduate Student Association Symposium (ERCGS), University of Kentucky, Lexington, 2006.

2nd place award, Materials Engineering and Sciences Division Poster Session, AIChE Annual Meeting, San Francisco, 2006.

Journal Publications:

S. Kalakkunnath, D.S. Kalika, H. Lin, R. D. Raharjo, B.D. Freeman, *"Molecular Dynamics of Poly(ethylene glycol) and Poly(propylene glycol) Copolymer Networks by Broadband Dielectric Spectroscopy"*, Macromolecules, **40(8)**, 2773-2781(2007)

H. Lin, B.D. Freeman, S. Kalakkunnath, D.S. Kalika, *"Effect of Copolymer Composition,Temperature and Carbon Dioxide Fugacity on Pure- and Mixed- Gas Permeability in Poly(ethylene glycol)-based Materials: Free Volume Interpretation",* Journal of Membrane Science, **291**, 131-139 (2007).

S. Kalakkunnath, D.S. Kalika, H. Lin, R. D. Raharjo, B.D. Freeman, *"Molecular Relaxation in Cross-Linked Poly(ethylene glycol) and Poly(propylene glycol) Diacrylate Networks by Dielectric Spectroscopy"*, Polymer, **48(2)**, 579-589 (2007).

S. Kalakkunnath, D.S. Kalika, *"Dynamic Mechanical and Dielectric Relaxation Characteristics of Poly(trimethylene terephthalate)"*, Polymer, **47(20)**, 7085-7094 (2006).

Journal Publications *(cont.)*

R.D. Raharjo, H. Lin, D.F. Sanders, B.D. Freeman, S. Kalakkunnath, D.S. Kalika, *“Relation between network structure and gas transport in poly(propylene glycol diacrylate)”*, Journal of Membrane Science, **283**, 253-265 (2006).

S. Kalakkunnath, D.S. Kalika, H. Lin, B.D. Freeman, *“Viscoelastic Characteristics of U.V. Polymerized Poly(ethylene glycol) Diacrylate Networks with Varying Extents of Crosslinking”*, Journal of Polymer Science Part B: Polymer Physics, **44(15)**, 2058-2070 (2006).

H. Lin, E. Wagner, J.S. Swinnea, B. D. Freeman, S.J. Pas, A.J. Hill, S. Kalakkunnath and D. S. Kalika, *“Transport and Structural Characteristics of Crosslinked Poly(ethylene oxide)”*, Journal of Membrane Science, **276**, 145-161 (2006).

S. Kalakkunnath, D.S. Kalika, H. Lin, B.D. Freeman, *“Segmental Relaxation Characteristics of Crosslinked Poly(ethylene oxide) Copolymer Networks”*, Macromolecules, **38(23)**, 9679-9687 (2005).

H. Lin, B.D. Freeman, T. Kai, S. Kalakkunnath, D.S. Kalika, *“The Effect of Cross-Linking on Gas Permeability in Cross-Linked Poly(ethylene glycol Diacrylate)”,* Macromolecules, **38(20)**, 8381-8393 (2005).

W.B. Lake, S. Kalakkunnath, D.S. Kalika, *“Crystallization, Melting and Rheology of Reactive Polyamide Blends”*, Journal of Applied Polymer Science, **94(3)**, 1245-1252 (2004).

S. Nene, S. Kaur, Sumod K., B. Joshi, Raghavarao K. S. M. S., *“Membrane Distillation for the Concentration of Raw Cane-Sugar and Membrane Clarified Sugarcane Juice”*, Desalination, **147**, 157-160 (2002).

Conference Proceedings:

H. Lin, V.A. Kusuma, B.D. Freeman, S.J. Pas, A.J. Hill, S. Kalakkunnath and D.S. Kalika, *"Membranes for Hydrogen Purification in Fuel Cell Applications"*, Proceedings of Mempro3: Intégration des Membranes dans les procédés, Nancy, France, April 5-7, 2006.

S. Kalakkunnath, H. Lin, B.D. Freeman, and D.S. Kalika, "*Relaxation Characteristics of Crosslinked Poly(ethylene glycol) Diacrylates and Their Relation to Gas Transport Properties*", Proceedings of the American Chemical Society, Div. of Polymeric Materials: Science and Engineering, 93, 332 (2005).

Conference Proceedings *(cont.)*

H. Lin, S. Matteucci, B.D. Freeman, S. Kalakkunnath, and D.S. Kalika, "*Novel Membrane Materials for* CO_2 *Removal from Mixtures with* H_2", Proceedings of the American Chemical Society, Div. of Fuel Chemistry, 50(2), 617 (2005).

Presentations:

Oral Presentations

S. Kalakkunnath, M.K. Danquah, S.T. Matteucci, R.D. Raharjo, B.D. Freeman and D.S. Kalika, "*Structure, Dynamics and Gas Transport Characteristics of Rubbery Polymer Networks and Nanocomposites*", AIChE Annual Meeting, San Francisco, 2006.

S. Kalakkunnath, H. Lin, B.D. Freeman, and D.S. Kalika, "*Dynamics of poly(ethylene glycol) Networks and Their Relation to Gas Transport Properties*", AIChE Annual Meeting, Cincinnati, 2005.

Poster Presentations

S. Kalakkunnath, S.T. Matteucci, V. Kusuma, B.D. Freeman and D.S. Kalika, "*Segmental Relaxation Characteristics of Rubbery Membrane Networks*", AIChE Annual Meeting, San Francisco, 2006.

S. Kalakkunnath, M. Borns, H. Lin, V. Kusuma, B.D. Freeman and D.S. Kalika, "*Dynamic Relaxation Characteristics of Rubbery Polymer Networks and Their Relation to Gas Transport*", Eastern Regional Chemical and Materials Engineering Graduate Symposium, Lexington, 2006.

S. Kalakkunnath, T.W. Humphries, and D.S. Kalika, "*Crystallization, Melting, and Dynamic Relaxation Characteristics of PTT and PTT Blends*", AIChE Annual Meeting, Cincinnati, 2005.

S. Kalakkunnath, H. Lin, S. Matteucci, B.D. Freeman, and D.S. Kalika, "*Dynamic Relaxation Characteristics of Crosslinked Poly(ethylene glycol) Networks and Composites*", AIChE Annual Meeting, Cincinnati, 2005.